CANADIAN THESES ON MICROFICHE

I.S.B.N.

THESES CANADIENNES SUR MICROFICHE

National Library of Canada
Collections Development Branch

Canadian Theses on
Microfiche Service

Ottawa, Canada
K1A 0N4

Bibliothèque nationale du Canada
Direction du développement des collections

Service des thèses canadiennes
sur microfiche

NOTICE

The quality of this microfiche is heavily dependent upon the quality of the original thesis submitted for microfilming. Every effort has been made to ensure the highest quality of reproduction possible.

If pages are missing, contact the university which granted the degree.

Some pages may have indistinct print especially if the original pages were typed with a poor typewriter ribbon or if the university sent us a poor photocopy.

Previously copyrighted materials (journal articles, published tests, etc.) are not filmed.

Reproduction in full or in part of this film is governed by the Canadian Copyright Act, R.S.C. 1970, c. C-30. Please read the authorization forms which accompany this thesis.

THIS DISSERTATION
HAS BEEN MICROFILMED
EXACTLY AS RECEIVED

AVIS

La qualité de cette microfiche dépend grandement de la qualité de la thèse soumise au microfilmage. Nous avons tout fait pour assurer une qualité supérieure de reproduction.

S'il manque des pages, veuillez communiquer avec l'université qui a conféré le grade.

La qualité d'impression de certaines pages peut laisser à désirer, surtout si les pages originales ont été dactylographiées à l'aide d'un ruban usé ou si l'université nous a fait parvenir une photocopie de mauvaise qualité.

Les documents qui font déjà l'objet d'un droit d'auteur (articles de revue, examens publiés, etc.) ne sont pas microfilmés.

La reproduction, même partielle, de ce microfilm est soumise à la Loi canadienne sur le droit d'auteur, SRC 1970, c. C-30. Veuillez prendre connaissance des formules d'autorisation qui accompagnent cette thèse.

LA THÈSE A ÉTÉ
MICROFILMÉE TELLE QUE
NOUS L'AVONS REÇUE

NL-339 (r. 82/08)

Canada

A REACTOR DESIGN STUDY FOR CHAR GASIFICATION KINETICS

by

VINCENZA M. ALLENGER

A thesis submitted to the School of Graduate Studies in partial fulfillment of the requirement for the degree of

MASTER OF APPLIED SCIENCE

in the

Department of Chemical Engineering
University of Ottawa

September 1982

ABSTRACT

A critical review of the char gasification literature revealed that many researchers fail to account for concentration and temperature gradients which may exist at three levels in gas-solid systems: within a single reacting particle, in the film surrounding the particle, and in the reactor as a whole. Furthermore, in many of the gasification studies, the fluid mixing state has not been clearly defined. Theoretical and experimental tests for evaluating these effects are summarized. The use of 'gradientless' reactors, to alleviate these problems in studying gasification reactions is discussed. The potential of gradientless internal recirculation flow reactors in studying gasification kinetics was investigated by designing and constructing such a reactor. The degree of gas-phase mixing in the reactor was determined from step-response data using a novel approach to remove the intrusion of measurement device dynamics which prevents unambiguous evaluation of the mixing in bench scale reactors commonly having short residence times.

ACKNOWLEDGEMENTS

I would like to express my gratitude to my supervisor, Dr. David D. McLéan for his guidance, advice and constructive criticism throughout the project.

I would also like to extend my appreciation to D. Lefebvre for his technical and analytical assistance during the early stages of this project.

Thanks are due to Dr. D. P. C. Fung for granting me permission to use his facilities to prepare coal char and G. Lett for analyzing the char samples.

The financial assistance received from the Natural Sciences and Engineering Research Council and from the Graduate School at the University of Ottawa is gratefully acknowledged.

TABLE OF CONTENTS

TABLE OF CONTENTS (CONT'D)

TABLE OF CONTENTS (CONT'D)

TABLE OF CONTENTS (CONT'D)

TABLE OF CONTENTS (CONT'D)

TABLES

TABLES (cont'd)

FIGURES

FIGURES (cont'd)

FIGURES (cont'd)

NOTATION

SYMBOL	DEFINITION
a_m	external surface/unit mass $[m_p^2\ k_g^{-1}]$
a_v	external surface area/unit reactor volume $[m_p^2\ m_r^{-3}]$
b	dilution ratio
b'	molar stoichiometric coefficient
C_A	concentration of gaseous component $[kmol\ m_f^{-3}]$
$\overline{C}_A$	mean concentration of reactant leaving vessel $[kmol\ m_f^{-3}]$
C_{AB}	concentration of species A in bulk stream $[kmol\ m_f^{-3}]$
C_{AS}	concentration of species A at surface $[kmol\ m_f^{-3}]$
C_b	bulk fluid concentration $[mol\ m_f^{-3}]$
c_p	fluid heat capacity at constant pressure $[kJ\ kg^{-1}K^{-1}]$
C_s^s	molar concentration of fluid reactant in front of solid surface $[kmol\ m_f^{-3}]$
d_p	particle diameter $[m]$

SYMBOL	DEFINITION
D_{12}	binary molecular diffusion coefficient $[cm^2\ s^{-1}]$
D_a	mixing dispersion coefficient for axial dispersion model
D_e	effective diffusivity for gas phase $[cm^2\ s^{-1}]$
D_{ea}	axial effective diffusivity $[m_f^3 m_r^{-1} s^{-1}]$
D_{eff}	effective diffusivity of solid $[cm^2\ s^{-1}]$
$D_{12,eff}$	effective diffusion coefficient for bulk diffusion $[cm^2\ s^{-1}]$
D_{er}	radial effective diffusivity $[m_f^3 m_r^{-1} s^{-1}]$
$D_{k,eff}$	effective diffusion coefficient for Knudsen diffusion $[cm^2\ s^{-1}]$
e	allowable error
E	exit age distribution
E_a	activation energy $[kJ\ kmol^{-1}]$
f_{u1}	calculated value of C/C_o for measurement device response at t_u
f_{u2}	calculated value of C/C_o for combined response at t_u
F	molar flow rate $[mol\ s^{-1}]$

SYMBOL	DEFINITION
FR	feed gas flowrate [$cm^3 min^{-1}$]
G	superficial mass velocity [$kg\ m_r^{-2}\ s^{-1}$]
h_f	heat transfer coefficient in film [$kJ\ m_p^{-2}\ s^{-1}\ K^{-1}$]
h_r	radiant heat transfer coefficient [$kJ\ m_p^{-2}\ s^{-1}\ K^{-1}$]
H_r	heat of chemical reaction [$kJ\ kmol^{-1}$]
I	internal age distribution
j_D	Chilton-Colburn factor
j_H	Chilton-Colburn factor
k_g	mass transfer coefficient [$m_f^3\ m_p^{-2}\ s^{-1}$]
k	reaction rate constant (1st order reaction) [s^{-1}]
k_r	first order rate constant [s^{-1}]
K_o	geometric parameter characteristic of porous solid [m]
l	fraction of total reactor volume that is behaving as a series plug flow region
L	characteristic dimension of solid particle [m]

SYMBOL	DEFINITION
L'	reactor length [m]
m	fraction of total reactor volume that is behaving as a parallel plug flow region
$\underline{M}^{-1}$	variance-covariance matrix for parameters (inverse of matrix $\underline{M}$)
M_A	molecular weight [kg $kmol^{-1}$]
n	reaction order
n	fraction of total reactor volume that is being backmixed
n	total number of data points
N	number of tanks in series
N_A	molar flux [kmol m^{-2} s^{-1}]
N_{Nu}	Nusselt Number = $h_f dp/\mu$
N_{Pr}	Prandtl Number = $C_p \mu / k_f$
N_{Re}	Reynolds Number = $UL\rho/\mu$
N_{Sc}	Schmidt Number = $\mu/\rho D_{12}$
N_{Sh}	Sherwood Number = $k_g L/D_{12}$
PS	coded particle size
q	heat flux [kJ m^{-2} s^{-1}]
Q	heat transfer rate from solid to fluid per unit mass [kJ kg^{-1}]

SYMBOL	DEFINITION
Q_R	radiant heat transfer rate [kJ s^{-1}]
r_p	particle radius [m]
$r_{v,obs}$	observed or measured reaction rate [kmol m^{-3} s^{-1}]
R	fraction of the total flow that is being completely mixed
R	universal gas constant [kJ $kmol^{-1}$ K^{-1}]
R_o	reactor radius [m]
RPM	impeller speed in revolutions per minute
SS_1	residual sum of squares for response 1
SS_2	residual sum of squares for response 2
t_1	mean residence time in one tank [s]
t_R	nominal holding time [s]
T	absolute temperature [K]
T_b	bulk fluid absolute temperature [K]
T_s	Temperature inside solid [K]
T_s^s	Temperature at solid surface [K]

SYMBOL	DEFINITION
T_B/R	residence time in backmix section [s]
$T_{PP}/(1-R)$	residence time in parallel plug flow section [s]
T_w	temperature of walls of cavity [K]
u	run number
u_t	unit step function
U	superficial fluid velocity $[m_f^3\ m_r^{-2}\ s^{-1}]$
v	superficial linear velocity $[MS^{-1}]$
v_o	volumetric flowrate $[cm^3\ s^{-1}]$
v_F	feed volumetric flowrate $[m_f^3\ s^{-1}]$
v_p	pump recycle rate $[m_f^3\ s^{-1}]$
V_B	volume of backmix region [mL]
V_D	volume of stagnant region [mL]
V_{PP}	volume of parallel plug flow region [mL]
V_{PS}	volume of series plug flow region [mL]

SYMBOL	DEFINITION
V_T	total volume of reactor vessel [mL]
W	weight of solid bed [kg]
x_o	feed stream conversion
$\underline{X}_1$	matrix of partial derivatives of response 1 with respect to the parameters
$\underline{X}_2$	matrix of partial derivatives of response 2 with respect to the parameters
X_τ	transformed variable for τ in minimization routine
X_B	transformed variable for T_{PP} in minimization routine
x_F	exit stream conversion
X_{PP}	transformed variable for T_{PP} in minimization routine
X_{PS}	transformed variable for T_{PS} in minimization routine
X_R	transformed variable for R in minimization routine
Y	co-ordinate
y_{u1}	measured value of C/C_o for measurement device
y_{u2}	measured value of C/C_o for combined response at tu
Z	co-ordinate

NOTATION

SYMBOL	DEFINITION
β	heat of reaction parameter defined by Equation 3-24
γ	Arrhenius number defined in Equation 3-22
γ^3	skewness
Δ	relative experimental error in conversion
δ	pore radius
ε	packed bed voidage $[m_f^3\ m_r^{-3}]$
ε_s	porosity of solid, internal void fraction of solid $[m_f^3\ m_s^{-3}]$
$\tilde{\varepsilon}$	emissivity of solid surface
ζ	ratio defined by Equation 3-21
ξ	radial coordinate inside particle $[m_p]$
η	effectiveness factor

SYMBOL	DEFINITION
Θ	reduced time = $t/\bar{t}_R$
θ_s	real value of parameter s
$\hat{\theta}_s$	estimate of parameter s
Λ	function defined in Equation 3-34
λ_e	effective thermal conductivity of packed bed with no fluid motion $[kJ\ m_r^{-1}\ s^{-1}\ K^{-1}]$
λ_{ea}	axial effective thermal conductivity in packed bed $[kJ\ m_r^{-1}\ s^{-1}\ K^{-1}]$
λ_{ea}^f	effective thermal conductivity of gas in axial direction in packed bed $[kJ\ m_r^{-1}\ s^{-1}\ K^{-1}]$
λ_{ea}^s	effective thermal conductivity of solid in axial direction in packed bed $[kJ\ m_r^{-1}\ s^{-1}\ K^{-1}]$
λ_{eff}	effective thermal conductivity of solid $[kJ\ m_r^{-1}\ s^{-1}\ K^{-1}]$

SYMBOL	DEFINITION
λ_{er}	radial effective thermal conductivity in packed bed $[kJ\ m_r^{-1}\ s^{-1}\ K^{-1}]$
λ_{er}^{f}	effective thermal conductivity of fluid phase in packed bed $[kJ\ m_r^{-1}\ s^{-1}\ K^{-1}]$
λ_{er}^{s}	effective thermal conductivity of solid phase in packed bed $[kJ\ m_r^{-1}\ s^{-1}\ K^{-1}]$
λ_f	thermal conductivity of fluid $[kJ\ m_f^{-1}\ s^{-1}\ K^{-1}]$
λ_s	thermal conductivity of solid at $s = 0$ $[kJ\ m_s^{-1}\ s^{-1}\ K^{-1}]$
μ	mean (centre of gravity of distribution about origin)
μ	fluid viscosity $[kg\ m^{-1}\ s^{-1}]$
π	pi
ρ	fluid density $[kg\ m^{-3}]$

SYMBOL	DEFINITION
σ	Stephan Boltzmann constant $[5.67 \times 10^{-8}$ kJ/M^{-2} s^{-1} K$^{-4}]$
σ^2	variance (spread of distribution)
σ^2_{u1}	variance of response 1 at t_u
σ^2_{u2}	variance of response 2 at t_u
τ	residence time in a single tank of measurement device tanks-in-series model [s]
τ	tortuosity factor
ϕ	Thiele modulus
X	ratio defined by Equation 3-27
ω	ratio defined by Equation 3-26

1 INTRODUCTION

Recently, the gasification of coal and biomass (bark, peat, woodchips, coconut shell, etc.) has received considerable attention in view of the growing interest in alternate forms of energy. There are various complete gasification systems in operation (Synthane, Lurgi, Kellogg, etc.), each having been developed to meet certain factors which include the availability of feedstock, the utilization of the product gas and the capital cost of the installation[1]. Even though this gasification technology has already been developed and is readily available, the renewed and vital role it plays today has provided the impetus for researchers to improve gasification processes in order to make them economically viable in a very competitive fuel market[2].

Coal/biomass gasification may be thought of as occurring in several steps[3]. First the carbonaceous material is heated at high rates where pyrolysis and devolatilization occur according to the following reaction:

$$\text{Coal/Biomass} + \text{Heat} \text{ ----- } \text{Volatiles } (CH_4, CO, CO_2, H_2, H_2O)\ (g) + \text{Tar}\ (l) + \text{Char}\ (s) \qquad \text{Equation 1-1}$$

The volatiles then react in the gas phase. The char or solid residue remaining after this step consists primarily of carbon together with

the major part of the ash components and some volatile matter. The subsequent heterogeneous reactions between the char and oxygen, steam, carbon dioxide and hydrogen account for the majority of the time required for particle burnout. Furthermore, as pointed out in a recent review[4], economic feasibility of producing SNG and efficiency of in situ gasification also hinge on this important char gasification step. In view of this, attempts for improvements in gasification technology might well be directed towards this aspect of the overall process.

Knowledge of the kinetics of the char gasification step is fundamental to the design and optimal operation of commercial gasifiers, to the development and testing of suitable catalysts (in terms of both activity and selectivity) and to the better understanding of the basic gasification mechanism involved. Many investigations into char gasification kinetics have been carried out on both a bench scale and pilot scale. Numerous types of experimental reactor systems have been used to study the kinetics in question. The experimental arrangements include gas flow and static systems in which the char may exist as a fixed or fluidized bed of granular particles[5,6], particles falling through a hot zone[7], or a single massive piece[8]. The operating variables encompass a wide range in temperatures (500-2300^{o}C), pressures (10^{-5}kPa-10^{3}kPa) and gas velocities (0-100 m/s). While some experiments involve the reaction of an appreciable portion of the char, others are confined to reactions at very low burnoff. In this myriad of experimental investigations, disagreements are evident. Table 1-1 and Figure 1-1

TABLE 1-1 *

ARRHENIUS FACTORS AND REACTION ORDERS FOR SOME GASIFICATION REACTIONS

Reaction	A [$kgm^{-2}s^{-1}k\ Pa^n$]	E/R [K]	n	Particle Type	Particle Size [μm]	Temperature Range [K]
O_2-C	1.32×10^{-1}	16400	0	Brown Coal Char	22-89	630-1812
	9.18×10^{-1}	8200	0.5	Brown Coal Char	22-89	630-2200
	2.01	9600	1	Semianthracite	6-78	1400-2200
	5.43	20100	1	Semianthracite	6-78	1400-2200
H_2O-C	3.19×10^2	25020	1	Graphite	-	1133-1233
	-	8240	1	Graphite	-	873-1273

	A_1	E_1/R	A_2	E_2/R		
CO_2-C	1.38×10^3	24000	1.4×10^{-4}	- 7500	Coke	1073-1363
	2.1×10^4	20200	2.0×10^{-11}	-27000	Coke	1199-1423

* Table adapted from Tables 1, 3 and 6 of Chapter 9 in Smoot, L.D. and D. T. Pratt, Pulverized Coal Combustion and Gasification Plenum Press NY C1979

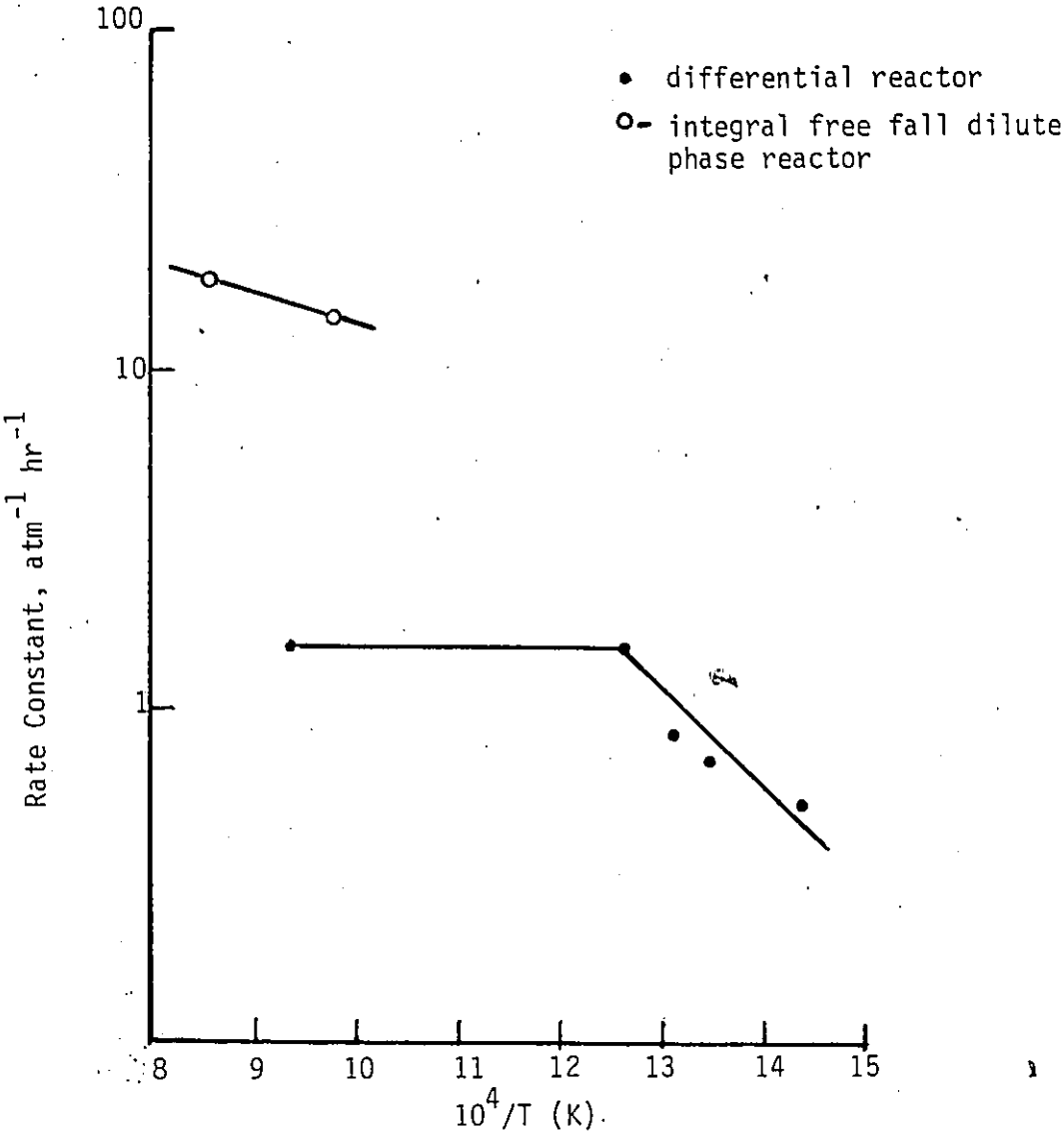

Figure 1-1 Effect of temperature and reactor type on hydrogasification (Adapted from Reference 86)

contain some examples of experimental findings of kinetic parameters which have been reported in the literature. In as much as values for reaction order n, preexponential factor A and activation energy E are dependent upon the nature of the feedstock, it is unclear why these kinetic parameters are found to vary considerably from investigation to investigation, even for very similar feedstocks. The discrepancies found in these instances, are generally attributed to differences in pretreatment and source of the char being investigated. Although activity and selectivity of the char gasification step have been shown to be influenced by these factors[120], the environmental history of the char during reaction (i.e. the heat up rate, temperature, pressure, composition of the gas phase, etc.) is an important factor which has often been poorly characterized. Proper interpretation of kinetic data depends upon reliable characterization of reaction conditions (temperature, reactant/product concentration, degree of mixing). In order to obtain reliable rate data and to facilitate data analysis, sound bench scale reactor design is critical. Unfortunately, there is little evidence in the gasification literature which indicates that reactor systems have been thoroughly evaluated.

Therefore, the preliminary objectives of the present work were:

1. to discuss the required features of laboratory reactor design for char gasification kinetics
2. to summarize and demonstrate the theoretical and experimental tests that may be applied to test an existing reactor system for temperature gradients, concentration gradients and residence time distribution

3. to summarize the types of reactors which have been used to date in char gasification studies and to evaluate them with respect to the above requirements

As a result of this evaluation of the status quo in reactor design for gasification kinetics, it was desirable to consider and discuss possible alternative reactor designs which showed promise in overcoming many of the shortcomings of the reactor systems in current use. One of the alternate designs, namely an internal recirculation flow reactor was constructed in order to investigate its potential in studying char gasification kinetics. The development, testing and use of the reactor are discussed in detail.

2 CHAR GASIFICATION

In char gasification the primary process is a heterogeneous reaction between carbon and hydrogen, oxygen, carbon dioxide and steam. Consequently, carbon (in the form of graphite) has been used by many experimenters as a first approximation to the carbonaceous material in their effort to study the gasification reactions listed in Table 2-1. The reader is referred to an excellent treatise on the gas reactions of carbon by Walker et. al[8]. The authors discuss quite thoroughly the rates and mechanisms of several gas-carbon reactions and the various factors that affect them. Considerable emphasis is placed on the role of mass transport. The dated review by von Fredersdorff and Elliott[9] which treats separately the topics of thermodynamics, physics, kinetics and diffusion in gasification reactions is also recommended as a summary of the work (mostly with pure carbon) done prior to 1960. Although much of the research carried out with pure carbon has contributed significantly to our understanding of the complex gas-char reactions, it has not been possible to predict char gasification rates from their carbon counterparts primarily because of inherent chemical differences. Char differs from pure carbon in that it contains chemically bound hydrogen, oxygen, sulfur and nitrogen as well as varying amounts of ash and mineral matter[3]. The latter items have been shown to influence reaction rates substantially through direct catalytic activity[10]. For these reasons, rate studies using char have been prompted. The reader's attention is focussed on a very comprehensive

TABLE 2-1

GASIFICATION REACTIONS

		Heat of Reaction [CAL/MOL]
Boudouard Reaction	$C_{(s)} + CO_{2(g)} \rightarrow 2CO_{(g)}$	41,200
Hydrogasification	$C_{(s)} + 2H_{2(g)} \rightarrow CH4_{(g)}$	-17,890
Carbon-Steam Reaction	$C_{(s)} + H_2O_{(g)} \rightarrow CO_{(g)} + H_2\ (g)$	41,000
Incomplete Combustion	$C_{(s)} + 1/2\ O_{2(g)} \rightarrow CO_{(g)}$	-26,400

review by Laurendeau[4] in which the kinetics of the char reactions with oxygen, hydrogen, steam and carbon dioxide are considered in great depth with the emphasis being placed on the use of intrinsic chemical reaction rates, i.e. the rate per unit surface area (internal plus external), in the study of these heterogeneous reactions. The basics of gas-solid reactions will now be examined briefly.

The char gasification reactions listed in Table 2-1 are non-catalytic heterogeneous reactions involving a solid (char) and a gas (oxygen, hydrogen, steam, carbon dioxide). Gas-solid reactions are considered to observe the following mechanism or sequence of steps:

1. external mass transport of gaseous reactant(s) from the bulk fluid to the outside surface of the porous solid
2. diffusion of the gaseous reactant(s) within the pores of the solid to the surface
3. chemical reaction with the solid including the adsorption of reactants and the desorption of products
4. diffusion of the gaseous products from interior sites to the outer surface of the solid
5. external mass transport of the gaseous products from the gas-solid interface to the bulk gas stream

It is very important to understand the relative significance of these steps in order to understand the overall rates of the reactions. Any single step 1 through 5 can be rate-determining and often a combination of steps ultimately determine the overall gasification

rates depending upon what reaction conditions (temperature, pressure, gas concentrations and velocities, particle sizes) are being studied. Operating conditions in which the surface reaction is controlling (i.e. step 3) must be used to determine the true kinetics of the char-gas reactions since at any other conditions, the external mass transport (steps 1 and 5) and the intraparticle diffusion (steps 2 and 4) may significantly affect the overall rate, the activation energy and the apparent order of reaction[11].

Since kinetic parameters must be determined through measurements on a reacting system, it is critical that the reactor be carefully described through an adequate design equation and that the experimental procedure and operating conditions be clearly defined.

The mathematical formulation for char-gas reactions in multiparticle systems (such as fixed beds, fluidized beds, entrained bed, etc.) is complex and as Wen[12] points out "a rigorous treatment seems unattainable even for the solid of the simplest geometry" because of a number of factors:

1. the changing size and shape of the char particles during the reaction
2. the changing intricate pore network within the porous char during reaction
3. the complicated velocity profile of the surrounding gas and
4. the complicated temperature distributions within the reactor due to high heats of reaction.

Szekely et. al[13] have outlined a general approach to formulating models of nonisothermal systems where there may be a significant change in the molar flow rate of the reacting gas. Their approach consists in statements of heat balances and component and overall mass balances on the gas and solid. Typical relationships that enter into these equations are correlations of heat and mass transfer coefficients, temperature dependence of property values and expressions for the solid rate of reaction.

As an example, a summary of the governing equations for a tubular packed bed flow reactor for the transient state and for a single reaction are given in Table 2-2. Models of chemical reactors, therefore, must be based on the physical phenomena of mass, heat and momentum transfer and on chemical reaction kinetics. Reactor design and operation which can simplify the formidable task of modelling is invaluable to obtaining and interpreting gasification rate data. In this light, the merits and demerits of various laboratory reactors in facilitating kinetic studies will be examined in Chapter 4.

It is clear that the mathematical model used to describe the reacting system should be representative of the actual conditions existing inside the reactor. No analytical solution to the complete set of partial differential equations listed in Table 2-2 exists. Numerical solutions of this set of equations, although feasible, require considerable computation and to my knowledge solutions of this type have not yet been attempted. In order to obtain the kinetics from a tubular fixed bed, simplifying assumptions must be made. The interpretation of kinetic data therefore depends upon the quality of these underlying assumptions. When assumptions are made about reactor

TABLE 2-2

GOVERNING EQUATIONS FOR TUBULAR FIXED BED REACTOR

MASS BALANCE ON KEY COMPONENT OF GAS

$$\partial(\varepsilon C)/\partial t = -\partial(UC)/\partial z - k_g a_v (C - C_s^s) + \varepsilon D_{er}(\partial^2 C/\partial r^2 + 1/r\,\partial C/\partial r) + \varepsilon D_{ea}\left[\frac{\partial^2 C}{\partial z^2}\right]$$

rate of acc of reactant	net convective flow of reactants in axial direction	net transfer of reactant from solid to gas	flow of reactant into the differential volume due to radial & axial dispersion

MASS BALANCE ON REACTING COMPONENT OF SOLID

$$\partial C_s/\partial t = D_{ea}(\partial(\xi^2 \partial C_s/\partial \xi)/\partial \xi)/\xi^2 - \rho_s r_A$$

Rate of Acc of reactant comp. of solid	effective diffusion within solid particle	rate of production or consumption of reactive component due to chemical reaction

HEAT BALANCE ON GAS

$$\varepsilon\partial(\rho_g c_p^f T_f)/\partial t = -\frac{\partial(U\rho_g c_p^f T)}{\partial z} + h_f a_v (T_s - T) + \lambda_{er}^f\left[\frac{\partial^2 T}{\partial r^2} + \frac{1}{r}\frac{\partial T}{\partial r}\right] + \lambda_{ea}^f\left[\frac{\partial^2 T}{\partial z^2}\right]$$

rate of acc of heat in gas	net convective axial heat flow into differential Volume	rate of heat transfer to solid	heat entering differential volume due to radial & axial dispersion in gas

HEAT BALANCE ON SOLID

$$\partial(\rho_s c_p^s T_s)/\partial t = \frac{\lambda_e}{\xi^2}\left[\frac{\partial}{\partial \xi}\left(\xi^2 \frac{\partial T_s}{\partial \xi}\right)\right] + \rho_s \Delta H_r r_A + \lambda_{er}^s\left[\frac{\partial^2 T_s}{\partial r^2} + \frac{1}{r}\frac{\partial T_s}{\partial r}\right] + \lambda_{ea}^s\left[\frac{\partial^2 T_s}{\partial z^2}\right]$$

rate of acc of heat in solid	rate of heat transfer to gas due to effective thermal cond. within solid	rate of heat consumed due to heterogeneous reaction	heat flow into differential volume due to conduction & radiation in axial and radial directions.

conditions, it is important that experimental as well as theoretical tests be applied whenever possible to verify them. In the next chapter, the essential and desirable features of bench scale reactors and these experimental and theoretical tests will be discussed in an effort to evaluate bench-scale reactors in the study of char gasification kinetics.

3 EXPERIMENTAL DESIGN

3.1 Essential and Desirable Features of System Design

Before embarking on an evaluation of reactor systems, it is worthwhile establishing those features of a reaction system which are desirable and in some cases essential for the accurate determination of char gasification kinetics from single particle or multiparticle systems. When only chemical kinetic information is of interest, one must ensure that temperature and concentration gradients within the reactor are controlled and accurately modelled. This can be classified as an essential feature of system design since chemical kinetics depend directly on the concentration of reacting species and on the reaction temperature. These gradients may exist at three levels in gas-solid systems: intraparticle*, interphase** and interparticle***. Each of these will be considered separately.

3.1.1 Intraparticle Gradients

---

* within individual particles

** between the external surface of the particle and the gas adjacent to it

*** between local gas regions and between char particles (sometimes referred to as intrareactor)

Concentration gradients inside a single reacting porous particle exist whenever the reactants cannot diffuse in to the pores of the solid from the solid-fluid interface sufficiently rapidly. A good description of pore diffusion can be found in References 14 and 15. Diffusion rates in porous solids cannot in general be predicted because of several complicating factors[13], namely:

1. The volume occupied by the solids is not available for diffusive transfer.
2. The actual diffusion path will not follow a straight line but will be quite tortuous and the extent of this tortuosity will necessarily depend on the pore structure of the solid.
3. The diffusion in the pore volume will be influenced by the pore walls when the pores are small enough and Knudsen diffusion will become important.
4. Under some conditions, significant total pressure gradients may be established within the solid. Under these conditions transfer due to a pressure gradient has to be considered.

The approach usually taken to model an actual solid is to assume that the laws of molecular diffusion are obeyed in the porous medium and then to define an effective diffusivity (which is smaller than the binary molecular diffusion coefficient) to incorporate the various factors mentioned

earlier as follows:

$$N_A = -D_{eff} \frac{dC_A}{dz} \qquad \text{Equation 3-1}$$

Pore diffusion in the solid may occur by either bulk or Knudsen diffusion or both. If the pores are large and the gas relatively dense, the process is that of bulk or ordinary diffusion*. The bulk diffusion coefficient per unit cross section of porous mass may be expressed in the following way:

$$D_{12,eff} = \frac{\varepsilon_s D_{12}}{\tau} \qquad \text{Equation 3-2}$$

where τ is the tortuosity factor, ε_s the internal void fraction or porosity of the solid, and D_{12} the ordinary molecular diffusivity. Typical values for porosity of coals are in the range 2-30%[16]. The porosity of chars is usually somewhat higher and depends upon the extent of gasification (30-70%).

Experimental values of gaseous diffusion coefficients are in most cases readily available but when this is not the case, gas phase diffusivities may be predicted quite accurately[17, 18]. Typical values are given in Table 3-1 for low temperatures. Extrapolation of these gas diffusivities to higher temperatures and pressures can be accomplished by using

---

* Pore size/mean free path of diffusing species > 10[4]

TABLE 3-1

GAS PHASE MOLECULAR DIFFUSION COEFFICIENTS

	1 Atmosphere	
Gas Pair	Temperature [K]	Diffusivity [cm^2/s]
$CO-CO_2$	315	0.18
	473	0.38
H_2-CH_4	316	0.81
H_2O-H_2	273	0.75
H_2O-CO_2	273	0.138
O_2-CO_2	273	0.139

any of a number of empirical correlations based on reduced temperatures and pressures (e.g. Slattery-Bird Equation, Chapman–Enskog Equation). D_{12} varies with T^n where n lies between 1.5 and 2 depending upon the temperature level. At low to moderate pressures, the diffusion coefficient of gases is inversely proportional to pressure or density[18]

If the gas density is low or if the pores are quite small or both** the molecules collide with the pore wall much more frequently than with each other. This is known as the Knudsen diffusion regime. In coals over 90% of the internal surface area is contained within a micropore ($\delta < 20 A^{\circ}$ or 200 nm) system that represents 50 to 80 percent of the total void space[16]. Knudsen diffusion is distinctly possible in this microporous network. A simplified approach to defining the Knudsen diffusivity $D_{k,eff}$ is given below[13]:

$$D_{k,eff} = \frac{4}{3} \left\{ \frac{8 R T}{\pi M_A} \right\}^{\frac{1}{2}} K_o \qquad \text{Equation 3-3}$$

where the term in the parenthesis can be interpreted as the root mean square of the velocity of the gas molecules of A; K_o is a parameter characteristic of the solid with the dimensions of length. Methods are available for estimating K_o for idealized geometries and can be found in Reference 13. Little information is available however on experimentally

---

** Pore size/mean free path of diffusion species < 0.1[4]

measured tortuosities and Knudsen diffusion coefficients for noncatalytic gas-solid reaction systems. The combined effects of both Knudsen diffusion and molecular diffusion in the transition region (for equimolar counterdiffusion) can be modelled to a good approximation by using the overall pore diffusion coefficient:

$$D_{eff} = \left[\frac{1}{D_{k,eff}} + \frac{1}{D_{12,eff}} \right]^{-1} \qquad \text{Equation 3-4}$$

Walker et. al[8] have found that D_{eff} is directly proportional to the square of the porosity for $\varepsilon_s < 0.40$ with the proportionality factor equal to 0.095 cm^2/s at NTP (20^oC, 1 atm) for spectroscopic carbon rods. Unfortunately the temperature and pressure dependence of D_{eff} were not studied. Recently, Desai and Yang[113] showed that the relation

$$D_{eff} = \varepsilon_s^2 D_{12}$$

for the effective diffusivity of carbon was limited to temperatures below 700^oC. In their modeling studies they found that at temperatures above 1300^oC the above relation predicts diffusivities that are too high by a factor of 74 to 80 as shown in Table 3-2. Because of the scarcity of the experimental data on effective diffusivities of char, a constant value is nearly always assumed in char gasification studies.

Temperature gradients inside a single porous particle may also exist whenever the thermal conductivity of the solid is

TABLE 3-2

EFFECTIVE DIFFUSIVITY OF CARBON AT HIGH TEMPERATURES

T (C)	D_{eff} * $[cm^2/s]$	τ	$\tau^2 D_{12}$ $[cm^2/s]$
1300	1.35×10^{-3}	64	0.1
1400	1.39×10^{-3}	65	0.11
1500	1.56×10^{-3}	61	0.12
1600	1.63×10^{-3}	60	0.13

* Obtained from modeling studies by Desai & Yang[113]

sufficiently low to hinder the transport of energy (by conduction within the solid). The usual approach taken for the representation of porous solids is to consider them homogeneous on a macroscopic scale and then to relate the heat flux to the temperature gradient by means of an effective thermal conductivity:

$$q_y = -\lambda_{eff} \frac{dT}{dy} \qquad \text{Equation 3-5}$$

If one assumes, in estimating the effective thermal conductivity of real porous solids, that the material consists of a continuous solid phase containing many closed and isolated pores filled with a gas that has a thermal conductivity much lower than that of the solid phase, then the thermal conductivity can be estimated by the following expression

$$\lambda_{eff} \doteq \lambda_s (1 - \varepsilon_s) \qquad \text{Equation 3-6}$$

where λ_s is the thermal conductivity of the solid at zero porosity. If on the other hand one assumes that the material consists of a gaseous continuous phase (of relatively low thermal conductivity) containing individual solid particles that are in point contact only, then the effective thermal conductivity of the porous solid depends on the thermal conductivity of the gas but is independent of the solid conductivity. Clearly these are two limiting cases. An actual porous solid will have an intermediate thermal conductivity.

It has been shown that the high porosity of coal makes its thermal conductivity very much dependent on the nature of the gas that suffuses its internal free space as demonstrated in the experimental work by Schumann and Voss[114] presented in Table 3-3. Other investigators have also found that heat conductivities are similarly affected by moisture content. Since chars have somewhat higher porosities, marginally lower effective thermal conductivities are expected. The effective thermal conductivities of chars are in the range $3\text{-}9 cals^{-1}cm^{-1}C^{-1}$ (4). It should be noted however that porosity and pore structure change with reaction so that strictly speaking both effective thermal conductivity (λ_{eff}) and effective diffusivity (Deff) are a function of the extent of reaction.

Reaction rates are significantly altered by the intrusion of these intraparticle temperature and concentration gradients. The classical approach adopted in studying gas-solid reactions has been to define the effectiveness factor η as the ratio of the actual reaction rate ($r_{v,obs}$) to that which would occur if all of the surface throughout the inside of the solid particle were exposed to reactant and product of the same concentration and temperature as that existing at the solid-gas interface.

$$\eta = \frac{r_{v,obs}}{r_v (C_s^s, T_s^s)}$$ Equation 3-7

TABLE 3-3

EFFECTIVE THERMAL CONDUCTIVITY OF COAL

Dry Coal

Sized - 10 + 12 m

$\varepsilon_s = 44\%$

	AIR	H_2
Effective Thermal Conductivity [cal s^{-1} cm^{-1} K^{-1}]	3.27×10^{-4}	7.03×10^{-4}
Gas Thermal Conductivity [cal s^{-1} cm^{-1} K^{-1}]	0.63×10^{-4}	4.6×10^{-4}

For the case where there is no pore diffusion limitation η approaches unity. Under isothermal conditions (i.e. no temperature gradients) η decreases in value as diffusion limitations become significant, but with a highly exothermic reaction (significant temperature gradient) η may exceed unity[19]. The effectiveness factor η is a function of the Thiele modulus, ϕ, as shown below.

$$\eta = \frac{\tanh \phi}{\phi} \text{ , where } \phi \propto L \lambda_{eff}^{\frac{1}{2}} D_{eff}^{-\frac{1}{2}} \quad \text{Equation 3-8}$$

It can be shown that for large particles (L large), small diffusivities or very rapid reaction rates, appreciable diffusion resistance can occur and must be considered.

Turkdogan et. al[62, 63] have conducted very extensive studies on the carbon-dioxide reaction with charcoal and coke using an electrobalance. The extent of pore diffusion in solid spherical carbon specimens was shown to depend on the size of the carbon sample, the concentration of the reactant gas and on the temperature. Pore diffusion offered less resistance with decreasing particle size, decreasing partial pressure of CO_2 and decreasing temperature. For a carbon dioxide partial pressure of 0.24 atm and a total pressure of 1 atm, the maximum critical sphere diameter for negligible pore diffusion resistance is about 2 cm at 900 - 950°C. At much lower pressures (0.025 atm) for 1 cm diameter cylinders negligible pore diffusion resistance extends to 1300°C.

3.1.2 Interphase Gradients

Steps 1 and 5 in the generalized mechanism of gas-solid reactions relate to the external mass transfer of reactant/product to/from the bulk fluid to/from the gas-solid interface. This mass transfer step has been extensively studied since the rates at which these species are transferred to and from the solid surface may play an important role in determining the overall rate of reaction. Mass transfer rates can be described by the usual mass transfer coefficient, k_g, in terms of an appropriate driving force as follows[15]:

$$N_A = k_g (C_{AB} - C_{AS}) \qquad \text{Equation 3-9}$$

where C_{AB} concentration of reactant/product A in bulk stream

C_{AS} concentration of reactant/product A at fluid/solid interface

N_A molar flux with respect to the fixed solid surface

Mass transfer coefficients for a particular reactor system can in general be obtained from numerous experimentally determined correlations[14, 15]. Frequently the mass transfer coefficient is expressed as a Chilton–Colburn j_D factor which is defined in terms of dimensionless groups as:

$$j_D = \frac{N_{Sh}}{N_{Re}\ N_{Sc}^{1/3}} \qquad \text{Equation 3-10}$$

The Sherwood, Schmidt and Reynolds numbers are defined as:

$$N_{Sh} = \frac{k_g L}{D_{12}} \qquad N_{Sc} = \frac{\mu}{\rho D_{12}} \qquad N_{Re} = \frac{U L \rho}{\mu}$$

where

μ	fluid viscosity
ρ	fluid density
U	superficial velocity of fluid
D_{12}	molecular diffusion coefficient
L	characteristic dimension of particle
k_g	mass transfer coefficient from bulk fluid to solid

In laboratory work, the Reynolds number (N_{Re}) will typically range from about 20 to as low as 0.1 or less. The following empirical correlation is recommended for packed beds in which the N_{Re} is between 3 and 2000 and the particle diameters are between 1.8 and 9.4 mm[19]:

$$\varepsilon j_D = \frac{0.357}{N_{Re}^{0.359}} \qquad \text{Equation 3-11}$$

For lower flow rates and smaller particle sizes, mass-transfer coefficients may be very low and a rough estimate may be obtained from the following ($0.0016 < N_{Re} < 55$)[112]

$$\varepsilon j_D = 1.09 \, (N_{Re})^{-2/3}$$

It must be stated however that at low flowrates, these average mass transfer coefficients may not be representative of the entire bed when there is a large degree of particle size distribution and hence distribution of voidage[19].

The rate of reaction at the solid surface for a first order reaction based on the interfacial surface area (r_A) can be expressed simply as the product of the reaction rate constant and the concentration of reactant at the interface.

$$-r_A = k_r C_{AS} \qquad \text{Equation 3-12}$$

At steady-state there is no accummulation of reactant at the interface and the rates expressed by Equation 3-9 and by Equation 3-12 must be equal. Combining these to eliminate the unknown surface concentration yields:

$$-r_{A,obs} = k_o C_{AB} = \left\{\frac{1}{k_g} + \frac{1}{k_r}\right\}^{-1} C_{AB} \qquad \text{Equation 3-13}$$

The meaning of external mass transfer resistance is clearly illustrated by Equation 3-13. When the mass transfer step is much more rapid than the surface reaction step (i.e. $k_g >> k_r$) then the observed reaction rate approximates the surface reaction rate because $k_o \rightarrow k_r$ and $C_{AB} \rightarrow C_{AS}$. However, the other limit is that of almost instantaneous reaction, (i.e. $k_r >> k_g$), the observed rate then corresponds to the fluid phase mass transfer step and is termed 'diffusion

controlling'. Appropriately Smith[14] points out that significant external mass transfer resistance leads to false activation energies and orders of reaction.

Fluid to particle heat transfer resistances must also be considered in gasification reactions. The heat transfer coefficient is defined in terms of the temperature difference between the bulk fluid T_b and surface T_s^s as

$$Q = h_f \, a_m \, (T_s^s - T_b) \qquad \text{Equation 3-14}$$

where Q = heat transfer rate from solid to fluid per unit mass

a_m = external surface/unit mass

h_f = film heat transfer coefficient

As in the case of the mass transfer coefficients, one has to rely for the most part on empirical correlation for obtaining the heat transfer coefficient. These empirical correlations also make use of a j-factor expression:

$$j_H = \frac{h_f}{c_p G} \, N_{Pr}^{2/3} \qquad \text{Equation 3-15}$$

where the dimensionless Prandtl number is defined as $c_p \mu / k_f$.

h_f = heat transfer coefficient

c_p = fluid heat capacity

G = superficial mass velocity

k_f = thermal conductivity of fluid

Satterfield[19] suggests the following correlation as a rough guide for estimating heat transfer coefficients at low flow rates ($0.1 \leq N_{Re} < 10$) in packed beds:

$$N_{Nu} = 0.07\ N_{Re}\ , \text{ where } N_{Nu} = \frac{h_f\ d_p}{\lambda_f}$$

It must be noted however that heat transfer coefficients evaluated from the j-factor expression do not include a radiation contribution. Smith[14] points out that in general, radiation effects are negligible below 400°C for fixed beds of pellets not greater than 6mm in diameter. Since gasification reactions occur at higher temperatures, the radiative heat transfer should be considered. A simple expression holds for describing the radiant flux received by a small pellet, located in a large cavity (e.g. thermogravimetric balance) the surface of which is isothermal, in the presence of a nonabsorbing gas[13]:

$$Q_R = \tilde{\varepsilon}\ \sigma\ (T_w^4 - T_s^4) \qquad \text{Equation 3-16}$$

where
- σ = Boltzmann's const $\doteq 1.37 \times 10^{-12}$ cal $cm^{-2}s^{-1}K^{-4}$
- Q_R = net radiative flux at the solid surface
- $\tilde{\varepsilon}$ = emissivity of the surface
- T_w = temperature of the walls of the cavity
- T_s = temperature of the solid surface

This is often a good approximation for radiative heat transfer to single pellets held in a tubular furnace (e.g. the thermogravimetric balance). A radiative heat transfer coefficient may be defined in the following manner

$$h_r = \tilde{\varepsilon}\, \sigma\, (T_w^2 + T_s^2)\, (T_w + T_s) \qquad \text{Equation 3-17}$$

for purposes of comparison with convective heat transfer coefficients.

The reactant gas and the solid surface may differ in concentration and temperature substantially[20]. Froment and Bischoff[15] point out that it is especially likely to find large temperature and concentration differences in laboratory reactors which have rather low flow rates through the reactor. When this is the case, heat and mass transfer processes must be considered simultaneously. For large interphase temperature gradients care has to be taken in selecting the mean or film temperatures at which property values such as diffusivity and gas density are evaluated. Thermal convection may also play a strong role in defining the flow conditions around the particle and should be taken into account in calculating both the heat- and mass-transfer coefficients[13]. External heat and mass transfer rates should therefore always be estimated in order to ascertain what role they play in the observed or measured rates.

3.1.3 Interparticle Gradients

In fixed beds, as in most bench scale reactors, the interaction of the solid particles and the nature of the gas flow through the reactor may lead to interparticle temperature and concentration gradients. These gradients occurring both radially and axially within the reactor as a whole are particularly difficult to evaluate and control. Heat conduction problems due to a low effective thermal conductivity of the entire bed can lead to severe radial gradients in cases where the reaction rate and heat release (or intake) are large and heating is being provided at the reactor wall. Since reaction rates for the most part vary exponentially with temperature, it is critical that the temperature profile inside the reactor be known explicitly. Models to predict the detailed temperature and conversion pattern in a reactor make use of the effective transport concept[14, 15]. A radial effective conductivity parameter λ_{er} and an axial effective conductivity parameter λ_{ea} have been defined by analogy to the mass transfer case:

$$q_r = -\lambda_{er} \frac{\partial T}{\partial r} \; , \; q_z = -\lambda_{ea} \frac{\partial T}{\partial z} \qquad \text{Equation 3-18}$$

Owing to the complex heterogeneous system, λ_{ea} and λ_{er}, the effective thermal conductivities, are properties of the bed that depend on a large number of variables such as gas flow rate, particle diameter, porosity, true thermal conductivity of

the gas and of the solid phases and the temperature level. Smith[14] points out that the axial effective thermal conductivity λ_{ea} is negligible in most cases except for very shallow beds and low gas velocities. Smith[14] discusses the use of an expression for estimating λ_{er} in packed beds based on a series mechanism of conduction, convection and radiation for various conditions of pressure, temperature and particle size. However, the correlation suggested has been tested only up to 400°C. In packed beds at moderate temperatures, convection is the predominant mode of heat transfer, however, thermal radiation may become significant at elevated temperatures and low gas flows. For example, radiation becomes important for 1mm particles at temperatures above 400°C and for 0.1mm particles above 1500°C[115]. Below 400°C radiation contributes between 10 and 15 percent of the bed conductivity[14]. Downing[13] has proposed the following expression for the effective thermal conductivity of a packed bed at high temperatures in the absence of fluid motion (T<700°C).

$$\lambda_e = \frac{(1-\varepsilon)\ \lambda_s\ k^*T^3}{\lambda_s + k^*T} + k^*T^3 \qquad \text{Equation 3-19}$$

where $k^* = .69\ \tilde{\varepsilon}\ d_p/10^8$

λ_s = thermal conductivity of solid

$\tilde{\varepsilon}$ = emissivity

λ_e = effective thermal diffusitivity of entire bed

ε = bed void fraction

Reaction conditions in gasification will usually be at atmospheric pressure or higher and at higher temperatures than those for which the above correlations apply. At temperatures above 700°C the radiation contribution accounts for about 80% of the total thermal conductivity of the bed[115]. The flow of gas in a reactor increases the effective bed conductivity[19]. The radial thermal conductivity is generally correlated by an empirical equation of the form

$$\lambda_{er} = A + B\, N_{Re} \qquad \text{Equation 3-20}$$

where A is the bed conductivity under stagnant conditions.

According to Satterfield[19], Reynolds numbers in the order of 200 would be required to double the bed conductivity over the value in the absence of fluid motion. Froment and Bischoff[15] have further distinguished between the effective thermal conductivity for the fluid phase λ_{er}^{f} and that for the solid phase λ_{er}^{s} in their approach. Although attempts are made to minimize radial temperature gradients, in order to approach isothermal operation, their occurence is usually inevitable when the heat of reaction is high. Isothermal operation (i.e. the implicit assumption that temperature gradients are minimal) of a bench scale reactor is highly desirable because of the greatly simplified governing mathematical model (no energy balances required for the gas and solid phase).

Concentration gradients in a reactor may be due to flow maldistributions, by-passing, axial dispersion and radial velocity gradients. Concentration differences greatly influence reaction rates and are difficult to predict. The effective transport concept has also been used to describe the nonisotropic effective diffusivity in packed beds. A radial effective diffusion parameter D_{er} and an axial effective diffusion parameter D_{ea} have been defined based on the void volume in the bed and are readily calculated from available correlations[13]. Experimental research has shown that when $L >> d_p$ and $P_e > 1$ for reasonable fluid velocities ($N_{Re} \simeq 10$), axial dispersion is unlikely to be significant[13, 14]. However, axial dispersion may be important where the bed is only a few particle diameters deep or when the linear gas velocity is small. Experimental results on radial dispersion are less extensive. Nevertheless for Reynolds numbers above 40, the radial Peclet number is independent of flow rates and approaches 10. The terms in the continuity equation that involve radial gradients are generally small for isothermal operation since the only way that concentration gradients can develop is through variation of the velocity with radial position[14]. Unfortunately, if radial temperature gradients exist then the reaction rate can vary signficantly with radial position and large concentration gradients develop. It is in the control of these interparticle gradients that reactor design plays a key role.

An understanding of the relative importance of intraparticle, interphase and interparticle gradients is fundamental to a complete description of data obtained from measurements of the overall rates of reaction in chemical reactors and to the validity of the mathematical models used to describe the reacting system. Failure to account for these gradients when they are significant leads to erroneous and meaningless rate expressions for scale-up or optimization.

3.1.4 Residence Time Distribution

Most of the bench scale reactors used to study chemical kinetics in char gasification are continuous flow reactors through which a fluid stream or solid stream or both are steadily being passed. If the volumetric flow rate of the stream is q and volume of the reactor is V, then the average or nominal holding time of the material ($\bar{t}_R$) in the vessel is given by V/q. However, it is not true that all the elements of matter passing through the system stay in the system for the same length of time; i.e. some elements of the stream may spend a longer period of time than $\bar{t}_R$ in the system (such as stagnant zones) whereas other elements are retained for a shorter time period (as in the case of bypassing). This distribution or spread of residence times is an important characteristic of the system and may have a profound effect on its performance as a reactor since, when chemical reaction takes place inside a flow reactor, the length of time each

element of reactants spends within the reactor affects the overall conversion[14]. An understanding of the mixing processes and the resulting residence-time distribution (RTD) can thus be classified as another essential feature of system design.

Two simple limiting cases, so-called ideal flow patterns are worth mentioning. At one extreme, the flow pattern in the reactor may be regarded as plug flow with no longitudinal mixing but with complete radial mixing. This flow pattern is characterized by an identical velocity and residence time of all the elements of the fluid stream within the reactor. Under these conditions there is no spread of the residence times and the residence time of the stream is a uniquely defined quantity. The other extreme is a completely mixed flow characterized by a well-defined residence time distribution of exponential form and the identical composition of the exit stream and the fluid within the reactor. It follows therefore that for completely mixed systems there is a large spread in the residence time distribution; some elements of the stream spend very little time in the reactor while other elements may be retained for much longer time periods than $\bar{t}_R$. The maximum effect of the residence time distribution (RTD) on conversion is evident from a comparison of plug flow and completely mixed flow in a reactor as shown in Figure 3-1 for first order kinetics ($r=kC$). As an example, when $k\bar{t}_R = 4$, the conversion for the case of complete mixing is 80% while for

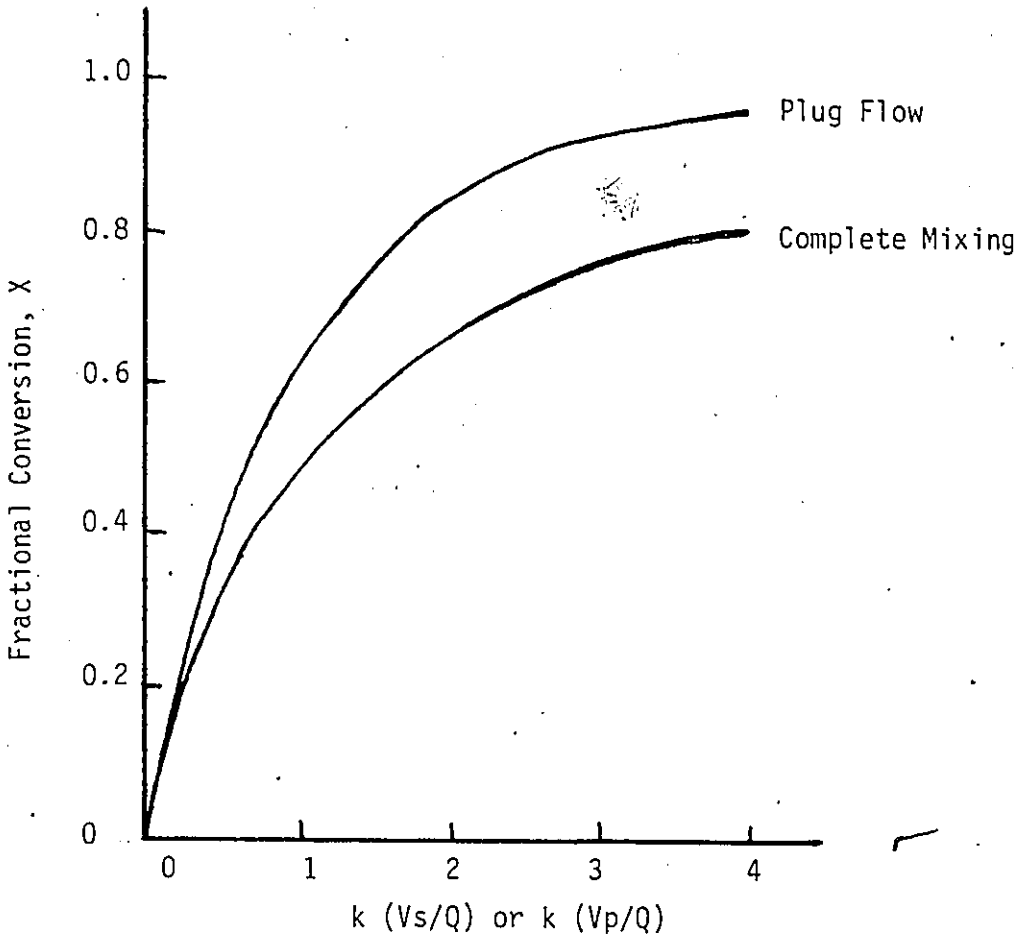

Figure 3-1 Effect of mixing (RTD) on conversion for 1st order kinetics
Reference 14, Figure 4-14, p. 178.

the plug flow case it is 98%. The differences would be larger for second order kinetics and smaller for half-order kinetics. For a reactor which followed neither ideal flow, but showed an intermediate RTD, the conversion would be between the two extremes.

While plug flow and completely mixed flow are idealizations, the design of reactors so that the flow pattern approaches either extreme is desirable because of the simplified governing mathematical equations. In general, however, a reactor will not have the characteristics of either of these two limiting case, i.e. nonidealities or deviations from the ideal flows will exist. These nonidealities can be on two levels: macromixing and micromixing. Residence time distribution is affected by both types of deviations. This implies that measurements of residence time alone cannot determine if the mixing process is on the microscopic or macroscopic scale. RTD concerns only the total period of time the elements have spent in the system rather than with the way the elements distributed their time in the various parts of the reactor. Since systems with differing flow pattern give rise to the same RTD, the RTD analysis should be looked upon only as supporting evidence on the validity of a reactor flow model.

3.1.5 Additional Features

In the previous two sections, the essential features of reactor design were discussed. In addition to these, practical

requirements dictate several desirable characteristics for bench-scale reactors. In any study of gas-solids reaction kinetics it is desirable to have a reactor system for which product sampling and analysis is simple and quick. Where small changes in gas composition must be observed (as for differential conversions) accurate analytical techniques are a necessity. A wide range of reactor operating conditions (e.g. gas flow rates, reactant composition, amount of solids, temperature, pressure) should be possible since the rate-determining step must be determined from the effects of changes in these conditions. Gas-solid reactors should also be designed with the object of facilitating the data analysis (i.e., by reviewing the design equations for the system). Finally, it is also preferable to keep the cost and difficulty of construction of these laboratory reactors low. These additional desirable features can greatly facilitate the investigator's work.

3.1.6 Summary

The desirable and essential features of reaction system design are summarized in Table 3-4. Although these features are generally common to any system for determining chemical reaction kinetics the inherent characteristics of char gasification reactions (i.e. high heats of reaction 50kcal/mol, severe operating temperatures ~ 1000^{o}C, unsteady state nature of system) makes the realization of these features

TABLE 3-4

ESSENTIAL AND DESIRABLE FEATURES OF SYSTEM DESIGN

ESSENTIAL FEATURES

- Controlled intraparticle, interphase, interparticle temperature and concentration gradients
- Well defined reaction temperature
- Well defined residence time distribution

DESIRABLE FEATURES

- Easy and quick product sampling and analysis
- Flexible operation
- Simple data analysis
- Low cost and simple construction and operation

particularly challenging. In the next three sections of this chapter analytical and experimental tests which can be applied to examine whether the essential design features have been achieved will be reviewed.

3.2 Analytical Criteria for System Design

Chemical reactor design must be based on four processes: chemical reaction kinetics and the transfer of mass, heat and momentum. These effects however should be studied independently in order to minimize the dependence of the data on the type and size of bench or pilot scale equipment. Physical effects in chemical reactors whether laboratory or pilot scale are often difficult to separate from the chemical rate processes. Therefore, prior to or in the early phases of a detailed kinetic study of a gas-solid reaction, certain preliminary tests should be carried out to establish whether the transfer processes are affecting the reaction to an appreciable extent. There are two ways of determining whether intraparticle, interphase or interparticle gradients are causing significant effects, first by experimentation and second by calculation. In this section, analytical criteria (developed mostly in the study of catalytic gas-solid reactions) to estimate the magnitude of these effects will be discussed. These criteria have been well reviewed by others[21, 22, 19] and so only a few of the most common and useful tests will be described herein. It should be stressed

that care should be exercised in using the criteria in gasification since many of the physical properties of the char undergoing reaction are changing with time (extent of reaction) and the criteria were developed for the steady state case (unchanging catalyst surface and properties).

3.2.1 Testing for Intraparticle Gradients

The classical test for determining whether concentration gradients exist within an isothermal solid particle consists in evaluating the ratio of the observed reaction rate to the rate if pore resistance controls.

$$\zeta = \frac{(r_{v,obs})\, L^2}{D_{eff}\, C_s^s} \qquad \text{Equation 3-21}$$

where $r_{v,obs}$ = observed reaction rate per unit particle volume

C_s^s = concentration of reactant at outer surface of solid particle

D_{eff} = effective diffusivity in a porous particle

L = ratio of particle volume to external particle surface area

The smaller the value of ζ, the smaller the concentration gradient throughout the solid particle. For an irreversible reaction of a single reactant whose kinetics can be represented by a power-law relationship $-r_{v,obs} = k\,(C_s^s)^n$, the effectiveness factor approaches unity ($\eta = 1 \pm .05$) if

$\zeta < 6 \quad n=0$
$\zeta < 1 \quad n=1$
$\zeta < 0.3, n=2$
$\zeta < 1/n$

and n is the reaction order. If the inequalities are satisfied then there are no pore diffusion limitations.

A diagnostic test for determining whether thermal gradients exist inside a solid particle has been derived by Mears[21] based on heat transfer by conduction inside the solid particle. This test is presented below:

$$\frac{|\Delta H_r|\ (r_{v,obs})\ L^2}{\lambda_{eff}\ T_s^s} < \left(\frac{T_s^s\ R}{E_a}\right) = \frac{1}{\gamma} \qquad \text{Equation 3-22}$$

where ΔH_r = heat of chemical reaction

λ_{eff} = effective thermal conductivity of porous particle

T_s^s = absolute temperature at surface of particle

E_a = intrinsic activation energy for chemical reaction

R = universal gas constant

When the inequality is satisfied the observed reaction rate does not differ by more than 5% of the isothermal reaction rate (reaction rate that would be observed if the particle had a uniform temperature profile) regardless of possible diffusion limitations.

The magnitude of the temperature difference inside a particle (without further complications of external mass and heat transfer resistances) was originally derived by Damkoëhler. The derivation based on simultaneous solution of heat and mass balances for a particle of any geometry can be found in References 14 and 15. The temperature difference is given by:

$$T_s - T_s^s = \frac{D_{eff}\,(C_s^s - C_s)(\Delta H_r)}{\lambda_{eff}} \qquad \text{Equation 3-23}$$

where T_s = absolute temperature at centre of porous particle

C_s = concentration of reactant at centre of porous particle

It can be seen that the maximum gradient, ΔT_{MAX} occurs for complete reaction, $C_s=0$, so that

$$\frac{T_s^s - T_s}{T_s^s} = \frac{(-\Delta H_r) D_{eff}\, C_s^s}{\lambda_{eff}\, T_s^s} = \beta \qquad \text{Equation 3-24}$$

This result holds for a particle of any geometry under steady-state conditions. The temperature gradient is therefore dependent on the heat of reaction, the transport properties of the particle, and the surface concentration of reactant. The so-called heat of reaction parameter β gives a simple method for estimating whether intrapellet temperature differences are significant.

For the absence of the combined effect of temperature and concentration gradients within the particle (i.e. $\eta \doteq 1 \pm .05$) and power law kinetics, Mears has proposed the following criteria which applies for both endothermic and exothermic reactions:

$$\zeta < \frac{1}{|n-\gamma\beta|} \quad (n \neq 0) \qquad \text{Equation 3-25}$$

In this criteria, the range of the Arrhenius number γ is from 10 to 40 while the range of the heat of reaction parameter β is -0.1 to 0.1 [for catalysts].

The intraparticle effects are not influenced by reactor type but rather by the kinetics and the physical structure of the solid. Hence, this check should be carried out regardless of the experimental set-up.

3.2.2 Testing for Interphase Gradients

Since the external surface gas concentration is not necessarily equal to the bulk fluid phase concentration surrounding the solid particle, the effects of a concentration gradient in the film must also be assessed. To determine whether interphase concentration gradients are significant under isothermal conditions, Levenspiel[23] has suggested looking at the ratio of the observed reaction rate (for reactions other than first order) to the rate if film resistance were controlling:

$$\omega = \frac{(r_{v,obs})\ L}{k_g\ C_b} < \frac{0.05}{n} \qquad \text{Equation 3-26}$$

where k_g = mass transfer coefficient between fluid and particle

C_b = concentration of reactant in bulk fluid

When the inequality is satisfied there are no film resistance limitations.

A criterion for detecting the onset of interphase temperature gradients has been proposed by Mears. If the observed rate is to deviate less than five percent from the true chemical rate (negligible diffusion resistance) the criterion requires that:

$$\chi = \frac{(r_{v,obs})\ |\Delta H_r|\ L}{h\ T_b} < \frac{0.05\ R\ T_b}{E_a} \qquad \text{Equation 3-27}$$

where h = heat transfer coefficient between fluid and particle

T_b = bulk fluid absolute temperature

The inequality shows that interphase heat transport limitations can be expected when reaction heats and rates are high and flow rates low (corresponding to low convective heat transfer coefficients).

A simple estimate of the magnitude of the temperature difference in terms of the concentration gradient has been derived by Smith[14] by performing an energy balance on the solid particle at steady state:

$$T_s^s - T_s = \frac{k_g |\Delta H_r| (C_s - C_s^s)}{h} \qquad \text{Equation 3-28}$$

It must be mentioned that the heat transfer coefficient, h, must include a convective term as well as a radiative term (radiation from the reactor wall, from other particles, between neighboring voids, etc.) when operating at temperatures above say 400°C. Mears[21] points out that temperature gradients become the source of deviation from ideality ($\eta \rightarrow 1$) long before concentration gradients do so. Also, when the Biot number (defined as $h\, d_p/\lambda_{eff}$), which expresses the ratio of thermal resistance of the particle to that of the film, is less than 10 (a condition usually met in bench scale reactors because of low flow rates) interphase resistance becomes limiting before intraparticle resistance.

Mears[21] has also derived a criterion using the perturbation approach for determining whether the combined intraparticle-interphase effects significantly affect the chemical rate. The criterion makes use of the Arrhenius number γ , the heat of reaction parameter β, the ratios χ , ω and the reaction order in power law kinetics:

$$\frac{(r_{v,obs})\, L^2}{D_{eff}\, C_b} < \frac{1 + 0.33\ \gamma\, \chi}{|1 - \gamma_b \beta_b|(1 + 0.33\ n\omega)} \qquad \text{Equation 3-29}$$

where γ_b and β_b are both evaluated at bulk fluid rather than at the surface conditions. Satterfield[19] has however indicated that criteria which treat two or more gradients simultaneously usually require that the values of several parameters be known with a degree of precision that is seldom available thereby limiting their scope. A prior calculation of the possible effects of both interphase temperature and concentration gradients should be carried out whenever possible.

3.2.3 Testing for Interparticle Gradients

Interparticle heat and mass transfer effects are manifest by radial and axial temperature and concentration gradients in the reactor as a whole. Heat conduction problems due to low effective thermal conductivity of the solid bed can lead to severe radial temperature gradients expecially where the reaction rate and heat of reaction are large. Other factors such as bypassing, axial dispersion and heat transfer resistance at the reactor wall also complicate the problem. It is in this domain more so than in the previous ones that reactor design is critical. Extensive studies have been conducted to determine diffusional and thermal effects in the tubular fixed bed reactor. For this reason, much of the discussion and tests which follow are based on the findings on integral packed bed reactors.

Analysis of integral tubular reactors is usually based on plug flow of the fluid through the reactor. Deviations from plug flow may be caused by several effects. The void fraction of a packed bed next to the wall is higher than at the centre[24]. Because of the lower resistance at the wall, the linear velocity next to the wall is greater. This contribution of wall flow to the total flow may be significant for low radial aspect ratios (R_o/R_p, reactor radius/particle radius) for example, 10 or less. At low Reynolds numbers molecular diffusion may cause significant axial dispersion. In general, it has been assumed that axial dispersion and axial heat conduction are negligible (ensuring plug flow) whenever the axial aspect ratio (L'/d_p, reactor length / particle diameter) is large, say above 30. Comparison of the actual and plug flow conversions for a first order reaction in a steady state flow reactor yields[15]:

$$\frac{k\bar{t}_R}{(k\bar{t}_R)_{PF}} \simeq 1 + \frac{k\,\bar{t}_R}{Pe_a} \simeq 1 + \frac{D_a}{\bar{v}L'} \ln (C_{AO}/C_A) \qquad \text{Equation 3-30}$$

This result shows that for a given plug flow conversion level, the reactor with axial dispersion will produce essentially the same results for large Pe_a ($Pe_a \to \infty$). For a given type of reactor, the axial dispersion coefficient is usually correlated using a characteristic local length, ℓ, (tube diameter, packing size, etc.) then

$$Pe_a = \frac{\bar{v}\, L'}{D_a} = \frac{\bar{v}\, \ell}{D_a}\,\frac{L'}{\ell} = Pe_{\ell,a}\ (L'/\ell) \qquad \text{Equation 3-31}$$

where $Pe_{\ell,a}$ is the local Peclet number for mass dispersion. Mears[21] has combined these findings to provide a formal criterion to determine whether the reactor length is sufficient to minimize axial dispersion effects for n^{th} order power law kinetics:

$$\frac{L'}{\ell} > \frac{1}{e}\,\frac{n}{Pe_{\ell,a}}\ \ln\frac{C_o}{C_f} = \frac{1}{e}\,\frac{k_b\,\bar{t}_R}{Pe_{\ell,a}} \qquad \text{Equation 3-32}$$

where L' = reactor bed length

k_b = apparent rate constant per unit bulk particle volume ($k_b = k\,(1-\varepsilon)\eta$)

$\bar{t}_R$ = space time

C_o, C_f = initial and effluent concentration of reactant

$\bar{v}$ = superficial linear velocity

n = integer exponent in power law expression

D_a = axial eddy diffusivity

e = allowable error

An allowable error of say five percent is usually the case for industrial reactors of the simple empty tube or packed bed types. This expression may not be true for laboratory studies especially in differential reactors or for reactors with more complicated flows leading to large characteristic dispersion lengths[15].

Radial heat transfer effects and to a lesser degree radial mass transfer effects are usually more serious than the axial conduction problem. In order to spread the heat release (in the case of an exothermic reaction) more uniformly and avoid 'hot spots', a technique by which the solid is diluted with inert material with dilution ratios decreasing with bed length has often been applied. Since dilution in large quantities introduces the hazard of bypassing, a check provided below should be performed to ascertain that this problem has been avoided[21]:

$$\frac{L'}{d_p} > 250 \frac{b}{\Delta} \qquad \text{Equation 3-35}$$

where b = dilution ratio

Δ = relative experimental error in conversion

Another technique which has been used to reduce radial temperature gradients is to decrease the reactor diameter and thus the radial aspect ratio. However, as this ratio is decreased, the contribution of heat transfer at the inside reactor wall becomes increasingly more serious. Mears has developed the following criterion for the observed reaction rate not to deviate more than 5% from the isothermal case, assuming plug flow and assuming that there are no concentration or temperature gradients inside particles or between particles and bulk fluid, and based on a lumped parameter model for the effective thermal conductivity of the entire bed.

$$\frac{|\Delta H_r|\ r_b\ R_o^2}{\lambda_e\ T_w} < \frac{0.4\ RT_w}{\Lambda\ E_a} \qquad \text{Equation 3-34}$$

where $\Lambda = 1$ for $R_o/R_p > 100$

$\Lambda = 1 + 16\ \frac{R_p\ Bi_h}{R_o}$ for $R_o/R_p < 100$

$$Bi_h = \frac{h_w\ R_p}{\lambda_e}$$

ε = bed void fraction

λ_e = effective thermal conductivity of entire solid bed

T_w = absolute temperature of reactor wall

R_o = reactor radius

R_p = solid particle radius

r_b = average reaction rate per unit bed volume

$$r_b = \frac{(1 - \varepsilon)}{(1 + b)}\ r_{v,obs}$$

The lower limit in the radial aspect ratio appears to be about 4 with a further reduction in reactor diameter leading to channelling near the reactor wall.

These interparticle gradients present severe problems. When varying the operating conditions does not succeed in minimizing the concentration and temperature gradients, the use of a distinct reactor type known to alleviate certain problems is advisable.

3.2.4 Summary

The analytical criteria presented are based on estimated values of pore diffusivity, thermal conductivity, axial dispersion, heat- and mass-transfer coefficients, nature of the kinetics and other coefficients. The accuracy with which such criteria can be applied varies widely and is limited by the certainty with which the properties can be obtained. The simple calculation procedures presented provide a method of reaching conclusions when experimentation is impractical. However, because of the possible inaccuracies it is often desirable to evaluate intraparticle, intraphase and interparticle effects experimentally whenever possible for the system under study.

3.3 Experimental Transport Checks

Although the analytical criteria presented in the previous section should be applied whenever possible, proper correlations for heat and mass transfer coefficients, thermal diffusivities and conductivities may not be readily available and the investigator must then resort to experimentation. Key experimental tests will be described in this section to determine whether the temperature and concentration gradients within the particle, in the film surrounding the particle and in the reactor as a whole are significant.

3.3.1 Intraparticle Transport

The classic experimental test for detection of intraparticle effects is to run the reaction using progressively smaller diameter particles. The lack of any dependence of rate of reaction per unit particle volume over an appreciable size range would indicate that intraparticle effects are minimal. However, by varying the particle size over too great a range, distortions in the flow field may be introduced thereby clouding the experimental results. Koros and Novak[25] have devised an alternate test which avoids complications due to distortions in the flow pattern. Their test is valid for first order reactions and is based on the fact that while in the kinetic regime (chemical reaction controlling) the rate of reaction is proportional to the number of sites per unit volume S, in the internal (pore) diffusion regime it is proportional to $S^{1/2}$. The test involves pelletizing mixtures of finely divided solid with an inert powder of comparable inert characteristics. If the fraction of the catalyst in the mixed pellet is f the ratio of the rates must also be equal to f in the kinetic regime.

3.3.2 Interphase Transport

The common experimental test to determine the existence of interphase effects is to check the effect of gas flow rate on the conversion while maintaining constant space velocity (W/F). Conversions should be independent of flow rate in the

kinetic regime while conversions should increase with flow rate if film diffusion is controlling. Chambers and Boudart[26] have warned however that this test may be insensitive at the low Reynolds numbers (Re < 10) usually encountered in the laboratory. In order for the test to be meaningful a wide range of flow rates must be used and conversions must be measured very precisely. The critical mass velocity (velocity no longer affects the rate) must be determined at the maximum temperature if diffusion resistance is to be negligible at all other temperatures[14]. It must be noted here that this test is particularly difficult in gasification studies because of the unsteady state nature of the reaction. Both film and pore diffusion are also characterized by low values for pre-exponential factors and activation energies in Arrhenius-type expressions for temperature dependence of rate constants. Such results should motivate a thorough check of the significance of these effects.

3.3.3 Interparticle Transport

There are no simple experimental tests for detection of interparticle or intrareactor gradients. Axial and radial temperature profiles can be detected with a network of thermocouples carefully placed throughout the reactor. However, one must be aware that the measurements obtained are average gas-solid temperatures and not true measurements of the actual temperature of the gas and of the solid. The gas flow

pattern in a reactor must be determined through residence time distribution studies. This will be the subject of the next section.

3.4 Determination of Residence Time Distribution

It is the purpose of this section to briefly outline the techniques of residence-time distribution measurements and modelling. Excellent extensive treatments on this topic can be found by Wen and Fan[27], Levenspiel and Bischoff[28] and Levenspiel[23].

3.4.1 Age Distribution Functions

Age distribution information, originally discussed by Danckwerts, gives a description of the flow pattern inside a vessel and information about the fraction of material that resides a certain time in the vessel. The most widely used age distribution functions are the internal and exit-age distributions. The internal age distribution, I, is a measure of the distribution of ages of elements in the vessel. The exit age distribution E, on the other hand, is a measure of the distribution of ages of all elements of the stream leaving the vessel where age is measured from the time the elements enter the vessel. It has been shown that $E(t) = -dI/dt$[26]. Age distribution information is useful in several ways. Reactor performance can be predicted with knowledge of the rate

equation and exit age distribution (also referred to as residence time distribution, abbreviated RTD) as stated below:

$$\overline{C}_A = \int_0^\infty C_A(\Theta)\, E(\Theta)\, d\Theta$$

where $\overline{C}_A$ is the mean concentration of reactant leaving the reactor unreacted and the concentration in an element $C_A(\Theta)$ depends on the residence time of the element according to

$$\frac{-dC_A}{d\Theta} = r_A(C_A(\Theta))$$

with $C_A|_{\Theta=0} = C_{AO}$, the feed concentration.

For linear systems the RTD leads to reactor design equations. For non-linear systems, age distribution information helps in selecting a suitable model which can give upper or lower limits on reactor performance. Age distribution also helps in detecting severe reactor shortcomings and problems such as short-circuiting, deadspace and non-uniform regions. The internal and exit age distributions for the idealizations of plug flow and complete mixing are given in Figures 3-2 and 3-3. Deviations of actual RTD from one of these two idealized flow patterns can often be detected by visual inspection of these curves as shown in Figure 3-4 in the case of dead space and in Figure 3-5 in the case of bypassing. Dead space or stagnant regions in the vessel can easily be seen from the E curve since for an ideal flow pattern the mean of E is at $\Theta = 1$

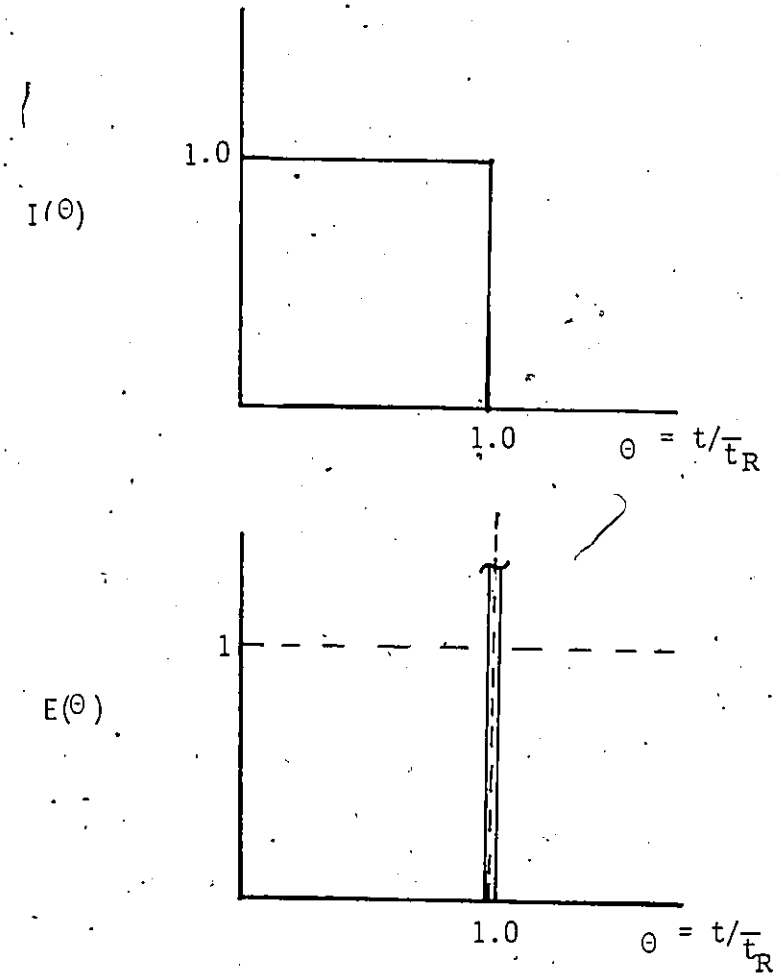

Figure 3-2 Internal (-a-) and Exit (-b-) Age Distribution for Plug Flow Reactor

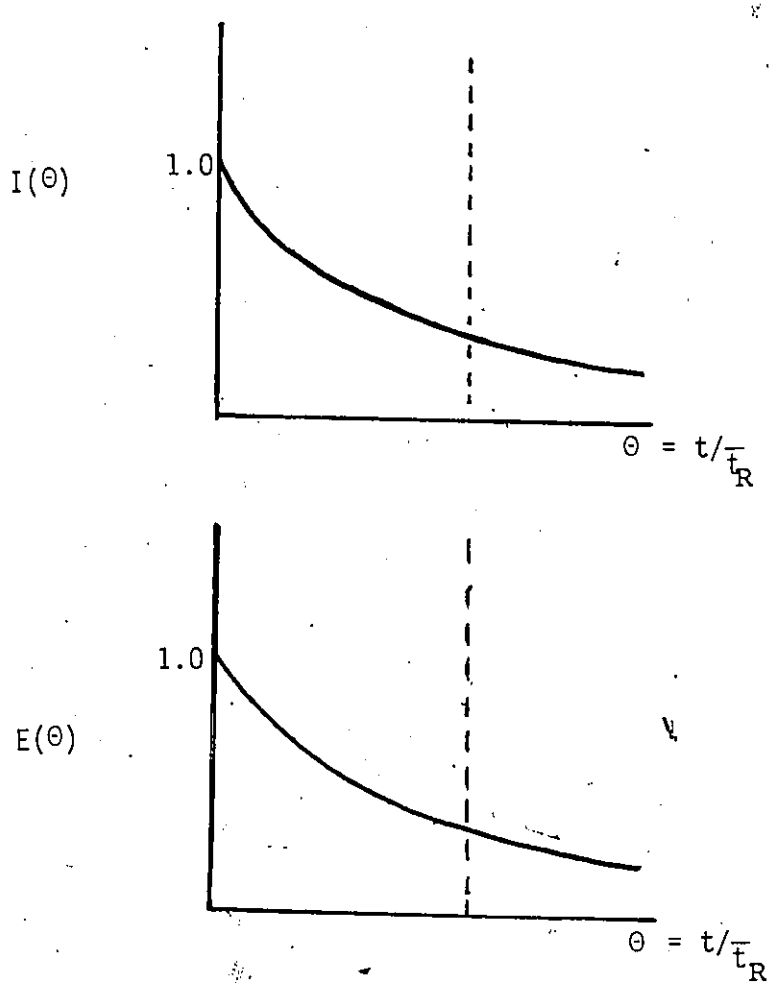

Figure 3-3 Internal and exit age distributions for backmix reactor

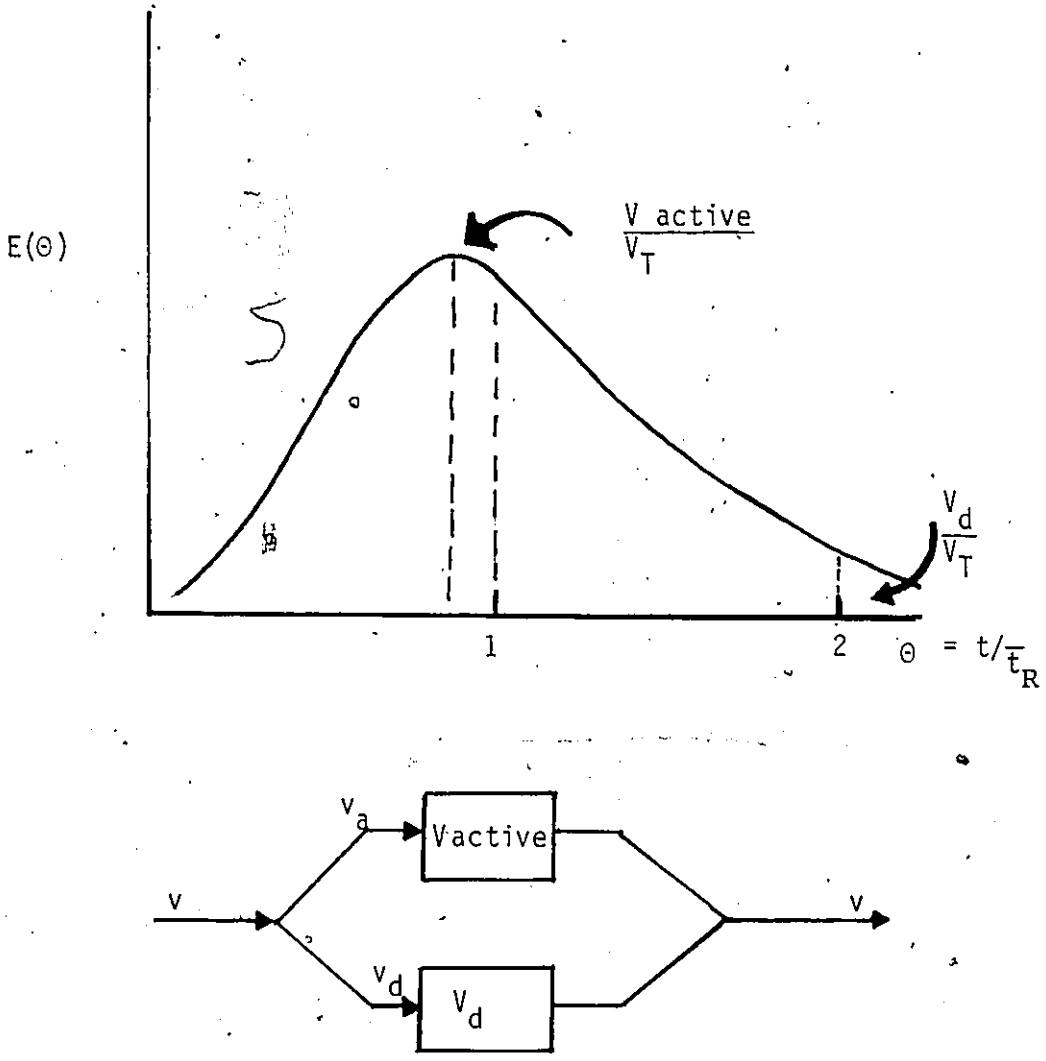

Figure 3-4 Diagnosing dead space from an exit age distribution

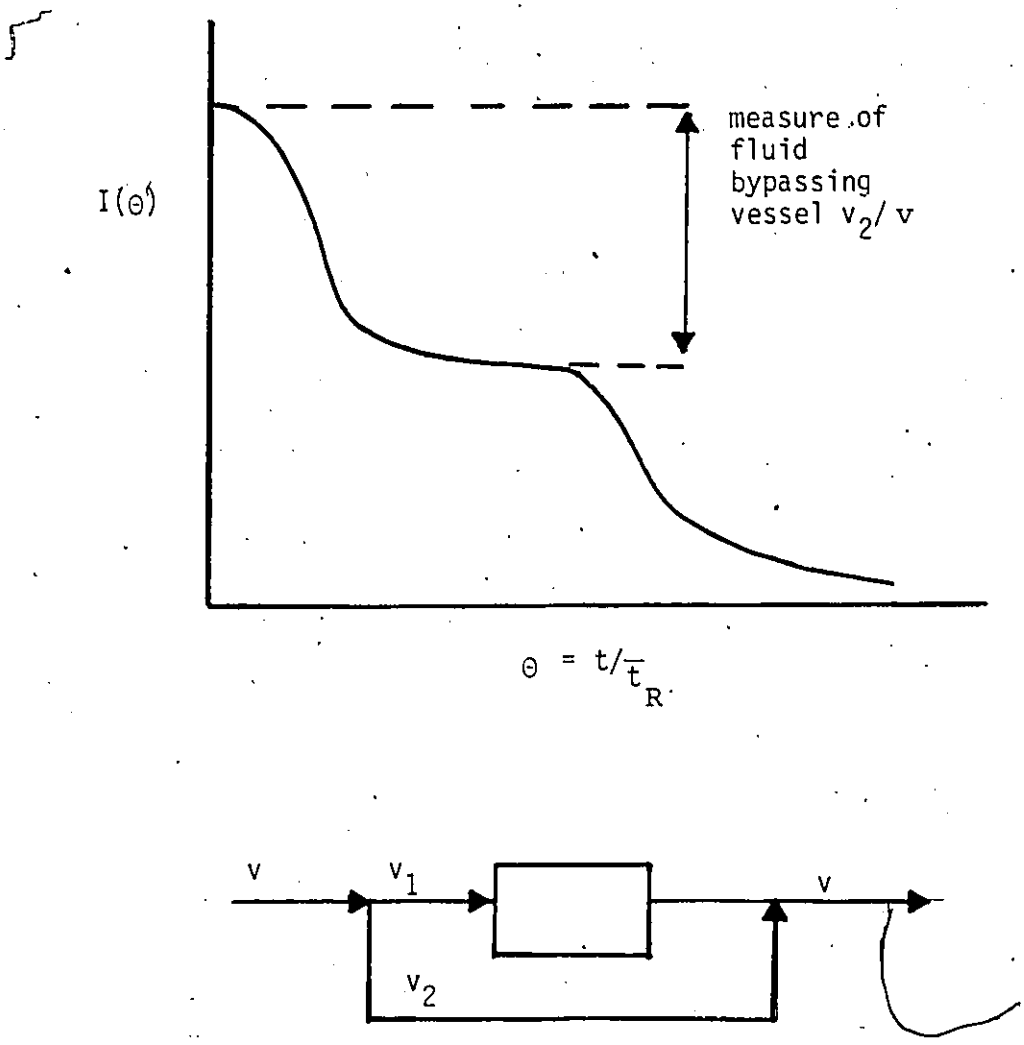

Figure 3-5 Diagnosing fluid by-passing from an internal age distribution

while stagnant zones move the mean to the left because of long tails in the distribution (corresponding to fluid held in the dead space which is extremely slow moving). Similarly fluid bypassing can be detected easily by the steps in an I-curve.

Both the internal and exit age distribution functions can be deduced experimentally from stimulus response techniques. These techniques have been used widely to derive age distribution functions. As illustrated below the tracer input signal (stimulus) may take on many forms. The advantages and disadvantages of several input tracer signals are listed in Table 3-5. The two most extensively studied are the pulse and step signals.

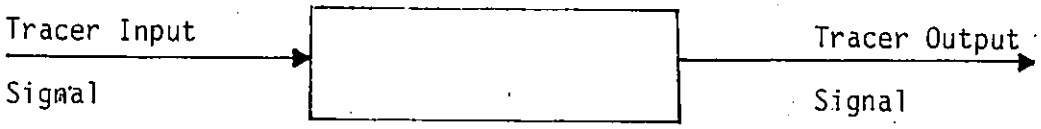

Experimentally the F curve can be obtained from the response at the exit of the system to a step change in tracerable quantity such as the concentrations of radioactive tracer or salt. Any tracer used in these experiments should be completely inert towards the system and should not alter the hydrodynamic flow characteristics being studied. When solids are present in the reactor, absorption or desorption of the tracer compound must

TABLE 3-5

AN EVALUATION OF TRACER INPUT SIGNALS

TRACER SIGNAL	ADVANTAGES	DISADVANTAGES
Impulse	. Output directly impulse response . Simplest model response . Brief disturbance in process	. Difficult to experimentally generate 'perfect impulse input'
Step	. Simple to generate . Output simply related to impulse response	. Long time of input stimulation required to achieve final 'lined out' response
Sinusoidal	. Only measurements of amplitude ratio and phase lag of output are required	. Relatively complex to experimentally generate a sine wave . Long process disturbance since initial transients must die out to achieve stationary response . Frequencies must be chosen in an optimum way
Random	. Lack of a need to generate any perfect specific input signal . Results related to general convolution properties of system	. Two signals must be measured . Deconvolution not always easy to perform numerically

not occur. An alternative approach used in gas phase studies is, if at a certain specified time t, the feed to the system is switched from one supply to another which has the same physical properties (e.g. density and viscosity) and the same flow rate before and after the switch, the concentration of the second fluid in the exit stream C may be observed as a function of time. A true tracer should give the same internal age distribution regardless of whether a + or - step input is made. The dimensionless concentration response C/C_0, which results is termed the F curve and leads directly to the internal age distribution as follows:

$$I(\Theta) = 1 - F(\Theta)$$

The response at the exit of the system to an instantaneous pulse tracer input yields the so called C-curve. This curve directly translates to the Exit Age distribution or RTD.

$$E(\Theta) = C(\Theta) = \frac{d\,F(\Theta)}{d\,\Theta}$$

The response to both a step tracer input (F-curve) and an impulse tracer input (C-curve) for a vessel whose flow pattern is described by one of the ideal flow models is illustrated in Figure 3-6 and Figure 3-7.

The Internal and Exit age distribution functions may be used as supporting evidence to check the validity of the

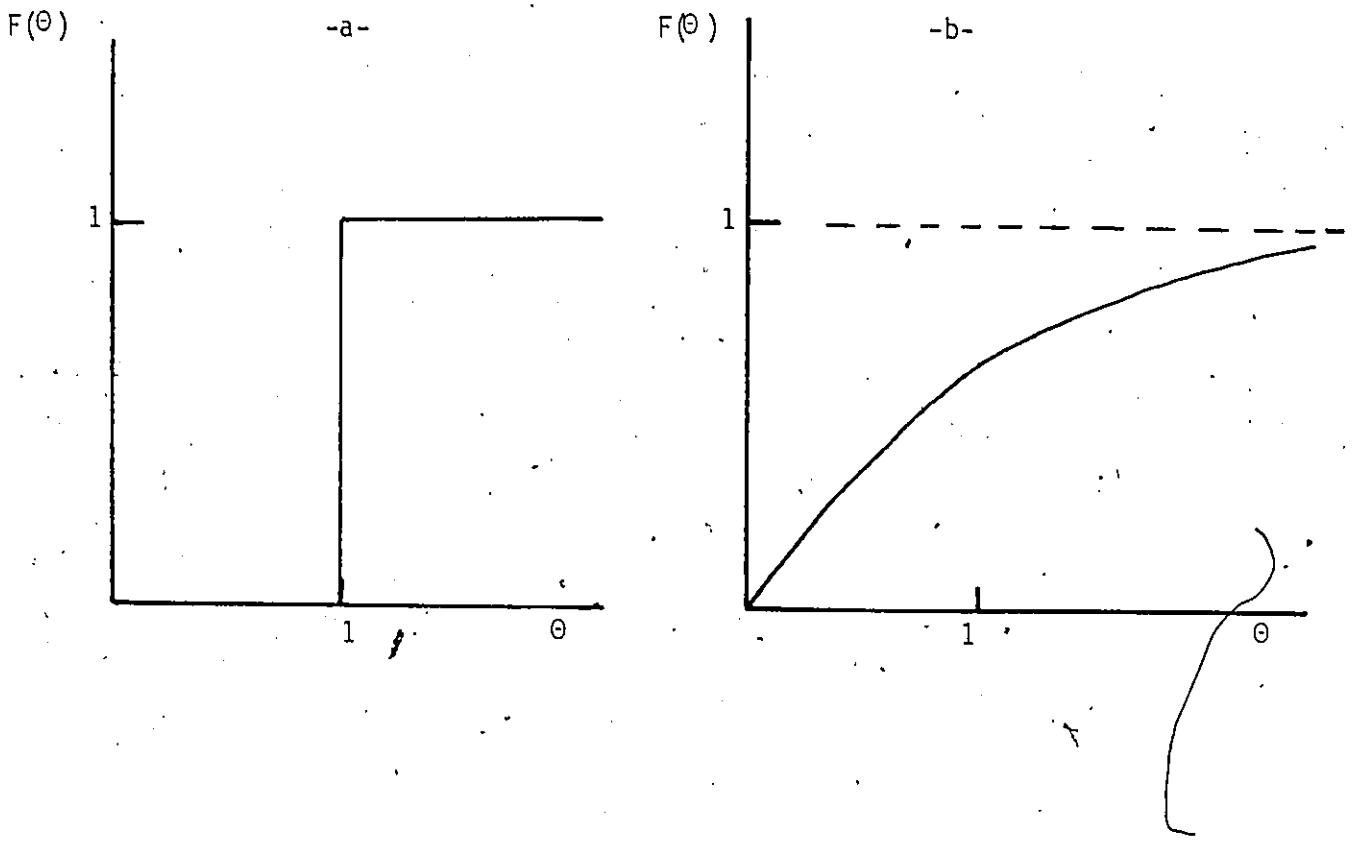

Figure 3-6 Step responses for a) plug flow and b) complete mixing

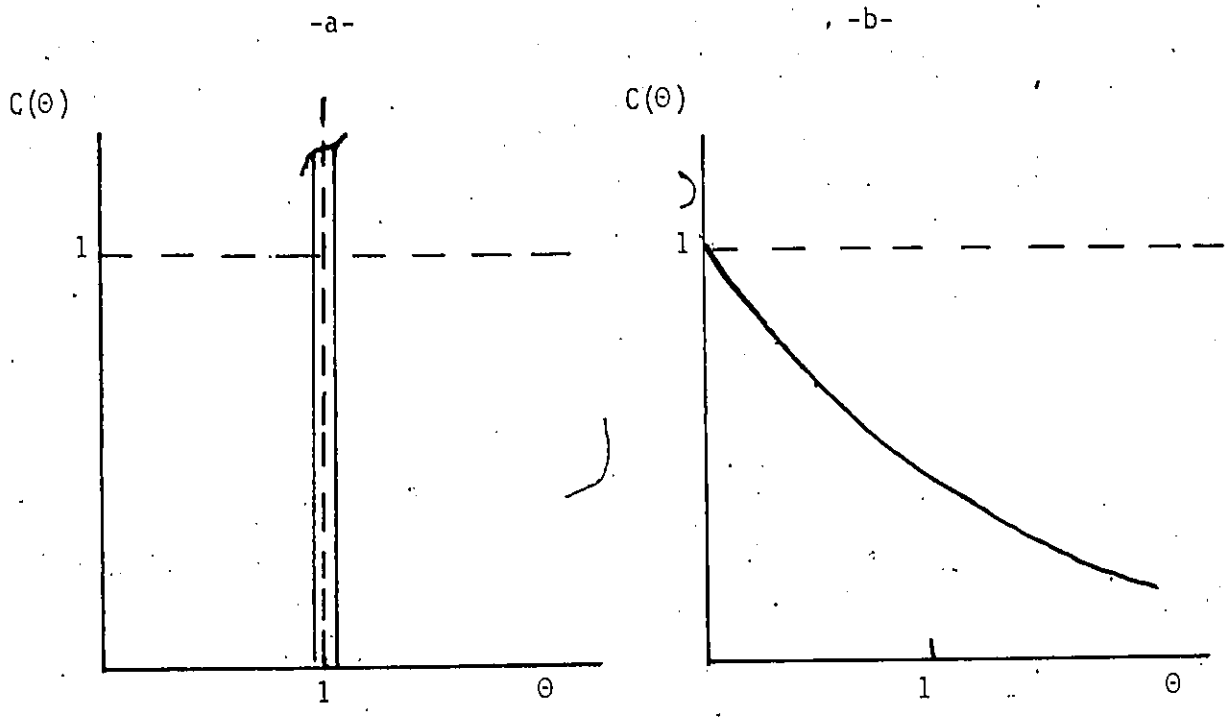

Figure 3-7 Pulse responses for a) plug flow and b) complete mixing

proposed flow model for a vessel. However, simulating the age distribution of the proposed model over the spread of the entire distribution using experimental data is difficult. The approach taken has in general been to compare the moments of the distributions. In order to completely characterize an arbitrary distribution function all moments are required, however, for practical purposes it has been deemed sufficient to use the first three moments in the tracer analysis. These moments are described in Table 3-6.

The basic probability distribution curves which have been used to represent the experimental age distribution function are the normal, the Poisson, the Gamma, and the binomial distribution functions. When the experimental data cannot be approximated by one of the above distribution functions, the age distribution curves are not directly useful since a correlation of age distribution curves for various types of equipment is not available and cannot readily be achieved. For this reason, mathematical models such as the dispersion models, combined models, and compartment models have been devised which contain parameters that can be correlated for various flow conditions and equipment geometries. These mathematical models are discussed in the next section.

3.4.2 Mathematical Models for Homogeneous & Pseudo-Homogeneous Systems

Mathematical models have been formulated with varying degrees of complexity in order to describe non-ideal flows.

TABLE 3-6

Moments of Probability Distribution Functions

Moment	Parameter	Description
1	μ	Mean (centre of gravity of distribution about origin
2	σ^2	Variance (spread of distribution curve)
3	γ^3	Skewness

There are several types of models that have found useful applications. Velocity profile or convective models are applicable to reactors of simple geometry in which the laminar flows of reacting mixtures are predominant. The information necessary to describe velocity profiles in a reactor is usually not available for complex reactors. For description of flow behavior in a real reactor one must rely on a model which contains empirical parameters and approximates the actual behavior closely. These parameters are then correlated as functions of fluid and flow properties, reactor configuration and other important features.

For relatively small deviations from ideality, one and two parameter models such as the axial dispersion model and the tanks-in-series or mixing-cell model are often used in describing the flow. This is often the case for tubular reactors and single phase flow in packed beds. The dispersion model in which the diffusion is superimposed on plug flow has been used for both homogeneous and heterogeneous systems in which axial symmetry can be assumed and in which the flow behavior is not far from that of plug flow. The mass balance for the one dimensional axial dispersion model is

$$\frac{\partial C}{\partial t} + U \frac{\partial C}{\partial z} = \frac{\partial}{\partial z}\left[D_a \frac{\partial C}{\partial z}\right] + r\,(C) \qquad \text{Equation 3-35}$$

where U = mean plug flow velocity through vessel

D_a = mixing dispersion coefficient

and the parameter D_a is found from experiments. One common approach to determining the parameter D_a is to perform a residence time distribution test on the reactor and choose the value of D_a so that the model solution and experimental output curve agree. The axial dispersion model can represent plug flow behavior when $D_a \rightarrow 0$.

Besides the dispersion model, the tanks in series model is the other model widely used to represent non-ideal flow. Here one assumes the fluid flows through a series of equal size ideal stirred tanks, and the parameters of the model are the number of tanks in the chain and the residence time in a single tank. For N-tanks in series the exit age distribution can be described by

$$E(\Theta) = \frac{N^N}{(N-1)!} \Theta^{N-1} \exp(-N\Theta) \qquad \text{Equation 3-36}$$

$$\Theta = \frac{t}{N\bar{t}_1}$$

$\bar{t}_1$ = mean residence time in 1 tank

The model parameter N, need not strictly be an integer for curve-fitting purposes. Plug flow is approached as $N \rightarrow \infty$. In many ways the dispersion model and the tanks in series model are similar and the two models are often used interchangeably.

Where there is no symmetry of flow pattern and relatively large mixing problems exist (such as channelling, dead space, bypassing) as encountered in real stirred tank reactors and fluidized beds whose flow patterns are closer to the complete mixing case, many different models with as many as six parameters have been proposed to describe the macromixing. Combined models were first suggested by Cholette and Cloutier[110] as early as 1953 to handle a real stirred tank flow. These models view the reactor as consisting of interconnected flow regions (plug, backmix, dispersed and stagnant flow) with various modes of flow (by-pass, recycle and cross flow) between and around the flow regions. The pattern generated by the various combinations of these elements can be used to fit a large variety of flow through different vessel geometries. Using these components, the problem then reduces to finding the volumes of the various regions and the rate of each type of flow occurring such that the response curves of the model match as closely as possible the response curves for the real vessel. The number of parameters used in a model is an indication of its flexibility in fitting a wide variety of situations and in addition suggests the complexity of the accompanying mathematics. In fitting a real reactor, one should aim for the simplest model which fits the response curves and whose various regions are suggested by the actual flow patterns and reactor geometries.

Cholette and Cloutier[110] concluded by matching experimental data (F-curve) for their stirred tank with a

number of alternative models that a model consisting of complete backmixing with short circuiting and dead space represented the real vessel adequately. Their two-parameter model (n, m) is shown below:

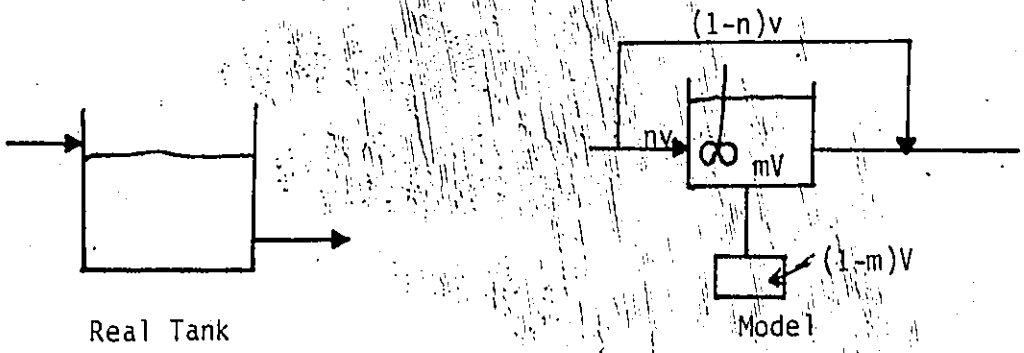

Several internal and exit age distribution curves of non-reacting systems for specific combined models are presented by Levenspiel and Bischoff[28]. Wen and Fan[27] present several combined models for an irreversible first order reacting system and their dynamic responses to a host of input tracer signals (ramp, pulse, step).

In addition to the combined models discussed, circulation models have been used to describe complex systems. Circulation models have been proposed mostly to describe fluid mixing in homogeneous stirred tanks. The basis is a region of intense shear and mixing around the impeller followed by recirculating flows around the rest of the tank. Weber et. al* proposed a circulation model which consists of a portion of the fluid recirculating the vessel; this portion of the fluid comprises m passes of plug flow. Van de Vusse* proposed another type

* as discussed in Wen and Fan [27]

of circulation model in which there are three main loops circulating in a tank: one receives feed stream, another delivers to the outflow stream, and all other loops combined together to form the third loop as shown in Figure 3-8. This results in a highly complicated model form. These models are unfortunately almost always complex and have a large number of parameters to be estimated.

All of the models presented thus far are essentially homogeneous models. Although many of these mixing models have frequently been applied to heterogeneous reactors such as packed beds and fluidized beds with some success, a gross approximation must be made to do so. It is assumed that the mass exchange between different phases is negligible and a homogeneous model can be applied to each phase separately. Alternatively it is assumed that the whole reactor consists of a homogeneous mixture. When these approximations cannot be made reasonably (often true of fluidized beds) heterogeneous models must be applied to the system.

3.4.3 Mathematical Models for Heterogeneous Systems

Ever since the fluidized bed technique was first applied to the making of synthesis gas from coal by the Winkler generator, fluidized beds have remained popular. However owing to the complex gas flow and solid particle movement within the fluidized bed, and other reactor types (e.g. spouted beds),

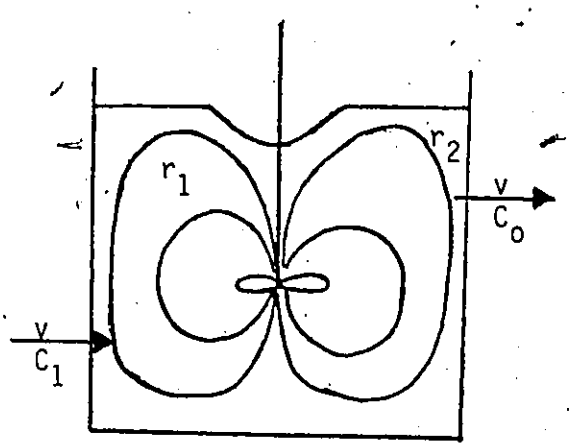

-a-

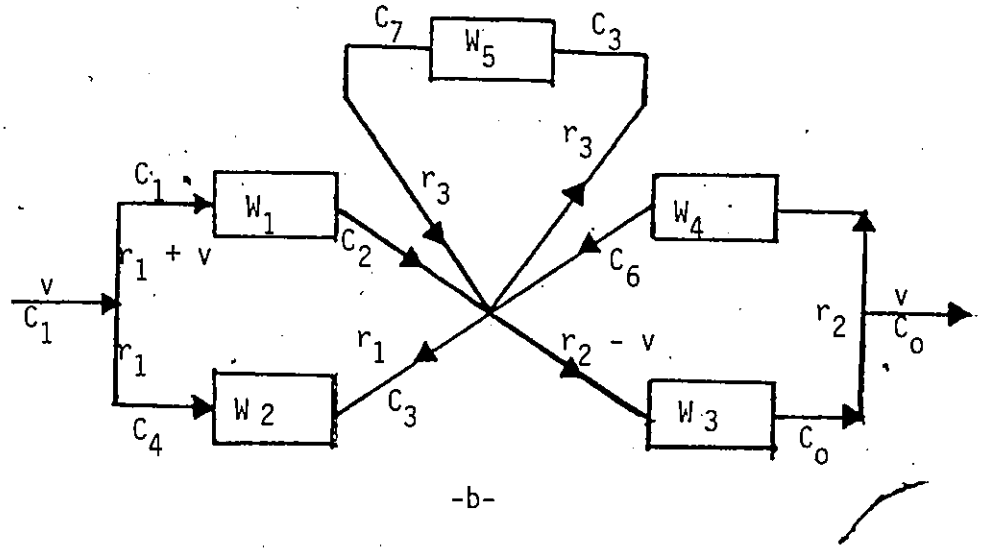

-b-

Figure 3-8 Physical Diagram (a) and Block Diagram (b) for a Circulation Model (adapted from Reference 27)

quite complex heterogeneous flow models have been applied to describe the system. Two phase models, residence time distribution models, bubbling bed models have all been used to some extent to describe flow behavior. It is beyond the scope of this short discussion to elaborate on these models. The reader is referred instead to the excellent summary by Wen and Fan[27] on heterogeneous models.

3.4.4 Mathematical Model Parameter Estimation

With multiparameter flow models, the accurate estimation of the parameters is not a simple task. There are various techniques that have been used for the actual parameter estimation, among which are direct non-linear regression in the time domain, comparison of time moments of the data and of the model, and fitting of data in the Laplace transform space. Some good reference material has been suggested by Bishoff and Froment[15].

Direct non-linear regression in the time domain is the most straightforward in principle since one is comparing the actual data with the model response. Also, the least squares, maximum likelihood, or other criterion is minimizing errors directly with the data. The primary disadvantage of this method is that the time-domain solution of the model must be available. The alternative of repetitive numerical solutions during an extensive parameter search routine can involve very

large amounts of computer time. Also, it has been shown[30] that the objective functions often have local in addition to global minima and/or long ridges because of correlation between the parameters---both of these cause difficulties.

The second technique is that of using time moments of the data to be compared with those of the model. The advantages are that they can be easily computed by numerical integration of the data and the integrations tend to somewhat smooth the data. Also, the moments can be readily found from the Laplace transform of the model without the necessity of a time domain solution. The main disadvantage is that the moments tend to emphasize the data for large values of time, and this data in the tail of the curve is usually not very accurate (because of low tracer concentrations). To decrease the importance of the tail, the moments can be defined with a weighting factor $[e^{-st}]$. With or without this modification, it is often difficult to decide just where to truncate the tail of the data curve. Finally, the results must be checked in a time-domain solution to ascertain that the model with moment evaluated parameters fits the actual data.

The last technique uses fitting (e.g. least squares) in the Laplace transform space since the Laplace Transform space solution for the model is easily obtained. This method necessitates numerical transformation of the time domain data

which is a serious drawback. The transformation can be carried out in the S domain or the frequency domain, ω . As for the previous method, the final results should be checked in the time domain since the fit obtained in the S-domain does not guarantee the best in the least squares sense in the time domain. This is not a necessary step in the ω -domain but the complicated expressions for the model in the frequency domain are quite discouraging[30, 31].

Numerical comparisons of the various methods have shown that the use of moments is the least accurate and sometimes leads to invalid parameter values. Direct fitting in the transform domain usually leads to valid parameter values but they are not always the same as would be found by time domain fitting. The final check is therefore always a comparison of the fit in the time domain. It appears, however, that the information contained in RTD experiments can sometimes only be used to determine a certain (small) number of parameters[30]. Unique discrimination will then require different types of experiments such as downstream injection of a tracer with measurements of backmixing. Then a crossplot can indicate which parameters are most sensitive to which type of experiments and how these combinations can be used to define the appropriate parameter combinations.

3.4.5 Summary

This section has demonstrated how the tracer experiment, the age distribution functions and mathematical models with appropriate parameter estimation techniques can be used to determine the flow pattern in a reactor. This task is of no less importance in laboratory reactors used for kinetic investigations. The major principles of experimental reactor design discussed heretofore, will be used to evaluate the bench scale reactors presently being used in gasification kinetic studies.

4 EVALUATION OF REACTOR SYSTEMS

4.1 Systems Reported in the Literature

The purpose of this section is to critically review laboratory reactors and experimental techniques used in the study of gasification kinetics. Major emphasis will be placed on evaluating the merits and limitations of these reactor schemes in view of the design features discussed in Chapter 3. Almost every conceivable gas-solid contacting pattern has been used in char gasification studies. The major types of bench-scale reactors used in studying char gasification kinetics are: the differential tubular fixed bed, the integral tubular fixed bed, the thermogravimetric balance, the fluidized bed and the transport reactor. In addition to these reactors, a number of miscellaneous contact devices (e.g. spouted beds) have been used and deserve brief mention. The reader is referred to Appendix A for a descriptive compilation of many gasification kinetics studies classified according to reactor type employed. This list is by no means exhaustive but it does provide a good sampling of the literature. Each of the major reactor types will be discussed in detail in the subsequent sub-sections of this chapter. Several excellent general reviews on the subject of laboratory reactors can be found in the papers by Weekman[32] and Doraiswamy and Tabjl[33] and in the books by Shah[34] and Anderson[35].

4.1.1 The Tubular Fixed Bed Flow Reactor

The bench-scale tubular flow reactor shown schematically in Figure 4-1 has been used extensively in gasification studies because it is simple and relatively cheap to construct. This reactor is also desirable because in some cases it represents a scaled-down version of a large commercial gasifier. In the fixed bed reactor, the solid char is confined in the tube and the reactant gas flows either upward or downward through the bed. The fixed bed reactor can be operated in a differential or integral mode. The basic difference between the differential and integral reactor is that the reactant conversion in the former is limited to a few percent (usually less than 10 percent). Since this difference significantly alters the interpretation of data the reactors will be discussed individually.

The integral reactor has the inherent advantage that large (finite) conversions are involved so that routine techniques are adequate for gas composition analysis. Determination of the kinetics of a reaction from the data in an integral fixed bed is usually based upon three main assumptions. First, the flow pattern of the gas inside the reactor is assumed to be plug flow (i.e. over any cross-section normal to the gas flow, the mass flow rate and the fluid properties such as pressure, temperature and composition are uniform). Secondly, the reactor is usually assumed to operate isothermally. Finally,

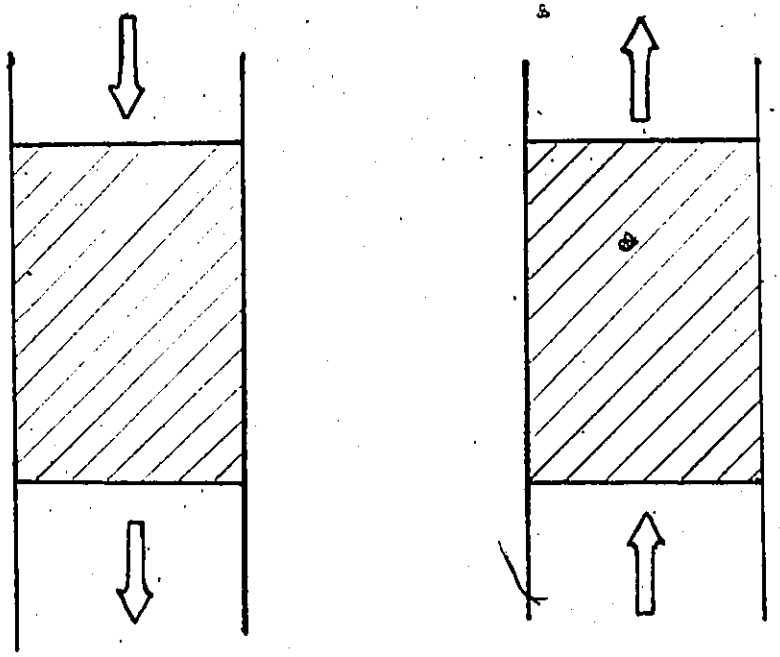

Figure 4-1 Schematic of fixed bed tubular flow reactor

the rates of film and pore diffusion are assumed to be much faster than the rate of chemical reaction. When these assumptions are made, the governing equations for the fixed bed tubular reactor given in Table 2-2 are greatly simplified and are given below:

Gas Phase Mass Balance

$$\varepsilon \frac{\partial C_A}{\partial t} = -U \frac{\partial C_A}{\partial z} - \rho_b r_A$$

Solid Phase Mass Balance

$$\frac{\partial C_s}{\partial t} = -b' \rho_s r_A$$

where r_A = rate of reaction of component A per unit mass [kmol/kg s hr]

ρ_b = solid bulk density [kg s /m_r^3]

ρ_s = density of solid [kg s /m_p^3]

C_s = molar concentration of reacting component A of gas [kmol/m_f^3]

ε = void fraction of bed

U = superficial velocity [m_f^3/m_r^2 hr]

b' = molar stoichiometric coefficient

However, as mentioned in the previous chapter, deviations from any one or all of the three assumptions occur in laboratory studies and the experimental and theoretical checks described earlier should be carried out.

Deviations from plug flow in integral fixed beds can arise in a number of ways from radial temperature gradients (due to heat of reaction and poor heat transfer through the bed) and from various dispersion effects (e.g. local density changes, packing turbulence, etc)[45]. In the report by the Institute of Gas Technology[46] on the gas reactions of carbon in an integral fixed bed, it is clearly stated that

"local variations in the fuel bed density and therefore in the distribution of the gas flow resulting in varying degrees of backmixing between reactant and products, varying radial concentration gradients and possible channeling and bypassing of portions of the fuel bed"

may have occurred especially at the high temperatures (1100°C). Nevertheless, no effort was made to ascertain to what extent these effects may have altered the kinetic results. As discussed earlier, the extent of nonideality in gas flow pattern can be identified by carrying out residence time distribution studies. These studies can be carried out in integral beds because the gas-solid contact times are relatively long in order to achieve high conversions. Channeling, often caused by non-uniform solid packing, is a problem which must be contended with in integral beds especially when the solid particles are introduced to the

reactor already at reaction temperature as in the work by Hunt et. al[47].

The major difficulty with the integral fixed bed is the problem of achieving isothermal operation during severely endothermic/exothermic reactions[14]. The isothermal assumption for integral beds must be checked carefully. There are numerous examples of large axial temperature differences in bench-scale integral beds. Some examples are given below:

"Three thermocouples were located in a six inch reactor zone, 1/2", 3" and 5 1/2" from the top of the zone. The maximum temperature occurred at the middle thermocouple and was considered the nominal temperature of the reaction. The top and bottom bed temperatures were generally within 35°C of the maximum temperature." (Haynes et. al[44] 750-950°C)

"Temperature control is less sensitive with this arrangement, nevertheless temperature variations of not more than 20°-30°F could be maintained in the carbon bed." (Hunt et. al[47], 1700-2000°F)

"At temperatures of 1800°F and above, we could not observe any consistent effect of temperature on the rate of gasification. Moreover during these tests at 1800°F and above, stainless steel screens which had been used to support the coal char charges were found to have MELTED, indicating

that very large temperature rises had occurred...sample temperatures could easily rise over 2500°F from a starting value of 2000°F, even with the high gas flow rates and small sample sizes used." (Feldkirchner & Huebler[48]).

The effect of these possible temperature gradients on the reaction rate constant for various temperature deviations and activation energies are shown in Table 4-1 following the analysis presented in Denbigh[45]. The magnitude of the ratio of the rate constants emphasizes the biggest concern in fixed bed reactors, achieving isothermality. Besides the obvious examples of this problem quoted above there are many examples in the literature where large differences in both interphase and intraparticle temperature and concentration appear. For instance when a simple calculation using the criterion (Equation 3-27) presented in Section 3.2.2 is carried out for the kinetic results described by Feldkirchner and Huebler[48] for steam gasification of bituminous char at a temperature of 1200K and 50 SCF/hr steam flow rate in an integral packed bed, one finds that as much as a 30°C temperature difference may exist between the gas film and the solid char surface (see Appendix B for details). Dilution of reacting solids with inert solids has been used to minimize the problem of hot spots in hydrogasification studies in integral beds. Feldkirchner and Huebler[48] used a ratio of 12 to 1 inert alumina particles to char throughout the bed to act as a heat sink with very limited success. Unfortunately, no tests

TABLE 4-1

The Effect of Temperature Deviations on Reaction Rate Constants

TEMPERATURE LEVEL [K]	TEMPERATURE DIFFERENCE [K] 10	20	30	100	ACTIVATION ENERGY [J/Kmol]
800	1.2*	1.4	1.7	5.3	1×10^8
	1.60	2.5	3.9	65.0	2.5×10^8
900	1.16	1.34	1.54	3.8	1×10^8
	1.44	2.1	2.9	28.2	2.5×10^8
1000	1.13	1.27	1.42	3.0	1×10^8
	1.35	1.80	2.4	15.4	2.5×10^8
1500	1.05	1.11	1.17	1.7	1×10^8
	1.14	1.30	1.48	3.5	2.5×10^8

* $$\frac{k_{T_1}}{k_{T_2}} = \frac{\exp(-E_a/RT_1)}{\exp(-E_a/RT_2)} = \exp\left[\frac{E_a \, \Delta T}{R \; T_1 T_2}\right]$$

were carried out to determine whether flow problems such as bypassing and channeling occurred as a result of the high dilution ratio. Although radial temperature gradients may also exist in integral fixed beds[14] (although to a lesser extent), they have rarely been looked at by workers studying gasification kinetics.

The third assumption in integral reactor data analysis, that of insignificant pore and film diffusion resistance, is not usually as troublesome as the nonisothermal behavior of the bed. The reason is that gas velocities and particle sizes can be varied substantially. However, increases in the gas velocity (e.g. to increase external mass transfer rates) and decreases in the particle size (e.g. to increase pore diffusion rates) can lead to substantial bed pressure drops. To account for the variation in pressure along the length of the reactor, a momentum balance must be introduced to describe the system. There is some evidence in the literature that mass transfer and pore diffusion effects which are significant have been neglected when interpreting rate data. Wicke[51] has made a significant contribution in his approach to isolate transfer effects from chemical reaction data. He describes experiments in which the experimental conditions can be arranged easily to measure on the one hand the true activation energy (i.e. with no diffusional resistance) and on the other hand with the full effect of diffusion. His results for the study of the Boudouard reaction are given in Table 4-2. It may be seen that

TABLE 4-2

Observed Activation Energies for Boudouard Reaction

REFERENCE	ACTIVATION ENERGY [kcal/mol]	TEMPERATURE RANGE [°C]	PACKED BED PARTICLES
Nicke[51] (full diffusion)	43 ± 1.5	850 - 1000	electrode carbon
(no resistance)	84 ± 3		and charcoal
Blakeley[53]	50 - 70	950 - 1100	coke
Mayers[42]	52	850 - 1150	graphite
Taylor and Bowman[54]	45	873 - 1063	subbituminous coal char
Smith and Tyler[5]	48.5	750 - 900	coke
	57	750 - 900	test electrode
	70	750 - 900	graphite

the activation energy for the diffusion limited case is half of the true activation energy as expected. Activation energies reported by other experimenters at similar temperature levels are included for comparison. Values of E_a for very similar materials are found to vary greatly although they all lie within the extremes reported by Wicke. These intermediate values indicate that possible diffusion limitations exist.

To summarize briefly, the integral tubular fixed bed flow reactor offers the following advantages:

- simple construction and operation
- flexible operating ranges
- long residence times for RTD determination

However, tnese advantages are often outweighed by the following limitations:

- difficulty in achieving isothermality
- complexity of the model form when nonidealities in flow prevail
- large pressure drops complicate data analysis

4.1.2 The Differential Tubular Fixed Bed Flow Reactor

The differential tubular reactor, unlike its counterpart, requires a small quantity of solid and operating conditions are such that the gas conversion is kept low (< 10%).

Interpretation of kinetic data from differential reactors is based on three main assumptions. First, because of the low gas conversions, the gas composition in the bed is assumed to be the average composition of the gas at the inlet and exit of the reactor. The change in composition between the inlet and exit streams must be large enough for precise measurement, otherwise the rate of conversion in the reactor cannot be accurately established. This restriction imposes a limitation on the applicability of the method. A material balance for the reactant gas over the differential bed yields a point reaction rate directly (equivalent to the rate in an integral bed at a position where the partial pressures of the reaction components are equal to those of the differential reactor) which is highly advantageous. If precise analytical methods of determining small composition changes are not available however, for the particular reaction, a close approach to a point value of the rate cannot be ascertained. In gasification studies, the analysis of gases such as O_2, H_2, CH_4, CO_2 and CO in low concentrations is required. Of these, accurate quantitative analysis of H_2 in the gas mixture is perhaps the most difficult to obtain[37].

The second assumption is that as a result of the high gas flow rates (short residence times) which are necessary to limit conversions, external mass transfer rates are fast enough to prevent significant interphase concentration gradients. In the study by Tyler and Smith[5] on the reactivity of coke to carbon dioxide, it was shown that operating conditions could be

attained to approach differential fixed bed behavior. These workers found through both experimentation and calculation that they could operate in a chemical reaction control region (i.e. rates of external mass transfer and pore diffusion were very fast). In view of the very short residence times inside the differential reactor, residence time distribution studies are difficult to carry out. With differential reactors however, nonideal flow does not present a serious problem because at low conversions, the effect of a distribution of residence times is small[45].*

The third assumption is that the reactor operates isothermally since low conversions lead to small overall heat effects. There are few examples in the gasification literature that show this assumption is being verified. Blackwood and McGrory[52] studied the carbon-steam reaction between 100 and 5000 kPa and 750-850°C using a differential fixed bed (17.6 cm^3 volume). The clear silica tube reactor, the thermocouple arrangement and the bed characteristics are shown in Figure 4-2. By adopting a space velocity of $2s^{-1}$ the authors were able to achieve steam decompositions of less than six percent so that the conditions approximate those of a differential reactor. In order to check for isothermality, nitrogen was allowed to flow through the bed at space velocities up to $4s^{-1}$ at a nominal temperature of 830°C.

---

* The reader is referred to Figure 3-1 where it can be seen that the effect of mixing at low conversions for 1st order kinetics is negligible.

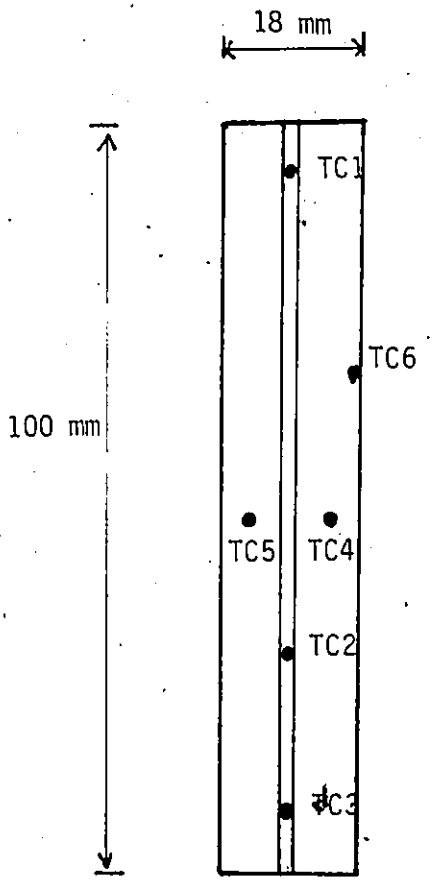

Bed Volume 17.6 cm^3
Bulk Density 0.59/cm^3
Bed Weight 9.9 g

Figure 4-2 Differential reactor used by Blackwood and McGrory[52]

They observed no significant variations in temperature in the central sheath, in the annular bed and at the wall. However, when steam was passed through the bed and subsequently reaction occurred, the temperature at the centre of the annulus rose above that of the wall and the central sheath by about 5 to 7°C at a space velocity of $2s^{-1}$. Kayembe and Pulsifer[36] studied the steam-char reaction at similar temperature levels using a differential packed bed and found 5 to 7°C temperature variations in the length of the solid bed. It appears, that even with conversions in the order of ten percent, achieving isothermality presents a challenge under gasification conditions. Differential beds have nevertheless been found to operate isothermally for gas-solid catalytic reactions (with high heats of reaction) at lower temperatures[14]. Smaller conversions ($\sim$ 5%) may be required to achieve isothermal operation in differential packed beds operating at very high temperatures.

Rate models found in a differential study have limited application since they may be valid only for the small range of conversions studied. This limitation can be overcome if synthetic feeds can be prepared to study reaction rates as a function of composition. Since the differential reactor gives the reaction rate directly, it is useful in analyzing complex reacting systems.

In summary therefore, low conversions in differential beds can lead to small changes in temperature, pressure and composition in the reactor. As a result, a high degree of analytical precision is required to measure the low gas concentrations.

4.1.3 The Thermogravimetric Balance

In the laboratory study of char gasification, the progress of the reaction can be followed by the weight change in the char sample as it is gasified. This gravimetric technique is generally applicable to many gas-solid reactions including decompositions, absorptions or adsorptions. Figure 4-3 is a schematic diagram of a typical system for studying gas-solid reactions using a recording balance. The initial investment for thermobalances and accessory equipment is usually very high.[56] Operating conditions for thermobalances range from vacuum to high pressure ($\sim$ 1000 psi) and from very low to very high temperatures ($\sim$ 2000^{o}C). For above 300 psi, near conditions of industrial gasification, a number of high pressure balances are available including quartz spring, electronic and commercial units (e.g. Cahn, etc.[56]). With regard to continuous weight measurement, these balances are capable of weighing specimen from the microgram range (microbalance) to as much as 100 grams. The solid specimen assume a variety of forms from granular particles contained in baskets to solid pellets formed under high pressure by extrusion.

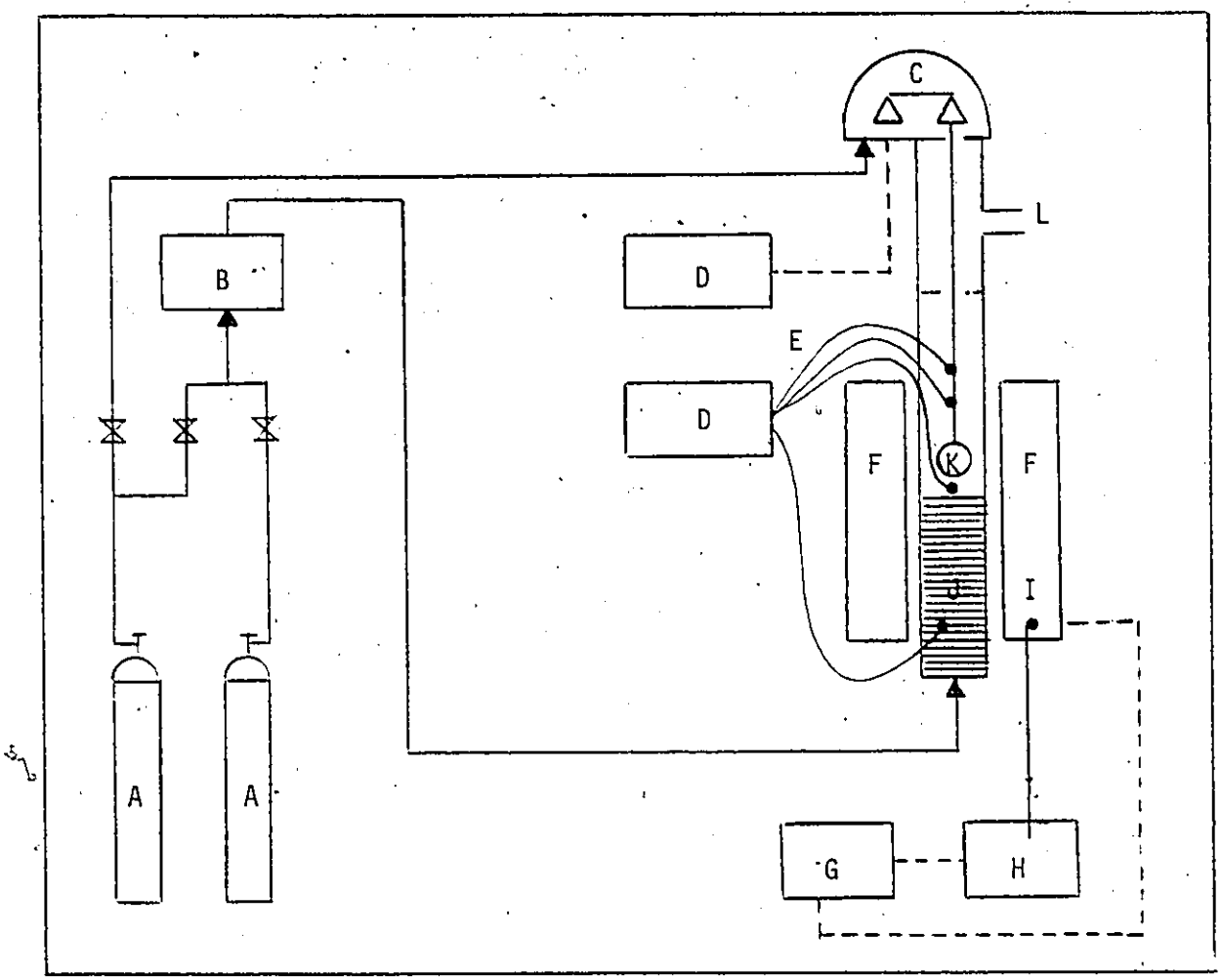

Figure 4-3 Schematic of Thermogravimetric Balance (adapted from Reference 13)

A	Gas Cylinders	G	Power Supply
B	Flowmeters	H	Controller
C	Balance	I	Control Thermocouple
D	Recorder	J	Packed Bed
E	Thermocouple	K	Sample
F	Furnace	L	Gases Out

The monitoring of the weight change of a very small sample of solid reactant offers a direct measure of the overall reaction rate without the need for analysis of all possible products. The microbalance is thus a differential reactor operating at point values of the partial pressure and the temperature. The usual assumptions made in interpreting the rate data from a microbalance are the same as those discussed in the previous section, i.e., because of the very low conversions (1-3%) operation is assumed to be isothermal and pore and film mass-transfer resistance are assumed to be very low. The thermobalance technique has led to defining an overall reactivity on a mass basis as follows:

$$R_m = -\frac{1}{w}\frac{dw}{dt}$$

where R_m overall char reactivity

w weight of unreacted char on a dry ash-free basis

Although this simple measure of conversion provides a measure of activity, a detailed analysis of the gas products is required to provide selectivity data. Product gas analysis for such small conversions requires expensive analytical equipment (e.g. mass spectrometer). The thermobalance has however emerged useful in quick determinations of the effects of various variables on the reactivity.

Gardner et. al[40] studied the catalyzed hydrogasification of chars using a thermobalance (0-1000°C,

0-1000 psi). Gas analysis was obtained by splitting a portion of the gas product stream to an infrared detector where methane content was continuously measured and a portion to a gas chromatograph where total gas composition was determined. They found that although the infrared measurement of methane production lead to qualitative agreement with the direct mass determination, quantitative agreement was not good. Two reasons for this poor agreement may be that precise regulation of the product stream flow rate is difficult and that axial dispersion and low concentrations in the gas product stream combine to make analysis difficult.

Ensuring isothermal operation in a thermobalance involves several factors. First, it is essential that the furnace (usually a tubular heater) have an adequate constant temperature zone where the reactant solid is placed. Second, the temperature of the furnace has to be maintained at the desired level within a specified accuracy through the use of a thermocouple which is placed close to the hottest part of the furnace heating element[13]. This is preferable to placing the thermocouple near the sample since the delay between a change in the power level to the furnace and the resulting temperature change at the pellet is so great as to render the system uncontrollable by the second method. This implies that the flow rate of the reactant gas must be held constant during a run and the apparatus must be given sufficient time to reach steady state before the run begins. Finally, thermoooupleś

must be placed around the specimen to assist the experimenter in arriving at an isothermal region surrounding the sample and for recording the nominal temperature during reaction. In the case of highly exothermic or endothermic reactions as in gasification, it would be advisable to place thermocouples inside the solid sample itself. Although very fine thermocouples are available and the leads may be twined around the suspension wire[13], it is still uncertain how this would interfere with the weighing or reaction of the sample.

Tien and Turkdogan[63] used an atmospheric pressure electrobalance to study the gasification of charcoal and coke with carbon dioxide. These workers checked the assumption that the carbon specimen were isothermal by making an approximate estimate of the intraparticle temperature gradient. The temperature gradient across a spherical pellet can be represented by the following:

$$\frac{1}{r^2}\left[\frac{d}{dr}\left(r^2\,\frac{dT}{dr}\right)\right] = -\frac{\rho R'|\Delta H_r|}{\lambda_{eff}}$$

where r = particle radius

ΔH_r = heat of reaction per unit mass carbon

R' = fractional mass loss per unit time

ρ = sample density

λ_{eff} = solid thermal conductivity.

Assuming a constant particle surface temperature T_s, the

gasification rate is computed (at T_s) and using the above heat balance the temperature at the centre of the sphere, T_c, is estimated. A mean temperature 1/2 (T_c + T_s) and a corresponding average reaction rate is then computed. The results of these approximate calculations are given in Figures 4-4 and 4-5 for the reaction of a coke sphere (2 cm diameter) in 100 kPa CO_2. For the case considered the temperature difference (T_s - T_c) becomes appreciable only at temperatures above 1100°C. For this endothermic reaction, the nonisothermal reaction rate is lower than the corresponding isothermal rate. Intraparticle temperature gradients will probably not be significant for smaller particles and lower temperatures. When solid pellets are used in the thermobalance this check should nevertheless be carried out.

Dutta et. al[38] used an atmospheric pressure thermobalance to study the gasification of several chars in carbon dioxide. This group studied the effect of sample holder on reaction rates. The three sample holders are described in Table 4-3. Although no actual data is presented, Dutta et. al conclude that no significant difference was found among the observed reaction rates in the three cases at a gasification temperature of 1000°C and a gas velocity of 4 cm/s. Calculations, based on the interphase concentration and temperature criteria presented in Chapter 3, were carried out for the cylindrical holder in order to determine the extent of possible diffusion and temperature effects for IGT char HT155

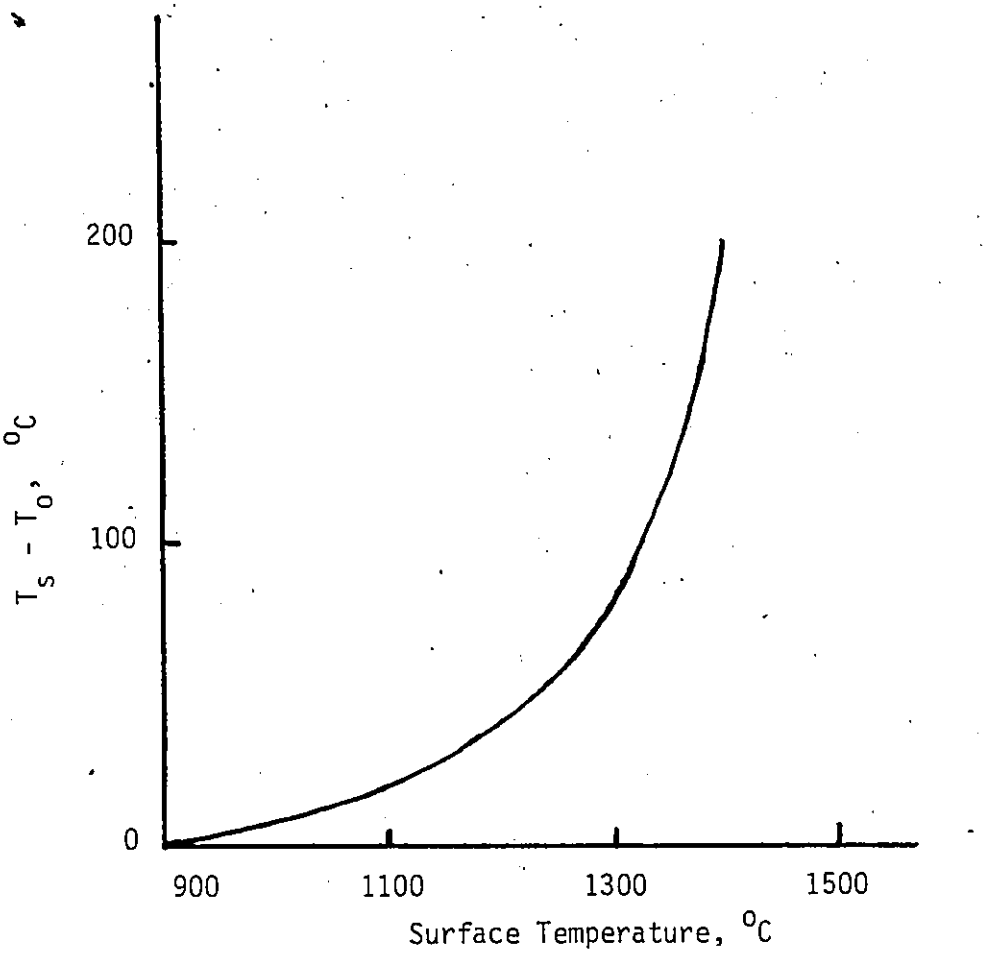

Figure 4-4 Approximate Temperature Difference between surface and center of a coke sphere as affected by temperature of oxidation in CO_2 at 1 atm.. (adapted from Reference 63).

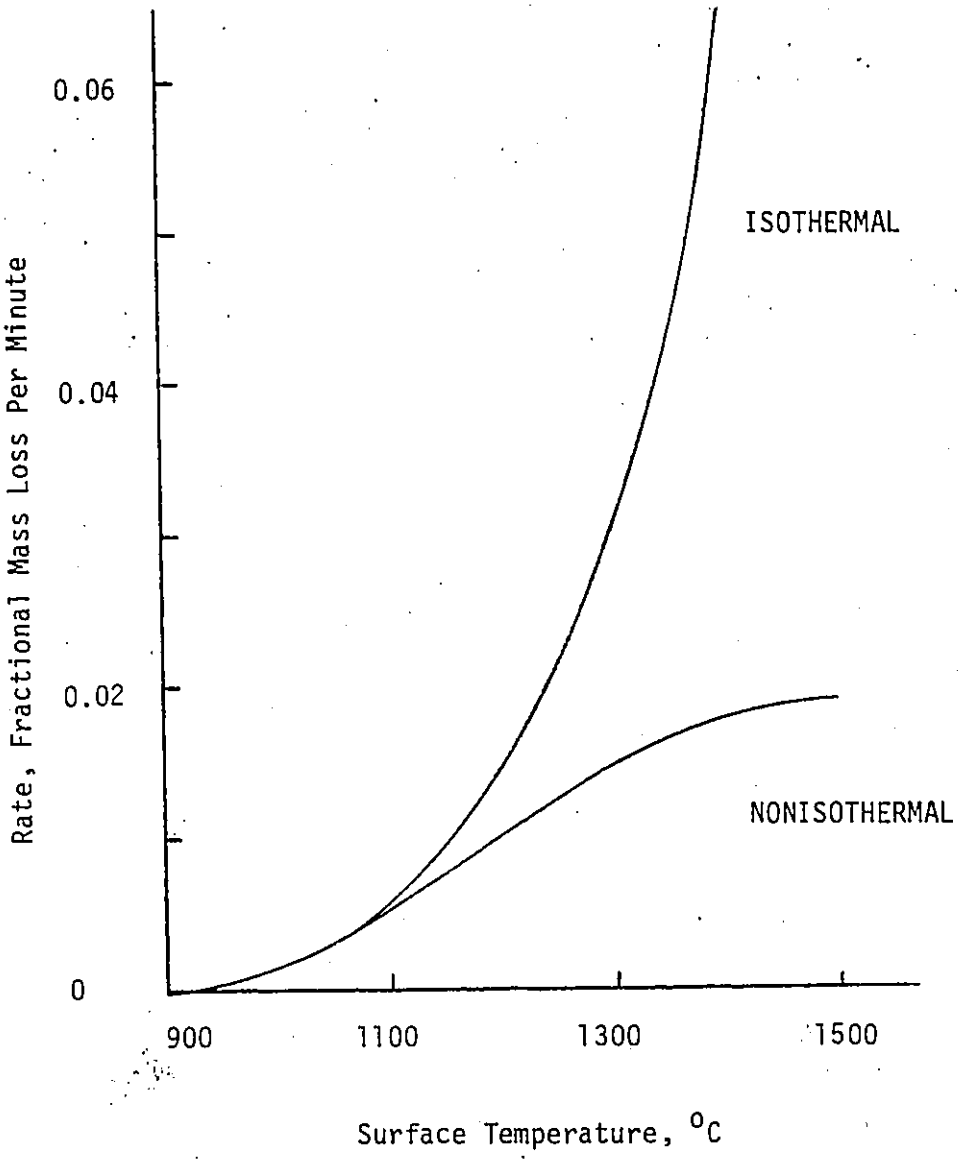

Figure 4-5 Comparison of Computed Rates of Oxidation for isothermal and non-isothermal conditions within the coke sphere (adapted from Reference 63).

TABLE 4-3

Thermogravimetric Balance Sample Holders

SAMPLE HOLDER	SHAPE	DIAMETER	HEIGHT	INITIAL CHAR WEIGHT
A	Petridish	8.5 mm	2 mm	3.75 mg
B	Crucible	8.5 mm	7 mm	18.5 mg
C	Perforated Cylinder	6 mm	15 mm	35.02 mg

reported in their study. These calculations are given in detail in Appendix C. The criteria reveal that although pore and film diffusion do not limit the observed rates, the assumption of isothermality may not be valid. An interphase temperature difference of as much as 20 to 80°C was calculated.

Composition and temperature differences may be present in the bulk gas phase inside the balance unless sufficient agitation is present to fully mix the gas surrounding the sample. This is particularly important for very large porous solid pellets. Costa and Smith[41] in their study of UO_2 describe the use of a modified thermobalance in which a small agitator is inserted close to the reacting solid to ensure uniform gas composition. This method has not been used to my knowledge in any gasification studies. It has not been ascertained as yet how the gas circulation affects the balance mechanism.

There is a large amount of evidence that, although the gas reactions are usually carried out with a gas flow rate sufficiently high that the progress of the reaction is insensitive to flow rate, interphase mass transfer may still be affecting the measured reaction rates. In Section 3.3.2 it was pointed out that this experimental test for film diffusion may be invalid at low Reynolds numbers, which is often the case in thermogravimetric balances. To facilitate mass (and heat)

transfer between the bed of particles and its environment, the thickness of the solid bed should be kept below 3 particle diameters especially for bed weights above 1 gram.[57]. Veraa and Bell[64] studied the catalytic gasification of several chars in steam in an electrobalance. These workers observed diffusional limitations on cylindrical char pellets, 0.13 cm by .3 cm at temperatures above 700°C and steam flowrates of 130 cm^3/min. According to Veraa and Bell, estimates were made of the gasification rates on the assumption that either internal or external mass transfer was rate limiting. No checks were carried out on possible temperature gradients within the pellet or in the film surrounding the pellet.

Otto and Shelef[65] used an atmospheric pressure microbalance to study the catalytic gasification of several coals. This group tried to assess diffusional effects by performing experiments with cylindrical solid specimen supported from the hangwire and with these specimen sliced into several disks (equal weight and diameter of original sample). With some catalysts, e.g. Ru, they found the reaction to be partly diffusion controlled. Rates for gasification were reported on a per unit surface area basis. The SA of the samples was measured in situ before and after gasification.

Otto and Shelef[65], Riede and Hanesian[66] and Pilcher et. al[67] all used very similar thermogravimetric

techniques and operating conditions to study steam gasification of graphite. The experimental details, operating conditions and activation energies reported by these workers are summarized in Table 4-4. The wide disparity in the activation energies reported supports the conclusion that true chemical kinetics are not being observed.

In summary the thermogravimetric method for all its simplicity in quick determination of char reactivity is fraught with limitations. Among these are the large investment required for the recording balance and for the analytical equipment and the uncertainty in weighing in highly sensitive balances when gas is recirculated and solid temperatures are measured. The need to carry out theoretical checks even for small samples in thermogravimetric balances has been demonstrated.

4.1.4 The Fluidized Bed

Bench-scale fluidized systems (Figure 4-6) represent potentially attractive alternatives to fixed bed operations for gas-solid contacting especially since many commercial scale processes for gasification utilize this technique (e.g. Synthane, Winkler, Hygas). The fluidized bed is quite popular in carrying out highly exothermic or endothermic chemical reactions since good solids mixing helps to minimize temperature variations[14]. The data analysis therefore is

TABLE 4-4

COMPARISON OF ACTIVATION ENERGIES FOR STEAM-GRAPHITE REACTION

REFERENCES	REYNOLDS NUMBER	REACTOR INTERNAL DIAMETER [cm]	CONTACT TIME [s]	SAMPLE DIMENSIONS [mm]	SAMPLE WEIGHT [g]	PARTIAL PRESSURE [atm]	TOTAL PRESSURE [atm]	TEMPERATURE [°C]	ACTIVATION ENERGY [kcal/mol]
Otto and Shelef (65)	20	-	-	9mm x 4mm	0.35	0.026	0.15	850-1130	80
Riede and Hanesian(66)	25	3.175	0.3	12.7 x 25.4	5.5	0.09-0.16	1	500-900	16.4
Pilcher et. al (67)	20	2.858	0.25	12.7 x 50.8	8.8	0.04-0.47	1	1000-1100	40
Mayers(42)	-	-	-	-	-	-	-	850-1000	49.7
								1000-1160	35.1

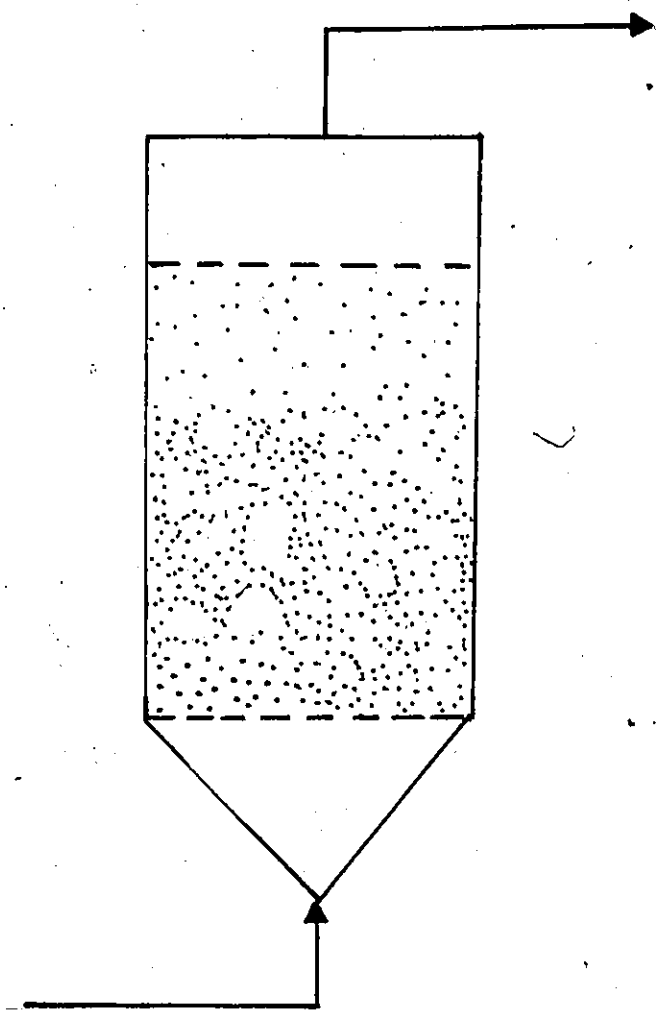

Figure 4-6 Schematic of a fluidized bed

usually based on the assumption that the entire reactor operates isothermally. The large power dissipation entailed in keeping the solids bed fluidized severely limits the particle size that can be handled (> 200 mesh). However, because of the small particles, pore diffusion is usually assumed to be rapid enough not to affect the measured reaction rates. Furthermore, the high gas velocities required for fluidization usually correspond to conditions where external mass transfer is extremely rapid and thus is not thought to affect the chemical reaction rate. The principle drawback for the fluidized bed is that the gas-solids contacting and the degree of backmixing are very difficult to define and so characterization and control of residence times is also difficult. Because of this, data analysis is often based on the assumptions that the solids are completely mixed and the gas flow is either plug flow or completely mixed. Two commonly found departures from the ideal behavior of gas-solid fluidized systems are channeling and slugging. Channeling corresponds to the preferential flow of the gas through certain vertical sections of the bed, thus under these conditions a part of the bed may become fluidized while the remainder stays in a packed state. Slugging, on the other hand, corresponds to the presence of rather large gas bubbles occupying most of the cross-section of the bed, the periodic collapse of the bed as particles fall through these large bubbles would then cause fluctuations in the pressure drop across the bed. It has been shown that[13] in most gas-solid fluidized systems, a portion

of the gas equivalent to the amount required to maintain the bed in a fluidized state is more or less uniformly distributed in the bed (emulsion phase) whereas the remainder passes through in the form of gas bubbles. Gas bubbles have a major influence on the operation of the fluidized systems. Their presence is responsible for the good solids mixing which is a desirable feature but on the other hand, that portion of the gas passing through the system in the form of bubbles is not brought into intimate contact with the bed of particles as is the gas contained in the continuous or emulsion phase. Using the bubbling bed model for fluid beds and a first order catalytic reaction, Levenspiel[23] has shown that the performance of the bed varies considerably depending on the bubble size (Figure 4-7). Even for smooth fluidization (small bubbles) some mixing occurs in the gas. For this state, the dispersion model with a suitable value of axial diffusivity may represent the mixing very well[14]. Large bubbles however do provide a means for the bypassing of the bed. The gas composition when slugging or channeling occurs is far from uniform and the gas enclosed in the bubbles contributes very little to the solid surface reaction thereby reducing the overall conversion. Many models have been proposed to account for the extent of mixing in fluid beds but reliable data for the mixing parameters are not yet available[14].

As noted earlier, another approximate way of accounting for mixing in the nonideal reactor is to measure the

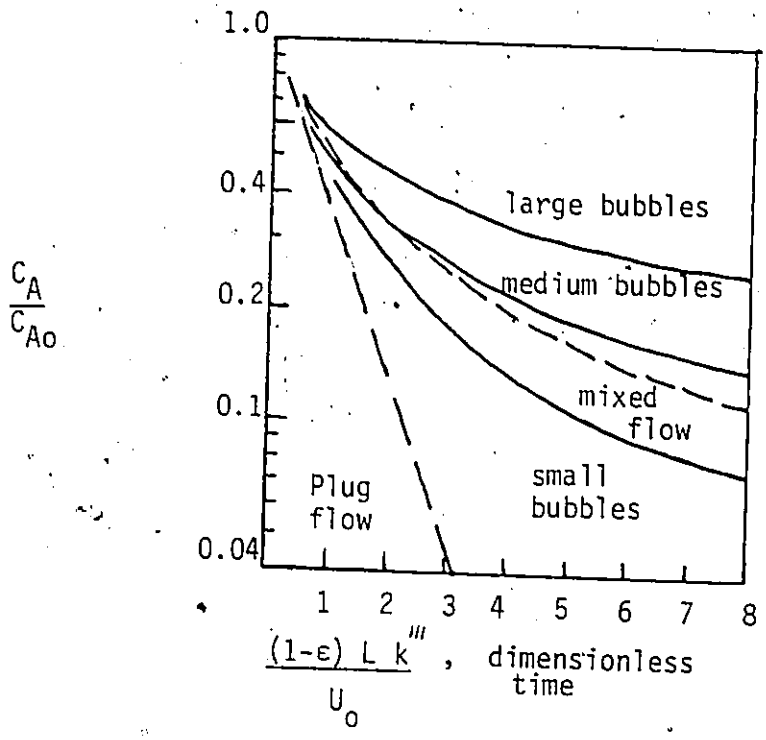

Figure 4-7 Performance of a fluidized bed as a function of bubble size (adapted from Reference 23).

distribution of residence times (gas phase). Gilliland and Mason[70] used this technique in studying the fluidized bed and found ambiguous results because of material transfer between the gas bubbles and the emulsion phase. The experimental findings of gas flow patterns in fluidized beds indicate that most laboratory units operate somewhere intermediate between plug flow and complete mixing and that kinetic results probably cannot be adequately analyzed on either basis.

Heat and mass transfer in fluidized beds can be thought to occur in three categories:

1. heat and mass transfer between the gas in the emulsion phase and the solid
2. heat and mass transfer between the gas in the bubble phase and that in the emulsion
3. heat transfer between bed and reactor walls.

Gas to solid heat and mass transfer rates have been shown to be very high. The region of transfer is confined to a thin layer at the bottom of the bed and the remainder of the bed is in equilibrium with the gas. The thickness of this layer to which effective concentration or temperature gradients are confined is in the order of 6-10 particle diameters[13]. Ayers[71] has experimentally determined gas temperature profiles in a fluidized bed with the solids and gas in crossflow

arrangement. He found that the gas temperature rapidly approached the temperature of the solids in less than 1 centimeter of the bed. Similar findings were reported in the area of mass transfer. Smith[14] has shown in a rough comparison of fixed and fluidized beds that the mass transfer rate between particle and gas for a fluid bed is approximately 2 orders of magnitude greater than that for a fixed bed. With this large transport rate, it is evident that the interphase concentration difference will be negligible. Smith also points out that similar results apply for external temperature differences.

Heat and mass transfer rates between the gas in the bubble and that in the emulsion are not easily evaluated. Overall heat or mass transfer coefficients between the two gas regions must be estimated from correlations or approximated by some other means. The difficulty in predicting these rates arises from the fact that bed properties such as the average bubble size and the ratio of solids in the bubble to volume of the bubble are not readily measurable.

Heat transfer rates between the reactor wall (when heating is supplied at the wall) and the emulsion phase or between the heating elements immersed in the bed (heating coil) and the emulsion phase are very high. Typical heat transfer coefficients range from about 200-600 kcal $m^{-2}h^{-1}C^{-1}$. This represents a major advantage of the fluidized bed for

highly endothermic/exothermic reactions. Nevertheless, for very small diameter laboratory reactors (2.5 - 10 cm ID) the wall effects may be significant. At high temperatures, thermal radiation may also become an important mechanism for bed to wall heat transfer; however, thermal radiation in fluidized beds is unlikely to play a significant role at temperatures below about 1000°C[13]. The foregoing discussion indicates that temperature can be kept essentially uniform in fluidized beds.

A few additional points must be mentioned about the fluidized bed. Because of the mode of operation, the range of operating variables is severely limited (small particle sizes, velocities between minimum fluidization velocity and elutriation velocity, etc). In gasification, the particles diminish in size and become less dense as chemical reaction progresses, these smaller or lighter particles may be elutriated as reaction proceeds. If the reactor is operated in a batch mode with respect to the solid particles, high burnoff may make particle carryover a problem. A preferred procedure would be continuous solids feed and removal. The distribution of the solids residence times will correspond to complete mixing when the fluidized bed height to diameter ratio does not exceed about 3:1[13].

Ergun[72] carried out both steam and carbon dioxide gasification of activated carbon and of graphite in a fluidized

bed and looked at the influence of flow pattern and diffusion on gasification reactions. Ergun emphasizes the importance of evaluating flow conditions in the bed in order to carry out experiments over wide ranges of temperatures and yet prevent nearly complete conversion. He noted that the gasification experiments in his fluidized bed could only be carried out over a limited range of gas flow rates and thorough mixing in the gas phase was not achieved, making it difficult to interpret the kinetic data.

The kinetics of lignite char gasification by steam and steam-hydrogen mixtures was investigated by Curran et. al[73] at 1600°F. The experimental work was carried out in a fluidized bed operated batchwise with respect to the solid charge and continuously with respect to the fluidizing gas. Most of the runs were made with an initial char bed weight of 5 or 10 grams. The char was mixed with fused periclase in order to hold a nearly constant fluidized bed height of 2 1/2 inches regardless of the initial char weight or burnoff level. This group attempted to overcome one of the major limitations of the fluidized bed (i.e. determining the mechanics of the fluid flow) by using a graphical extrapolation procedure to yield differential rate data. These data were obtained from the two integral rates corresponding to initial char bed weights of 5 and 10 grams by linear extrapolation to zero bed weight (Figure 4-8). This procedure, however, also has its limitations since extrapolation far beyond the experimental range is unreliable.

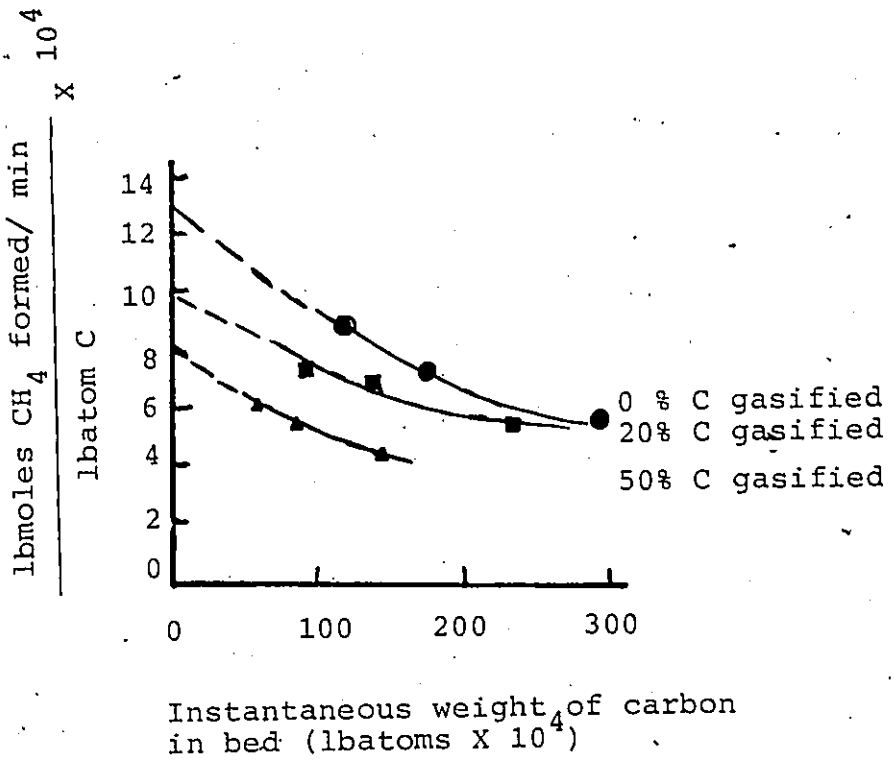

Figure 4-8 Rate of reaction as a function of bed weight. Extrapolation plot to obtain differential methane formation rates. (Adapted from Reference 73)

Johnson[74] has developed specific kinetic correlations for char gasification. The gasification data obtained by Zielke and Gorin[75] and Goring et. al[76] and the bulk of the data obtained in studies at IGT[46] with pilot scale fluid beds and with the thermobalance were used to evaluate parameters over a wide range of conditions in the quantitative model developed. These correlations for low rate gasification were used to predict carbon oxides and methane formation rates by May et. al[77] for batch gasification of Disco char with steam-H_2 mixtures in a fluid bed. In computing these values, it was assumed that the fluid bed was completely backmixed with respect to both gas and solids. It was found that carbon oxide yields were adequately predicted for the systems examined, however experimental methane yields obtained are generally higher than predicted. They give no clear explanation for the discrepancy. Incomplete mixing in the gas phase may have occurred thereby increasing the conversion to CH_4.

Feistel et. al[78] in their study of steam gasification of coal in a small scale pilot plant internally heated fluidized bed found that the reaction rate constants determined from experiments in the fluid bed were somewhat lower than those measured in a laboratory scale differential bed. The reason they suggest is that in the upper layers of the fluidized bed hydrogen (in significant percentages) is present and it reduces the reaction rates.

The fluidized bed has a distinct advantage in that isothermal operation can be maintained under conditions of high heats of reaction. Unfortunately the fluid flow behavior of the bed is not easily characterized and remains a major limitation in its use for gasification kinetic studies.

4.1.5 Transport Reactors

Transport reactors may be divided into two types, the entrained bed and the free fall reactor. In entrained bed gasifiers shown schematically in Figure 4-9a, pulverized coal and/or coal char and gasifying medium are fed cocurrently through a heated tube. The solid particles are thus suspended in the gas and are progressively carried over in the effluent stream. In the free fall reactors depicted in Figure 4-9b, the gas and solids do not have the same residence times and the contacting may be either co- or countercurrent. The objective in these transport reactors, as in the case of the fluidized bed, is usually to obtain data for the purpose of reactor scale-up (Kopper-Totzck, Bi-gas). In the transport reactor, rapid heating is obtained with very short residence times but at the same time sufficient quantities of products are available for analysis (and sometimes for characterizing the flow). Solid particles leaving transport reactors consist of partially reacted particles which are either suspended in the carrier gas and product gas (in the case of entrained beds) or moving independently of the gas stream at some velocity v. The

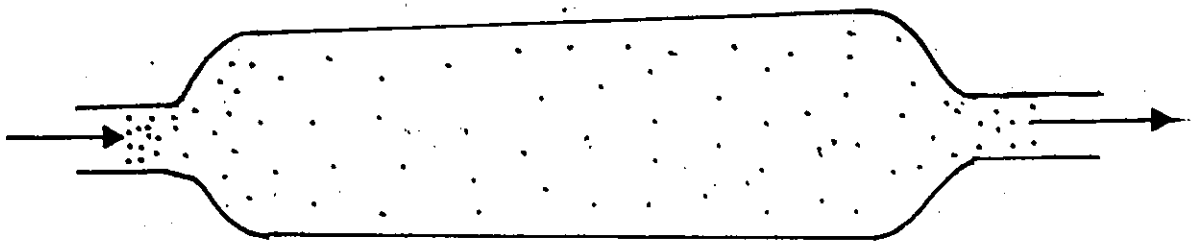

-a-

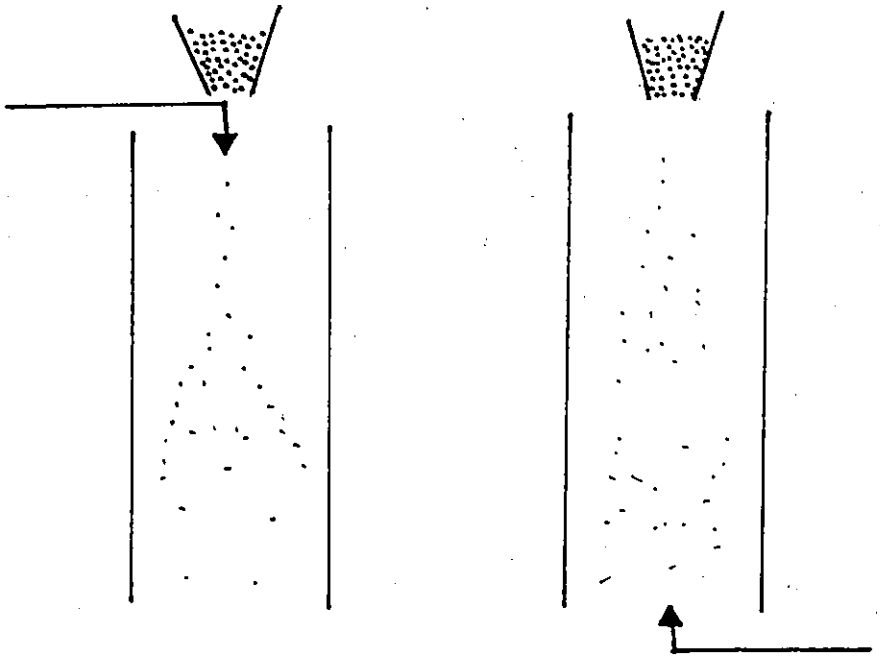

-b-

Figure 4-9 Schematic of a) entrained bed b) free fall reactor

solid particles must be removed from the gas stream by use of settling chambers, filters, condensers, etc. The experimental apparatus is usually quite elaborate.

Coates[81] has studied the kinetics of coal/char gasification in a low-pressure, low residence time (0.012 - .343 s) entrained flow reactor. Finely ground coal was rapidly mixed with oxidizing combustion gases produced from a pre-mixed flame of pure oxygen and hydrogen. Reaction tubes of 4 5/8" in length with inside diameters varying between 3/4 - 2" were tested. The use of smaller diameter reaction tubes permitted testing at lower residence times. The coal was entrained into a stream of carrier gas (either N_2 or H_2) flowing between 13-15 scfh. The reaction temperature was measured but not controlled. It ranged from 1200 - 1400K. The temperature in the reactor (i.e. a nominal gas-solid temperature) increased with the amount of combustion gas fed to the reactor per pound of coal. Figure 4-10 reproduced from Coates publication is a graph of conversion versus reactor residence time without regard for variations in other operating variables. Although Coates draws some conclusions from these graphs, it must be noted that any effect due to residence time would be masked by a moderate temperature change since the primary variable governing the composition of the reactor products is temperature.

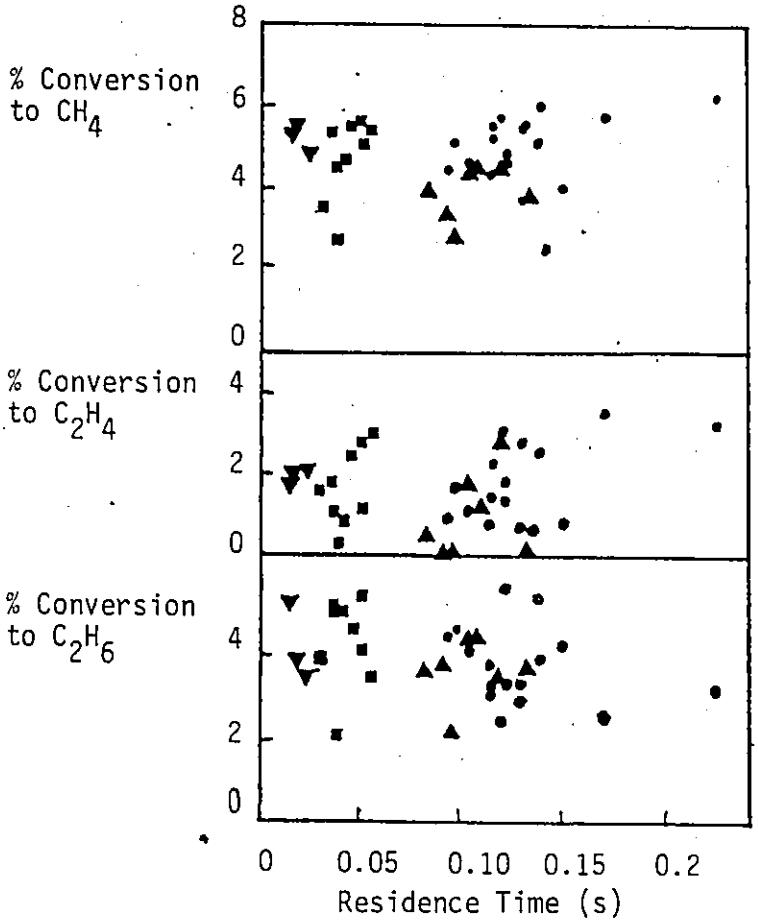

Figure 4-10 Conversion data showing small effect of average reactor residence time.

- • Reactor diameter 2 in, H_2 carrier
- ▲ Reactor diameter 2 in, N_2 carrier
- ■ Reactor diameter 1.25 in, H_2 carrier
- ▼ Reactor diameter 0.75 in, H_2 carrier

Coal feed rate 1.2 lb/hr

In another study, Coates[82] obtained kinetic data from a high temperature entrained flow gasifier. The reaction chamber was 7.6 cm ID by 28 cm in length. Pulverized coal was blown into the top of the reaction chamber with recycled product gas. The recirculation rate near the point where the feed streams were injected was estimated to be approximately 150% of the mass flow of the feed streams. The kinetic data were analyzed assuming the reactor to be completely mixed. Diffusion rates of steam and carbon dioxide to the surface of the char particles were considered by calculating the diffusion limited reaction rates. These were estimated to be of the order of 3000-6000 min^{-1}, several hundred times greater than the measured reaction rates. It is in general reasonable to assume very rapid intraparticle and interphase heat and mass transfer for conditions existing in entrained flow reactors. However, since most transport reactors are long narrow tubes with no external agitation other than that provided by the gas, the completely mixed assumption is questionable.

Johnson[83] discussed the use of a continuous dilute-phase entrained bed in studying the hydrogasification of lignite. The reactor had a unique feature of variable temperature control along the length of the reactor which permits the establishment of various desired gas-solid time-temperature histories. Results were reported for both isothermal conditions and for conditions of constant gas-solid heat-up rate ($50^{o}F/s$) in the temperature range 900-1550^{o}F

and pressures from 18 to 52 atmospheres. The helical-coiled transport reactor measured 1/16" ID with a total length of 200 feet and a vertical height of 2 1/2 feet. The particle size was between 170-200 mesh. Such small particles flowed essentially at gas velocities and calculated temperature differences between the gas and solids and between the reactor tube wall and the flowing gas-solid stream were negligible. This assumption seems reasonable in view of the small particles and provided the apparatus has been given enough time to reach steady state before the run begins. Gas-solids residence times for the isothermal tests ranged from 5 to 14 s. Data analysis was based on the assumption that the gas and solids were in plug flow through the coil and slippage of the solids relative to the gas flow was negligible. Differential conversions were achieved in all experiments by using sufficiently small solid/gas feed ratios (0.02 by volume) in order to facilitate the quantitative kinetic analysis.

In free-fall reactors, the solid particles are usually introduced at the top of the reactor and are allowed to fall through the reactor. Uncertainties arise in the measurement[7] and/or calculation[85] of residence times based on terminal velocities. This is perhaps the most serious drawback of this type of reactor.

Feldmann and coworkers[86] found a simple rate model adequate to correlate hydrogasification data obtained from an

integral free-fall dilute phase reactor. The first-order rate constant k during their investigation depended guite heavily on the type of reactor used as was shown in Figure 1-1. When a differential bed was used to generate low temperature data they observed a wide disparity in reaction rate constants for methane formation. Although some tentative explanations were offered, the assumptions made about the transport reactor (i.e. total backmixing) were never verified.

Dotson et. al[7] used a visual method for measuring solid residence times in their kinetic study of the steam carbon reaction in a free-fall reactor. In these experiments, residence time was the time required for carbon to travel from the feeder bowl at the top of the reactor to a collection plate and this time was measured with a stopwatch. When the residence time was estimated from Stokes law and the linear velocity of the steam in the reactor, the time calculated at 2000^{o}F was 37% longer than the measured time. Furthermore, the longitudinal temperature profile for a 3 in. ID by 6 1/2 ft. long reactor was measured once at nominal temperatures between 1800 - 2500F. These profiles were used to correct the data for deviation from the nominal furnace temperature. It was implicitly assumed that the particle temperatures were identical with these profiles which is not likely when there is a distribution of particle sizes.

One can see from the number and the type of assumptions that have to be made with these reactors that the reliability of the kinetic data is questionable.

4.1.6 Miscellaneous Reactors

While packed beds, thermogravimetric balances, fluidized beds and transport reactors account for the majority of gas-solid contacting schemes, it may be of interest to briefly mention some of the alternate contacting arrangements that have been used. Among these are the spouted bed, the electrofluid reactor, the batch reactor and the diffusion cell.

Spouting refers to a gas-solid contacting process somewhat similar to fluidization. A schematic diagram of a spouted bed is given in Figure 4-11. In spouted beds, the upward motion is very rapid and is restricted to a well defined central core (spout). In the remainder of the bed there is never any upward motion of particles, rather a packed bed moving steadily downward and to some extent inward. This steady motion eliminates backmixing of particles in the annulus. At the same time, the fairly fast bed turnover tends to reduce the temperature differences associated with packed beds. The spouting process does not require the small particles necessary for fluidization however the spouted bed does share some of the disadvantages of the fluid bed, namely, the gas flow pattern and the solid flow pattern are not clearly defined and require

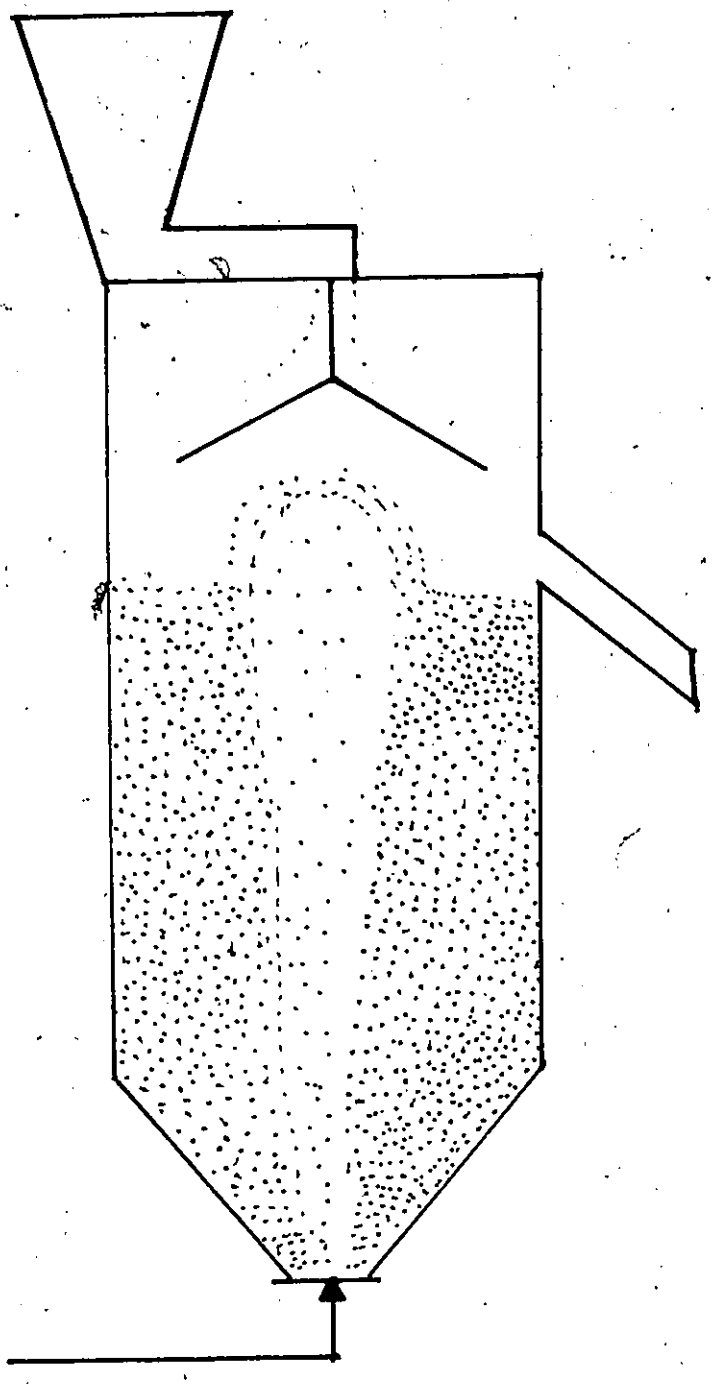

Figure 4-11 Schematic of spouted bed

substantial modelling. Carbonization, pyrolysis and gasification have been carried out using spouted beds[87][88]. A model which predicts the exit char volatile matter from low temperature carbonization of coal in a spouted bed has been forwarded by Ratcliffe and Rigby[87]. Gas composition profiles, temperature profiles and the gas velocity distribution were all measured experimentally in their spouted bed (6" ID by 30" length). At the present time Foong et. al[89] are investigating the possibility of using spouted beds on a commercial scale for steam gasification.

The electrofluid reactor is an electrically heated fluidized bed of conducting solids. It offers several important advantages over the other systems for carrying out reactions which are favored by high temperatures and require substantial energy inputs. These advantages are due to the direct conversion of electrical energy to heat within the reacting system. Pulsifer and Wheelock[90] have investigated the use of such a reactor in steam gasification of chars. The electrical characteristics of the reactor have proven to be very complex and do not lend themselves to accurate analysis. The resistivity of the fluid bed is apparently affected by gas velocity, temperature, particle size and the electrical conductivity of individual particles.

A modified version of the batch reactor has been used by Butler and Snelson[91] in their investigation of coal

gasification. All experiments were carried out using stainless steel tubing .375 inch OD with .035 inch wall thickness and length approximately 8 inches. Water and coal were weighed and inserted into the tube. The air was evacuated from the tube and replaced by argon. The two ends of the tube were welded shut. The tubes were then transferred to a heated oven and the temperature range studied was between 400-700°C. The length of time the sample remained in the oven varied between 15 and 60 minutes. The tubes were then removed from the oven after the allotted time and allowed to cool to room temperature. The reaction products were removed from the reactor and the volume, pressure and temperature of the collected gas were recorded for calculation of product yield and distribution. These experiments are very time-consuming and the exact reaction time is difficult to determine.

A diffusion-cell technique has been used for measuring the chemical reaction rates in the diffusion/chemical reaction combined controlled region in studies of the reaction between CO_2 and both graphite and chars in the temperature range 1200-1600°C[92]. In this method (see Figure 4-12) a solid sample is placed on the bottom of a cell (1-1.6 cm ID, 1-2.5 cm depth). The reactant gas is passed over the open end of the cell. The reaction system is maintained at a constant temperature and pressure. Weight of the cell is continuously measured and recorded on a thermobalance so that the overall rate of the gas-solid reaction can be calculated. The intrinsic surface reaction rate has to be extracted from the

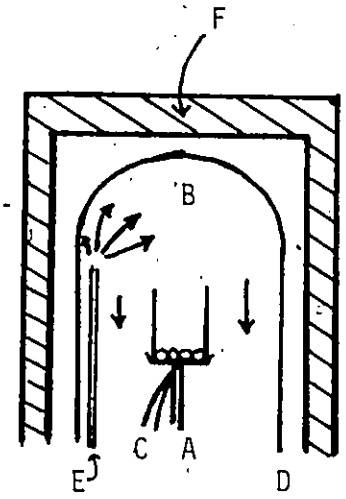

Figure 4-12 Schematic of diffusion cell apparatus

A, to automatic recording balance
B, gas flow
C, thermocouple
D, alumina bell jar
E, alumina bleeder
F, high temperature furnace

solution of the diffusion equations which govern the system. Estimation methods of determining diffusion coefficients in the high temperature range are inadequate and limit the usefulness of this approach in gasification studies.

4.1.7 Summary

A summary of the advantages and disadvantages associated with major bench-scale char gasification reactors used to date is given in Table 4-5. It appears from the reported investigations that the essential design features of bench scale reactors discussed in Chapter 3 are difficult to predict and control in the reactors presently in use. Either the maintenance of isothermality (absence of internal and external temperature gradients) or the assumption of an ideal flow pattern or both are often highly suspect. Bench-scale reactors which were specifically designed to address and facilitate these problems have been in use in catalytic engineering research for several years. The subsequent subsection is devoted to exploring the potential of these so-called 'gradientless' reactors in the study of noncatalytic gasification reactions.

4.2 Selected Alternative Reactor Systems

The term differential reactor refers to a reactor in which the gas conversion is limited to not more than a few percent. Furthermore, the gas and solid composition, pressure and

TABLE 4-5

An Evaluation of Bench-scale Char Gasification Reactors

REACTOR TYPE	ADVANTAGES	DISADVANTAGES
1. Differential Tubular Fixed Bed	. simple to construct and inexpensive . each run gives directly a value for the rate of reaction at the average concentration in the bed . due to small conversions, heat effects will be small, isothermality is more easily maintained . backmixing effects negligible due to low conversions	. small conversions require high analytical precision for product analysis . rate model has limited application to small range of conversion studied . short residence times limit ability to ascertain flow pattern
2. Integral Tubular Fixed Bed	. simple to construct and inexpensive . most closely ressembles large industrial packed bed and useful for modelling their complex operation . finite conversions facilitate analytical analysis . RTD studies may be carried out	. difficult to maintain isothermality (significant temperature variations from point to point especially for gas-solids systems) . channeling and other deviations from plug flow often encountered . high reactor pressure drop . analysis for complex kinetics is very difficult
3. Thermogravimetric Balance	. quick and direct measure of carbon consumption rate (reactivity) . small sample size required . can operate at high temperature and either high or low pressures	. expensive and fragile . low gas conversion does not permit product gas analysis . residence time distribution studies not easily carried out . high balance sensitivity limits gas recirculation rate . different sample holders and sample pellets have shown concentration and temperature gradients

TABLE 4-5

An Evaluation of Bench-scale Char Gasification Reactors (cont'd)

REACTOR TYPE	ADVANTAGES	DISADVANTAGES
4. Fluidized Bed	. direct bench-scale scale-up to industrial reactor (Synthane, Winkler, Hygas, etc.) . fluidization provides rapid heat transfer and thus isothermal conditions can be approached . product gas distribution can be obtained	. gas mixing not well defined even with mechanical agitators (complex dynamics) . limited operating range for gas flowrates . limited particle size for fluidization
5. Transport Reactor	. direct bench-scale scale-up to industrial reactor (Kopper-Totzek, Bi-gas, etc.) . sufficient conversion can be attained for product gas analysis . residence time distribution studies may be carried out	. complicated auxiliary equipment for quick product separation . representative sampling may present a problem . isothermality difficult to maintain . relatively short residence times since high velocities are necessary to avoid slippage . flow patterns for gas and solid must be determined

temperature must be uniform throughout the reactor for true differential operation. A reactor operating in this way is highly desirable for kinetic studies. As discussed earlier a laboratory packed bed reactor may possibly be operated in a differential mode but in practice it is difficult to do so over a very wide range of operating conditions. This limitation as well as the other major drawbacks of the differential reactor (precise product gas analysis required, need for synthetic feeds) can be overcome by the use of an external recycle reactor. This reactor is able to achieve high overall conversions through low conversions per pass. This basic concept of the external recycle reactor has been used to design other reactors for studying gas-solid catalytic reaction kinetics, namely the continuous stirred tank and the internal recirculation reactor. A good discussion of these so-called 'gradientless' reactors can be found in the publications by Carberry[22], Bennett et. al[94] and Doraiswamy and Tabjl[33]. Schematic drawings of these three reactor types are provided in Figures 4-13, 4-14 and 4-15. In each case, a small amount of catalyst is used and the relative velocity of the gas with respect to the solid is increased over that achieved in an ordinary laboratory fixed bed reactor. This improves the heat- and mass-transfer characteristics external to the solid particles. The possibility of using these reactors to study gasification kinetics will now be explored.

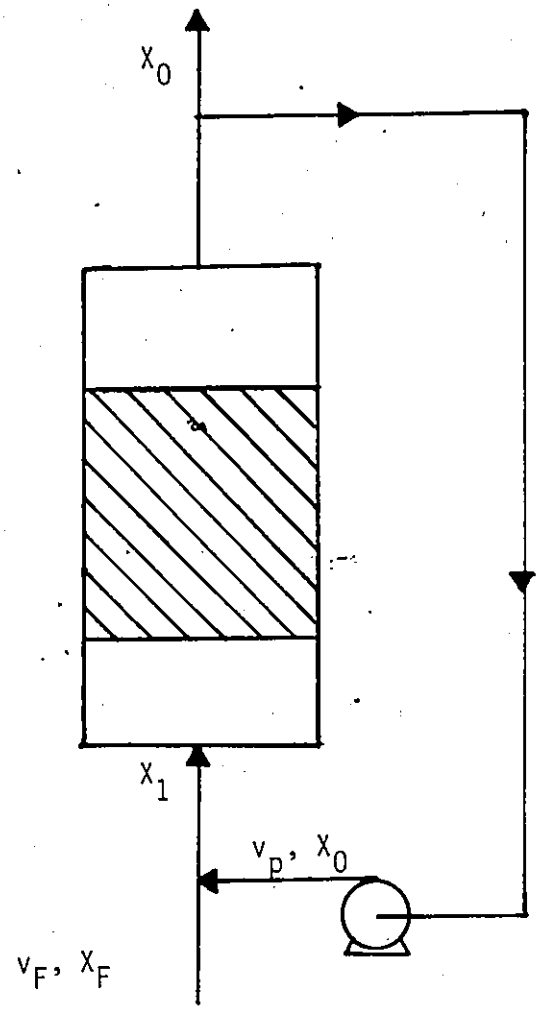

Figure 4-13 Schematic of external recycle reactor

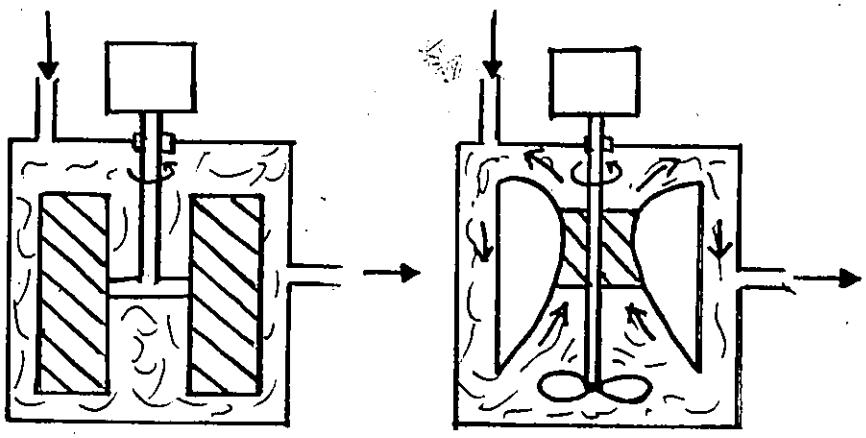

Figure 4-14 Schematic of continuous stirred tank reactor, two versions

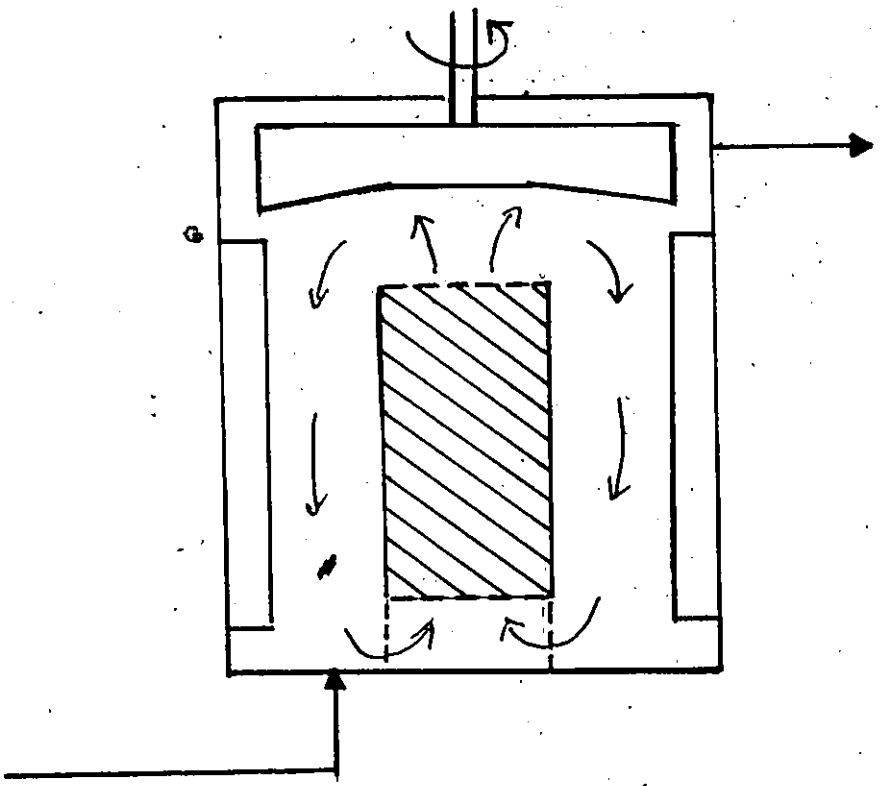

Figure 4-15 Schematic of internal recycle reactor

4.2.1 The External Recycle Reactor

The schematic of an external recycle reactor in Figure 4.13 provides the notation for the following discussion. Feed v_F at conversion x_F is admitted steadily to the system and effluent at conversion x_o is withdrawn at the same rate (assuming no volume change on reaction). Within the loop, a pump recirculates gas at a rate v_p. The conversion rate across the bed of volume V per pass is

$$r_A = \frac{v_p + v_F}{V} \quad (x_o - x_1) \qquad \text{Equation 4-1}$$

The average overall rate based on feed and effluent is

$$\bar{r} = \frac{v_F}{V} \quad (x_o - x_F) \qquad \text{Equation 4-2}$$

By material balance,

$$x_1 = \frac{v_p\, x_o + v_F\, x_F}{v_p + v_F} \qquad \text{Equation 4-3}$$

In order for equation 4-1 to express differential rates, then $x_1 \to x_o$ or in terms of Equation 4-3, $v_p >> v_F$. If the recycle flow is made much greater than the net feed, then the overall rate must equal the rate per pass:

$$r_{A,F} = (x_o - x_F)\frac{v_F}{V} = (x_o - x_1)\frac{(v_F + v_p)}{V} \qquad \text{Equation 4-4}$$

Consequently, while the conversion per pass is differential, overall conversion is integral. One obtains therefore a direct measure of the rate of reaction from the measured difference between inlet and outlet concentrations.

With recirculation rates 10 to 15 times the feed rate, the reactor tends to operate nearly isothermally[22]. High velocities past the bed of particles may eliminate almost completely external mass-transfer influence on the reactor performance. This can be achieved simply by varying the recycle rates to establish the minimum rate beyond which mass transfer effects are negligible. The degree of mixing can be controlled and calculated from the recycle rate. It has been shown[22] that at large values of v_p/v_F (> 25) the reaction proceeds at or very closely to discharge conditions found for the ideal continuous stirred tank reactor.

Finding the limits of the recycle flow rate is a critical point in the construction of a recycle reactor for kinetic studies. If a high recycle flowrate is chosen, which means the internal volumes of pump used and pipes are large compared to the reactor volume, the time needed to reach steady state will be long. If on the contrary, a low recirculation flow rate is chosen, it will be difficult to maintain constant gas concentrations throughout the solid bed. Nystrom[95] discusses the derivation of a criterion for determining the highest recirculation flow rate required in a recycle reactor

in order to be free from gradient effects. The criterion is given below:

$$q > 40 \frac{D_{eff} V (1-\varepsilon)}{d_p^2} \qquad \text{Equation 4-5}$$

where D_{eff} = solid effective diffusivity

V = total bed volume

ε = bed porosity

d_p = solid particle diameter

q = volume flow capacity of pump F/C_T

C_T = total concentration in bulk flow

F = molar flow rate

A critical hardware problem and expense associated with the external recycle reactor is the recycle pump. The recycle pump should have the following characteristics: noncontaminating, leaktight, low hold-up and capable of operating against a moderate back pressure. Some pumps have been developed for specific applications which meet these requirements[96, 97], but a pump which will satisfy the diverse needs of a wide range of conditions characteristic of gasification studies is not available.

An external recycle reactor, in which control of gas concentration was achieved by adjustment of the feed rate, has been used recently to study the kinetics of the carbon-dioxide-carbon reaction[98]. The influences of

reaction temperature, gas concentrations, degree of burnoff and methods of pretreatment upon the reactivity of carbon black were determined. The temperature range for the reaction (900-1200C) made it necessary to separate the reactor bed from the recycle pump. Temperature control in this external recycle system was complicated by the necessity to thermostat several items, viz., the reactor tube, the pump and the recycle loop. Perhaps most important, because of the large volume of the connecting loop necessary for heating and cooling the system components; the system had a relatively slow response to changes. Very little detail is provided in the publication on the experimental apparatus. It is also not known what recycle ratio was used and whether diffusional effects were hindering the progress of the reaction.

4.2.2 The Continuous Stirred Tank Reactor

The continuous stirred tank reactor illustrated in Figure 4-14 has many equivalent design versions. In the Carberry reactor[22] for example, the solid particles are placed in wire mesh containers forming the arms of the stirrer and the whole basket is rotated at high speeds. The agitation promotes good heat transfer and can lead to isothermal operation[22]. The rotational speed (up to 5000 rpm) and the gas feed rate can be adjusted to achieve perfect mixing. The high linear velocities achieved tend to minimize external mass transfer effects. Bennett[94] has demonstrated that residence time

distribution studies can be carried out easily. When the complete mixing assumption holds, a direct measure of the reaction rate can be found by measuring the inlet and outlet gas concentrations as stated below:

$$r_{A,F} = \frac{x_{A,o} - x_{A,F}}{W/F_{A,o}} \qquad \text{Equation 4-6}$$

Since these conversion levels are finite, gas composition can be accurately measured.

The catalyst baskets which have been used vary in form. Figure 4-16 illustrates a few. While the external recycle reactor often poses recycle pump difficulties, the CSTR may often exhibit agitator seal problems especially at high reaction temperatures. This type of reactor does not lend itself to temperature measurements of the solid bed because of the rotation and so the use of this type of reactor is not recommended for reactions involving high heats of reaction (due to the uncertainty in predicting the solid temperature)[33]. A common experimental difficulty of these reactors is how to determine whether all the solids see the gas uniformly. Also, in the Carberry reactor for instance, the bulk mass transfer characteristics may vary substantially between the particles close to the axis and those far from the centre[19]. Since in these reactors, the true gas velocity relative to the catalyst is not known and varies radially as well, it is not

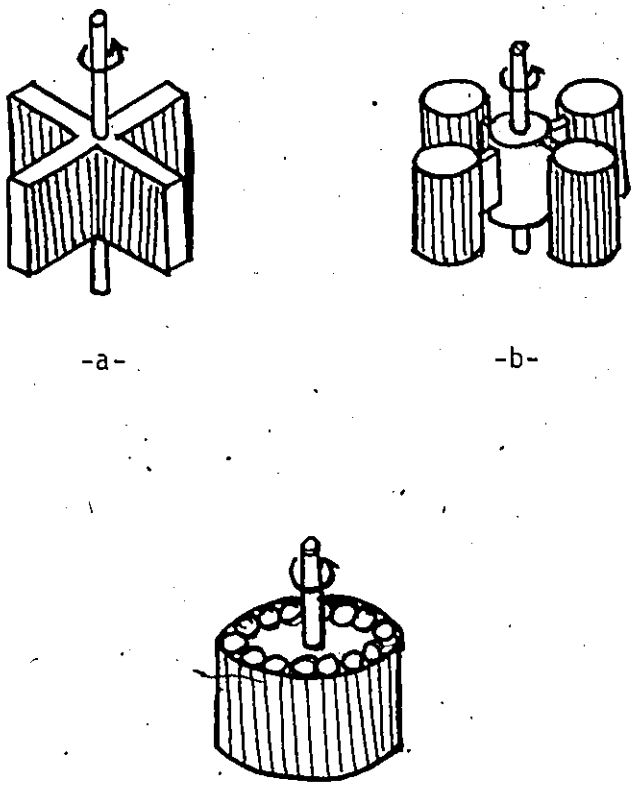

-a-

-b-

-c-

Figure 4-16 Catalyst baskets used in CSTR

a four rectangular paddle baskets for single layer of catalyst pellets

b four cylindrical baskets made of wire mesh for catalyst of any form

c wire mesh circular basket

possible to predict heat- and mass-transfer coefficients. In the revolving basket reactor, one must also ensure that bypassing of the feed gas to the exit does not occur. For a finely powdered solid (and in the case of a shrinking solid reactant) special containment methods must be devised. Although the CSTR has been used successfully in many catalytic gas-solids reaction studies, the disadvantages outlined above make it of limited potential in gasification studies.

4.2.3 The Internal Recirculation Reactor

In an internal recirculation reactor, gas phase mixing is achieved by recirculating the reaction mixture through a stationary solid bed using a specially designed impeller. Berty[99] has demonstrated that the recirculation rate may be determined by the rotational speed of a centrifugal blower mounted on the top or bottom of the solid chamber. The flow rate of the reacting mixture and the degree of recirculation through the catalyst bed are well defined quantities for these reactors and the actual rate of internal recycle can be estimated by experiment[99]. Well-mixed isothermal conditions can be achieved with proper choice of impeller speed, gas flow rate and particle size. Internal recirculation reactors have proven to be versatile and have been employed in a number of gas-solid catalytic reactions successfully. The solid particles can be of any form or size since the solid bed

is stationary. Nominal bed temperatures can also be measured. Heat- and mass-transfer rate correlations obtained in a fixed bed reactor can be applied to this type of reactor to determine possible diffusional resistances. In comparison with the CSTR, an internally recycled reactor possesses two merits of some practical importance. First, the mounting and replacement of the solid is more simply carried out without any danger of unbalancing the stability of the rotating parts. Second, the effect of imperfect mixing in the internal recycle reactor can be estimated from a knowledge of flow rate through the solid bed[33]. Residence-time distribution studies can also be carried out with this reactor to determine flow pattern. As in the case of the CSTR, a direct measure of reaction rates result from the difference between inlet and outlet reactant gas concentration.

Two technological problems emerge in the design of an internal recycle reactor because of the insertion of an agitator shaft into the reaction chamber. The first problem is to protect the shaft bearing from overheating when high temperature reactions are studied. This problem may be solved by cooling the bearings or by using a long shaft with the bearings placed at one end safely removed from the high temperature zone. Both these methods of tackling the overheating problem have limitations and use of one method or the other depends upon the specific reaction conditions. The second problem is to seal effectively against leakage along the

shaft and along the reactor/shaft connections. The sealing problem for high pressure studies at moderate temperatures (500°C) has been solved using a magnetic drive[100]. However, high temperature sealing still presents a challenge.

Mahoney[100] has employed a version of the internal recycle reactor modified for operation at high temperatures and pressures (1100°F maximum up to 1000 psig, 1000°F maximum up to 2000 psig) which are prevalent in petroleum processing. The studies were concerned with the reactions of n-heptane catalyzed by a commercial platinum-on-alumina catalyst. Process conditions were constant so that the catalyst deactivated at a constant temperature and pressure. Experiments were conducted using particles which ranged from 1/12 inch extrudates to small 40 mesh particles.

Berty[99] has recommended that a lower pressure limit of 45 psig be used "because at lower pressures and corresponding low gas densities it is difficult to maintain good mass velocities". High mass velocities are required to minimize the thickness of the stagnant boundary layer between the external catalyst surface and the bulk gas phase. Kuchcinski and Squires[116] however have shown that the internal recycle reactor can also be used at low pressure i.e., 1 atm, provided certain conditions are met. They found that the reactor could behave as a perfectly mixed vessel when the recycle ratio was greater than about 20.

4.2.4 Summary and Conclusions

The differential reactor with recirculation by means of an external pump, the stirred tank reactor and the internal recirculation reactor have been described and discussed in view of pointing out the major merits and demerits of these reactors for undertaking gasification kinetic studies. A summary of these findings is given in Table 4-6. The most important basic requirement of these reactors is that they should be operated under gradientless conditions. Physical measurements should therefore be carried out in order to evaluate the reactor behavior both with respect to the heat and mass transfer and mixing characteristics under different conditions of flow rate and stirring speed. Except for construction difficulties the internal recirculation reactor shows great potential in gasification studies. An internal recirculation reactor has been constructed in order to evaluate this potential for investigating gasification kinetics. The design, development and testing of the reactor are the subject of the following chapter.

TABLE 4-6

Alternative Bench-scale Char Gasification Reactors

REACTOR TYPE	ADVANTAGES	DISADVANTAGES
1. External Recycle Reactor	. high degree of overall conversion can be obtained with essentially differential conversion per pass . isothermal operation possible . concentration gradients are easily minimized (with sufficiently high recirculation)	. critical hardware problem and expense to obtain a noncontaminating, leaktight, low hold-up pump that withstands moderate temperatures . for low recirculation rates many of the disadvantages of the integral tubular bed exist
2. Continuous Stirred Tank	. agitation promotes good heat transfer and leads to isothermal operation . RTD studies easily carried out direct measure of reaction rate . integral conversions simplify analysis of product composition	. surface temperature of solids difficult to measure . solids may not "see" bulk gas uniformly . containment of small particles difficult (especially at high conversions) . construction complicated by mechanical moving parts
3. Internal Recirculation	. well-mixed isothermal conditions can be achieved . sampling and product analysis are simplified . RTD can be accurately measured . solids temperature can be measured . fixed bed heat-and mass-transfer correlations can be used	. difficult construction, mechanical difficulties include protecting the shaft bearing from overheating and sealing effectively against leakage along the shaft

5. TESTING AN INTERNAL RECYCLE REACTOR

5.1 Introduction

An internal recirculation flow reactor was constructed in order to investigate its potential in overcoming the shortcomings of the current bench-scale reactors used for studying char gasification kinetics. Descriptions of the reactor and its operation are given in the following sections. An evaluation of the reactor performance based on the results of tests carried out to determine mixing characteristics and possible temperature gradients within the reactor is presented. As a result of this evaluation no gasification runs were performed with the experimental set-up. A description of the ancillary equipment required to carry out steam gasification at atmospheric pressure and high temperatures as well as a product analysis system is nonetheless provided for future work with a modified version of this reactor or with alternate reactors.

5.2 Experimental Equipment and Materials

The experimental equipment set up in the present study is shown in Figure 5-1. It consists essentially of an internal recirculation reactor, a heating system, a system for generating steam and varying the steam partial pressure, equipment for removing unreacted steam and facilities for sampling, metering and analyzing the product gases. Each of these will be described in detail subsequently.

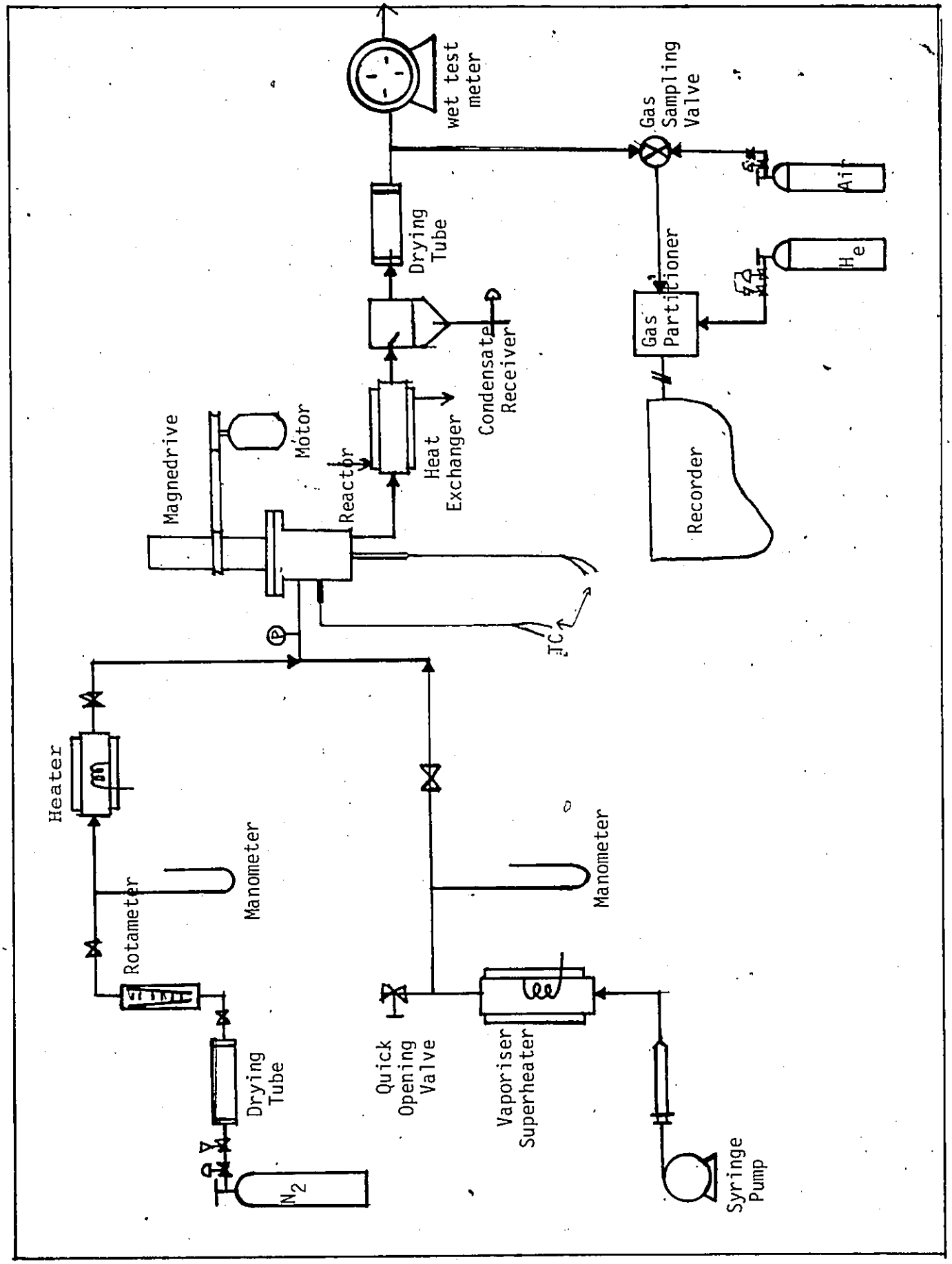

Figure 5-1 Schematic of experimental apparatus

5.2.1 The Reactor

The bench-scale internal recirculation reactor used in the present study is shown in Figure 5-2. The two components of the reactor assembly are the stirrer drive unit with stirrer shaft and the reaction vessel. A detailed view of the reaction vessel internals is provided in Figure 5-3. The reactor shell was constructed of 316 stainless steel which can withstand temperatures up to 1100°C at moderate pressures. The cylindrical vessel measured 17.8 cm by 5.72 cm outer dimensions. The total free volume of the reaction vessel was 30 mL $\pm$ 1 mL and the volume available for the solids is 14.5 cm^3. Up to 15 grams of char could be charged in the annular solid basket (7.6 cm height, 1.6 cm OD, .3 cm ID). The solid was supported by a fine mesh stainless steel screen. Four vertical baffles were placed at right angles to one another on the inner wall of the chamber. The feed gases entered the reaction chamber at constant rate through a 0.16 cm inlet port at the top of the vessel and the product gases left through a 0.16 cm outlet port at the side of the reactor. The gas in the chamber was recirculated by means of a flat-blade impeller mounted at the top of the chamber. A schematic of the impeller is shown in Figure 5-4. A thermowell was fixed inside the annular basket to permit temperature measurement with a chromel-alumel thermocouple embedded in a stainless steel tube sheath, throughout the height of the solids bed. A second chromel-alumel thermocouple inserted horizontally through a

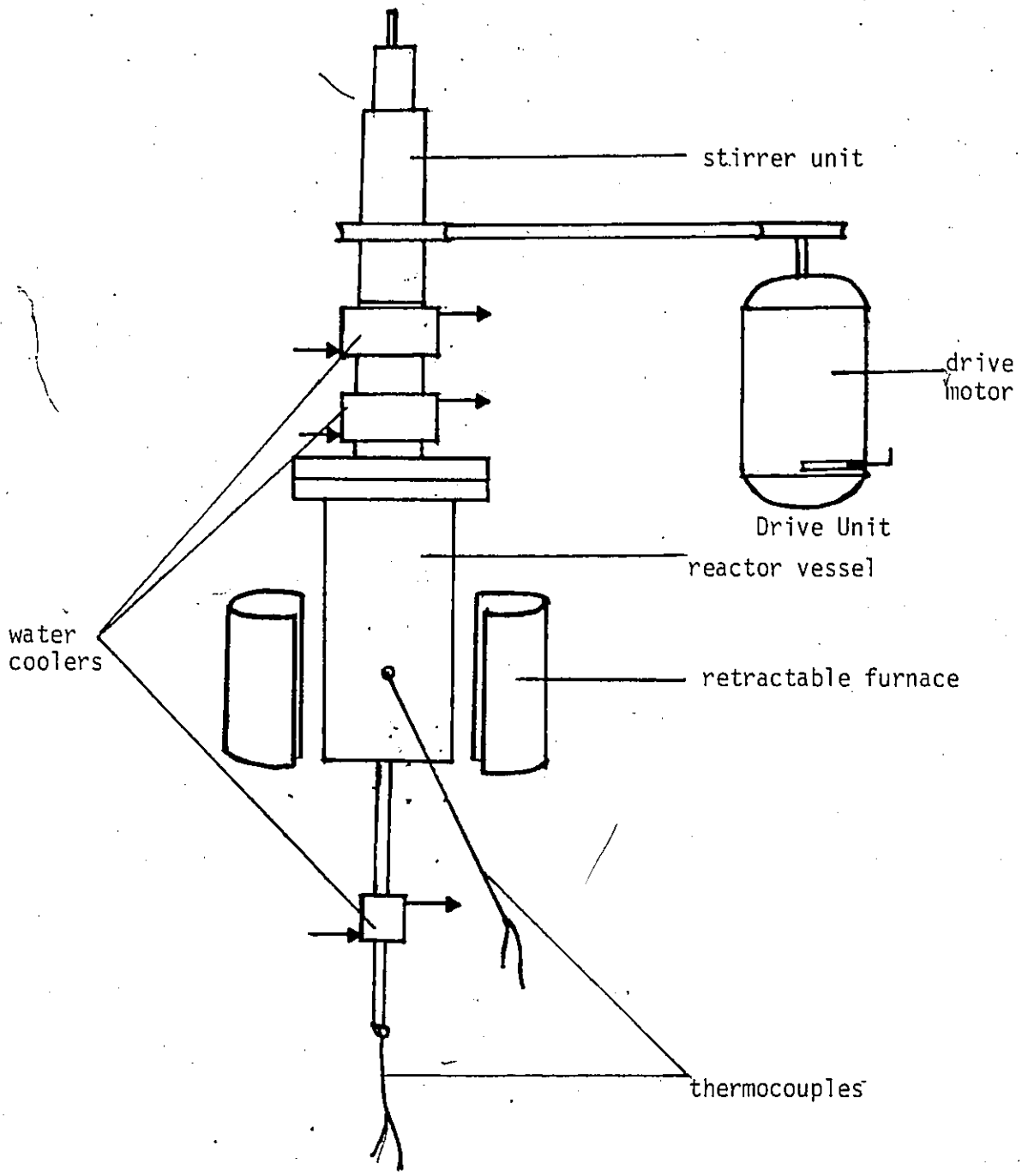

Figure 5-2 Reactor Assembly

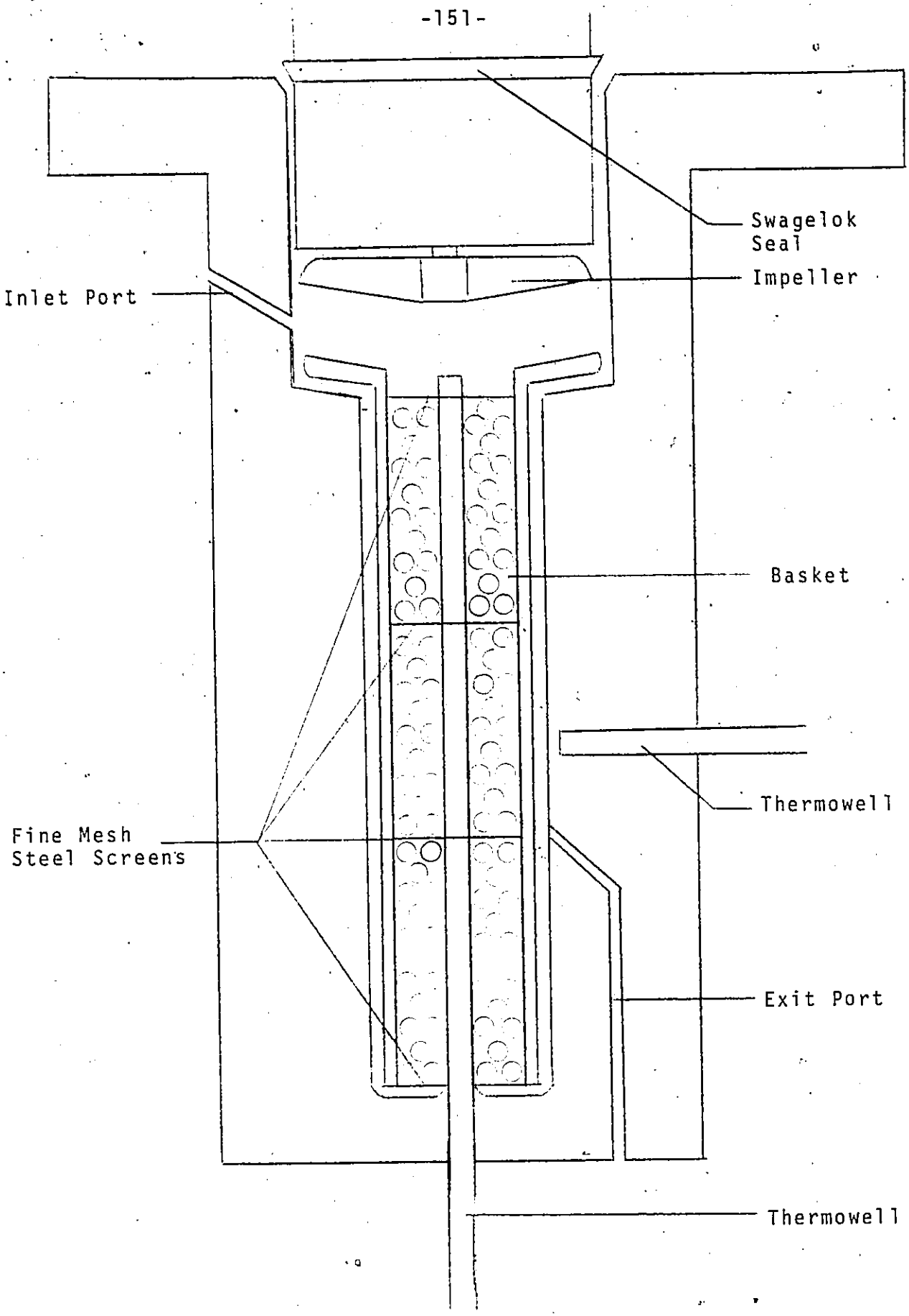

Figure 5-3 Reaction Chamber Internals

Scale 1 cm = 0.25 inch

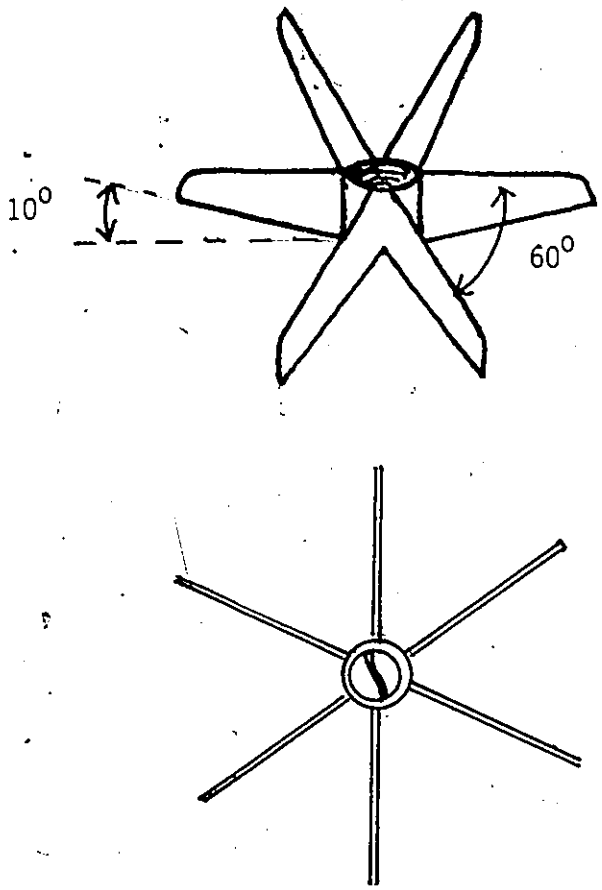

Figure 5-4 Impeller

nole in the side of the furnace with the hot junction placed against the outside wall of the reaction chamber was used for temperature control purposes.

A completely sealed, magnetically coupled drive was used to rotate the impeller at speeds up to 1900 RPM. Since the standard magnedrive assembly supplied by Autoclave Engineers can withstand a maximum temperature of about 600°F. A modified version of this assembly was used, a schematic of which is given in Figure 5-5. There are two ways of protecting the shaft bearings (graphite or teflon) from overheating when high temperature reactions are studied. The first way is to cool the bearings with water jackets and the second is to use a long shaft with the bearings placed at one end safely removed from the high temperature zone. Both methods were combined in an effort to minimize the inherent weaknesses of the solutions when used separately. The magnedrive is bolted to the reactor and a stainless steel ring, similar to a "Swagelok fitting", at the top of the neck of the reactor vessel prevents gas leakage along the joining flange even at high temperatures.

Heating for the reactor was supplied by 2 semi-cylindrical 0.1 m long Lindberg furnaces (model 5010-1063-00A) which could attain temperatures of 1200°C. Because of the length of time required for this short heater to reach temperatures of the order of 1000°C (4 hrs), a booster heater which consisted of a tightly wound coil of resistance elements was embedded in the insulation surrounding the furnace. Electrical leads from the

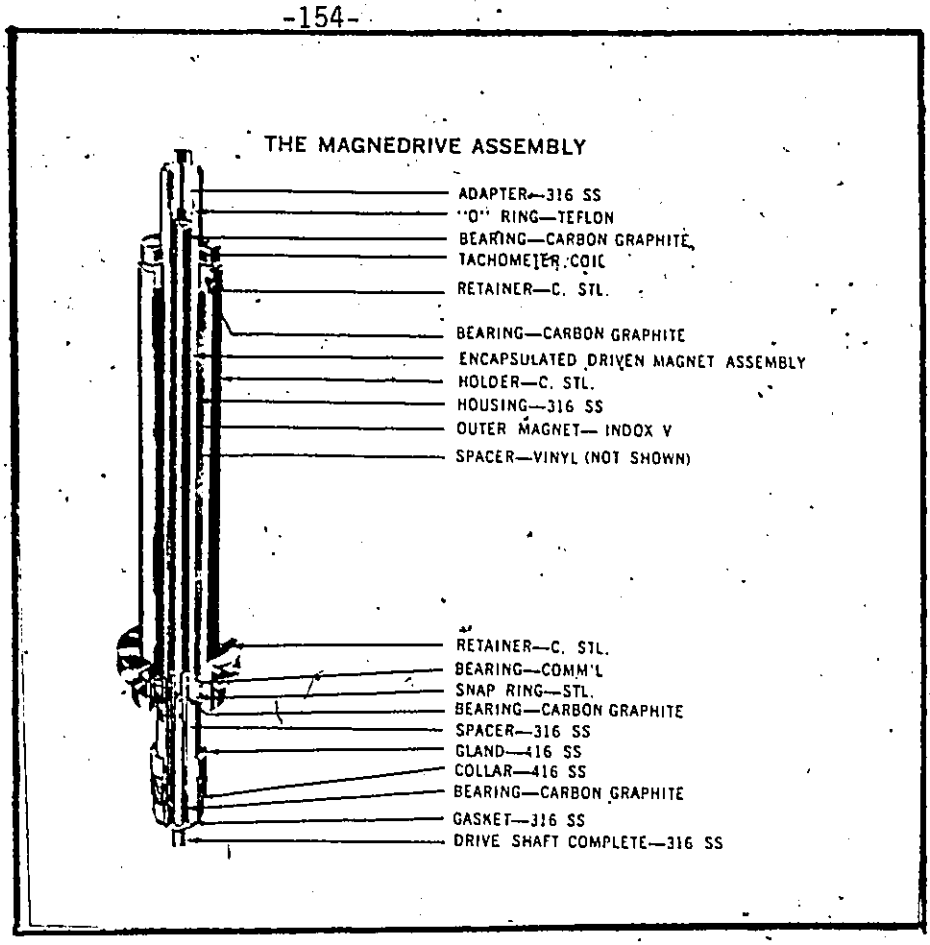

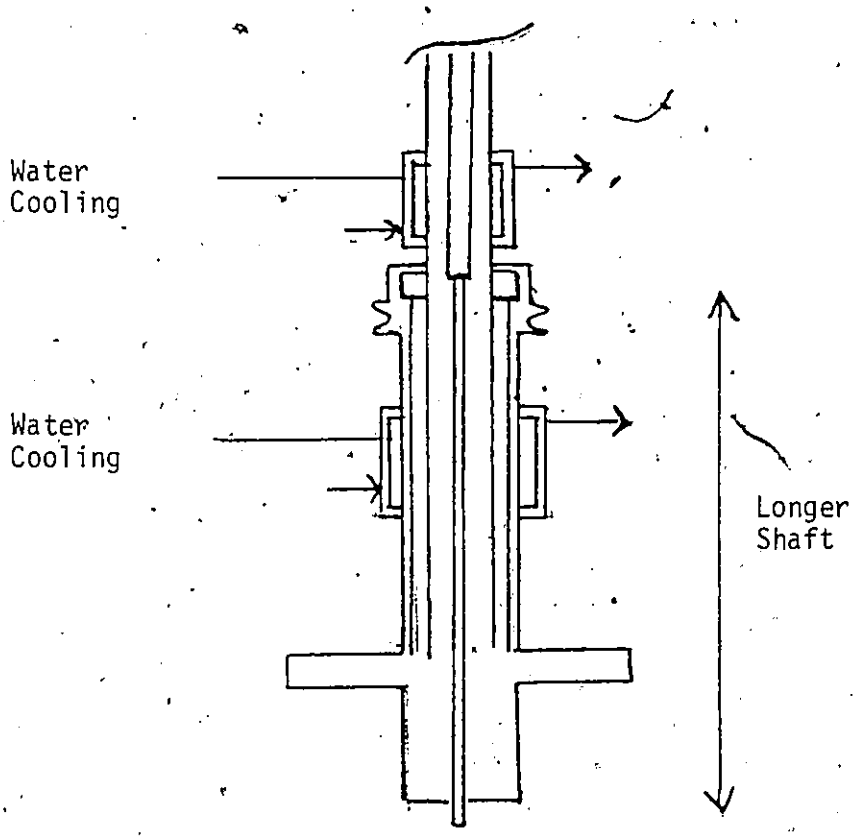

Figure 5-5 Modified Magnedrive Assembly

Lindberg heater were connected to an automatic on-off Honeywell controller actuated by a type K thermocouple. The current to the booster heater was controlled manually with voltage step-down through a rheostat.

Kaowool blanket and Kaowool bulk fibre were used to insulate the reactor/heater system. Kaowool, a trade name for ceramic fiber provided by Babcock and Wilcox, is non-combustible, has a low thermal conductivity and maintains its structural integrity up to 1300°C.

5.2.2 The Feed System

Distilled water, stored in three 20 milliliter gas tight syringes was supplied at constant flow rate by a syringe pump to an electrically heated vaporiser-superheater where steam was generated and superheated ($\sim$ 300°C). The Sage Model 355 syringe pump offered a continuously variable flow range. The pump was calibrated with the syringes to deliver the required water flow to the superheater (0.002 - 0.02 gm/s). The vaporiser-superheater was made from stainless steel tubing and measured 0.013 m ID by 0.3 m in length. The syringe needles were welded to the superheater at one end and the other end of the heater was fitted with a quick opening valve. The entire vaporiser was packed with crushed quartz particles (.004 m - .006 m diameter). The tube was wound with a heating coil connected to a variable transformer and insulated with 0.06 m of Kaowool.

Nitrogen could be circulated through the reactor during the heat-up time and could be used as the inert gas in the experiments. The inert gas supply train consisted of a tank of high purity nitrogen which discharged to a 0.15 m long drying tube (0.01 m ID) containing indicating drierite ($CaSO_4$) followed by a 0.3 m long purifying tube containing copper turnings (to remove traces of O_2) maintained at 300°C. The nitrogen flow was measured with a Matheson type 602 rotameter in the (0-3 L/s) range. The rotameter was calibrated against a standard wet test meter. The gas was passed to the vaporiser-superheater if H_2O / N_2 mixtures were to be used or directly to the reactor during the warm-up period. The process line connecting the vaporizer to the reactor inlet was wound with insulating tape to prevent condensation of the steam.

5.2.3 Product Analysis

The product gas, steam and inert diluent gas at the reactor exit could be carried through 0.3 cm ID stainless steel tubing to a double-pipe heat exchanger for condensation of the unreacted steam. The condensate was collected in a 60 ml plastic receiver which could be emptied regularly. The product and diluent gases were separated from the water in the condensate collector. The main stream of effluent gases was subsequently passed through a 20 cm long 1.25 cm ID drying tube filled with anhydrous calcium sulfate (Drierite) and through a calibrated wet test meter. Experiments were carried out to

investigate whether reaction products such as CO and CO_2 would be adsorbed on the Drierite. These experiments described in Appendix D determined the allowable size of the drying tube. A small gas stream was continuously sent through a sampling valve for analysis. Sampling of the gas at 12 minute intervals was achieved through an air actuated 6 port automatic Valco sampling valve with a loop volume of 0.5 mL and a digital timing system provided by Chromatographic Specialties (Digital Valve Sequence Programmer).

A system for product gas analysis was designed, calibrated and tested although no gasification runs were performed. This system will form the basis of product analysis systems for future work and thus will be described briefly.

The gas samples were analyzed on a Fisher-Hamilton Model 29 dual column/dual detector gas partitioner. The detector was kept at a nominal temperature of 70°C and the cell current maintained at 225 ma. Helium supplied at 18 psig and a flowrate of 40 cm^3/min was used as a carrier gas. The chromatographic system consisted of 3 columns kept at ambient temperature as shown in Figure 5-6. The first column consisted of 2.4 meters of .64 cm ID aluminum tubing packed with 30% DEHS on 60/80 mesh Chromosorb P. Its function was to separate CO_2 from the other gases in the mixture. The gas sample thus separated was detected and recorded as two successive peaks, one for the mixture of nitrogen, oxygen, carbon monoxide,

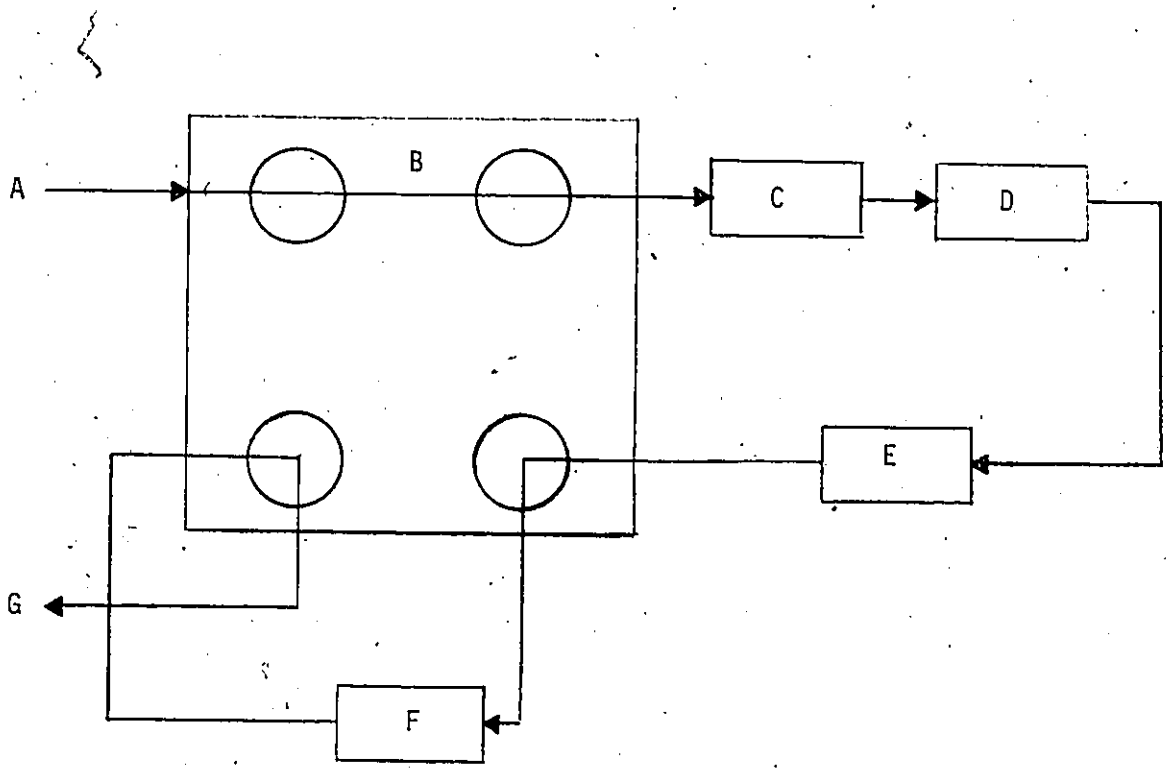

Figure 5-6 Chromatographic system for product gas analysis

A Carrier gas inlet	E Column 1
B Reference	F Columns 1 and 2
C Sample Inlet	G Exhaust
D Drying Tube	

FIGURE 5-3

REACTION VESSEL

hydrogen and methane and one for the carbon dioxide respectively. The columns in position number 2 were in series and consisted of 1.8 meters of .64 cm ID copper tubing packed with 60/80 m Chromosorb W followed by 1.22 meters of .64 cm ID copper tubing packed with 60/80 mesh Molecular Sieve 13X. The molecular sieve column separated H_2, O_2, N_2, CH_4 and CO in that order. However because of the short length of the molecular sieve column used, a spacer column was needed so that the time for hydrogen elutriation was far enough from the CO_2 peak to enable detection. Since the Chromosorb W packing is inert, Column 2 served as the delay column. This column therefore ensured that the first peak from column 3 (H_2 peak) did not overlap with the CO_2 peak on a chromatogram.

Since the DEHS and MS 13X columns readily adsorb water (103) a process which gradually causes deactivation of the column and results in the loss of separation of the gases, reactivation or conditioning is necessary. Column 1 was conditioned at 100°C overnight housed in a Varian Model 1400 Gas Chromatograph and Column 2 was conditioned at 325°C overnight in the same chromatograph. Helium gas was allowed to flow through the columns during conditioning at a rate of 10 cm^3/min.

Complete gas mixture separation was accomplished in approximately 10 minutes. A typical chromatogram for a prepared gas sample is shown in Figure 5-7. Gas concentrations

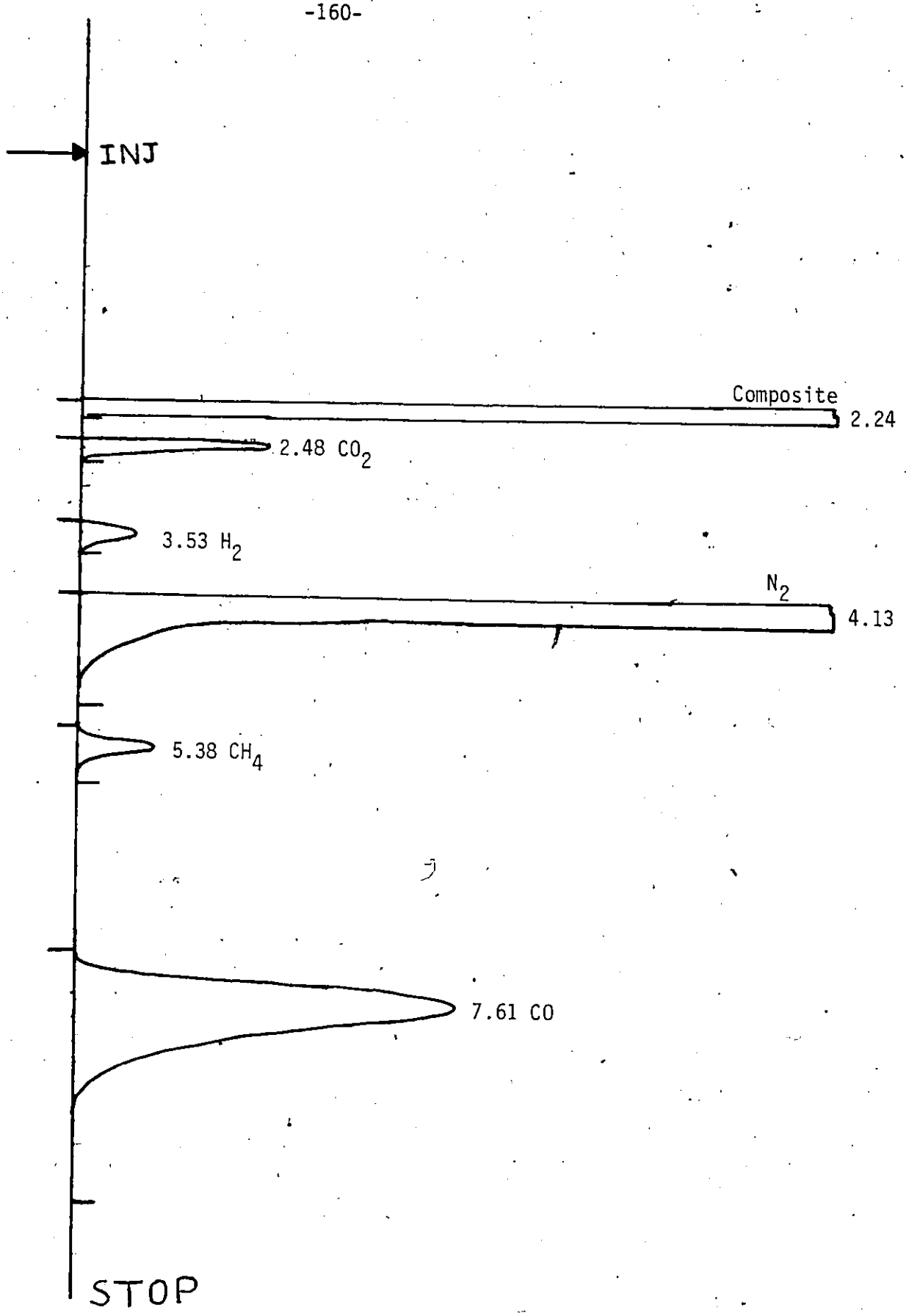

Figure 5-7 Typical gas separation and analysis

could be determined from a chromatogram obtained on a Hewlett-Packard Model 3380S integrator with the aid of calibration curves. There are several procedures available for gas calibration, namely direct calibration, internal normalization and normalization of areas (correction factors). The method adopted here is direct or absolute calibration. Blends of the components (H_2, CO, CO_2, CH_4, N_2) were prepared and chromatograms were made with these mixtures. The value of the peak area was then plotted against the amount of sample injected, thereby determining the calibration factors. Once these factors were known the actual amount of component in an unknown sample could be calculated from peak area and sample size. This method is especially useful for gases since blends of exactly known composition are not easily made. A method of injecting a known fixed sample size (0.5 ml sample loop, 1 psig pressure) was used as described in detail in Appendix E. The main disadvantage of this procedure for calibration is that calibration is time consuming. Also, frequent spot checks are necessary since the sensitivity of the detector must remain constant from run to run and day to day in order to compare results with the calibration graph. After screening experiments, when the composition range of the reaction product gas is more or less known, the most exact analysis of the mixture may be obtained by comparison of the chromatogram with chromatograms obtained from synthetic mixtures of approxiately the same composition. Analyses of two synthetic mixtures prepared by Matheson Gas Products are also given in Appendix E.

5.2.4 Materials

The char used in this investigation was prepared from Byron Creek coal by a devolatilization technique described in detail in Appendix F. The coal and coal char analyses are presented in Table 5-1 and 5-2 respectively. Char obtained from a sub-bituminous 'A' (Forestburg) coal was used in some of the preliminary experiments. It was obtained from Dr. B. Lu, University of Ottawa.

Indicating Ascarite II (8 mesh) was supplied by the Arthur H. Thomas Co., Philadelphia, USA and indicating Drierite (8 mesh) was supplied by Chromatographic Specialties, Brockville, Ontario.

Gases used for calibration purposes and for mixing studies were all high purity or ultra-high purity grade (99.8% min) supplied by Matheson Gas Co., Whitby, Ontario.

5.3 Gas Phase Mixing Tests

Residence time distribution studies were performed on the bench-scale internal recirculation flow reactor described in Section 5.2.1 in order to determine the operating conditions (agitator speed, gas flow rate, solid particle size) under which the completely mixed assumption prevailed. To investigate the degree of mixing in the gas phase of the

TABLE 5-1

ANALYSIS OF BYRON CREEK COAL

		As Received
Moisture	%	1.99
Ash	%	14.96
Volatile	%	25.69
Fixed Carbon	%	57.36
Carbon	%	72.96
Hydrogen	%	4.23
Sulphur	%	0.78
Nitrogen	%	1.13
Ash	%	14.96
Oxygen (by diff)	%	3.95

TABLE 5-2

ANALYSIS OF BYRON CREEK CHAR

		As Received
Moisture	%	1.14
Ash	%	21.5
Volatile	%	3.50
Fixed Carbon	%	73.86
Carbon	%	74.5
Hydrogen	%	0.952
Sulphur	%	0.32
Nitrogen	%	1.28
Ash	%	21.5
Oxygen (by diff)	%	-

reactor, the classical stimulus-response experimental technique was used. For ease of experimentation and data analysis, the response of the non-reacting system to a step change in feed gas composition was monitored and modelled. Normally, for relatively large reactor volumes the dynamics of the measuring device (which usually have fast responses) can be ignored. However, for the small laboratory reactors the response time of the measurement device can be of the same order of magnitude as that of the reactor itself (1-2s). No evidence that this problem has been tackled by other workers could be found. It was necessary therefore, in this study to use a different approach with respect to the analysis of the step response data. The approach adopted here to handle the problem of deriving the RTD of the reactor when the measuring instrument dynamics are included is to model the two contributions to the experimentally measured response curve separately. Appropriate models were therefore found to simulate the behavior of both the instrument and the reactor. In this section, the experimental procedure, the basic approach, the instrument model, the reactor model, the data analysis and the mixing test results are discussed.

5.3.1 Experimental Apparatus

The experimental scheme adopted to impose the step change in inlet gas composition is given in Figure 5-8. To generate step changes, a 4-way manual switching valve was used. Known

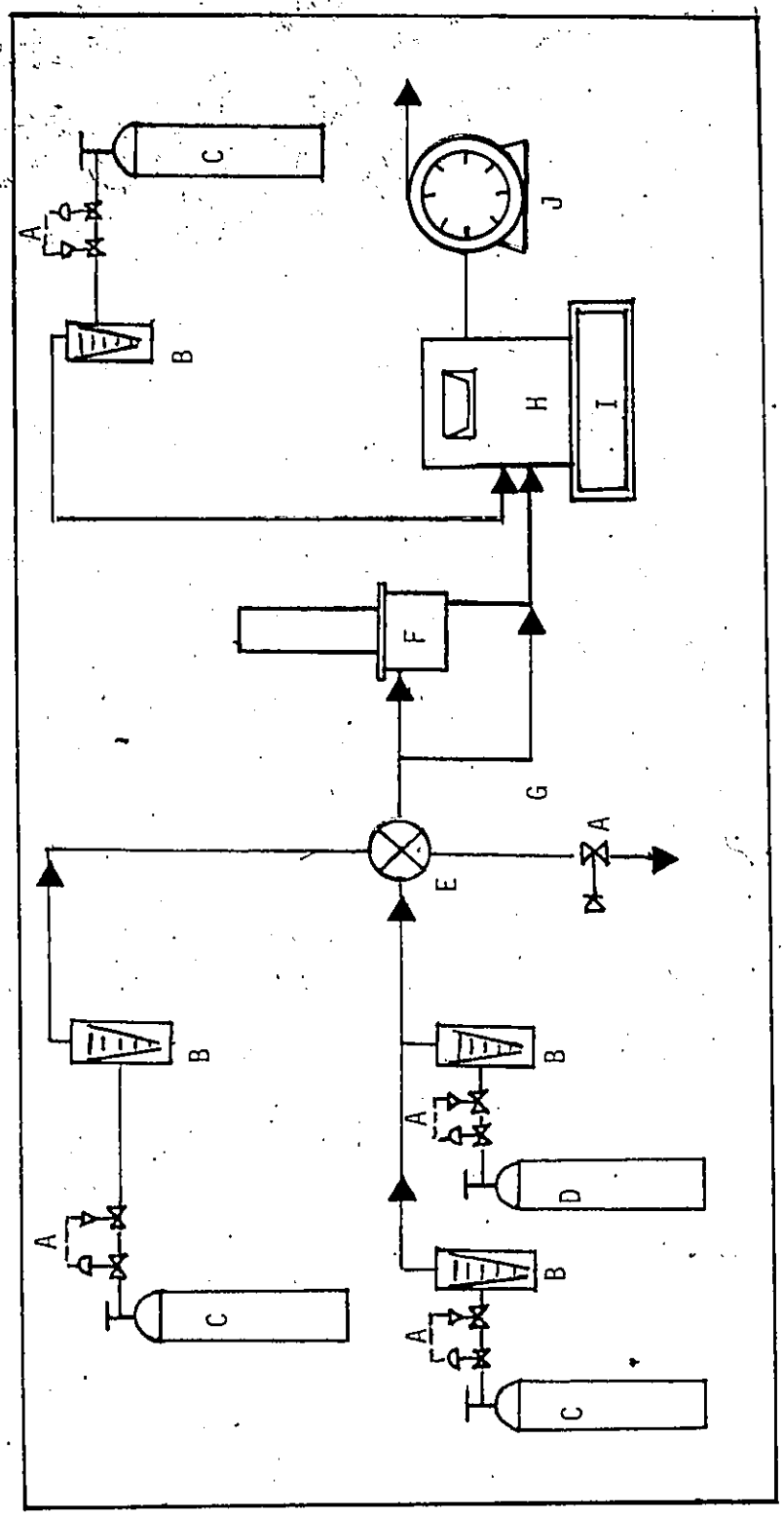

Figure 5-8 Schematic flow diagram of experimental apparatus for mixing studies

A needle valve
B rotameter
C He gas cylinder
D N_2 gas cylinder
E 4-way switching valve
F reactor
G bypass line
H thermal conductivity cell
I power supply
J wet test meter

compositions of feed gases were prepared from cylinder gases by adjustment of the rotameters. The needle valve on the vent stream was adjusted so that when a stream was switched from the reactor to the vent, there was no change in flow rate. The remaining needle valves were adjusted so that both gases flowed at the same rate. One stream from the 4-way valve could be directed either through the reactor or through a temporary bypass around the reactor. In this study, step changes from either pure He to pure N_2 or from pure He to He/N_2 mixtures were conducted by switching the 4-way valve from one position to another at a specified time. Negative step changes (e.g. N_2 to pure He) could similarly be applied. The physical properties of He and N_2 are similar and both gases are inert to the char.

The outlet stream from the reactor was fed continuously through a Gow Mac Model 40-001 thermal conductivity cell, consisting of 4 WX filaments. The heated cabinet was maintained at a constant temperature of $100^{o}C$. A current of 200 ma was maintained in the bridge circuit.

Analysis of the RTD data is greatly simplified if there is a linear relationship between thermal conductivity and gas composition. The results of tests carried out to ensure that such a linear relationship existed are shown in Figure 5-9. The linearity is clearly verified. Additional tests showed that the linearity of the response did not depend on flow rate

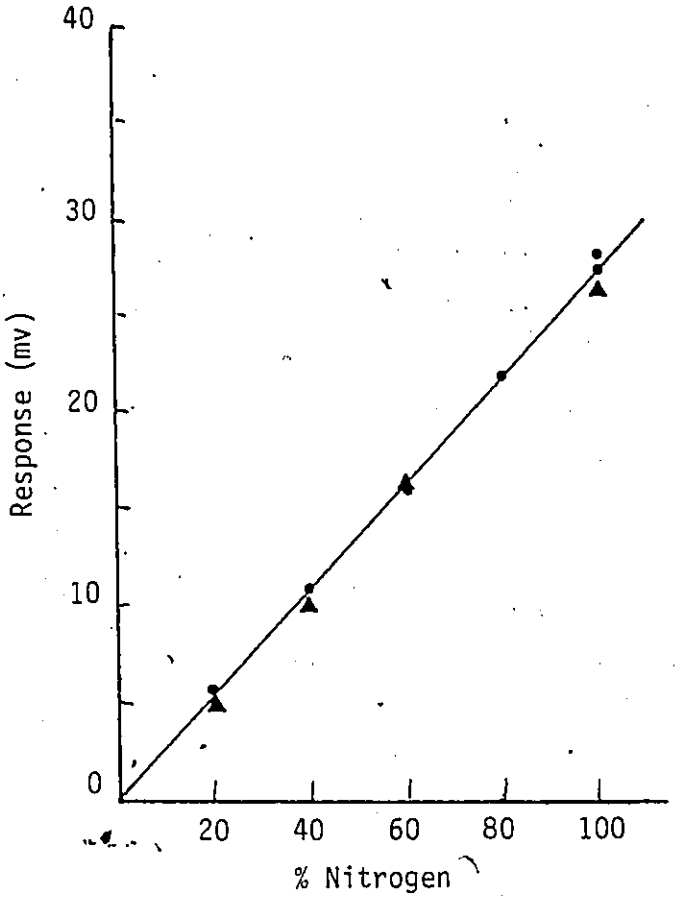

Figure 5-9 Instrument Calibration Curve

▲ 1000 $cm^3 min^{-1}$ gas flowrate

● 100 $cm^3 min^{-1}$ gas flowrate

when varied from 100 cm^3/min to 1000 cm^3/min. The signal from the thermal conductivity cell was recorded on a WATANABE linear mark V high speed recorder.

5.3.2 Experimental Procedure

Before each run, approximately 5 grams of sized char was weighed and set aside. Quartz particles of the same size fraction were also prepared. The solids basket was then filled with the char and quartz as shown in Figure 5-10 with fine mesh stainless steel screens separating the layers. The manner of packing was identical to that planned for actual gasification experiments. In order to ensure consistency in the packing, the packing technique was not varied. The volume of each section (i.e.; A,B,C) was kept constant. The magnedrive assembly was then bolted to the reactor and the pressure in the vessel increased to 30 psi. If no pressure change was observed on a Bourdon pressure gauge on the upstream side of the reactor within one half hour, the reactor was considered leaktight and the test continued. The appropriate gas flowrates were then established for the reference gas through the cell, the gas exiting the reactor and the gas being vented by adjusting the needle valves. The bridge current was then turned on. The thermal conductivity cell was always kept heated to the proper temperature. At this time the magnedrive was activated and the correct rotational speed was determined with the use of a stroboscope. Once a steady baseline was achieved on the

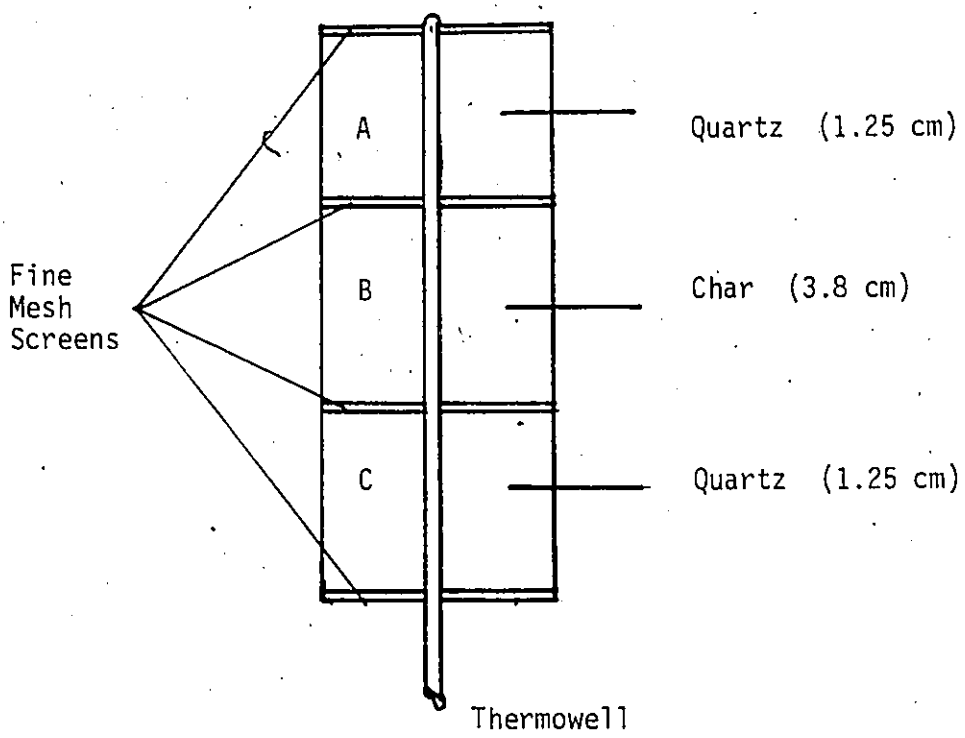

Figure 5-10 Schematic of bed packing

recorder with helium flowing through the reactor, the 4-way valve was manually switched to N_2 (or to N_2/He mixtures in case of calibration) and the output of the thermal conductivity cell recorded. At the same time the step change was introduced, a stopwatch was started and once the output on the recorder reached a new steady level (corresponding to 100% N_2) both the stopwatch and the recorder were turned off. In this way, the time at which the step input was applied was determined by the elapsed time and the chart speed. At the end of each run, the alternate char/quartz layers were carefully removed by first pulling out the screen and then pouring out the material.

The ranges of the operating variables explored are listed in Table 5-3. A 2^3 factorial design described in Table 5-4 was used to examine the effects of these variables on mixing.

With the high gas flowrates used and the small reactor volume (30 mL^3), the average residence time of the gas in the reactor was in the order of 2-3 seconds. In this time scale, it became important to measure the thermal conductivity cell's response to a step change as a function of flow rate. The instrument response was determined by imposing a step change in the feed gas from He to N_2, with the feed gas stream entering the temporary bypass line. The recorder time constant is in the order of milliseconds and can be ignored.

TABLE 5-3

Range of Operating Variables

Gas Flow Rate	:	500 - 1000 cm^3/min
Impeller Rotational Speed	:	0 - 1800 rpm
Particle Size	:	0.2 - 1.4 mm

TABLE 5-4

2^3 Factorial Design for Mixing Tests

Char/Quartz Particle Size [mm]	Gas Flowrate [cm^3/min]	Impeller Speed [rpm]
0.2 – 0.4	500	0
	1000	0
	500	1800
	1000	1800
0.4 – 1.0	500	0
	1000	0
	500	1800
	1000	1800
1.0 – 1.4	750	900
	750	900

All of these experiments were conducted at room temperature because this greatly reduced the time involved for the tests. Bennett et. al[94] have reported RTD studies by Brown (using an internal recycle reactor) carried out at room temperature and at reaction temperature (300°C). It was noticed that as the temperature was increased to reaction temperature, natural convection improved mixing even with no agitation. This is thought to be true for the present study where temperatures are much higher (600-1000°C).

5.3.3 Modelling Approach

As was mentioned in the introduction to this section, deriving the RTD of a bench scale reactor from response data in which the measurement device dynamics cannot be ignored is a problem which (to my knowledge) has not been tackled. It was necessary therefore to develop a means of handling it. The basic approach adopted here is to model the reactor and the instrument dynamics separately. A simple empirical model (the tanks in series model) has been shown to adequately describe the measurement device contribution. The recirculation reactor, on the other hand, was modelled using a mixed model which allows for possible deviations from complete mixing as represented by the parameters in the model.

The step-response curves for the measurement device and for the combined reactor/measurement device are continuous concentration-time curves. On the other hand, the estimation

of parameters in the models for the reactor and for the measurement device requires discrete data. Discretization by sampling the continuous data presents no problem in itself, however the question of the number and spacing of samples arises. The important factor here is that the discrete data points selected should allow accurate reconstruction of the continuous data.

A problem which does arise however is that the data taken from any one step response curve is autocorrelated. One of the basic assumptions involved in standard parameter estimation methods is that the response measurements are independent. Thus using data from only one step response curve would lead to unreliable parameter estimates. Several correlated error models and parameter estimation techniques for a simple system with cumulative errors are available in the literature[103-108]. However, the search for an appropriate correlated error model is very time-consuming and requires considerable computation. To circumvent this problem it was decided to obtain uncorrelated data via experimentation. This was accomplished by repeating the step response experiments at each of the desired operating conditions a number of times and only one data point was taken from each of the continuous concentration curves generated. Since the duration of these experimental tests was relatively short ($\sim$ 30 min) this represented a viable and favorable alternative. The response data used to fit both the measurement device model and the combined measurement device/reactor model were obtained in this manner.

5.3.4 Measurement Device Model

The thermal conductivity cell's response to a step change in feed gas at a gas flowrate of 500 cm^3/min is shown in Figure 5-11. The transient portion of the response takes place in approximately 1.2 seconds. This short response time would usually be negligible, however because the nominal reactor residence times are in the same order of magnitude, the dynamics of the cell had to be accounted for. The thermal conductivity cell's response curve has been modelled successfully with the tanks in series model(N equal size backmix tanks in series). An advantage of this mathematical representation is that the parameter N gives a measure of the approach to a perfect plug flow response (Figure 5-12). The exit age distribution for the model can be expressed as follows[23]:

$$E(t) = \frac{1}{\tau}\left(\frac{t}{\tau}\right)^{N-1}\frac{1}{(N-1)!}\exp\left(\frac{-t}{\tau}\right)$$

where t = time

τ = residence time in a single tank

N = number of tanks in series

Since the exit age distribution is the time derivative of the F-curve, the above expression can be integrated (details are found in Appendix G) to obtain the step response:

$$F(t) = C(t)/C_o = (1/\tau)^N \exp(-t/\tau)\sum_{r=o}^{N-1}\left[\frac{(-1)^r\, t^{N-1-r}}{(N-1-r)!\,(-1/\tau)^{r+1}}\right]$$

Equation 5-1

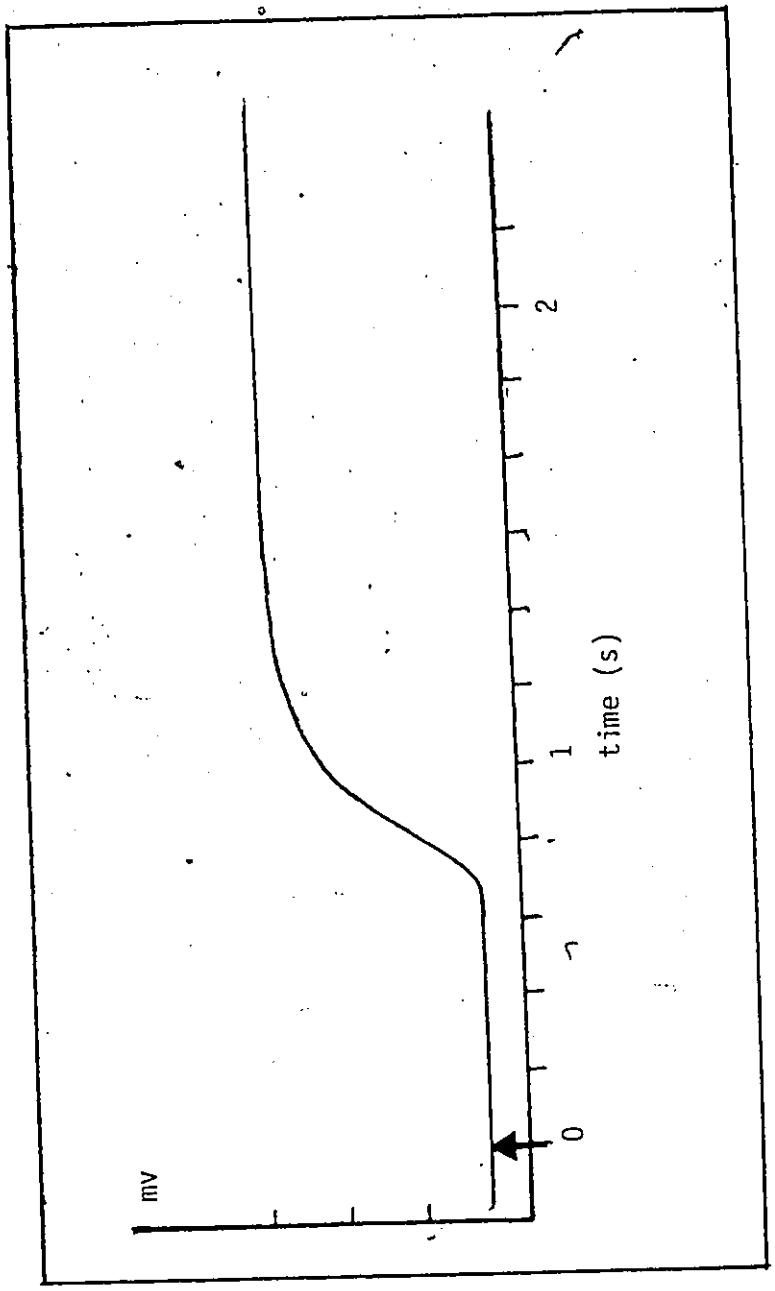

Figure 5-11 Actual Measurement device step response, gas flowrate 8.3 cm^3/s

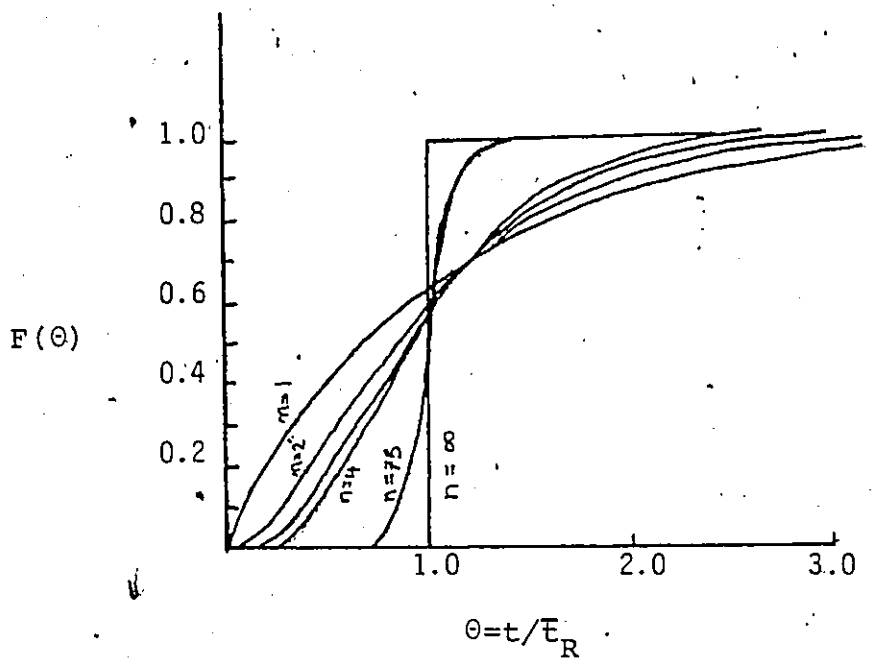

Figure 5-12 F-curve for N tanks in series model.

A nonlinear least squares technique can be used to obtain the parameters τ and N in the model provided the data satisfied the least squares assumptions. Uncorrelated data, obtained in the manner described in the previous section, were used in fitting the model. Figure 5-13 shows the results of modelling the measuring instrument using uncorrelated response values. For comparison, Figure 5-14 shows the results of fitting the model to the correlated response values obtained from one concentration-time curve. There is more scatter in the uncorrelated data which reflects the uncertainty in the data points obtained from different experiments. This scatter is not unrealistic when one notes the time scale of 1 second. The trend in the residuals (predicted concentration value at t_u less the measured value at t_u) in Figure 5-14 is typical of autocorrelated data.

The two parameters τ and N in the tanks in series model were obtained by using a non-linear parameter estimation technique in the Fortran package called NONLIN. The parameter N presented a problem since values of N were restricted to positive integer values. Therefore in order to estimate N, the value of N in the model was fixed and the value of τ obtained by minimizing the residual sum of squares. The value of N was then changed and the procedure repeated. Several values of N then generated the graph shown in Figure 5-15. The ideal number of tanks to use to model the instrument response is that value of N corresponding to the minimum in the parabolic

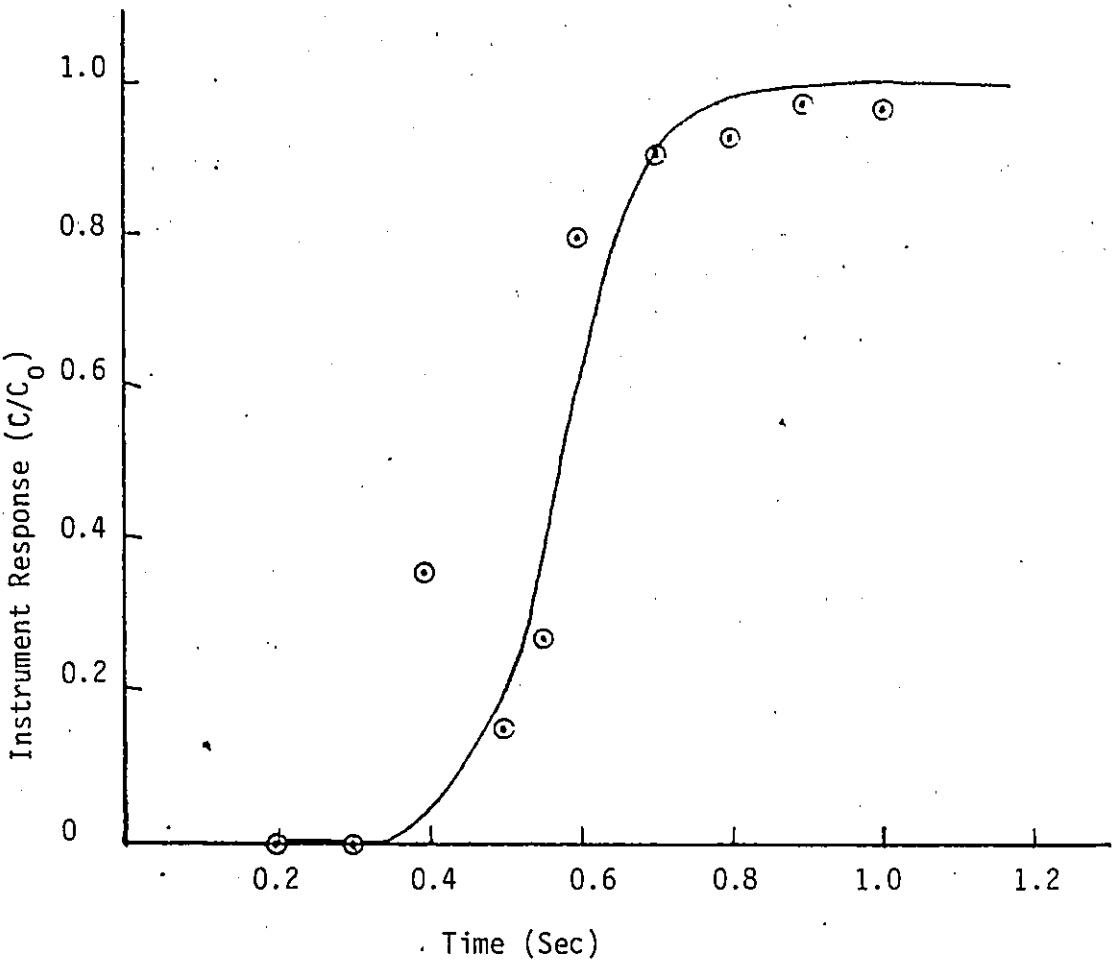

Figure 5-13 Instrument Response Curve Fit with Independent Data, Gas Flowrate: 1000 cm^3/min, N = 40, τ = .014s

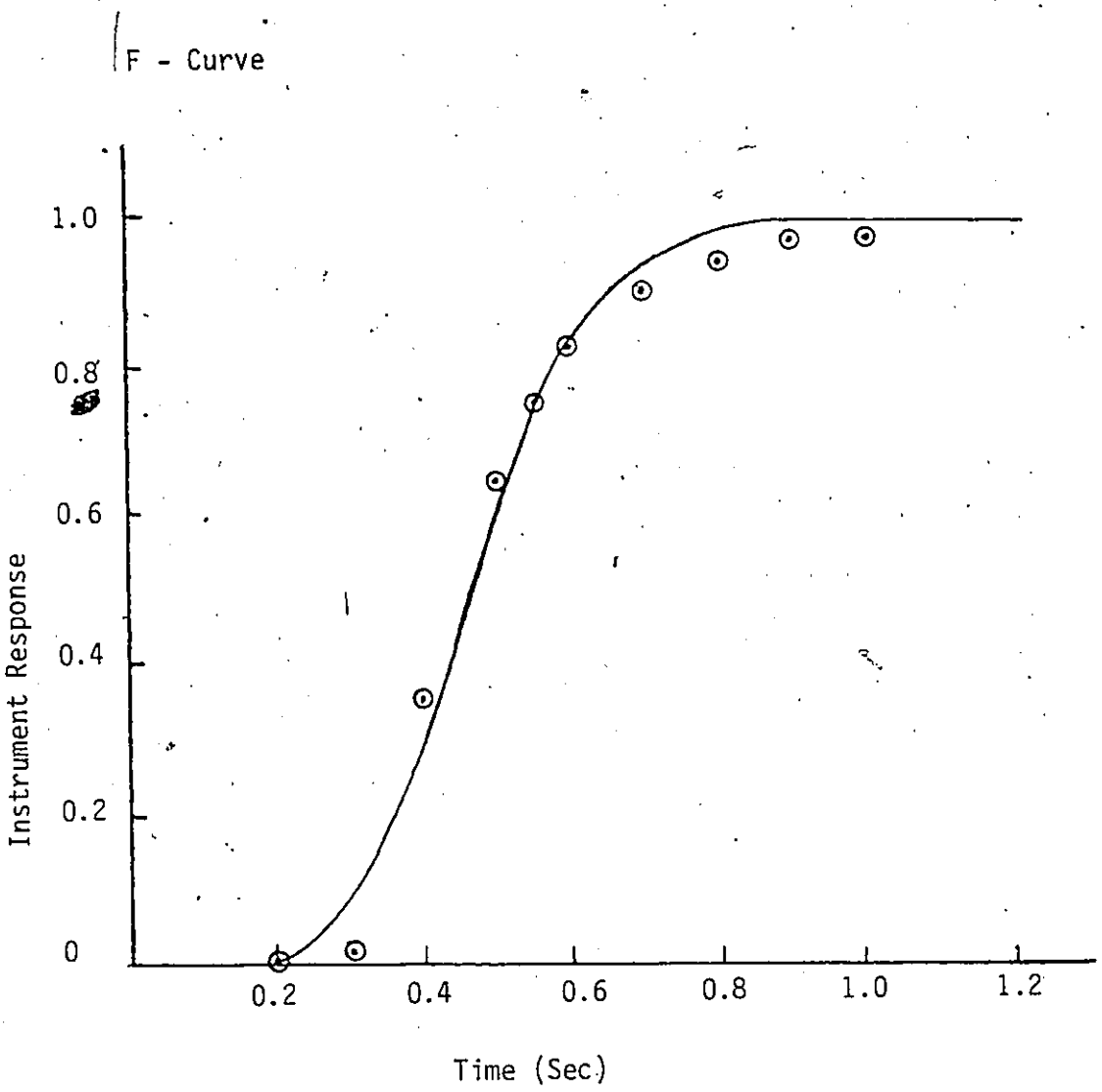

Figure 5-14 Instrument Response Curve Fit with Autocorrelated Data, Gas Flowrate 1000 cm^3/min, N = 12, τ = 0.039s.

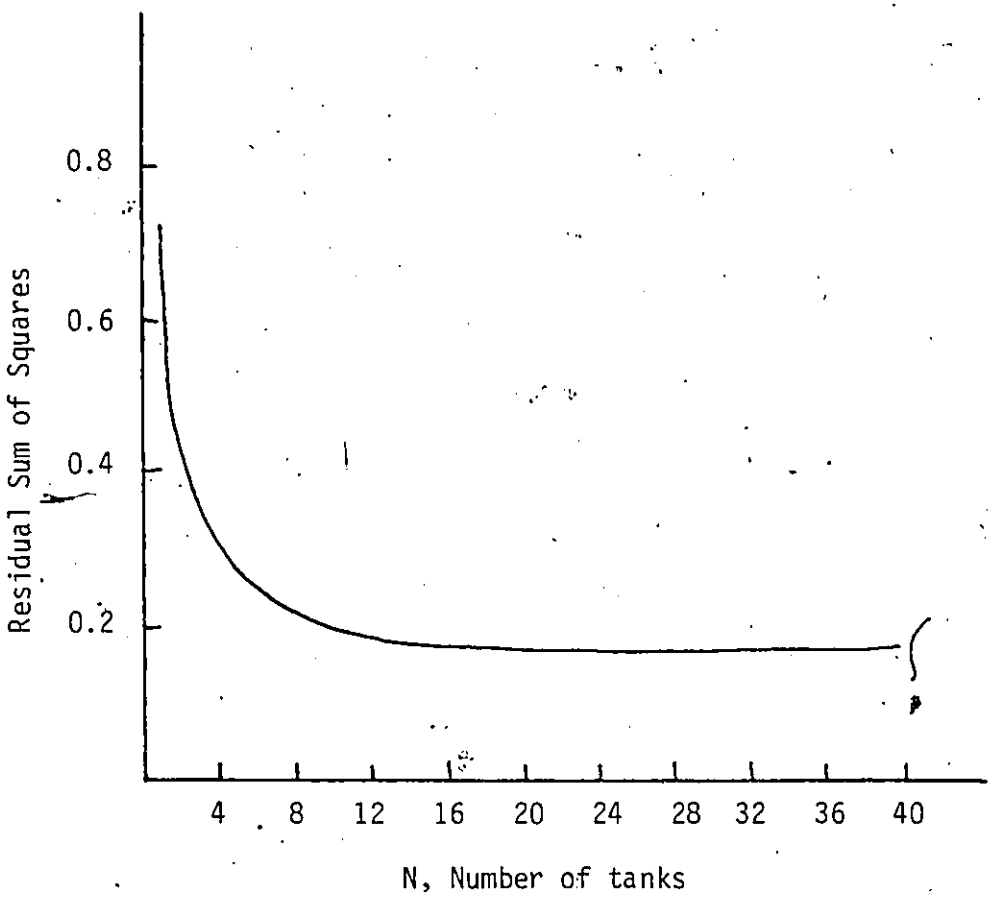

Figure 5-15 Sum of squares surface as a function of N

Gas Flowrate 1000 cm^3/min

curve. Unfortunately for gas flow rates above 750 cm^3/min the number of tanks exceeded 40 which surpassed the computer calculation range. However, the shape of the curve in Figure 5-15 suggests a very shallow sum of squares surface so that very little improvement was taking place as N increased beyond 20. The best-fit models in the least squares sense for the instrument response at three feed gas flowrates are presented in Figures 5-16, 5-17 and 5-18. These values of τ and N were used as initial guesses for the multiresponse parameter estimation in the combined reactor/measurement device model.

5.3.5 Reactor Model

Many approaches exist to model the mixing characteristics of reactors. Some of these were discussed in Section 3.4. For the purpose of modelling the internal recirculation reactor used in this study, a mixed model was chosen because

1. complete mixing behavior could be described

and

2. the extent and nature of any deviation from complete mixing behavior could be described.

A schematic of the reactor mixed model is given in Figure 5-19. The three different flow regions were suggested by the internal structure of the reactor. The series plug flow region (T_{PS}) represents a time delay encountered in the inlet and exit lines of the reactor. The parallel plug flow region (T_{PP}) represents that portion of the feed gas moving from the

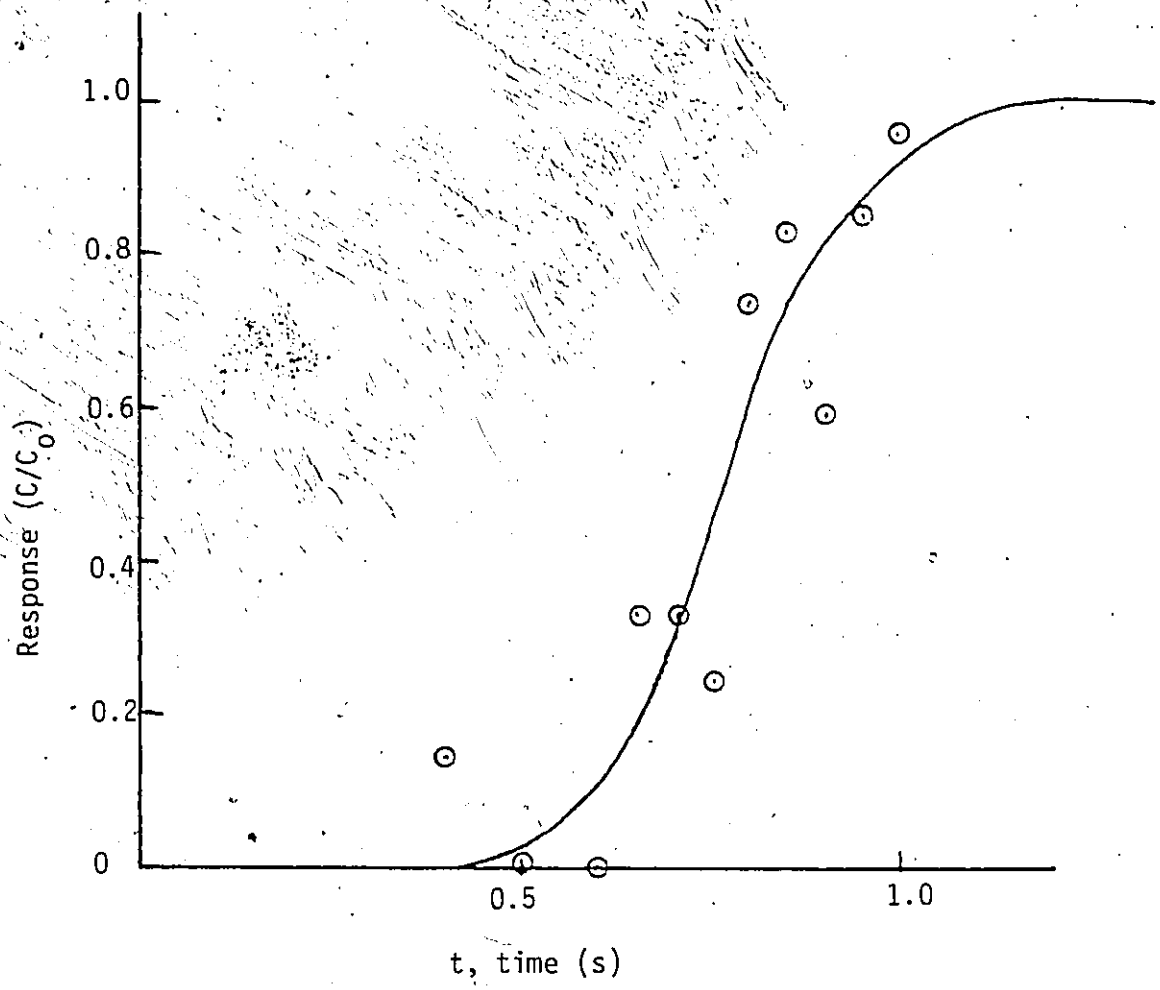

Figure 5-16 Measurement device model fitted to uncorrelated data, gas flowrate 500 cm^3/min, N = 26, τ = 0.03 (s)

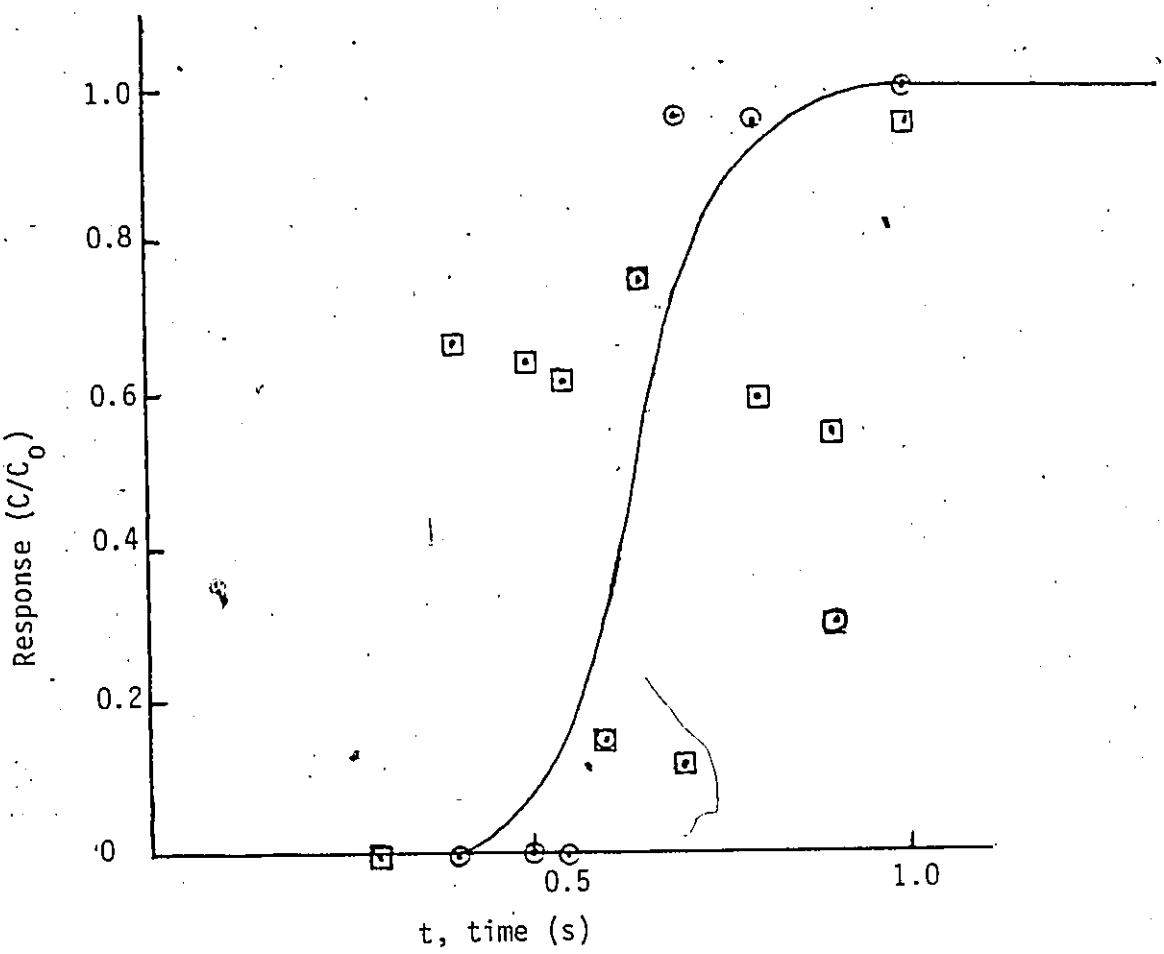

Figure 5-17 Measurement device model fitted to uncorrelated data, gas flowrate 750 cm^3/min, N = 40, τ = 0.016 s.
Data from two separate experiments.

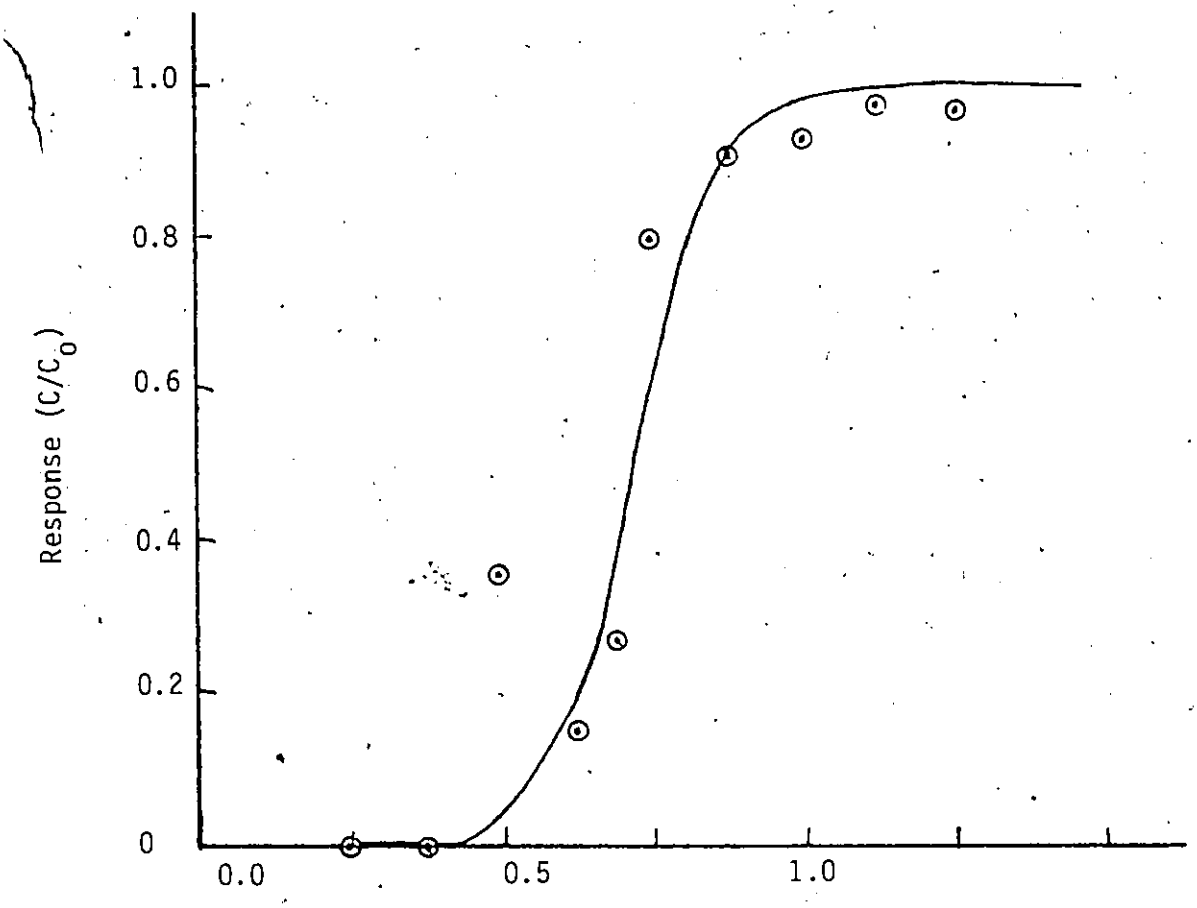

Figure 5-18 Measurement device model fitted to uncorrelated data, gas flowrate 1000 cm^3/min, N = 40, τ = .0143s

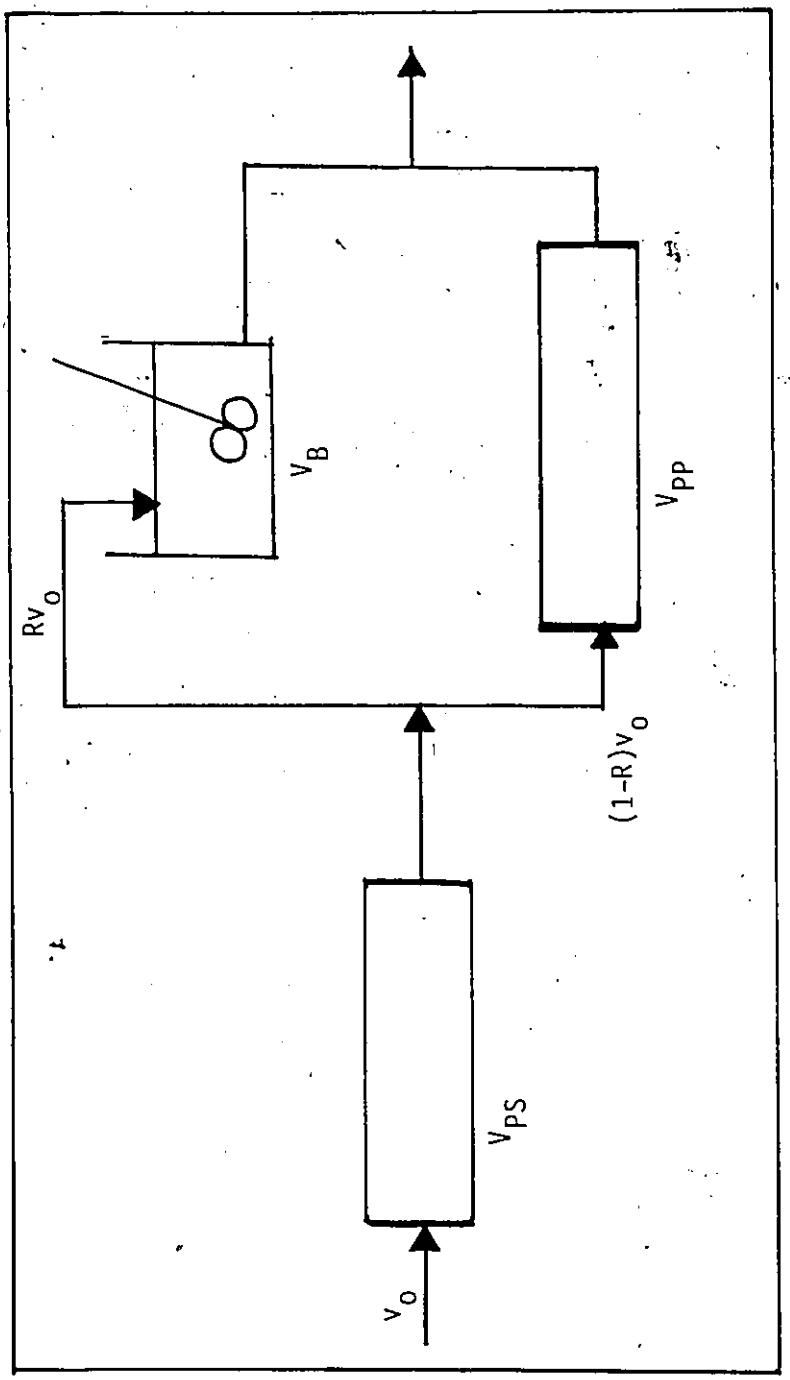

Figure 5-19 Schematic representation of reactor mixed model

reactor inlet to the reactor exit without being backmixed (e.g. gas flow up magnedrive shaft, gas flow short-circuiting solid bed, etc.). The backmix region (T_B) represents that portion of the gas which is being completely mixed. If the free volume in the reactor assembly is denoted by V_T(mL) and l, m and n correspond to those fractions of the total volume of the reactor that behave as the gas regions just described then one can define the following parameters:

$$T_{PS} = \frac{lV_T}{v_o} = \frac{V_{PS}}{v_o} \; ; \quad T_{PP} = \frac{mV_T}{v_o} = \frac{V_{PP}}{v_o} \; ; \quad T_B = \frac{nV_T}{v_o} = \frac{V_B}{v_o}$$

where v_o is the feed gas flow rate

T_{PS} is the residence time of the gas in the series plug flow region

T_B/R is the residence time of the fluid in the backmix region

R is the fraction of the feed gas flow being backmixed

$\frac{T_{PP}}{(1-R)}$ is the residence time of the fluid in the plug flow region in parallel with backmix region

V_{PS} volume of series plug flow region

V_{PP} volume of parallel plug flow region

V_B volume of completely mixed region

V_T total reactor volume

The step response of this reactor mixed model is derived in Appendix H and is summarized below in the time domain:

$$F(t)= R\left[1-\exp\left(\frac{R}{TB}\right)(T_{ps}-t)\right]u_t(T_{ps})+(I-R)u_t\left(\frac{Tpp}{(I-R)} + T_{ps}\right) \quad \text{Equation 5-2}$$

This is a very flexible model and depending upon the values of the parameters R, T_{pp}, T_{PS} and T_B several special cases can be described:

1. As $R \to 1$, $T_{pp} \to 0$, $T_{PS} \to 0$ — complete mixing behavior is approached

2. As $R \to 1$, $T_{pp} \to 0$ — complete mixing and plug flow sections exist in series (e.g. inlet and outlet lines of a completely mixed system are a significant portion of the total reactor volume)

3. $0 < R < 1$, $T_{pp} \to 0$ — some bypassing (short-circuiting) is occurring

4. $0 < R < 1$, $T_{pp} > 0$ — parallel plug flow region exists

5. As $R \rightarrow 0$ — plug flow behavior is approached

6. V_T ($V_B+V_{PP}+V_{PS}+V_D$) — dead space or stagnant zone exists

< known reactor volume

It is evident that the model chosen is general enough to cover a wide variety of flow situations that may exist within the reactor.

The reactor response to a step change in feed gas concentration cannot be determined independently of the measuring device. Therefore, the two models, the measurement device model discussed in the previous section and the reactor mixed model presented here must be combined to fit the step response data. A schematic representation of the combined reactor/measurement device model is depicted in Figure 5-20. The step response of this combined model can be derived most easily in the Laplace Domain as shown in Appendix I. The mathematical equation is given below:

$$F(s) = (1/\tau)^N \, (1/(s + 1/\tau))^N \left[R \exp(-T_{PS}s)/s \;\; (R/T_B/(s+R/T_B)) + (1-R) \exp(-s(T_{PS} + T_{PP}/(1-R)))/s\right] \qquad \text{Equation 5-3}$$

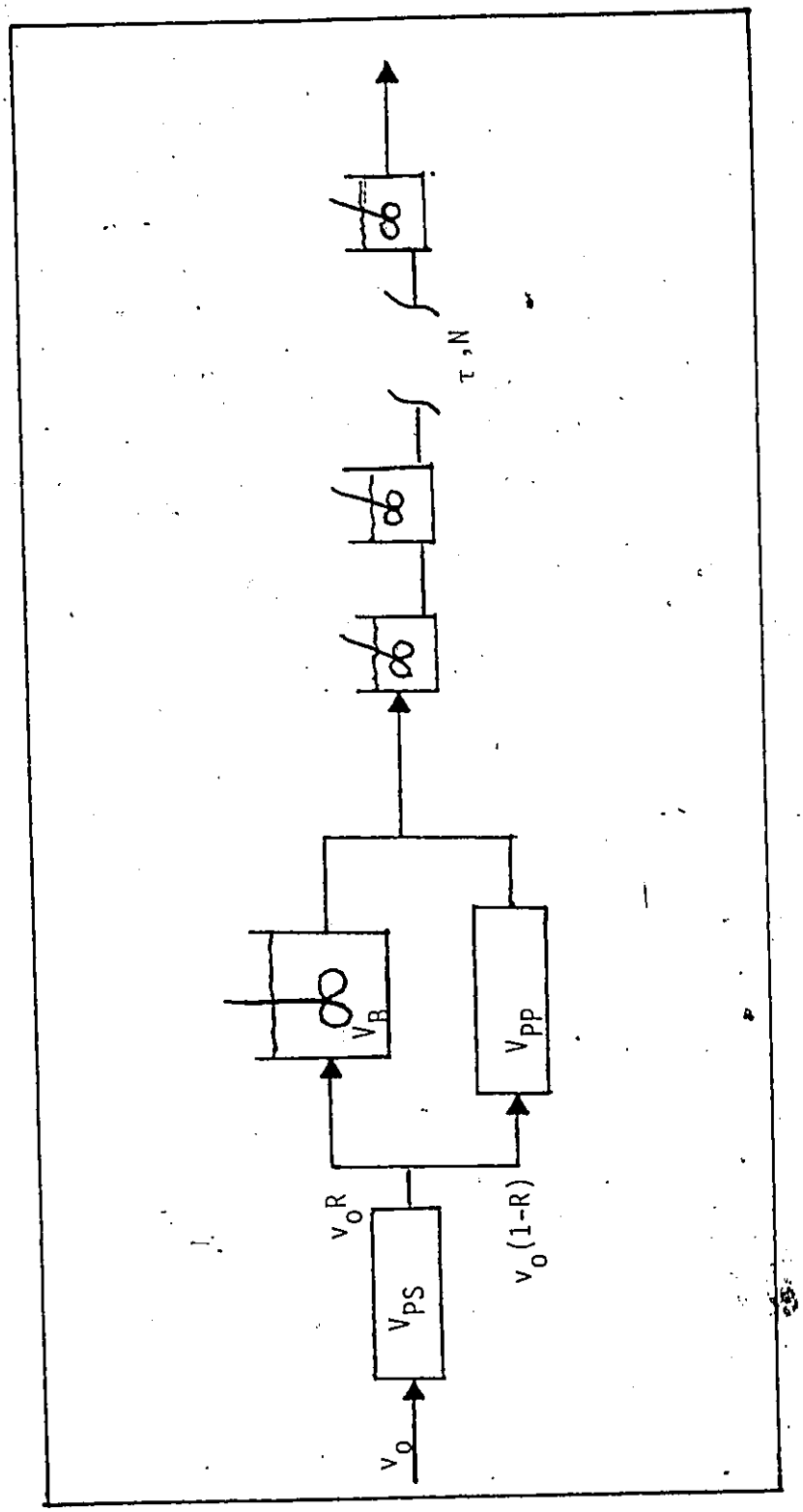

Figure 5-20 Schematic representation of combined reactor/measurement device model

Analysis of the combined reactor/measurement device data alone using this model may yield misleading results since deviations from complete mixing behavior could be mistakenly accounted for by the instrument. The independent determination of the instrument response model as described in the previous section and the multiresponse parameter estimation technique discussed in the next section will help to avoid this pitfall.

5.3.6 Parameter Estimation

Conclusions about the mixing characteristics of the reactor are based upon the values of the parameters found in the mixed model. Reliable and precise estimates of these parameters are needed therefore to determine the significance of possible flow nonidealities. Multiresponse parameter estimation techniques offer some means of improving the precision of the parameter estimates for two or more responses. Since step response data was collected not only for the reactor/measurement device system but also for the measurement device alone, and since the mathematical expressions for the combined reactor/measuring device model and for the measuring device model share some common parameters, namely τ and N, multiresponse techniques can be used to fit the data simultaneously from the two responses.

A sample of the type of data collected with the mixing experiments is listed in Table 5-5. If it is assumed that there is no correlation for a single set of data between the

TABLE 5-5

Responses to a Step-Change in Feed Gas

ELAPSED TIME (s) t_u	RESPONSE 1 y_{1u}	RESPONSE 2 y_{2u}
0.2	0	0
0.3	0	0
0.4	0.358	0
0.5	0.151	0
0.55	0.275	0
0.6	0.80	0
0.7	0.909	0
0.8	0.936	0.0980
0.9	0.977	0.0471
1.0	0.966	0.1568
1.3	1	0.2353
1.7	1	0.4471
2.2	1	0.5490
2.7	1	0.6941
3.2	1	0.8078
3.7	1	0.8627
4.2	1	0.9019
4.8	1	0.9451
5.3	1	0.9490

Response 1: Instrument Response for Gas Flow rate 1000 cm^3/min

Response 2: Combined Reactor/Measuring Device Response for Gas Flow Rate: 1000 cm^3/min, Particle Size: 1.0 - 1.4 mm, Impeller Speed: 1800 rpm

observed instrument response value at t_u and the observed combined response value at t_u, then the appropriate criterion to use is to minimize the following weighted sum of squares[117].

$$SS = SS_1 + SS_2$$

$$SS_1 = \sum_{u=1}^{n} (y_{u1} - f_{u1}(t_u, \underline{\theta}))^2/\sigma_{u1}^2$$

$$SS_2 = \sum_{u=1}^{n} (y_{u2} - f_{u2}(t_u, \underline{\theta}))^2/\sigma_{u2}^2$$

Equation 5-4

where t_u is the value of the independent variable, time, for the u 'th observation.

y_{u1} experimental value of C/C_o for measurement device response at t_u.

f_{u1} calculated value of C/C_o for measurement device response at t_u with parameters

$\underline{\theta}$ vector of parameter values

y_{u2} experimental value of C/C_o for combined reactor/measuring device response at tu

f_{u2} calculated value of C/C_o for combined response at t_u with parameters $\underline{\theta}$

σ_{u1}^2 variance of instrument response at t_u

σ_{u2}^2 variance of combined response at t_u

This sum of squares is a generalization of the nonlinear least squares parameter estimation technique. The assumptions

involved are justified in the present context because the two responses were measured independently with very similar experimental arrangements.

The mathematical model form given in Equation 5-3 for the combined model (f_{u2}) is in the Laplace domain. In order to compare the actual experimental data with the model response in the time domain using the criterion just presented, it was necessary to obtain the time domain solution of the model. An IMS library algorithm (FLINV) was used to find the inverse Laplace of the model function at every required time value. The advantages of direct non-linear regression in the time domain over parameter estimation in the Laplace domain were discussed in Section 3.4.4. Briefly, regression in the time domain is preferred because one is comparing the actual data with the model response and so the criterion is minimizing errors directly with the data. Laplace domain techniques require transformations of the actual data to the S-domain. If the original data have constant variance, this may not be true of the transformed data. Also, a fit obtained in the S-domain does not guarantee the best in the least squares sense in the time domain.

Estimates of the parameters were obtained by using the criterion presented in Equation 5-4 and the IMS library minimization routine ZXMIN. ZXMIN is a general Fortran program which obtains the minimum of a function of n variables by a

Quasi-Newton method. Several parameter transformations were found useful in obtaining convergence. Since the parameters T_B, T_{PS} and T_{PP} must be positive real numbers, the simple transformations $T_B = X_B^2$, $T_{PS} = X_{PS}^2$, $T_{PP} = X_{PP}^2$, allowed the routine to search over all possible values of X. Similarly, the value of R, the fraction of the gas flow which is being backmixed must be in the range zero to unity. In order for the minimization routine to search over all possible values of X_R, the following transformation was found helpful, $R = \exp(-X_R^2)$. As the value of X_R approaches zero, R approached unity. As the value of X_R gets very large ($\pm \infty$), R tends to zero. The minimization routine was highly sensitive to estimates of τ, the tanks-in-series parameter. It was necessary to use the following transformation on the parameter τ in order to limit the range over which the search for τ could be carried out, $\tau = \mathrm{SIN}^2(\pi X_\tau^2/2X10^4)$. As X_τ varies between 0 and ± 100, the value of τ ranges from 0 to 1. Initial estimates for τ which were obtained with the measuring device response as described earlier, proved useful. A procedure similar to that used for obtaining the initial estimate for N was adopted in estimating the values of N in the multiresponse case. Transformations of both the independent variable (time) and dependent variable (concentration ratios) by a simple multiplication by a constant was also necessary since the inversion algorithm (FLINV) encountered some difficulty when the time vector contained a wide range of values. Scaling the

time vector by a factor of 20 and the concentration ratios by a factor of 4 improved convergence to the accuracy required.

An approximate $100(1-\alpha)\%$ confidence interval for each of the parameters τ, T_B, T_{pp}, T_{ps} and R was calculated as shown below[148].

$$\hat{\theta}_s - t_{\nu,\alpha} \sqrt{m^{ss}} \leq \theta_s \leq \hat{\theta}_s + t_{\nu,\alpha} \sqrt{m^{ss}} \qquad \text{Equation 5-5}$$

where $\hat{\theta}_s$ is the estimated value of the parameter s

$t_{\nu,\alpha}$ is the t-value from tables for ν degrees of freedom at the $(1-\alpha)$ confidence level

m^{ss} are the elements of the inverse of the following matrix:

$$\underline{M} = \underline{X}_1^T \underline{X}_1 / \sigma_{11}^2 + \underline{X}_2^T \underline{X}_2 / \sigma_{22}^2$$

The matrix $\underline{X}_i$ is the nxp matrix whose elements are $\{x_{us}\}$ shown below:

$$\{x_{us}\} = \left\{ \frac{\partial f_i (t_u, \underline{\theta})}{\partial \theta_s} \right\} \Bigg| \underline{\theta} = \hat{\underline{\theta}}$$

where n = total number of time values or independent runs

p = total number of parameters

$\underline{\theta}$ = the vector of p parameters to be estimated

$\hat{\underline{\theta}}$ = the vector containing p estimates of the parameter

The variance σ_{11}^2 was estimated by $(SS_{11}/(n-p))$. The variance σ_{22}^2 was estimated by $S_{22}/(n-p)$. A copy of the fortran program and output is provided in Appendix J.

5.3.7 Results and Discussion

Parameter estimates obtained from using the multiresponse criterion and approximate 95% confidence limits are given in Table 5-6. It can be seen that in all cases, T_{PP} and therefore V_{PP} the parallel plug flow volume are negligible and R the fraction of the total flow which is being backmixed is unity. The approximate confidence intervals for these two parameters encompass 0 and 1 respectively. These parameters were subsequently deleted from the combined model. It was not found necessary to search over different values of N because of the closeness of the value of τ found in the multiresponse case to that value found in the single response case.

The completely mixed volume (V_B) and the series plug flow volume (V_{PS}) corresponding to T_B and T_{PS} respectively as well as the 95% confidence limits are given in Table 5-7. The fit of this four parameter model (T_B, T_{PS}, τ , N) to a typical set of experimental data is shown in Figure 5-21. There are no significant trends in the residual plot shown in Figure 5-22, therefore the model appears to be adequate. Since the estimates from the single response fitting of the measurement device model yielded estimates of N and τ

TABLE 5-6

Parameter Estimates for Combined Reactor/Measurement Device Model

Operating Conditions			Parameters					
Particle Size (mm)	Feed Gas Flowrate (cm^3/min)	Impeller Speed (rpm)	T_B (s)	T_{PS} (s)	T_{PP} (s)	R	τ (s)	N
-	1000	1800	1.56 ± 0.19	0.675 ± 0.124	0.05 ± 0.098	1.0 ± 0.006	0.014 ± 0.0007	40
0.2-0.4	500	-	2.46 ± 0.30	0.502 ± 0.198	-	-	0.030 ± 0.0012	26
	500	1800	2.93 ± 0.37	0.265 ± 0.232	-	-	0.030 ± 0.0012	26
	1000	-	1.34 ± 0.21	0.155 ± 0.106	-	-	0.014 ± 0.0007	40
	1000	1800	1.40 ± 0.28	0.493 ± 0.218	-	-	0.014 ± 0.0008	40
0.4-1.0	750	900	2.10 ± 0.21	0.243 ± 0.129	-	-	0.016 ± 0.001	40
	750	900	2.23 ± 0.35	0.306 ± 0.213	-	-	0.016 ± 0.001	40
1.0-1.4	500	-	3.05 ± 0.20	0.636 ± 0.128	-	-	0.030 ± 0.0012	26
	500	1800	2.82 ± 0.20	0.871 _ 0.130	-	-	0.030 ± 0.0012	26
	1000	-	1.50 ± 0.06	0.203 ± 0.066	-	-	0.014 ± 0.0007	40
	1000	1800	1.59 ± 0.07	0.203 ± 0.071	-	-	0.014 ± 0.0007	40

TABLE 5-7

Specific Volumes of Components of Reactor Mixed Model

Operating Conditions				
Particle Size [mm]	Gas Flowrate [cm^3/min]	Impeller Speed [rpm]	V_B (mL)	V_{PS} (mL)
-	1000	1800	25.9 ± 2.7	11.3 ± 3.6
0.2-0.4	500	0	20.5 ± 2.2	4.17 ± 1.4
	500	1800	24.4 ± 2.7	2.17 ± 1.9
	1000	0	22.3 ± 3.1	2.58 ± 1.5
	1000	1800	23.3 ± 4.2	8.21 ± 3.2
0.4-1.0	750	900	26.2 ± 2.3	3.0 ± 1.4
	750	900	27.9 ± 3.9	3.88 ± 2.3
1.0-1.4	500	0	25.4 ± 1.7	5.33 ± 0.9
	500	1800	23.5 ± 1.5	7.25 ± 0.9
	1000	0	25.0 ± 1.8	3.33 ± 1.0
	1000	1800	26.4 ± 1.9	3.33 ± 1.0

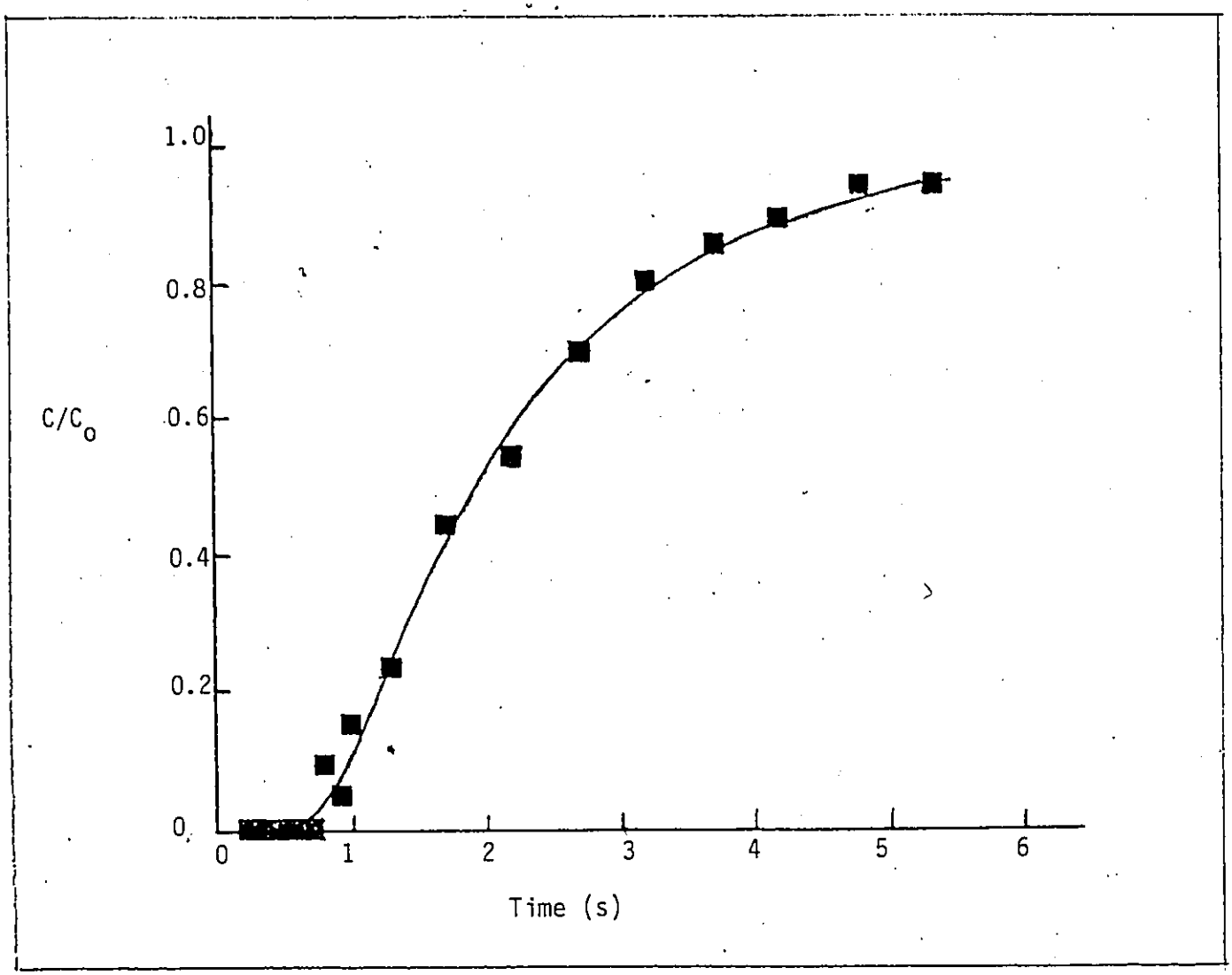

Figure 5-21 Combined Reactor/Measurement Device Step Response
Particle Size 1.0 - 1.4 mm, Impeller Speed 1800 rpm,
Gas Flowrate 16.7 $cm^3\ s^{-1}$

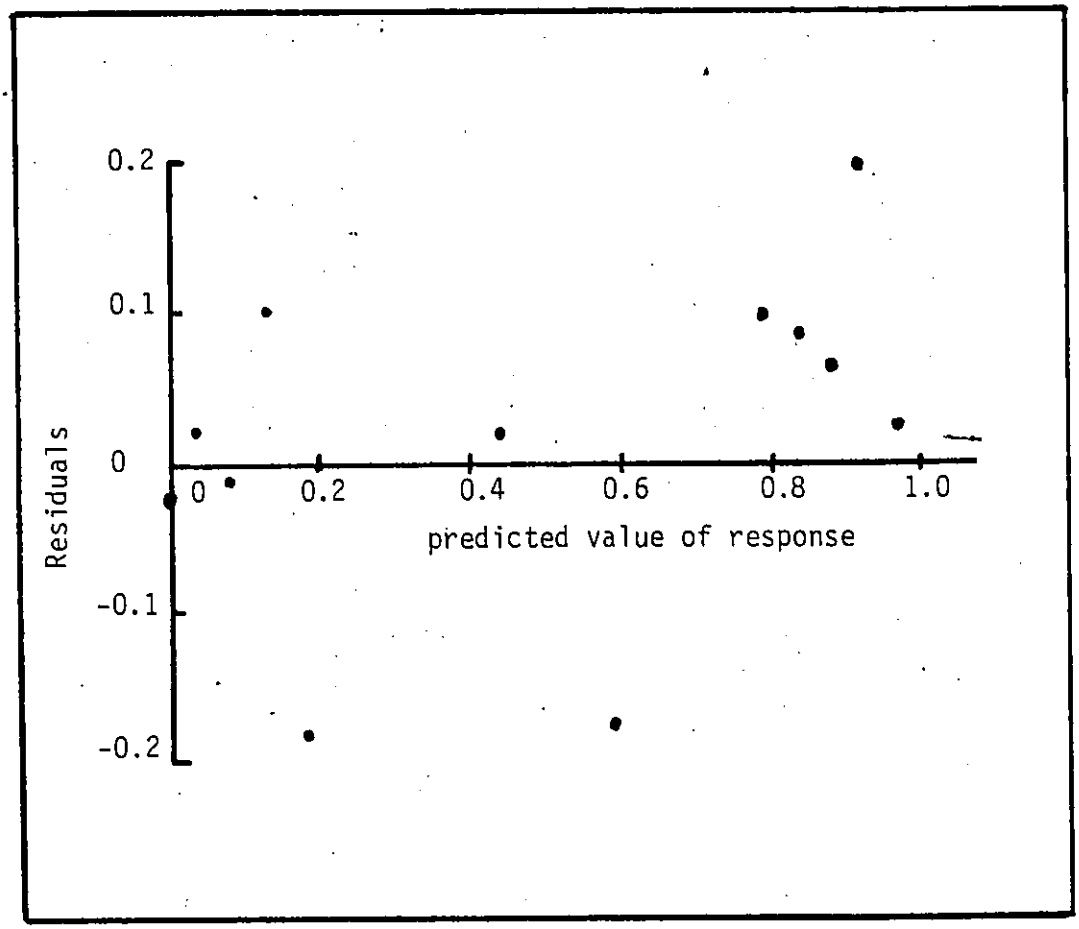

Figure 5-22 Residuals for combined reactor/measurement device model Particle Size 1.0 - 1.4 mm, Impeller Speed 1800 rpm, Gas Flowrate 16.7 $cm^3\ s^{-1}$

which were not significantly different from those obtained from the multiresponse fitting, a graph showing the fit of measurement device model to the data is unnecessary.

The empty reactor volume found by water displacement experiments (i.e. by measuring the volume of water required to fill the reaction chamber) was found to be 30 mL $\pm$ 1 mL. The volume of the connecting lines to and from the reactor are estimated to be in the order of 1 mL. The total reactor volume found through the mixing experiments is 37.2 $\pm$ 6.1 mL. This is therefore consistent with the water displacement tests in the lower half of the interval.

Estimated theoretical voidage volumes in the char bed corresponding to the different particle sizes were found based on Leva's correlation, details of which may be found in Appendix K. A comparison of the total volume available for the gas found by the modelling and that estimated based on the voidages is presented in Table 5-8. The total gas volumes found with the two methods are consistent.

Analysis of the factorial design led to the following expression for the backmix volume:

$$V_B = 24.50 + 0.55\left[\frac{RPM-900}{900}\right] + 0.41\left[\frac{FR-750}{750}\right] + 0.115PS \quad \text{Equation 5-7}$$

where RPM = impeller speed

FR = feed gas flowrate

TABLE 5-8

Comparison of Free Gas Volume in the Reactor

Operating Conditions					
Particle Size [mm]	Feed Gas Flowrate [cm^3/min]	Impeller Speed [rpm]	Calculated V_T (mL)		Estimated* V_T (mL)
0.2-0.4	500	0	24.6 ± 3.6		
	500	1800	26.6 ± 4.3	Avg	28.1 ± 9.1
	1000	0	24.9 ± 4.6	26.9	
	1000	1800	31.5 ± 7.4		
0.4-1.0	750	900	29.2 ± 3.7	Avg	
	750	900	31.9 ± 6.1	30.6	28.6 ± 5.0
1.0-1.4	500	0	30.8 ± 2.6		
	500	1800	30.8 ± 2.4	Avg	
	1000	0	28.4 ± 2.7	30.0	28.6 ± 5.0
	1000	1800	29.8 ± 3.0		

* Based on an Empty Reactor Volume Between 32-42 ml

PS = particle size = 0 for particles 0.4 - 1.0 mm
-1 for particles -0.2 - 0.4 mm
+1 for particles 1.0 - 1.4 mm

The volume of the reactor which is being completely mixed can be increased therefore by increasing the impeller speed, increasing the feed gas flowrate, and decreasing the bed pressure drop by using larger particles. The small plug flow region, which under the operating conditions examined accounted for 8 to 12 percent of the reactor volume, may only be reduced by using feed gas flowrates above 1000 cm^3/min since the impeller speed of 1800 rpm is at the maximum tolerance, and particles larger than 1.4 mm will present pore diffusion problems.

5.4 Other Tests

5.4.1 Gas Flow Pattern in Solids Bed

Tests were carried out in order to determine whether the gas flow through the solid char bed was uniform for those operating conditions which most closely approached the complete mixing assumption. For this purpose, the annular basket was charged with indicating drierite ($CaSO_4$) and indicating

ascarite II as shown in Figure 5-23. Helium with a small amount of CO_2 was fed to the reactor for 30 minutes. During use, the normally light greenish brown color of Ascarite II should gradually turn to white due to absorption of CO_2 and formation of sodium carbonate. At the end of the allotted time, the reactor was taken apart and the layers visually inspected. This experiment was repeated with various quantities of CO_2 added for varying lengths of time (up to 1 1/2 hrs). The results of all these experiments were the same. The layers of ascarite which should have turned white with the formation of Na_2CO_3 in the presence of CO_2 did not change color. Layer A was always very moist so that a small amount of reaction with carbon dioxide was taking place. However, very little if any color change was observed even in this layer. In the upper layers the ascarite was progressively less moist. This would indicate that some of the gas must be bypassing the solid bed since the quantities of CO_2 and the flowrates of the feed gas used should have made the ascarite turn white. Approximate calculations of the pressure head developed by the impeller (see Appendix L) show that the suction provided may not be sufficient to allow for recirculation through the ascarite/drierite bed.

5.4.2 Temperature Profile

The three Chromel Alumel Type K thermocouples used in measuring the reactor temperature were checked against a

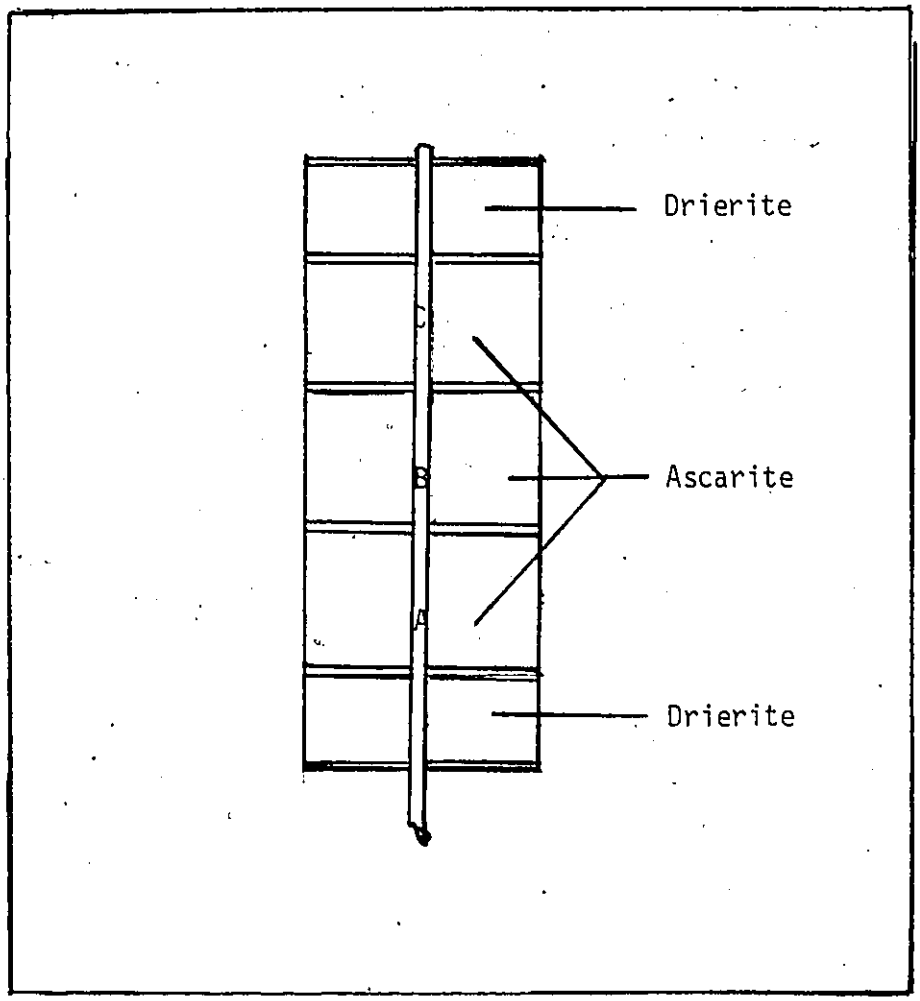

Figure 5-23 Schematic of solid packing for gas flow determination

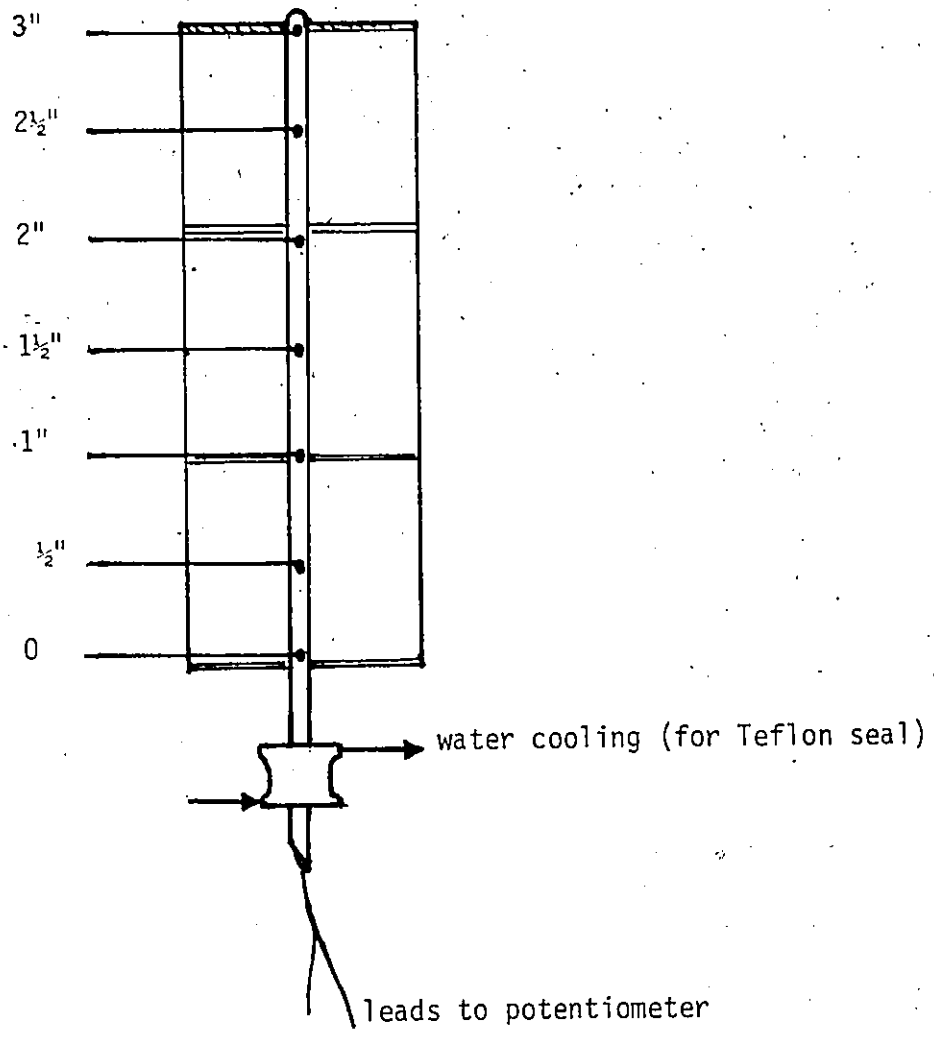

Figure 5-24 Thermocouple arrangement inside reactor bed

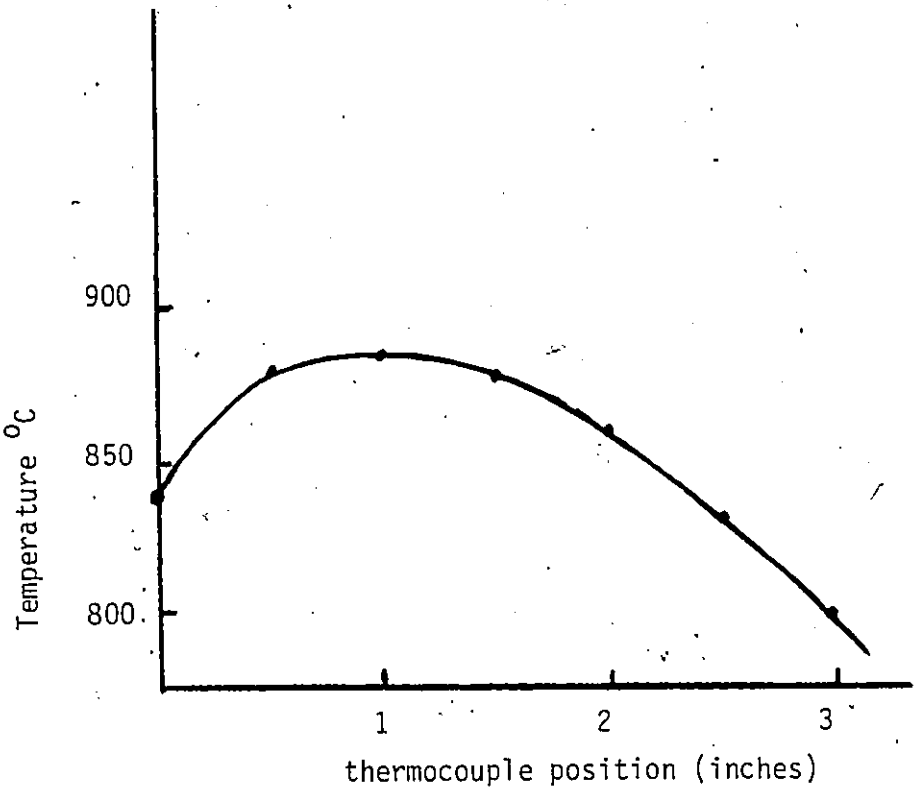

Figure 5-25 Axial temperature profile in char bed

mercury thermometer up to 650°C and against a pyrometer over the range 400-1000°C with a Leeds and Northrup model 8686 millivolt potentiometer. As expected, at temperatures above 600°C there was very little difference in the millivolt readings from all three thermocouples (∿ .3 mv equivalent to 8°C). The positioning of the thermocouples inside the reactor is illustrated in Figure 5-24. The central TC could be moved throughout the height of the solid bed. With N_2 flowing through the reactor, the reactor was heated to 800°C. The magnedrive was activated and the temperature inside the central sheath was measured at the different positions. The axial temperature profile for the nonreacting system found in this manner is given in Figure 5-25. It can be seen from this profile that a large temperature gradient exists throughout the solid bed. This gradient may be due to a number of reasons. First, despite the heavy insulation, the influence of the water cooling (needed to keep the shaft bearings below 300°C) on the temperature in the reaction chamber is significant, i.e. a large driving force exists for conduction of heat up the shaft. A longer shaft may improve this problem in the upper third of the bed however, increasing the length of shaft further is not possible because of problems encountered in vibrations of the impeller shaft. The reason for the large temperature drop in the bottom 1/3 of the solid bed is due to conduction of heat along the thermocouple well to the exterior of the reactor where water cooling is provided to keep the Teflon seal in operation. The seal allows the thermocouple to

be moved vertically in the bed. This problem could have been circumvented by using a multipoint thermocouple inside the well with the leads connected to a multipoint potentiometer. Finally, since there is some evidence of poor gas circulation in the char bed, this too may contribute to the existing temperature gradient.

The radial temperature profile inside the solid bed cannot be assessed with the present reactor. Nevertheless, there appears to be a large temperature difference between the temperature of the controlling thermocouple ($800^{o}C$) and the central thermocouple. Some of this difference can be accounted for by conduction of heat across the steel surfaces. Isothermal operation even for the nonreacting system could not be achieved with this reactor without some major modifications. It was therefore decided to assess the potential of the reactor based on the testing carried out up to this point and to determine whether further testing was warranted.

5.5 Conclusion

Analysis of the reactor model parameters has revealed that the internal recirculation reactor designed and built in this study is not completely mixed under any of the operating conditions examined. A small plug flow region (in the order of 10% of the total available volume) exists in series with the

completely mixed section. This plug flow region is too large to be entirely accounted for by the inlet and exit lines to the reactor. This suggests that some minor changes in the reactor design or in the operating conditions are necessary to obtain complete mixing in the reaction chamber. Because of the nature of the reactor, modifications to it are both expensive and time-consuming.

Testing carried out to determine the reactor temperature profile has shown that even for the non-reacting system, isothermality has not been achieved. It remains quite a challenge in reactor assembly construction to minimize conduction up the shaft at elevated temperatures.

The problems enumerated above are serious since recirculation reactor data analysis is based on the assumptions of isothermality and complete mixing. In view of this, no gasification experiments were conducted with this reactor.

6 CONCLUSIONS AND RECOMMENDATIONS

6.1 Conclusions

1. A critical evaluation of bench-scale reactors in current use for studying gasification kinetics has led to the following conclusions:

   a. Many investigators fail to completely characterize the reactor system and use unfounded assumptions about the system to derive gasification kinetic models from the measured rate data.

   b. Two major weaknesses in the reactor systems in use have been identified. First, in all the reactors (with the exception of the fluidized bed, perhaps), the maintenance of isothermality is difficult. Second, the degree of gas phase mixing in the reactors does not usually approach the mixing state generated by either of the ideal flows.

2. Three alternative reactors which have some potential in overcoming the major limitations of the reactors presently being used in char gasification have been identified, namely, the internal and external recirculation reactors and the continuous stirred tank reactor.

3. Experimental testing has been carried out on an internal recirculation reactor designed and built in this study. Two distinct problems have not been overcome: severe conduction along the rotating shaft and reaction chamber design for complete mixing behavior to prevail.

4. The approach presented in this study for deriving the residence time distribution for small reactors where the measurement device dynamics are significant has been shown to be a useful tool for testing the gas phase mixing assumptions.

6.2 Recommendations for Future Work

It is recommended that further work with a modified version of the reactor discussed in this study be considered because of the potential of using an internal recycle reactor to study gasification kinetics. Modifications to the present reactor are needed in two major areas. First, the reaction chamber internals should be modified so that the fluid flow approaches complete mixing and second, the magnedrive assembly bearings and seals should be changed to allow operation at higher temperatures without the need for cooling. The latter may be accomplished by investigating the possibility of using ceramics instead of teflon and graphite as materials. Several suggestions for designing the reaction chamber so that complete mixing is approached are given below:

1. increase the capacity of the drive motor so as to increase the impeller RPM.
2. obtain the pressure drop versus flow relationship for the solid bed.
3. obtain the velocity head developed by the impeller as a function of its rpm by building a precursor to the reactor with special pressure taps.

The solid bed dimensions and the impeller design can be determined from 1, 2 and 3 accordingly.

If sufficient funds are available, commissioning this work to Autoclave Engineers is recommended.

REFERENCES

1. Verma, A., "An Overview of Coal Gasification Technology", Preprint 26th CCEC, Toronto, Oct. 3-6 (1976).

2. Littlewood, Kenneth, "Gasification: Theory and Application", Prog. Energy Comb. Sci., Vol. 3, p. 35-71 (1977).

3. Smoot, L.D. and D.T. Pratt (ed.), "Pulverized - Coal Combustion and Gasification", Plenum Press, New York (1979).

4. Laurendeau, N.M., "Heterogeneous Kinetics of Coal Char Gasification and Combustion", Prog. Energy Comb. Sci., Vol. 4, No. 4, p. 221 - 270 (1978).

5. Tyler, R. J. and I.W. Smith, "Reactivity of Petroleum Coke to CO_2 Between 1030 and 1180K", Fuel, Vol. 54, p. 99 - 104 (Oct. 1975).

6. Curran, G.P., Carl E. Fink and Everett Gorin, "Kinetics of Lignite Char Gasification", Ind. Eng. Chem. Proc. Des. and Dev., Vol. 8, No. 4, p. 559 - 567 (Oct. 1969).

7. Dotson, J.A., W.A. Koehler and J.H. Holden, "Rate of the Steam-Carbon Reaction by a Falling Particle Method", Ind. Eng. Chem., Vol. 49, No. 1, p. 148 - 154 (1957).

REFERENCES (cont'd)

8. Walker, P.L., F. Rusinko and L.G. Austin, "The Gas Reactions of Carbon", Adv. Catal., Vol. 11, p. 133 - 221 (1959).

9. von Fredersdorff, C.G. and M. A. Elliott, "Chemistry of Coal Utilization", H.A. Lowry, (Ed.), Supplementary Volume, John Wiley and Sons, New York, New York, p. 1142 (1963).

10. Jenkins, R.G., S. Nandi and P.L. Walker Jr., "Reactivity of Heat-Treated Coals in Air at 500°C", Fuel, Vol. 52, p. 288 - 293 (Oct. 1973).

11. Carberry, J.J., "Heat and Mass Diffusional Intrusions in Catalytic Reactor Behavior", Catalysis Reviews, Vol. 3, p. 61 - 90 (1970).

12. Wen, C.Y., "Noncatalytic Heterogeneous Solid Fluid Reaction Models", Ind. Eng. Chem., Vol. 60, No. 9, p. 34 - 54 (1968).

13. Szekely, J., J.W. Evans and H.Y. Sohn, "Gas Solid Reactions", Academic Press, New York (1976).

14. Smith, J.M., "Chemical Reaction Kinetics", 2nd Ed, McGraw-Hill Book Co., New York (1970).

REFERENCES (cont'd)

15. Froment, G.F. and K.B. Bischoff, "Chemical Reactor Analysis and Design", John Wiley and Sons, New York (1979).

16. Berkowitz, N., "An Introduction to Coal Technology", Academic Press, New York (1979).

17. Bird, R.B., W.E. Stewart and E.N. Lightfoot, "Transport Phenomena", Wiley, New York (1960).

18. Reid, R.C., J.M. Prausnitz and T.K. Sherwood, "The Properties of Gases and Liquids", McGraw-Hill Book Co., New York (1977).

19. Satterfield, C.N., "Heterogeneous Catalysis in Practise", McGraw-Hill Book Co., New York (1980).

20. Yoshida, F., D. Ramaswami and O.A. Hougen, "Temperatures and Partial Pressures at the Surfaces of Catalyst Particles", A.I. Ch. E. Journal, Vol. 8, No. 1, p. 5 - 11 (1962).

21. Mears, D.E., "Tests for Transport Limitations in Experimental Catalytic Reactors", Ind. Eng. Chem. Proc. Des. Dev., Vol. 10, No. 4, p. 541 - 547 (1971).

REFERENCES (cont'd)

22. Carberry, J.J., "Designing Laboratory Catalytic Reactors", Ind. Eng. Chem., Vol. 56, No. 11, p. 39 - 46 (1964).

23. Levenspiel, O., "Chemical Reaction Engineering", 2nd Ed., John Wiley and Sons Inc., Toronto (1972).

24. Szekely, J and J.J. Poveromo, "Flow Maldistribution in Packed Beds: A Comparison of Measurements with Predictions", A.I. Ch. E. Journal, Vol. 21, No. 4, p. 769 - 774 (1975).

25. Koros, R.M. and E.J. Novak, "A Diagnostic Test of the Kinetic Regime in a Packed Bed Reactor", Che. Eng. Sci., Vol. 22, p. 470 (1967).

26. Chambers, R.P. and M. Boudart, J. Catal., No. 6, p. 141 (1966).

27. Wen, C.Y. and L.T. Fan, "Models for Flow Systems and Chemical Reactors", Marcel Dekker Inc., New York (1975).

28. Levenspiel, O. and K.B. Bischoff, Adv. Chem. Eng., Vol. 4, Academic Press, New York (1963).

29. Johnson, J.L., L.T. Fan and Y. Wu, Ind. Eng. Chem. Proc. Des. Dev., 10, p. 425 - 431 (1971).

REFERENCES (cont'd)

30. Michelson, M.L., "A Least Squares Method for Residence Time Distribution", Chem. Eng. J., 4, p. 171 - 179 (1972).

31. Bashi, H. and D. Gunn, A.I. Ch. E. Journal, Vol. 23, p. 40 (1977).

32. Weekman, V.W. Jr., "Laboratory Reactors and Their Limitations", A.I. Ch. E. Journal, Vol. 20, No. 5, p. 833 - 840 (1974).

33. Doraiswamy, L.K. and D.G. Tajbl, "Laboratory Catalytic Reactors", Cat. Rev. - Sci. Eng., 10 (2)., p. 177 - 219 (1974).

34. Shah, Y.T., "Gas Liquid Solid Reactor Design", McGraw-Hill, New York, p. 149 - 175 (1979).

35. Anderson, R.B. and P.T. Dawson, "Experimental Methods in Catalytic Research", Vol. II (1976).

36. Kayembe, N. and A.H. Pulsifer, "Kinetics and Catalysis of the Reaction of Coal Char and Steam", Fuel, 55 p. 211 (1976).

37. Thompson, B., "Fundamentals of Gas Analysis by Gas Chromatography", Varian, California (1977).

REFERENCES (cont'd)

38. Dutta, S., C.Y. Wen and R.J. Belt, "Reactivity of Coal and Char in CO_2 Atmosphere", ACS Div. of Fuel Chem. Preprints, Vol. 20, No. 3, p. 103 - 114 (1975).

39. deWasch, A.P. and G.F. Froment, "A Two Dimensional Heterogeneous Model for Fixed Bed Catalytic Reactors", Chem. Eng. Sci., Vol. 26, p. 619 - 634 (1971).

40. Gardner, N., E. Samuels and K. Wilks, "Catalyzed Hydrogasification of Coal Chars", ACS. Div. of Fuel Chem. Preprints, Vol. 18, No. 2, p. 43 (1973).

41. Costa, E.C. and J.M. Smith, A.I. Ch. E. Journal, Vol. 17, No. 4, p. 947 (1971).

42. Mayers, M.A., "The Rate of Reduction of CO_2 by Graphite", J. Amer. Chem. Soc., Vol. 56, 70, 6 (1934).

43. Butt, J.B. and V.W. Weekman Jr., "Characterization of Activity Selectivity and Aging Properties of Heterogeneous Catalysts", A.I. Ch. E. Symposium Series, No. 143, Vol. 70, p. 27 - 41 (1974).

REFERENCES (cont'd)

44. Haynes, W.P., S.J. Gasior and A.J. Forney, "Catalysis of Coal Gasification at Elevated Pressure", ACS Div. Fuel Chem. Pre., Vol. 18, No. 2, p. 1 (1973).

45. Denbigh, K.G., "Chemical Reactor Theory", Cambridge University Press, Cambridge (1965).

46. ———, Institute of Gas Technology Research Bulletin, No. 39, Vol. 1, (1954 - 1964).

47. Hunt, B.E., S. Mori, S. Katz and R.E. Peck, "Reaction of Carbon with Steam at Elevated Temperatures", Ind. Eng. Chem., Vol. 45, No. 3, p. 677 - 680 (1953).

48. Feldkirchner, H.L. and J. Huebler, "Reaction of Coal with Steam-Hydrogen Mixtures at High Temperatures and Pressures", Ind. Eng. Chem. Proc. Des. Dev., Vol. 4, No. 2, p. 134 - 142 (1965).

49. Vadovik, C.J. and J.M. Eakman, "Kinetics of Potassium Catalyzed Gasification", ACS Fuel Division, Vol. 23, No. 3 (1978).

50. Chan, E.M. and M.M. Papik, "Gasification of Hat Creek Coal", Can. J. Chem. Eng., Vol. 54, p. 645 (Dec. 1976).

REFERENCES (cont'd)

51. Wicke, E., "Contributions to the Combustion Mechanism of Carbon", 5th Symposium on Comb., Comb. Inst. Reinhold Publishing Corp., New York (1955).

52. Blackwood, J.D. and F. McGrory, "The Carbon-Steam Reaction at High Pressure", Aust. J. Chem., Vol. 11, p. 16 - 33 (1958).

53. Blakeley, T.H., "Gasification of Carbon in Carbon Dioxide and Other Gases at Temperatures above 900K", in Proceedings of the 4th Conference on Carbon, Buffalo, New York, 1959, p. 95 - 105 (1960).

54. Taylor, R.W. and D.W. Bowman, "Rate of Reaction of Steam and CO_2 with Chars Produced from Subbituminous Coals", California University, Livermore, USA, UCRL 52002 (1976).

55. Ergun, S. and M. Mentser, Chem. Phy. Carbon, P.L. Walker (ed.), Vol. 1, p. 203 - 263 (1965).

56. Cadenhead, D.A. and N.J. Wagner, "Microbalances in Adsorption and Catalysis", Chapter 6 in "Experimental Methods in Catalytic Research", Vol. II, (R.B. Anderson and P.T. Dawson, ed.) , Academic Press, New York (1976).

REFERENCES (cont'd)

57. Delmon, B., "Introduction a la Cinetique Heterogene", Editions Technip, Paris (1969).

58. Jenson, G.A., Ind. Eng. Chem. Proc. Des. Dev., Vol. 14, No. 3 (1975).

59. Fuchs, W. and P.M. Yavorsky, "Gasification of Hydrane Char in Reactions with CO_2 and Steam", ACS Div. Fuel Chem. Pre., Vol. 20, No. 3, p. 115 - 133 (1975).

60. Zahradnik, R.L. and R.J. Grace, Adv. Chem. Series, No. 131, p. 126 - 144 (1974).

61. Coates, R.L., "Coal Processing Technology", A.I. Ch. E. Pub., New York, New York, p. 89 - 94 (1977).

62. Turkdogan, E.T., V. Koump, J.V. Vinters and T.F. Perzak, "Rate of Oxidation of Graphite in CO_2, Carbon, Vol. 6, p. 467 - 484 (1968).

63. Tien, R.H. and E.T. Turkdogan, "Incomplete Pore Diffusion Effect on Internal Burning of Carbon", Carbon, Vol. 8, p. 607 - 621 (1970).

REFERENCES (cont'd)

64. Veraa, M.J. and A.T. Bell, "Effect of Alkali Metal Catalysts on Gasification of Coal Char", Fuel, Vol. 57, p. 194 - 200 (1978).

65. Otto, K. and M. Shelef, "Catalytic Steam Gasification of Graphite: Effects of Intercalcated and Externally Added Ru, Rh, Pd and Pt", Carbon, Vol. 15, p. 317 - 325 (1977).

66. Riede, B.E. and D. Hanesian, "Kinetic Study of Carbon-Steam Reaction", Ind. Eng. Chem. Proc. Des. Dev., Vol. 14, No. 1 (1975).

67. Pilcher, J.M., P.L. Walker Jr. and C.C. Wright, "Kinetic Study of Steam-Carbon Reaction", Ind. Eng. Chem., Vol. 47, No. 9, p. 1742 - 1749 (1955).

68. Elliott, M.A., H. Perry, J. Jonakin, R.C. Corey and M.L. Khullar, Ind. Eng. Chem., Vol. 44, No. 5, p. 1074 - 1082 (1952).

69. Tuddenham, W.M. and G.R. Hill, Ind. Eng. Chem., Vol. 47, No. 10, p. 2129 (1955).

70. Gilliland, E.R. and E.A. Mason, "Gas Mixing in Beds of Fluidized Solids", Ind. Eng. Chem., Vol. 44, p. 218 (1952).

REFERENCES (cont'd)

71. Richardson, J.F. and J. Ayers, Trans. Inst. Chem. Eng., Vol. 37, p. 314 (1959).

72. Ergun, S., "Kinetics of the Reaction of CO_2 and Carbon", J. of Phys. Chem., 60, p. 480 (1956).

73. Goring, G.E., G.P. Curran, R.P. Tarbox and E. Gorin, "Kinetics of Carbon Gasification by Steam", Ind. Eng. Chem., Vol. 44, No. 5, p. 1051 - 1065 (1952).

74. Johnson, J.L., "Kinetics of Bituminous Coal Char Gasification with Cases Containing Steam and Hydrogen", ACS Div. of Fuel Chem. Preprints, Vol. 18, No. 1, p. 228 (1973).

75. Zielke, C.W. and E. Gorin, "Kinetics of Carbon Gasification", Ind. Eng. Chem., Vol. 49, No. 3, p. 396 - 402 (1957).

76. ibid, Ind. Eng. Chem., Vol. 47, No. 4, p. 820 - 825 (1955).

77. May, W.G., R.H. Mueller, and S.B. Sweetser, "Carbon-Steam Reaction Kinetics from Pilot Plant Data", Ind. Eng. Chem., Vol. 50, No. 9, p. 1289 - 1296 (1958).

REFERENCES (cont'd)

78. Feistel, P.P., K.H. vanHeek and H. Juntgen, "Gasification of a German Bituminous Coal with H_2O, H_2 and H_2O/H_2 Mixtures", ACS, Div. of Fuel Chem., Vol. 22, No. 1, p. 53 - 83 (1977).

79. Binford, J.S. Jr. and H. Eyring, J. Phy. Chem., Vol. 60, p. 486 (1956).

80. Montet, G.L. and G.E. Myers, Carbon, Vol. 6, p. 627 - 636 (1968).

81. Coates, R.L., "Kinetic Data from a High-Temperature Entrained Flow Gasifier", ACS. Div. Fuel Chem., Vol. 22, No. 1, p. 84 (1977).

82. Coates,R.L., C.L. Chen and B.J. Pope, "Coal Gasification in a Low Pressure Low Residence Time Entrained Flow Reactor", ACS, Div. Fuel Chem., Vol. 18, No. 1, p. 165 (1973).

83. Johnson, J.L., "Kinetics of Initial Coal Hydrogasification Stages", ACS Div. Fuel Chem. Pre., Vol. 22, No. 1, p. 17 - 37 (1977).

84. Pulsifer, A.H., T.M. Knowlton and T.D. Wheelcock, Ind. Eng. Chem. Proc. Des. Dev., Vol. 8, No. 4, p. 539 - 545 (1969).

REFERENCES (cont'd)

85. Wen, C.Y. and J. Huebler, "Kinetic Study of Coal Char Hydrogasification" Ind. Eng. Chem. Proc. Des. Dev., Vol. 4, No. 2, p. 143 - 154 (1965).

86. Feldmann, H.F., "The Role of Chemical Reaction Engineering in Coal Gasification", Adv. Chem. Series 148, p. 132 - 155 (1975).

87. Ratcliff, J.S. and G.R. Rigby, "Low Temperature Carbonization of Coal in a Spouted Bed, Prediction of Exit Char Volatile Matter", Mech. Chem. Eng. Trans., p. 1 - 6 (1969).

88. Ray, T.B. and S. Sarkar, "Kinetics of Coal Pyrolysis in Spouted Bed", Indian Chem. Eng., Vol. XVIII, No. 2, p. 11 - 19 (1976).

89. Foong, S.K., C.J. Lim and A.P. Watkinson, "Coal Gasification in a Spouted Bed", Can. J. Chem. Eng., Vol. 58, p. 84 (1980).

90. Pulsifer, A.H., T.M. Knowlton and T.D. Wheelcock, "Coal Char Gasification in an Electrofluid Reactor", Ind. Eng. Chem. Proc. Des. Dev., Vol. 8, No. 4, p. 539 - 545 (1969).

REFERENCES (cont'd)

91. Butler, R. and A. Snelson, "Coal Gasification Studies - Part I: Single Stage Complete Gasification of Coal Using Water as the Hydrogen Source", Fuel Processing Tech. I, p. 297 - 304 (1977).

92. Yang, R.T. and M. Steinberg, "A Diffusion Cell Method for Studying Heterogeneous Kinetics in the Chemical Reaction/Diffusion Controlled Region. Kinetics of C + $CO_2 \rightarrow 2CO$ at 1200-1600°C.", Ind. Eng. Chem. Fund., Vol. 16, p. 235 (1977).

93. Ingle, A.N., "Gasification of Coal in a Spouted Bed", M. Tech. Dissertation, Indian Institute of Technology, Bombay (1975).

94. Bennett, C.O., M.B. Cutlip. and C.C. Yang, "Gradientless Reactorsand Transient Methods in Heterogeneous Catalysis", Che. Eng. Sci., Vol. 27, p. 2255 - 2264 (1972).

95. Nystrom, M.G., "Choice of Recirculation Flow Rate in a Gradient-Free Reactor with a Porous Catalyst", Chem. Eng. Sci., Vol. 33, p. 390 - 391 (1978).

REFERENCES (cont'd)

96. Hanson, F.V. and J.E. Benson, "An Inexpensive Non-Contaminating Gas Recirculation Pump", J. Catal., 31, p. 471 - 472 (1973).

97. Gray, J.A., P.J. Donatelli and P.M. Yavorsky, ACS Div. Fuel Chem. Pre., Vol. 20, No. 4, p. 103 (1975).

98. Lowe, A. and E. Bilgesu, "Kinetics of Reaction and of Reactivity Change of a Gas Solid Reaction in a Recycle Reactor with Variable Feed", Chem. Eng. Sci., Vol. 35, p. 1307 - 1315 (1980).

99. Berty, J.M., Chem. Eng. Progr., 70, p. 78 - 84 (1974).

100. Mahoney, J.A., "The Use of a Gradientless Reactor in Petroleum Reaction Engineering Studies", J. Catal., 32, p. 247 - 253 (1974).

101. Northam, D.B. and C.W. vonRosenberg Jr., Fuel, Vol. 58, (April 1979).

102. McNair, H.M. and E.J. Bonelli, "Basic Gas Chromatography", Varian Aerograph, Walnut Creek, California, 2nd Ed., (1966).

REFERENCES (cont'd)

103. Jaech, J.L., J. Am. Stat. Ass., 59, p. 863 (1964).

104. Mandel, J., J. Am. Stat. Ass., 52, p. 552 (1957).

105. Mandel, J., J. Am. Stat. Ass., 6, p. 225 (1964).

106. Lyttkens, E., Proceedings Symp: Time Series Analysis, Edit. Rosenblatt Wiley, p. 49 (1963).

107. Nelson, L.S. (ed.), "Regression Analysis of Cumulative Data", Tech., Vol. 6, No. 2 (1964).

108. Beck, J.V., Tech., Vol. 16, No. 1 (Feb. 1974).

109. Perry, R.H. and C.H. Chilton (ed.), "Chemical Engineers' Handbook", 5th Ed., McGraw-Hill Book Co., New York (1973).

110. Cholette, A. and L. Cloutier, Can. J. Chem. Eng., Vol. 37, p. 105 (1959).

111. Otto, K., L. Bartosiewicz and M. Shelef, Fuel, Vol. 58, p. 85 - 91 (1979).

112. Wilson, E.J. and G.J. Geankopolis, Ind. Eng. Chem. Fund, 5, p. 9 (1966).

REFERENCES (cont'd)

113. Desai, N.J. and R.T. Yang, "Kinetics of High Temperature Carbon Gasification Reaction", A.I. Ch. E. Journal, p. 239 (March 1982).

114. Schumann, J.E. and V. Voss, Fuel, 13, p. 249 (1934).

115. Schotte, W., A.I. Ch. E. Journal, Vol. 6, No. 1, p. 63 (1960).

116. Kuchinski, G.R. and R.G. Squires, J. Catal., 41, p. 486 - 488 (1976).

117. Draper, N.R. and W.G. Hunter, "Design of Experiments for Parameter Estimation in Multiresponse Situations", Biometrika, 53, 3 and 4, p. 525 (1966).

118. Gadsby, J., C.N. Hinshelwood and K.W. Sykes, "The Kinetics of the Reactions of the Steam-Carbon System", Proc. Roy. Soc. (London), A187, p. 129 - 151 (1946).

119. Johnstone, H.F., C.Y. Chen and D.S. Scott, "Kinetics of the Steam-Carbon Reaction in Porous Graphite Tubes", Ind. Eng. Chem., Vol. 44, No. 7, p. 1564 - 1569 (1952).

REFERENCES (cont'd)

120. Jolley, L.J. and A. Poll, "Effects of Reactivity and Some Other Variables on Gasification of Coke with Steam", J. Inst. Fuel, Vol. 26, p. 33 - 44 (1953).

121. Blackwood, J.D. and A.J. Ingeme, "The Reaction of Carbon with Carbon Dioxide at High Pressure", Aust. J. Chem., Vol. 13, p. 194 (1960).

122. Vastola, F.J. and P.L. Walker Jr., "The Reaction of Graphite Wear Dust with CO_2 and O_2 at Low Pressures", J. de Chi. Phy., Vol. 58, p. 20 (1961).

123. Blackwood, J.D., "The kinetics of the System Carbon-Hydrogen-Methane", Aust. J. Chem., Vol. 15, p. 397 (1962).

124. Feldkirchner, H.L. and H.R. Linden, "Reactivity of Coals in High-Pressure Gasification with H_2 and H_2O", Ind. Eng. Chem. Proc. Des. Dev., Vol. 2, No. 2, p. 153 - 162 (1963).

125. vanHeek, K.H. and H. Juntgen, J. Inst. Fuel, 46, p. 249 - 257 (June 1973).

126. Wilson, W.G., L.J. Sealock Jr., F.C. Hoodmaker, R.W. Hoffman, D.L. Stinson and J.L. Cox, Adv. Chem. Series, 131 (1974).

REFERENCES (cont'd)

127. Smith, J.W. and R.J. Tyler, Comb. Sci. Tech., Vol. 9, p. 87 - 94 (1974).

128. Smith, J.W. and R.J. Tyler, Fuel, Vol. 51, p. 312 - 321 (1972).

129. Gulbransen, E.A. and K.F. Andrew, Ind. Eng. Chem., Vol. 44, No. 5, p. 1034 - 1051 (1952).

130. Walker, P.L. Jr., R.J. Foresti, C.C. Wright, Ind. Eng. Chem., Vol. 45, No. 8, p. 1703 - 1710 (1953).

131. Blakely, J.P. and L.G. Overholser, Carbon, Vol. 3, p. 269 - 275 (1965).

132. Giberson, R.C. and J.P. Walker, Carbon, Vol. 3, p. 521 - 525 (1966).

133. Blake, J.H., G.R. Bopp, J.F. Jones, M.G. Miller, and W. Tambo, Fuel, Vol. 46, p. 115 (1966).

134. Walker, P.L. Jr., M. Shelef and R.A. Anderson, Chemistry and Physics of Carbon, Vol. 4, p. 287 - 383 (1968).

135. Turkdogan, E.T. and J.V. Vinters, Carbon, Vol. 10, p. 97 - 111 (1972).

REFERENCES (cont'd)

136. Turkdogan, E.T. and J.V. Vinters, Carbon, Vol. 8, p. 39 - 53 (1970).

137. Kertamus, N.J., M.A. Paisley and W.L. Sage, ACS Div. Fuel Chem., Vol. 18 No. 3, p. 112 (1973).

138. Nandi, S.P., R. Lo and J. Fischer, ACS Div. Fuel Chem., Vol. 20, No. 3, p. 88 - 98 (1975).

139. Walker, P.L. Jr. and E.J. Hippo, ACS Div. Fuel Chem., Vol. 20, No. 3, p. 45 - 51 (1975).

140. Wilks, K.A., M.Sc., Case Western University (1974).

141. Biederman, D.L., A.J. Miles, J. Vastola and P.L. Walker Jr., Carbon, Vol. 14, p. 351 - 356 (1976).

142. Otto, K. and M. Shelef, Paper Presented at 6th International Congress on Catalysis, London (July 1976).

143. Strange, J.F. and P.L. Walker Jr., Carbon, Vol. 14, p. 345 - 350 (1976).

144. Chauhan, S.P. and J.R. Longanback, ACS Div. Fuel Chem. Pre., Vol. 23, No. 3 (1978).

REFERENCES (cont'd)

145. Tomita, A., O.P. Mahajan and P.L. Walker Jr., ACS Div. Fuel Chem. Pre., Vol. 22, No. 1, p. 4 - 6 (1977).

146. Chauhan, S.P., H.F. Feldmann, E.P. Stambaugh, J.H. Oxley, ACS Div. Fuel Chem. Pre., Vol. 20, No. 4, p. 207 (1975).

147. Koba, K. and S. Ida, Fuel, Vol. 59, p. 59 (1980).

148. Himmelblau, D.M., "Process Analysis by Statistical Methods", John Wiley and Sons Inc., New York (1970).

APPENDIX A

Compilation of Char Gasification Bench-Scale Kinetic Studies

APPENDIX A

Compilation of Char Gasification Bench Scale Kinetic Studies

REFERENCES	REACTOR TYPE	CARBON/CHAR CHARACTERISTICS	SAMPLE PRETREATMENT	OPERATING CONDITIONS	COMMENTS
118	Integral Fixed Bed L 10 cm D 3.1 cm	Charcoal 35 gm 8-10 B.S.S.	Active charcoal (from carbonization & steam activation) of coconut shell & briquetted coal	T: 700 - 800°C P: 10-760 mm H_g F: 1200 cc/min	Steam-carbon reaction kinetics
119	Differential Tubular Bed D 1.5 cm Integral	Porous graphite tubes length .75" length 9" 20 gm	Partial degassing in vacuum & flushing with N_2	T: 862-938°C P: 1 atm F: 900 ml/min	Steam-carbon reaction kinetics
47	Integral Fixed Bed 3in ID	High temperature pitch coke .078-.033"		T: 1800-2500°F P: 1 atm	Steam-carbon reaction kinetics at high temperature
120	Integral Fixed Bed L = 1.25 in D = 2-3 in	Coke .4 mm particles 30 gm	Coke was first flushed with nitorgen at required temperature.	T: 800-950°C P: 1 atm F: 35-75 lph (NTP)	Reactivity of coke and steam vs Rank, Particle Size, Steam Flow, etc.
9	Integral Fixed Bed D = 3 in L = 5 in	Pitch coke -10 + 40 US sieve		T: 1700-2100°F P: 1 atm	Carbon reaction with steam & CO_2 - Obtained & interpreted reaction rate data
52	Differential Tube Reactor 1.8 cm	Coconut charcoal 8.8 gm -7 + 14 mesh	Charcoal heated to 950°C in 2 hrs maintained for 1 hr and cooled to atmospheric temperature in 2 hrs in N_2 stream	T: 750-830°C P: 1-50 atm	Steam-carbon reaction. To examine effect of H_2 addition to steam gasification
121	Differential Tube Reactor	Purified carbon 7.5 gm		T: 790-870°C P: 5-40 atm	Carbon-carbon dioxide reaction at high pressure

APPENDIX A

Compilation of Char Gasification Bench Scale Kinetic Studies (cont'd)

REFERENCES	REACTOR TYPE	CARBON/CHAR CHARACTERISTICS	SAMPLE PRETREATMENT	OPERATING CONDITIONS	COMMENTS
122	Fixed Bed	Carbon wear dust spectrographic graphite	Sample heated to 850°C in vacuo for 3 hours	T: 500-600°C P: low 2.7-16 uHg	Carbon-carbon dioxide low-pressure gasification
123	Differential tubular bed	Coconut-shell charcoal 8.8 gm -7 + 14 mesh		T: 650-870°C P: 40 atm	Kinetics of system C-H_2-methane
124	Differential D= 2 in L = 60 in	Bituminous coal char anthracite -16 +20 m		T: 1700°F P: 2500 psia	Kinetics of H_2/H_2O/C system at high pressure
46	Differential reactor D = 1 1/4 in	Coal char from Pittsburgh seam coal -16 +20 USS 2.5-5 gm		T: 1700-2100°F P: 1000 psig F: 50 scf/hr	Carbon - H_2/H_2O kinetics
125	Differential fixed bed	Variety of coals	Slow heating 10°C/min to required temperature pyrolysis & gasification	T: 400-1100°C P: 1-70 atm	Non-isothermal kinetics of steam gasification
44	Fixed bed L = 6 in D = 3/4 in	Bituminous coal 20 - 60 mesh	Pretreated at 450°C with steam-air mixture to remove caking properties	T: 1500-1800°F P: 300 psi F: 2000 $cm^3 N_2/hr$	Catalytic study of steam gasification
126	Fixed bed D = 1 in	Sub-bituminous coal 60-100 mesh 100 gm coal 110 gm catalyst		T: 650°C P: 2 atm	Catalytic study of steam gasification (N_i, alkali carbonate catalysis)

APPENDIX A

Compilation of Char Gasification Bench Scale Kinetic Studies (cont'd)

REFERENCES	REACTOR TYPE	CARBON/CHAR CHARACTERISTICS	SAMPLE PRETREATMENT	OPERATING CONDITIONS	COMMENTS
127, 128	Fixed bed	Brown coal char 89-22 um	Partial combustion of pulverized brown coal	T: 357-487°C P: 1 atm	Reactivity of char to O_2. - intrinsic reactivity
5	Fixed bed L = 12-15 mm = 1.66	Petroleum coke -14 +25 mesh 3 gm	Coke sample brought to temperature in nitrogen atmosphere	T: 750-950°C P: 1 atm F: 660-1330 cm^3/min NTP	CO_2 gasification kinetic studies intrinsic rate measurement
36	Fixed bed 15 mm°D 1 meter long	Western Kentucky & Bear coal chars 149-177 mm 5 gm	Mixing of char with catalyst in slurry. Evaporation of H_2O at low temperature	T: 600-850°C P: 1-2 atm F: 1 ml/min	Kinetic & catalytic study of coal-steam gasification
54	Differential flow packed bed	Chars from Roland & Felix seam subbituminous Wyoming coals 35 gm	Coal first pyrolysed in H_2, or CO_2. Char sample prepared by heating coal at 800°C in flowing argon	T: 475-675°C P: 1 atm F: 45-425 l/hr steam	C-H_2O, C-CO_2 reaction Analysed data in terms of average initial rates for 0-20% burnoff and average final rates for 70-100% burnoff
78	Differential packed bed	German bituminous coal		T: 600-1100°C P: 1-70 atm	Steam/H_2 gasification
49	Integral fixed bed D = 1 in L = 30 in	Illinois coal #6 20 gm	Purge catalyst impregnated char with helium & raise temperature	T: 1200-1300°F P: 0-500 psig F: 3-100 gm/hr steam	Catalytic steam gasification conversions high
159	Thermogravimetric	AGKSP spectroscopic graphite 0.27 gm 9.91 l; 0.71 ID; 0.47 OD [cm]	Specimen were boiled in distilled H_2O desicated, washed in absolute methanol, and then heated to 1000°C in vacua for 1 hr	T: 500-900°C P: 7.6 cm H_g V	Reaction: CO_2-C Purpose: To determine the nature of the time dependence of the reaction rate for several temperatures, the nature & the role of surface oxide in the reaction, and the role of traces of impurities on the rate of the reaction.

APPENDIX A

Compilation of Char Gasification Bench Scale Kinetic Studies (cont'd)

REFERENCES	REACTOR TYPE	CARBON/CHAR CHARACTERISTICS	SAMPLE PRETREATMENT	OPERATING CONDITIONS	COMMENTS
130,8	Thermo-gravimetric	Spectroscopic carbon reactor tube: 1 1/2" ID, carbon rods 2" long x 1/2" OD and 1/8" hone in centre 8.8 gm	Extrusion into rod	T: 925-1305°C P: 1 atm F: 2200 cc/min	Reaction: CO_2 - C Purpose: Investigate mass transfer and diffusional effects
131	Thermo-gravimetric	Speer moderator - 2 graphite & ATJ graphite 15 gm 2.54 cm D sperical specimen	Specimen was degassed for 4 days under vacuum at 1025°C prior to use	T: 775-925 & 875-1025°C P: 1 atm F: 300 cc/min	Reaction: H_2O vapor/CO_2-C Purpose: To study oxidation rates of two different graphites and to compare the results
132	Thermo-gravimetric	TSC nuclear graphite 8 gm 1.08 cm ID 5.08 cm l cylindrical solid specimen	Specimen was exposed to helium at the set temperature for 18-24 hours	T: 790-850°C P: -	Reaction: H_2O vapor/H_2-C Purpose: Mechanistic study of H_2O-H_2-C gasification
133	Thermo-gravimetric	Cokes & calcined chars from subbituminous coals 200-500 mg -16 + 20 mesh U.S. granular		T: 900-1100°C P: 1 atm V: 10-15 cm/s F: 2879-4730 cc/min	Reaction: CO_2-C Purpose: To develop a test that would compare reactivities of granular carbons and to gain some knowledge of the influence of rather mild thermal treatment on the reactivity of these cokes
134	Thermo-gravimetric	Spectroscopic graphite SP-1		T: 800-1000°C P: 1 atm	Reaction: CO_2-C Purpose: Catalytic study using F_e, N_i, C_o as catalysts for gasification
135	Thermo-gravimetric	Electrode graphite spheres 1/8"-7/8"D blocks			

APPENDIX A

Compilation of Char Gasification Bench Scale Kinetic Studies (cont'd)

REFERENCES	REACTOR TYPE	CARBON/CHAR CHARACTERISTICS	SAMPLE PRETREATMENT	OPERATING CONDITIONS	COMMENTS
136	Thermo-gravimetric	Coconut charcoal, 1% ash, electrode graphite AUC & (.03%) metallurgical coke (7.5 % ash) 70-200 mg granules (.5 mm D) -10 ± 16 m		T: 700-1400°C P: 10-3-40 atm F: 1200 cc/min - 1500 (STP)	Reaction: CO_2-C Purpose: A kinetic and mechanistic study of gasification using CO_2 and mixtures of CO & CO_2
46	Thermo-gravimetric	Ireland-Mine, Pittsburgh, etc. Bituminour coal char 0.5-1.5 g granules: -20+40 USS (wire-mesh basket)	Several pretreatment modes: nitrogen, air pretreated	T: 815-1040°C P: 1-40 atm	Reaction: H_2-C Purpose: Kinetic study of hydrogasification using hydrogen and steam-hydrogen mixtures: Modeling
40	Thermo-gravimetric	Pittsburgh Seam Ireland Mine Bituminous Coal 1.5 - 2.5 g granules: 18x35 mesh	No pretreatment for char A, and preoxidation using air for char B	T: 1000°C P: 136 atm F: 4700-19000cc/min	Reaction: H_2-C Purpose: To study the kinetics of catalysed hydrogasification at high temperatures and pressures
10	Thermo-gravimetric	Variety of coals (20) 5-30 mg A0 x 100 US mesh granular	Sample heated in a stream of dry nitrogen to a max. temp. at a const. heating rate and held there for 2 hrs.	T: 500°C P: 1 atm F: 500 cc/min	Reaction: Air-C Purpose: To develop a simple reactivity test to be used on a wide range of coal chars & to obtain some measure of the variables which affect it
74	Thermo-gravimetric	Pittburgh #8 chars & Ireland coal mine char (Bituminous) -20 +40 USS granular-basket (2-3 diameter layer)	Air pretreatment	T: 840-1210°C P: 0-80 atm	Reaction: H_2-C Purpose: Study kinetics of char gasification using hydrogen and hydrogen-steam mixtures

Compilation of Char Gasification Bench Scale Kinetic Studies (cont'd)

REFERENCES	REACTOR TYPE	CARBON/CHAR CHARACTERISTICS	SAMPLE PRETREATMENT	OPERATING CONDITIONS	COMMENTS
137	Thermo-gravimetric	Metallurgical coke coal char from FMC pulverized graphite	Preheat in N_2 atmosphere	T: 1800-2240°F P: 1 atm	Shrinking core model for gasification of graphite using SO_2 to get CO + elemental sulfur
38	Thermo-gravimetric	Several coals: IGT, Hydrane, Pittsburgh, etc. 15-30 mg -35 +60m granular-platinum pan	Varied	T: 840-1100°C P: 1 atm F: 200 cc/min	Reaction: CO_2-C Purpose: Find relationship between reactivities and physical characteristics of samples, i.e. porosity, surface area, etc.
138	Thermo-gravimetric	4 coals of low rank 10 mg 35 x 80 mesh granular plan	Coal pyrolysed in N_2 at H.R - 8°/min to 900°C & held there for 2 hours	T: 750-900°C P: 1 atm	Reaction: Both H_2O-C and O_2-C Purpose: To determine the apparent activation energy for the separate reactions and to estimate the value of the relative rates at a common temperature
66	Thermo-gravimetric			T: 500-900°C P: 1 atm F: 5-15 cm/s	Reaction: H_2O-C Purpose: Kinetics
139	Thermo-gravimetric	Variety of coals 5-10 mg 40 x 100 m granular, pan	Coal was heated at a rate of 10°/min to 1000°C in N_2 and held there until no further weight loss occured. Demineralizing	T: 900°C P: 1 atm F: 300 cc/min	Reaction: CO_2-C Purpose: To study different factors which affect char reactivity and to compare with air-C reaction results

APPENDIX A

Compilation of Char Gasification Bench Scale Kinetic Studies (cont'd)

REFERENCES	REACTOR TYPE	CARBON/CHAR CHARACTERISTICS	SAMPLE PRETREATMENT	OPERATING CONDITIONS	COMMENTS
140	Thermo-gravimetric	FMC char: Illinois #6 coal + some others. 2 gm 18-35 m granular, basket	Coal was pyrolysed at 1550°F -catalyst impregnation -preoxidation -varied pretreatment	T: 650-850°C P: 34 atm	Reaction: H_2O-C Purpose: To look at the effect on reactivity of dual catalyst systems, varying catalyst concentrations, catalyst annialing & catalyst preparation
141	Thermo-gravimetric	SP-1 pure natural graphite GRAPHON 1/16" or 1/32" thick plates 0.38-0.58 g	Heat-treated to 2500°C in A_r to remove impurities adden on compaction. Then plates were burned off to 12% wt loss at 1100°C	T: 950-1150°C P: low pressure F: 11.61 liters reactor volume	Reaction: CO_2-C Purpose: To study the kinetics at low pressure and H_2 inhibition
65	Thermo-gravimetric	6 coals of different rank single crystal SP-1 graphite 9 mm ID specimen -200 m pellet	-surface area measurement conditions for sample SA measurement -devolitalized in N_2 at 25°/min up to 1000°C	T: 700-1200°C P: 1 atm	Reaction: H_2O-C Purpose: To study the effects of N_i and K catalysts on the gasification of several coals. Gasification rate experessed/ unit SA
142	Thermo-gravimetric	Graphimets & SP-1 graphite 0.35 gm pellet 9mm D 4mm height cylindrical	Samples heated to 850°C in vacuo	T: 520-1150°C P: 1 atm F: Recirculation of balance volume - 6 1/5 min	Reaction: H_2O-C Purpose: To study the effects of different catalysts on steam gas rates. Product retardation looked at
143	Thermo-gravimetric	SP-1 spectroscopic graphite. Plates = 3/8"x1"x1/16 thick or 3/8"x1"x1/32 thick	Plates were gasified to 10% wt loss at 1150°C on a flowing 10% CO-90% CO_2 atm prior to any measurements	T: 900-1007°C P: .02 atm-.2 atm	Reaction: CO_2-C Purpose: To use a simple well-defined (spectroscopically) graphite to study Langmiur-Hinshelwood kinetics

APPENDIX A

Compilation of Char Gasification Bench Scale Kinetic Studies (cont'd)

REFERENCES	REACTOR TYPE	CARBON/CHAR CHARACTERISTICS	SAMPLE PRETREATMENT	OPERATING CONDITIONS	COMMENTS
144	Thermo-gravimetric	Montour #4 mine of Pittsburgh #8 seam treated with C_aO and N_aOH (BTC) 1/16" long 3/16" D cylindrical + 20 gm pellets	BTC pretreatment using C_uO + N_aOH to avoid caking	T: 1200°C P: 102 atm	Reaction: H_2-C Purpose: Study a novel treatment process for catalyst incorporation and define a comparative reactivity index at a given conversion X for two samples as $R_x=t_{AX}/t_{BX}$
145	Thermo-gravimetric	Several US coals of different rank 5-10 mg 40x100 m pan, granular	Coal carbonized in N_2 at 1000°C for 2 hours (at a rate of 10°C/min)	T: 900°C P: 1 atm	Reaction: Air, H_2, CO_2-C Purpose: To study the reactivities of different chars and the effects of minerals in the coal on gasif. rates, char pretreatment, etc.
146	Thermo-gravimetric	Pitts. #8 Illinois #6 raw, caking bituminous coals 0.5-1 gm, -50 to +10 m granular, basket (.63 OD)	Initial hydrogasif. stage with different temperatures 700-900°C	T: 700-1000°C P: 68 atm F: 0.04-0.23 l/s 2500 cc/min	Reaction: H_2-C Purpose: To determine the kinetics of hydrogasification of char with H_2-CH_4 mixtures
64	Thermo-gravimetric	Western sub-bituminous coal 400 mg 1/2" D 1/8" thick pellets	The pellets were charred in H_e at 900°C for 7 min.	T: 700-900°C P: F: 130 cc/min	Reaction: H_2O=C Purpose: A study of the effects of alkali metal catalysts on steam gasification of char using H_2O-H_e mixtures
111	Thermo-gravimetric	2 low rank coals (lignite) one high rank (Pittsburgh seam coal) 0.5 gm 9 mm ID cylindrical pellets	Coal pellets were devolatilized in flowing N_2 at a heating rate of 20°C/min and kept at 1000°C for 2 hrs.	T: 850°C P: .5 atm F:	Reaction: H_2O-C Purpose: To study catalysis of carbon-steam gasification by ash components from two lignites

APPENDIX A

Compilation of Char Gasification Bench Scale Kinetic Studies (cont'd)

REFERENCES	REACTOR TYPE	CARBON/CHAR CHARACTERISTICS	SAMPLE PRETREATMENT	OPERATING CONDITIONS	COMMENTS
147	Thermo-gravimetric	Metallurgical coke 3 mm particles	Coking time 22 hr at 1200°C	T: 1200°C P: 1 atm F: 21 min^{-1}	Gasification with steam and CO_2 mixtures
73	Fluidized bed	Disco char from Pittsburgh seam coal 65-150 m 1 lb or 25" height 1 1/2" ID	Varied pretreatment times (0-24 hrs) using N_2 at 1600°F	T: 871°C P: 1 atm F: .39 ft/s CO_2 .55 ft/s H_2O	Reaction: H_2O-C, CO_2-C Purpose: To look at the effect of high temperature pretreatment on reactivity of low-temperature char to steam and CO_2
73	Fluidized bed	Disco char from Pittsburgh seam coal 65-150 m, 1 lb or 25" height 1 1/2' ID	N_2 pretreatment for 1 hour at 1600°F	T: 871°C P: 1 atm-30 atm	Reaction: H_2O-C Purpose: To look at the effect of pressure and carbon burnoff on the rate of gasification of char in steam-hydrogen mixtures
72	Fluidized bed	Activated carbon, graphite & ceylon graphite 1-12 gm 1.8 mm-.081 mm 2.22 cm ID tube	No pretreatment	T: 700-1400°C P: 1 atm	Reaction: CO_2-C Purpose: A study of the kinetics and the mechanization of the reaction
55	Fluidized bed	Graphite, activated carbons, metallurgical cokes 3 gm 0.08 - 1.8 mm 2.22 cm ID	No pretreatment	T: 700-1500°C P: 1 atm F: 180 cc/min STP	Reaction: CO_2-C, H_2O-C Purpose: To summarize the work of Ergun & Mentser at B of Mines on gasification of C using H_2O and CO_2. They use a mechanistic approach to the kinetics of the reactions
75,76	Fluidized bed	Disco char 65-100 mesh 0.4 lb 1 1/2" ID	Pretreated for 1 hr at the reaction temperature in N_2 (.44 ft/s velocity)	T: 8.16-927°C P: 1 atm	Reaction: H_2-C, H_2O-H_2C Purpose: To study the rate of gasification of carbon in pure hydrogen & hydrogen-steam mixtures in an effort to correlate results in a single empirical correlation

APPENDIX A

Compilation of Char Gasification Bench Scale Kinetic Studies (cont'd)

REFERENCES	REACTOR TYPE	CARBON/CHAR CHARACTERISTICS	SAMPLE PRETREATMENT	OPERATING CONDITIONS	COMMENTS
85	Fluidized moving bed	Bituminous coal +40 - 325 m (.0029" avg) +40 - 80 m (.0095" avg) Bed Height: 2, 4.7, 7, 9 (ft)	Pretreated by low-temperature oxidation	T: 704-927°C P: 34-136 atm F: .01-.59 ft/s	Reaction: H_2-C Purpose: To study the kinetics of coal char hydrogasification on pilot plant scale
6	Fluidized bed	High sodium, lignite char from North Dakota 35x65m 5-10g, 2 1/2" height of bed Reactor 7" x 1"	Coal was carbonized in N_2 at 565°C and devolitalized by heating in fluid bed in H_2 at 1400°F for 1 hr and 6 atm	T: 816°C-871.1°C P: 11-20 atm	Reaction: H_2O-C Purpose: To study the steam gasification kinetics of lignite char
58	Fluidized bed	Kentucky #9 coal minerals 30/35 m, 50/60 m, 200/270 m, 100 g, height 7"	N_2 flow through apparatus	T: 1040-1430°C P: 1 atm	Reaction: H_2O-C Purpose: To study the kinetics of coal mineral carbon with steam. They use the shrinking core model to describe kinetics
59	Fluidized bed .8 cm ID 1.78 m long	Hydrane char 5 gm		T: 750-900°C P: 70 atm F:	Reaction: H_2O-C, CO_2-C Purpose: To obtain kinetic information concerning the water gas reaction (reaction with steam). The char used contains 50% of initial carbon of raw coal. To improve hydrane process
7	*Falling Particle* 3" ID 6 1/2' long	Coke + graphite 200-230 m	Petroleum coke devolitilized and shrunk at 1350°C in absence of air then mixed with binder. Graphite baked in oven at 750°C for 20 hrs. Graphitization occured during 7 hrs at app. 2850°C	T: 1800-2500°F P: 1 atm	Reaction: Steam-Carbon Purpose: To examine the effect of temperature on the reaction rate

APPENDIX A

Compilation of Char Gasification Bench Scale Kinetic Studies (cont'd)

REFERENCES	REACTOR TYPE	CARBON/CHAR CHARACTERISTICS	SAMPLE PRETREATMENT	OPERATING CONDITIONS	COMMENTS
60	Entrained flow	Pulverized Coal		T: 746-1180°C P: 15-97 atm F:	Reaction: H_2-H_2O-C Purpose: To understand & improve Bi-gas process gasifier. Kinetic study of pertinent rate equations
61	Dilute phase reactor 3" ID; 5 ft	Pittsburgh seam coal Illinois #6 lignite 50 x 100 m	None	T: 650-1000°C P: 68-136 atm	Reaction: H_2-C Purpose: To investigate the direct conversion of coal methane using entrained concurrent flow of coal in hydrogen
81	Entrained flow 3" ID 11" long	Pulverized coal Utah Bituminous coal	None	T: 1066°C. P: 150 psi	Reaction: H_2O-O_2-C Purpose: To examine a pressurized entrained flow gasifier with the intent of decreasing industrial reactor size
82	Entrained flow with recirculation	Highly volatile low sulfur bituminous coal 70-80% - 200 m	None	T: 1130-1730°C P: 10 atm F: steam to coal feed rates 0.5g/g	Reaction: O_2-Coal, Char-CO_2, H_2O Purpose: To obtain kinetic data from high temperature entrained flow gasifier which is a scaled down version of the existing gasifier well-mixed
61	Entrained flow reactor 1 1/4", 3/4" tubes	Highly volatile bituminous coal - 200 mesh	Coal is dried, ball milled and screened Entrain coal in stream of carrier gas H_2,N_2	T: 650-1370°C P: 1 atm F: 13-15 scfh avg. residence time 0.12 - .343 s	Reaction: Oxidizing combustion gases Purpose: To investigate the potential for increased volatility and also the production of unsaturated hydrocarbons as a result of rapid pyrolysis using partial combustion gases

Compilation of Char Gasification Bench Scale Kinetic Studies (cont'd)

REFERENCES	REACTOR TYPE	CARBON/CHAR CHARACTERISTICS	SAMPLE PRETREATMENT	OPERATING CONDITIONS	COMMENTS
83	Dilute phase transport reactor helical coiled (integral)	Montana lignite .0029" to .0035" 250-200 mesh		T: 480-840°C P: 18-52 atm F: 5-50 scf/hr residence times	Reaction: H_2-H_e-Char Purpose: To study the rapid-rate methane formation reaction in both isothermal & with constant gas-solid heat-up rate (50°F/s)
80		Single crystals of graphite	Graphite annealed at 2300°F in vacuo by electron beam heating	T: 850-1075°C P: 1 atm	Reaction: H_2O-graphite Purpose: To determine rates of reaction by measuring the rates of increase in diameters of etch pits produced from lattice vacancies
84	Electrofluid reactor charged (Fluidized bed)	Variety of coal chars 20-200 mesh	Chars produced by pyrolysis at varying temperatures	T: 1500-1960°F P: 1 atm Batch F:	Reaction: Char-steam Purpose: To discover the electrical properties & behavior of coal gasification in bench scale electrofluid reactor. Bench scale-continuous-large scale. To investigate the pertinent parameters for scale-up purposes
87,88, 89,93	Spouted bed	Ranigahj coal 1.2-2.05 mm 0.8-3.6 mm Western Canadian Coals		T: 600°C-1000°C P: 1 atm	Reaction: Air-steam-coal Purpose: To study 1. low-temperature carbonization, 2. kinetics of coal pyrolysis, 3. gasification of coal, air-steam-jet-coal

APPENDIX A

Compilation of Char Gasification Bench Scale Kinetic Studies (cont'd)

REFERENCES	REACTOR TYPE	CARBON/CHAR CHARACTERISTICS	SAMPLE PRETREATMENT	OPERATING CONDITIONS	COMMENTS
97	Free-fall Dilute-phase reactor	Pittsburgh, Illinois #6		T: 725-900°C P: 103-205 atm	Reaction: Hydrogasification Purpose: To consolidate kinetic information yielded from hot-rod, free-fall dilute phase reactors
68	Vortex Tube *Adiabatic*	Pulverized bituminous C coal -200 m (80%)	None	T: 1300-2700°F P: 1 atm	Reaction: Coal+O_2+steam Purpose: To assess the potentialities of this type of reactor for producing synthesis gas and to obtain basic information on the critical variable affecting gasification under these conditions
69	*Impinging* *Jet*	AGKS spectroscopic graphite	Addition of catalyst via heating & slurrying	T: 975-1100°C P: low	Reaction: Steam-Carbon Purpose: Examine catalytic effects of Cobalt, Iron, Nickel and Vandaium Oxide on reaction rate
79	*Furnace Tube*	Spectroscopic graphite electrode	None	T: 900-1300°C P: 1-40 m	Reaction: Steam-Carbon Purpose: Kinetic study at high temperatures
101	Explosion chamber	Pem-Rilton 'Sea coal' hvBA bituminous 200 mesh (70%)	None	T: 2000°C P: 1-11 atm	Reaction: Carbon-Steam Purpose: Rapid non-steady state coal gasification at very high temperatures is investigated
92	Diffusion cell	Char, graphite.		T: 1000-1600°C P: 1 atm	Reaction: CO_2-C Purpose: Study intrinsic rates in chemical reaction diffusion regime

APPENDIX B

Testing for Film Temperature Gradients

Feldkirchner and Huebler[48] in their study of steam-hydrogen gasification using a thermobalance reported the following operating conditions and results:

TGA BALANCE TUBE DIAMETER	1 inch
SUPERFICIAL GAS VELOCITY	50 SCF/HR
PARTICLE SIZE	-16+20 (.0328 - .039 inch)
TOTAL PRESSURE	1000 psi
BULK DENSITY OF SOLID	50 lb/ft^3
SOLID THERMAL CONDUCTIVITY	3.3 - 8.6 x 10^{-4} cal/scm C
EMISSIVITY	0.53
BED POROSITY	0.40
AVERAGE BED TEMPERATURE	1700F
GASIFICATION RATE	(0.4 - 6 $\frac{\text{lb C}}{\text{lb hr}}$)

CROSS-SECTIONAL AREA OF TUBE $\frac{\pi D^2}{4} = \frac{\pi (1)^2}{4} \times 2.54^2 = 5.067\ \text{cm}^2$

SUPERFICIAL MASS VELOCITY OF GAS:

$$\frac{1.416 \times 10^6\ \text{cm}^3/\text{hr}}{22{,}400\ \text{cm}^3/\text{mol}} \cdot \frac{1}{5.062\ \text{cm}^2} \cdot \frac{1}{3600\ \text{s}} \cdot \frac{18\ \text{g}}{\text{mol}} = 0.062\ \text{gcm}^{-2}\text{s}^{-1}$$

PARTICLE SIZE .091 cm diameter

VISCOSITY (steam 1700F) = 425 x 10^{-4} cp = 425 x 10^{-6} poises

Reynolds Number: $N_{Re} = \frac{dpG}{\mu} = \frac{(0.091)(0.062)}{425 \times 10^{-6}} = 13.28$

MASS TRANSFER number $j_D = 0.84\ N_{Re}^{-0.51} = 0.22$

HEAT TRANSFER $j_H = 1.076\ j_D = 0.242$

CONVECTIVE HEAT TRANSFER COEFFICIENT

$$h_c = \frac{c_p G j_{H_{z/3}}}{(c_p \mu / k)} = \frac{(0.5)(0.062)(0.242)}{(0.7)^{2/3}} = 9.52 \times 10^{-3} \text{ cal cm}^{-2} \text{s}^{-1} \text{C}^{-1}$$

RADIATIVE HEAT TRANSFER COEFFICIENT

$$h_r = 1.37 \times 10^{-12} (.53) (4T^3)$$

$$h_r = 1.37 \times 10^{-12} (.53)\ 4\ (1200\text{K})^3$$

$$= 5.02 \times 10^{-3} \text{ cal cm}^{-1} \text{s}^{-1} \text{C}^{-1}$$

$$h = h_c + h_r = 0.0145 \text{ cal cm}^{-2} \text{ s}^{-1} \text{C}^{-1}$$

Using the appropriate criterion for determining whether interphase temperature gradients exist,

(Equation 3-27) $$\Delta T_f = \frac{r_{v,obs} L \Delta H_r}{h}$$

For, $r_{v,obs} = 0.4$ gC/gC hr

$$\frac{r_{v,obs} L H_r}{h} = \frac{\frac{1 \text{ mol}}{12 \text{ gC}} \quad \frac{1 \text{ hr}}{3600 \text{ s}} \quad \frac{0.4 \text{ gC}}{\text{gC hr}} \quad \frac{0.8 \text{gC}}{\text{cm}^3} \quad (0.091) \frac{\text{cm}}{\text{cal}} \quad (41000) \frac{\text{cal}}{\text{mol}}}{0.0145 \frac{\text{cal}}{\text{cm}^2 \text{ s C}}}$$

$$\Delta T_f = 1.91\ ^\circ\text{C}$$

For $r_{v,obs} = 6$ gC/gC hr, $\Delta T_f = 29\ ^\circ\text{C}$

APPENDIX C

Testing for Transport Limitations

Dutta et al[38] in their study of the reactivity of coal char with carbon dioxide at atmospheric pressure in a thermobalance report the following findings:

Thermobalance diameter:	19 mm
Sample holder dimensions:	cylinder 6 mm x 15 mm (35 mg)
CO_2 flowrate:	150 ml/min (NTP)
Reaction temperature:	1000°C
Char sample:	IGT char #155
	density = 1.54 g/cm^3
	porosity = 0.767
Reactivity:	0.067 min^{-1}
Activation Energy:	59.26 kcal/mol
Heat of Reaction:	41 kcal/mol

Since the resistance to gas flow is so much less outside of the wire mesh cylinder, it is not unlikely that the entire holder and contents behave as a single pellet. It will be treated as such in the following analysis.

Effective length:

$$L = \frac{\text{volume of holder}}{\text{external surface area}}$$

$$L = \frac{\pi D^2 h / 4}{\pi D^2 / 2 + \pi D h}$$

$$L = 1.25 \text{ mm} = 1.25 \times 10^{-3} \text{m}$$

Linear Velocity: $$U = \frac{150\ cm^3/min \quad \frac{1273}{298}}{\frac{\pi}{4}\ (1.9)^2\ cm^2}$$

$U = 226$ cm/ min

$U = 136$ m/hr

Carbon Dioxide Physical Properties at 1000°C

Density: $$\rho = \frac{P}{RT} = \frac{1\ atm}{(82.05)\ (1273)} = 9.6 \times 10^{-6}\ \frac{mol}{cm^3} = 9.6\ \frac{mol}{m^3}$$

$$\rho = 0.4224\ kg/m^3$$

Viscosity: $$9.4 \times 10^{-7}\ \frac{lb_f\ s}{ft^2} \times \frac{1}{0.020886\ lb_f\ s/ft^2}\ \frac{N\ s/m^2}{} = 4.5 \times 10^{-5}\ \frac{kg}{m\ s}$$

$\mu = 4.5 \times 10^{-5}$ kg/m s

Kinematic Viscosity: $\nu = \rho/\mu = 1.07 \times 10^{-4}\ m^2/s$

$\nu = 0.385\ m^2/hr$

Thermal Conductivity: $$0.046\ \frac{Btu}{hr\ ft\ ^oF} = 0.0685\ \frac{kcal}{hr\ m\ K}$$

Effective Diffusivity:* Porosity ranges from 0.30-0.77

*Walker et. al[8] $$D_{eff} = 0.14\ \Theta^2 \left[\frac{T}{298}\right]^{1.3}$$

Average porosity, Θ, 0.53

Temperature 1273 K

$D_{eff} = 0.113\ m^2/hr$

Effective Thermal Conductivity of Char: 0.004 - 0.005 cal/cmsk

= 1.8 kcal/hrmK

PREDICTION OF MASS TRANSFER COEFFICIENT: (RANZ and MARSHALL correlation)

Reynolds Number: $N_{Re} = \frac{UL}{\nu} = \frac{(135\ m/hr)(1.25 \times 10^{-3} m)}{0.385\ m^2/hr}$

$= 0.438$

Schmidt Number: $N_{Sc} = \frac{\nu}{D_{CO-CO2}} = \frac{0.385}{0.788} = 0.489$

Molecular Diffusion coefficient calculated using Slattery-Bird Equation as follows:

	A	B
	CO	CO_2
Tc	132.9	304.2 K
Pc	34.5	72.8 atm

$(T_{CA}\ T_{CB})^{5/12} = 83.07$

$(T_{CA}\ T_{CB})^{1/2} = 201.1$

$(P_{CA}\ P_{CB})^{1/3} = 13.59$

$M_A = 28$

$M_B = 44$

$\left(\frac{1}{M_A} + \frac{1}{M_B}\right)^{1/2} = 0.242$

At 1273 K, $\left[\frac{T}{(Tc_A\ Tc_B)^{1/2}}\right]^b = \left[\frac{1273}{201.1}\right]^{1.823} = 28.9$

$D_{CO_2-CO} = (2.745 \times 10^{-4})(28.9)(0.242)(83.07)(13.59)$

$= 2.16\ cm^2/s$

$= 0.79\ m^2/hr$

Sherwood Number: $Nsh = 2 + 0.6\ (N_{Re})^{1/2} (N_{Sc})^{1/3}$

$= 2 + 0.6\ (0.438)^{1/2} (0.489)^{1/3}$

$= 2.313$

Mass Transfer Coefficient: $kg = \frac{D\ Nsh}{L} = \frac{(0.778)(2.313)}{1.25 \times 10^{-3}}$

$k_g = 1440\ m/hr$

Calculation of Rate of Reaction:

According to Dutta et.al,

$$\frac{dx}{dt} = a\ k_v\ C_A\ (1-X)$$

$$a = 1 + 100\ X\ Be^{-BX}$$

$$k_v = k\bar{v}_o\ e^{-E/RT}$$

IGT char: $k_{vo} = 0.113 \times 10^{15}\ cm^3/mol\ min$

$T = 1273$

$= 0.75$

$= 5.5$

$X = 0.20$

$a = 1 \pm 100\ (0.2)(.75)(5.5)e(-5.5)(0.2) = 1.0436$

$$k_v = 0.113 \times 10^{15} \exp(-59{,}000/(1.987 \times 1273)) = 8376.5 \frac{cm^3}{mol\ min}$$

$$r_{obs} = dx/dt = (1.0436)(8376.5)(9.6 \times 10^{-6})(1 - 0.2) = 0.067 \frac{gC}{gC\ min}$$

$$r_{v,obs} = \left[0.067 \frac{gC}{gC\ min}\right]\left[\frac{1\ gmol\ C}{12\ gC}\right]\left[\sigma_a \frac{gC}{cm^3}\right]$$

where σ_a = the apparent density of the char
= 1.3-1.5 (Laurendeau)

$$r_{v,obs} = (4.3 \times 10^{-3} - 8.5 \times 10^{-3}) \frac{mol\ C}{min\ cm^3}$$

$$r_{v,obs} = (2.6 \times 10^{5} - 5.2 \times 10^{5}) \frac{mol\ C}{hr\ m^3}$$

Convective Heat Transfer Coefficient

Prandtl Number: $Np_r = 0.72$

Nusselt Number: $N_{Nu} = 2 + 0.6\ (0.438)^{1/2}(.72)^{1/3}$

$= 2.356$

Heat Transfer Coefficient: $h = \frac{kg\ Nu}{L}$

$$h = \frac{0.685 * 2.356}{1.25 \times 10^{-3}} = 129 \frac{kcal}{hrm^2K}$$

Radiative Heat Transfer Coefficient

$$h_r = \tilde{\varepsilon}\ \sigma\ (T_E^2 + T_S^2)(T_E + T_S)$$

For $T_E \sim T_S = T$, $h_r = 4\ \tilde{\varepsilon}\ \sigma\ T^3 = 4(0.53)\ (1.37 \times 10^{-12})(1273)^3$

$= 5.99 \times 10^{-3}$

$= 6 \times 10^{-3} \frac{cal}{cm^2 s\ K}$

$h_r = 216\ kcal\ m^{-2}h^{-1}K^{-1}$

Transport Criteria

Pore Diffusion:

Equation 3-18, $\dfrac{r_{v,obs}\, L^2}{D_{eff}\, C_s^s} < \zeta$ where $\zeta \begin{cases} 6 & n=0 \\ 1 & n=1 \\ 0.3 & n=2 \end{cases}$

$$\frac{(3.9 \times 10^5)(1.25 \times 10^{-3})^2}{(0.113)\ (9.6)} = 0.56$$

This result is conclusive if the reaction rate is known, no pore diffusion limitation is expected.

Film Diffusion:

EQN. 3-26, $\dfrac{r_{v,obs}\, L}{k_g\, C_b} < \dfrac{0.05}{n}$

$$\frac{(3.9 \times 10^5)(1.25 \times 10^{-3})}{(1440)(9.6)} = 0.035$$

No film diffusion is suspected. An approximate calculation of the mass transfer rate will help to confirm this conclusion:[63]

$$J_{CO_2} = -k_g \frac{P}{RT} \ln\left[\frac{1 + N_{CO_2}}{1 + N^*_{CO_2}}\right]$$

Avg Particle Size: 0.0333 cm

X-section of gap between cylinder and wall: 2.55 cm^2

X-section of empty tube: 2.84 cm^2

Avg. linear velocity at 1000°C: 4 cm/s

$Nco_2 = 1$ i.e. pure CO_2 feed

$Nco_2^* = 0$

$$J_{CO_2} = 2400 \text{ cm/min} \times 10^{-5} \times \ln 2 = 1.66 \times 10^{-2} \text{ mol min}^{-1}\text{cm}^{-2}$$

$$J_{CO_2} = 1.66 \times 10^{-2} \text{ mol/min cm}^2 \left[\frac{44 \text{ g } CO_2}{\text{gmol } CO_2}\right]\left[\frac{12 \text{ gC}}{44 \text{ g}CO_2}\right] = 0.2 \frac{\text{g}}{\text{min cm}^2}$$

Initial Weight of Char: .035 g

Char Density ($\sim$ 1.54 g/cm^3)

Number of particles = (assuming spherical geometry)

$$\left(\frac{0.035}{1.54}\right) \Big/ \left(\frac{\pi (0.0333)^3}{3}\right) = 586$$

Rate of Reaction :

$$\frac{(0.067)\text{min}^{-1} \quad 0.035 \text{ gC}}{586 \ (\pi(0.0333)^2) \text{ cm}^2}$$

$$= 1.15 \times 10^{-3} \frac{\text{g}}{\text{min cm}^2}$$

Ratio of reaction rate to mass transfer rate

$$\frac{1.12 \times 10^{-3} \text{ g/min cm}^2}{0.2 \text{ g/min cm}^2} = 0.006$$

The mass transfer through the film does not appear to be rate limiting.

Intraparticle Temperature Gradient

Equation 3-19 $\quad \dfrac{\Delta H_r \, r_{v,obs} \, L^2}{\lambda_{eff} T_s^s} < \dfrac{T_s^s \, R}{E_a}$

$$\frac{(41)(5.2 \times 10^5)(1.25 \times 10^{-3})^2}{(1.8)(1273)} = 0.014; \quad \frac{1273(1.987)}{(1000)(59)} = 0.04$$

No temperature gradient is suspected inside the particle.

Temperature Gradient Across the Film

$$\frac{\Delta H_r \, r_{v,obs} \, L}{h \, T_b} < 0.05 \, \frac{^{\circ}R \, T_b}{E}$$

$$\frac{\Delta H_r r_{v,obs} L}{h \, T_b} = \frac{(41)(5.16 \times 10^5)(1.25 \times 10^{-3})}{(129 + 216)\ (1273)} = 0.06$$

$$\frac{0.05 \, RT_b}{E} = \frac{(0.05\ (1.987 \times 10^{-3})\ (1273)}{59} = 0.02$$

A temperature difference across the film appears to be likely. The magnitude of this temperature difference is calculated below.

$$\frac{r_{v,obs} L \, \Delta H_r}{h_c + h_r} = T_g - T_s$$

$$\frac{r_{v,obs} L \, \Delta H_r}{h_c + h_r} = \frac{(5.16 \times 10^5)(1.25 \times 10^{-3})(41)}{(129.1 + 216)}$$

$$(T_g - T_s) = 80 \ ^{\circ}C$$

This represents a sizeable temperature difference.

APPENDIX D

Experimental Tests for Absorption of CO/CO_2 on Commercial Drying Agent

Experimental tests were carried out in order to determine whether Drierite, a tradename for anhydrous calcium sulfate, could be used as a drying agent for the moist effluent gas from the reactor. The reaction products present in the effluent gas include CO and CO_2. It was necessary to determine whether these gases would be significantly absorbed by the drierite (or by a thin H_2O layer which covers the drierite when it is spent). These tests would also help to determine the maximum size of the drying tube that could be used in gasification.

The experimental setup used to carry out these investigations is shown in Figure D-1. Basically, the gases were supplied from high pressure cylinders at or near atmospheric pressure. The flowrates of both gases were measured with calibrated rotameters. The composition of the gas mixture was checked by bleeding some gas to the gas partitioner. The main gas stream was sent through a 0.5" ID transparent plastic tube of varying length packed with drierite (64 mesh). Most of the gas mixture exiting the drying tube was subsequently vented while a small fraction of this gas was again sent to the partioner for analysis. Moist air could be sent through the drying tube to deactivate parts of the packing.

The results from these tests are shown in Figures D-2 for CO_2 and D-3 for CO. The blanks are analys s of the gas mixture before it enters the drying tube. For carbon dioxide, Table D-1 shows no significant difference between the analysis before or after the drying tube regardless of how used the tube was. On the other hand, Table D-2 shows that there is some difference in the carbon monoxide analysis. The carbon monoxide content in the exit line from the drying tube is somewhat lower after the tube was approximately half spent. In order to avoid any loss of CO the maximum size of the product drying gas tube for the gasification runs was 20 cm.

TABLE D-1

Carbon Dioxide Analysis

Blank Runs (A)	Drierite Runs (B)
$n_A = 14$	$n_B = 32$
$x_A = 730,540$	$x_B = 732,314$
$s_A = 6772$	$s_B = 10,133$
$s_A^2 = 45.9 \times 10^6$	$s_B^2 = 102.7 \times 10^6$
$\nu_A = 13$	$\nu_B = 31$

$$\frac{s_B^2}{s_A^2} = \frac{102.7}{45.9} = 2.24$$

$$F(31,13,0.95) = 2.38$$

$$\frac{s_B^2}{s_A^2} < F$$

The variances of A and B are the same

$$s_p^2 = \frac{\nu_A s_A^2 + \nu_B s_B^2}{\nu_A + \nu_B} = 85.9 \times 10^6$$

100 $(1 - \alpha)$% confidence interval for $(\mu_A - \mu_B)$ is

$$(\bar{X}_A - \bar{X}_B) \pm t_{\nu,\, \alpha/2}\ s_p \left(\frac{1}{n_A} + \frac{1}{n_B}\right)^{\frac{1}{2}}$$

$$t_{44,0.05} = 2, \quad s_p = 9269$$

$$-1774 \pm 5932$$

Interval contains zero, therefore $\mu_A = \mu_B$.

TABLE D-2

Carbon Monoxide Analysis

Blank Runs (A)	Drierite Runs (B)
$n_A = 14$	$n_B = 32$
$x_A = 1{,}098{,}796$	$x_B = 1{,}091{,}491$
$s_A = 6317.4$	$s_B = 11{,}312$
$s_A^2 = 39.9 \times 10^6$	$s_B^2 = 127.9 \times 10^6$
$\nu_A = 13$	$\nu_B = 31$

$$\frac{s_B^2}{s_B^2} = 3.0185$$

$$F(32,13,0.99) = 3.6$$

$$\frac{s_B^2}{s_A^2} < F$$

The two variances are the same

$$s_p^2 = \frac{\nu_A s_A^2 + \nu_B s_B^2}{\nu_A + \nu_B} = 101.9 \times 10^6$$

100 $(1 - \alpha)$% confidence interval for $(\mu_A - \mu_B)$ is

$$(X_A - X_B) \pm t_{\nu,\, \alpha/2}\ s_p \left(\frac{1}{n_A} + \frac{1}{n_B}\right)^{\frac{1}{2}}$$

$$t_{44,0.05} = 2,\ s_p = 10{,}095$$

$$7305 \pm 6460$$

Interval does <u>not</u> contain zero, therefore $\mu_A \neq \mu_B$.

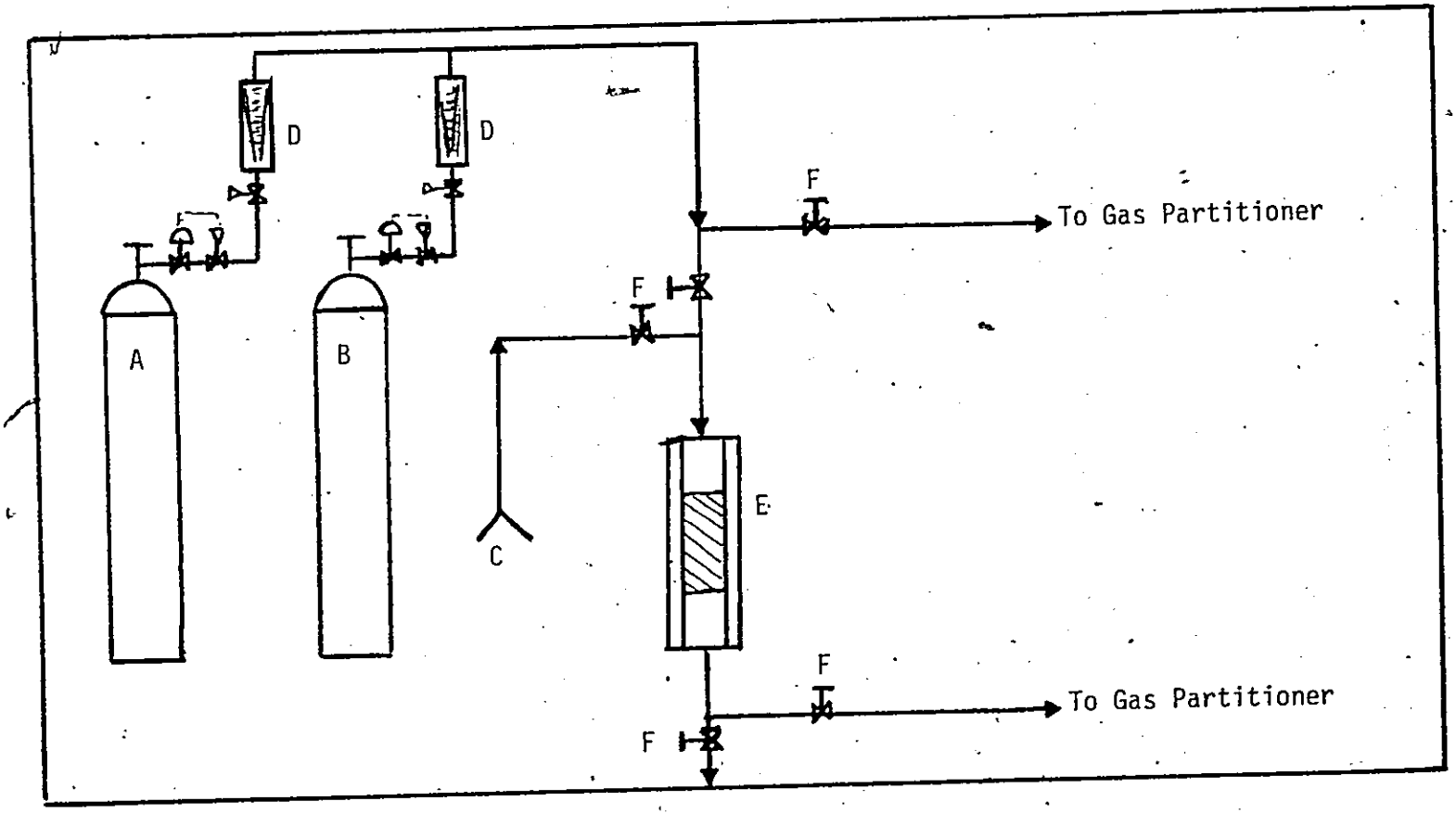

Figure D-1 Experimental arrangement used in testing absorption of CO, CO_2 mixtures on drying agent.

A CO cylinder
B CO_2 cylinder
C Moist air
D Rotameter
E Drying Tube
F On-off valves

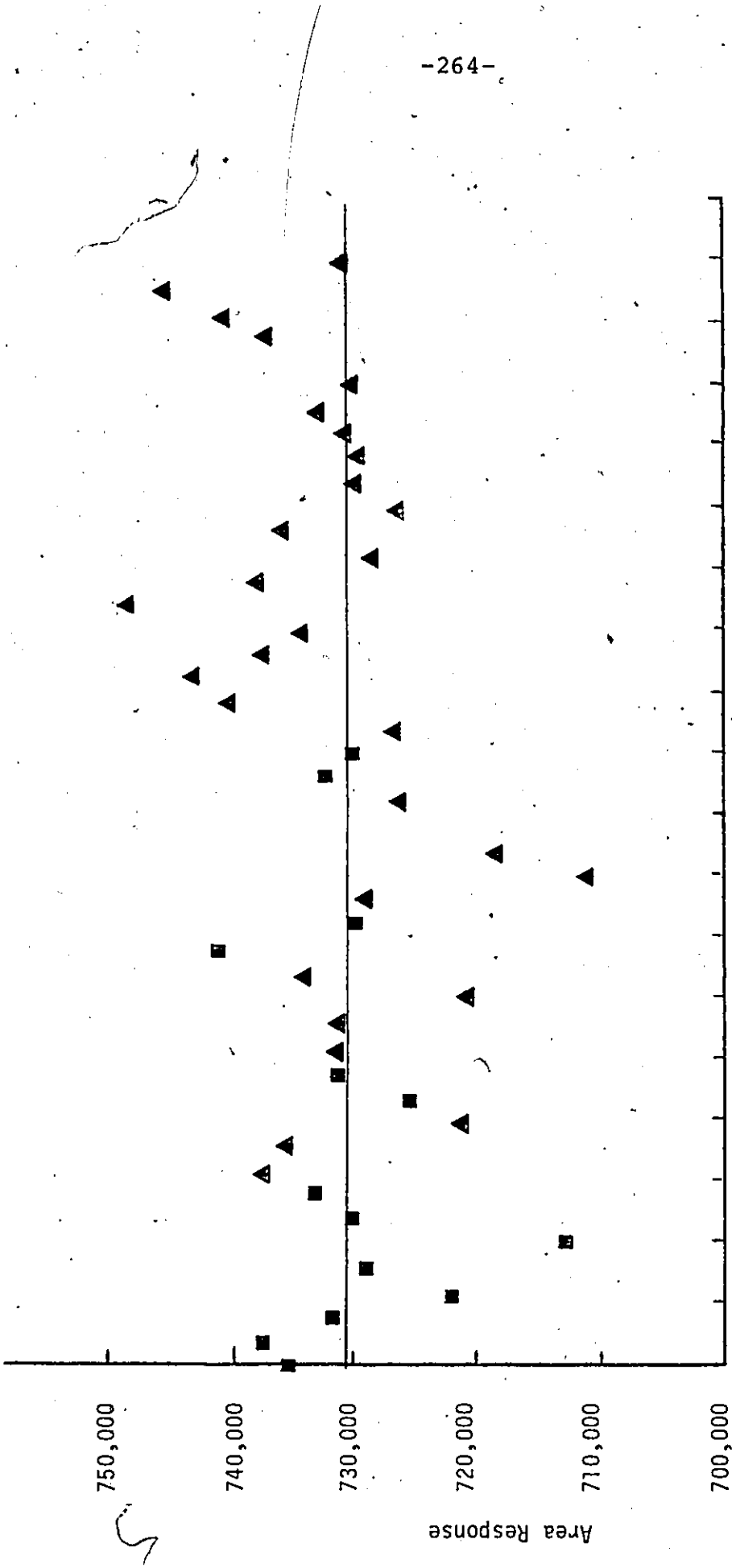

Figure D-2 Carbon Dioxide area response, total flow 400 cm^3/min.

FIGURE 5-19

Schematic Representation of Reactor Mixed Model

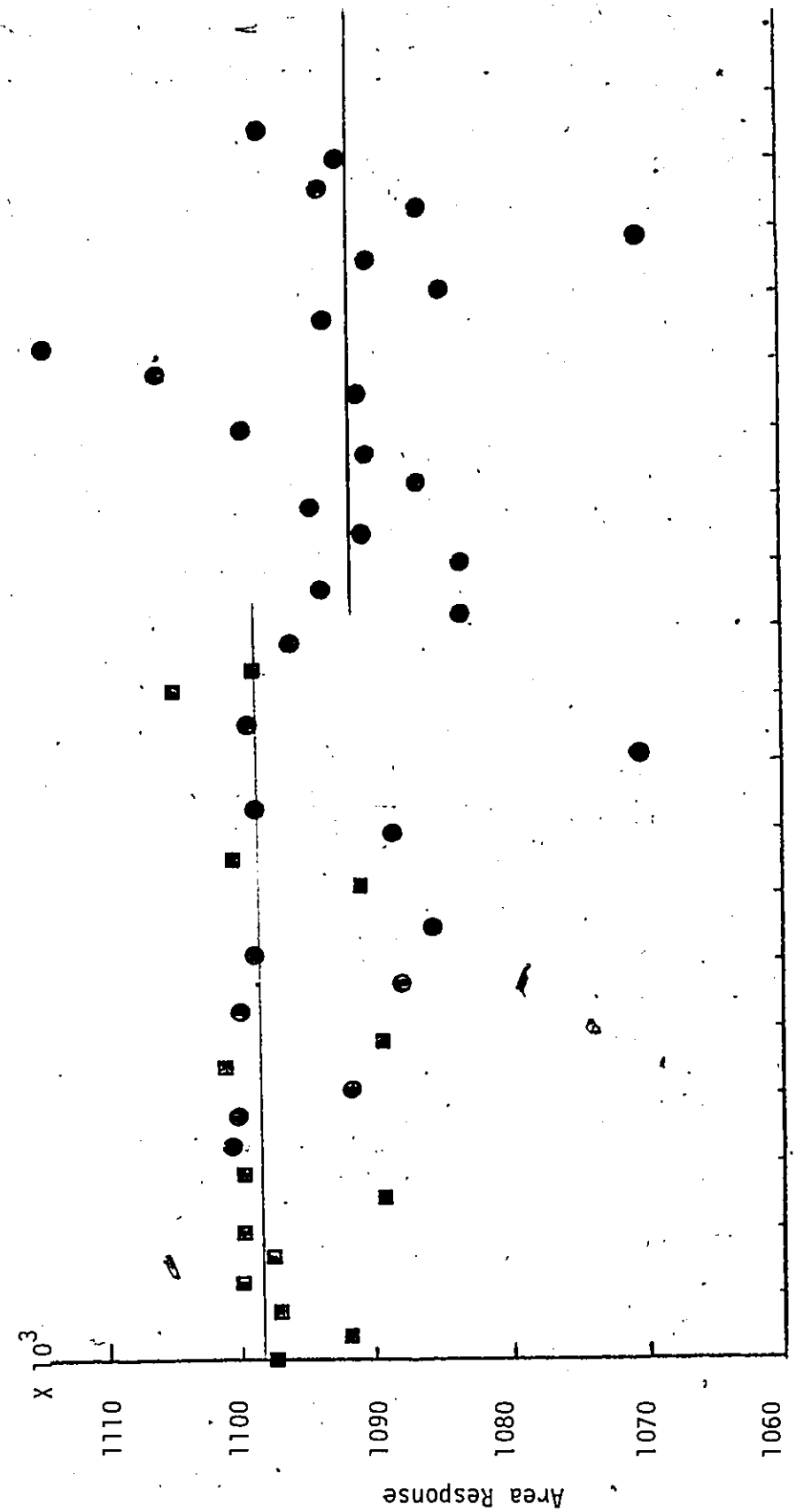

Figure D-3 Carbon Monoxide area response, total flow 400 cm^3/min,

FIGURE 5-20

Schematic Representation of Combined Reactor/

Measurement Device Model

APPENDIX E

Calibration Procedure for Gas Partitioner

The experimental setup used to determine calibration factors for each of the product gas components on the gas partitioner is shown schematically in Figure E-1. Mixtures of ultra-high purity gases were metered through calibrated rotameters and a small bleed stream was continuously sent to the partitioner. A constant pressure of 1 psi was maintained upstream of the gas sampling valve so that the amount of gas in the 0.5 mL sample loop could be kept constant. Three to five samples were taken of every gas mixture prepared. The He gas flowrate through the partioner was 40 cm^3/min at about 18 psig throughout the calibrations. The integrator slope sensitivity was kept at 0.03 mv/m.

The calibration curves for N_2, CO, CO_2, CH_4 and H_2 are given in Figures E-2 to E-6. Two commercially prepared gas mixtures were analysed on the partitioner and a comparison of the gas analysis is given in Table E-1. The analyses compare favorably with the exception of perhaps hydrogen. However, Matheson Gas Products Co. did not analyze for H_2 separately and report it as a difference which may be misleading.

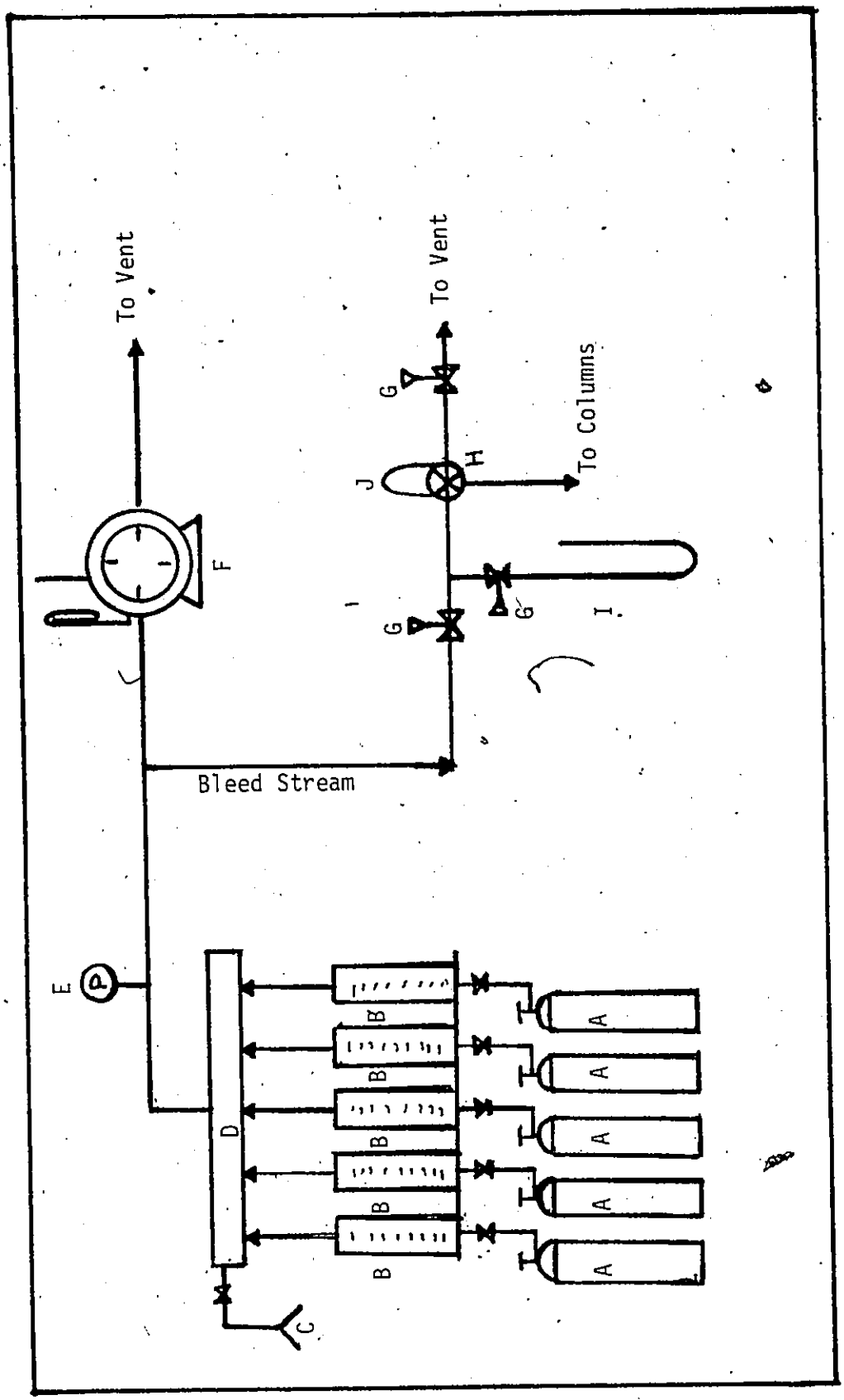

Figure E-1 Flowsheet for Gas Partitioner Calibration

A Gas cylinder
B Rotameters
C Vacuum pump
D Mixing chamber
E Pressure gauge
F Wet test meter
G Needle valves
H Gas sampling valve
I Mercury manometer
J 0.5 ml sample loop

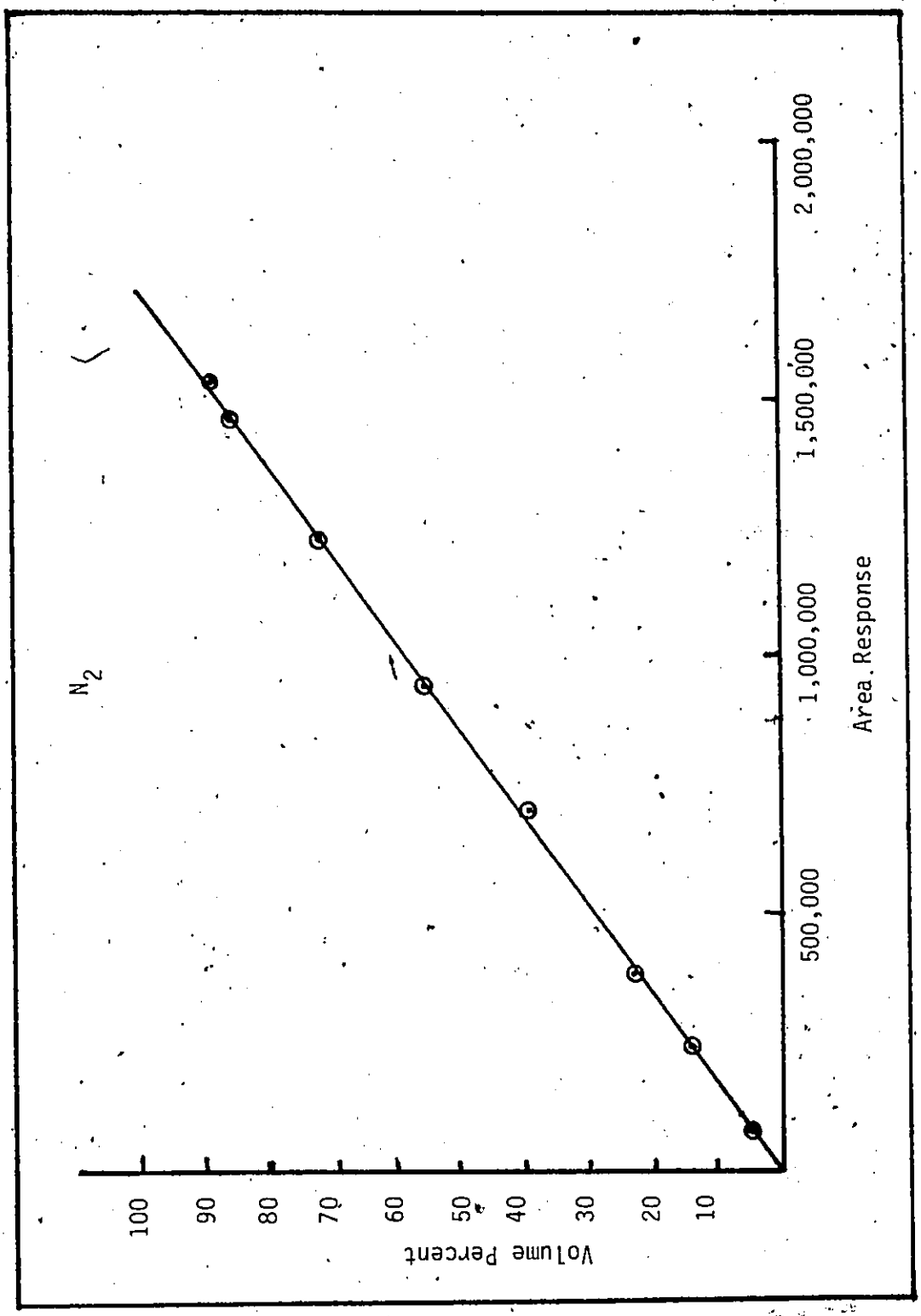

Figure E-2 Calibration Curve for Nitrogen Gas

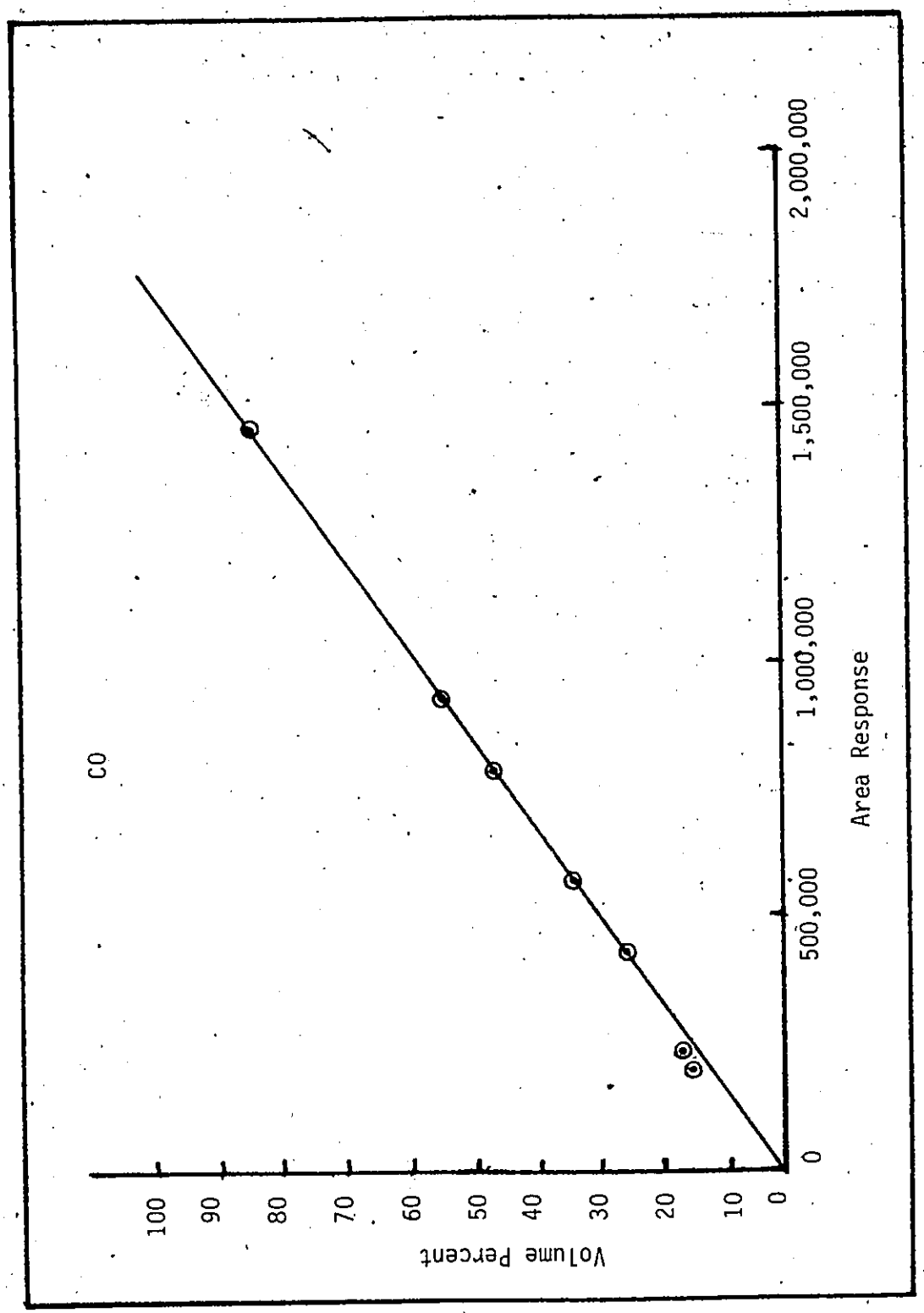

Figure E-3 Calibration Curve for Carbon Monoxide Gas

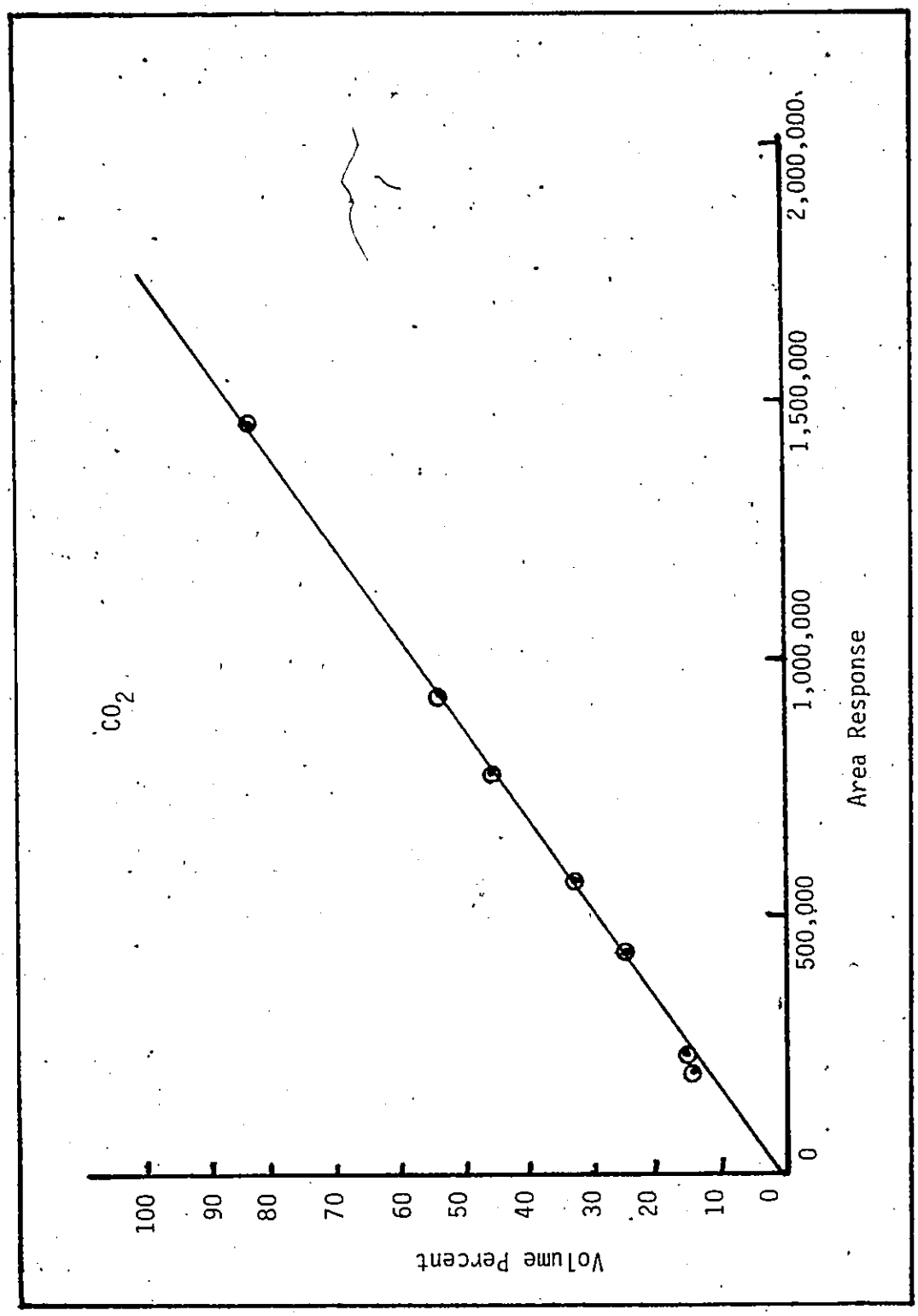

Figure E-4 Calibration Curve for Carbon Dioxide Gas

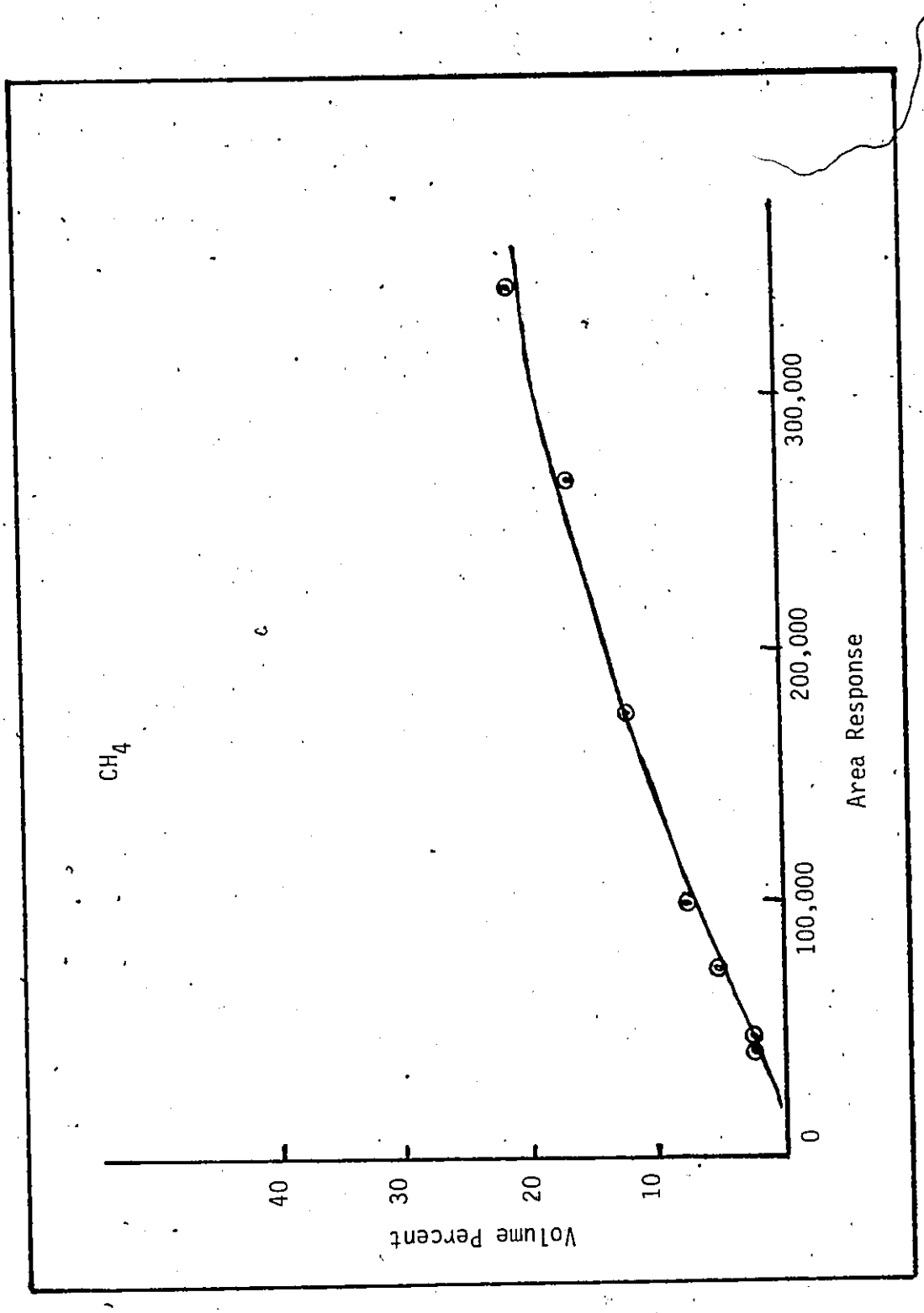

Figure E-5 Calibration Curve for Methane Gas

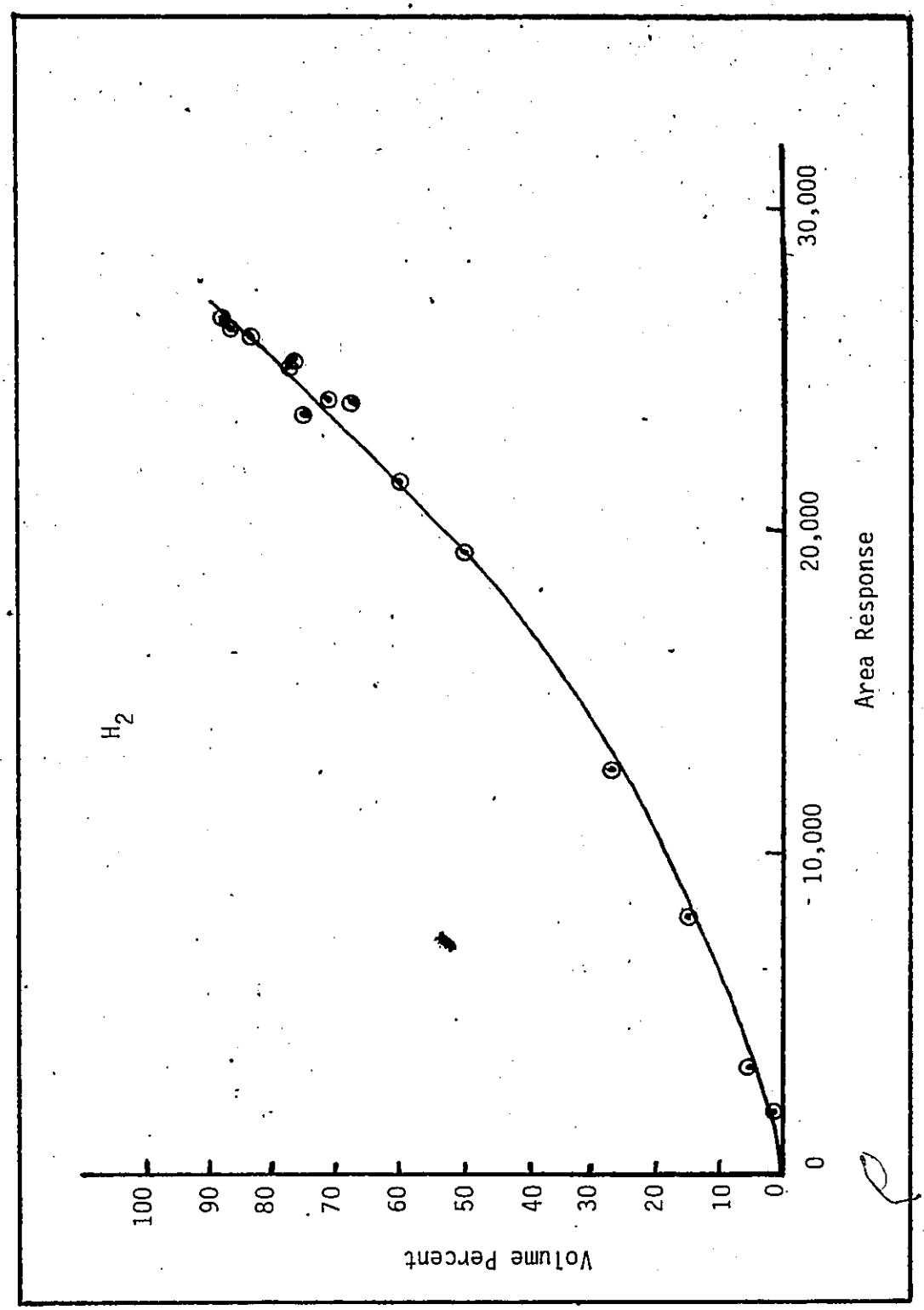

Figure E-6 Calibration Curve for Hydrogen Gas

TABLE E-1

Comparison of Analysis of Commercial Gas Mixtures

	Species	Matheson Analysis mole %	from Calibration Curves mole %
	CO_2	30.2 ± 0.6	30.5
	CO	21.0 ± 0.4	21.6
#1	N_2	10.1 ± 0.2	10.5
	CH_4	16.1 ± 0.3	16.8
	H_2	22.6 (by difference)	14.1
		100.0	93.5
	CO	3.06 ± .06	3.0
#2	CO_2	2.93 ± .06	2.6
			70.5 (N_2)
	Air	93 (by difference)	23.9 (O_2 by difference)
		100	100

APPENDIX F

Devolatilization Procedure for Coal

A coal char sample was produced from Byron Creek Coal in the apparatus shown in Figure F-1 by the following procedure:

1. 200 grams of coal are placed in the furnace tube at room temperature.

2. Nitrogen flow through the tube is started and maintained at 3 L/min.

3. Furnace is turned on and the warm up rate is controlled by dial settings on the Lindberg furnace.
   Start-up: Room Temperature $20^{o}C$
   After 8 minutes: Temperature $250^{o}C$ [$30^{o}C$/min]

4. Dial Setting is placed at 4. The warm up rate is $7.5^{o}C$/min for 40 minutes. ($T = 550^{o}C$)

5. Dial Setting was placed at 8. The warm up rate is $10^{o}C$/min for 25 minutes. ($T = 800^{o}C$)

6. The sample is kept at $800^{o}C$ for 20 minutes.

7. The furnace is then turned off but N_2 is kept flowing through the apparatus.

8. When the furnace has cooled sufficiently ($\lesssim 150^{o}C$), the sample is removed, weighed and placed in a sample bottle, purged with N_2 and sealed.

This procedure yields approximately 150 grams of char. The temperature time history during charring can be seen in Figure F-2.

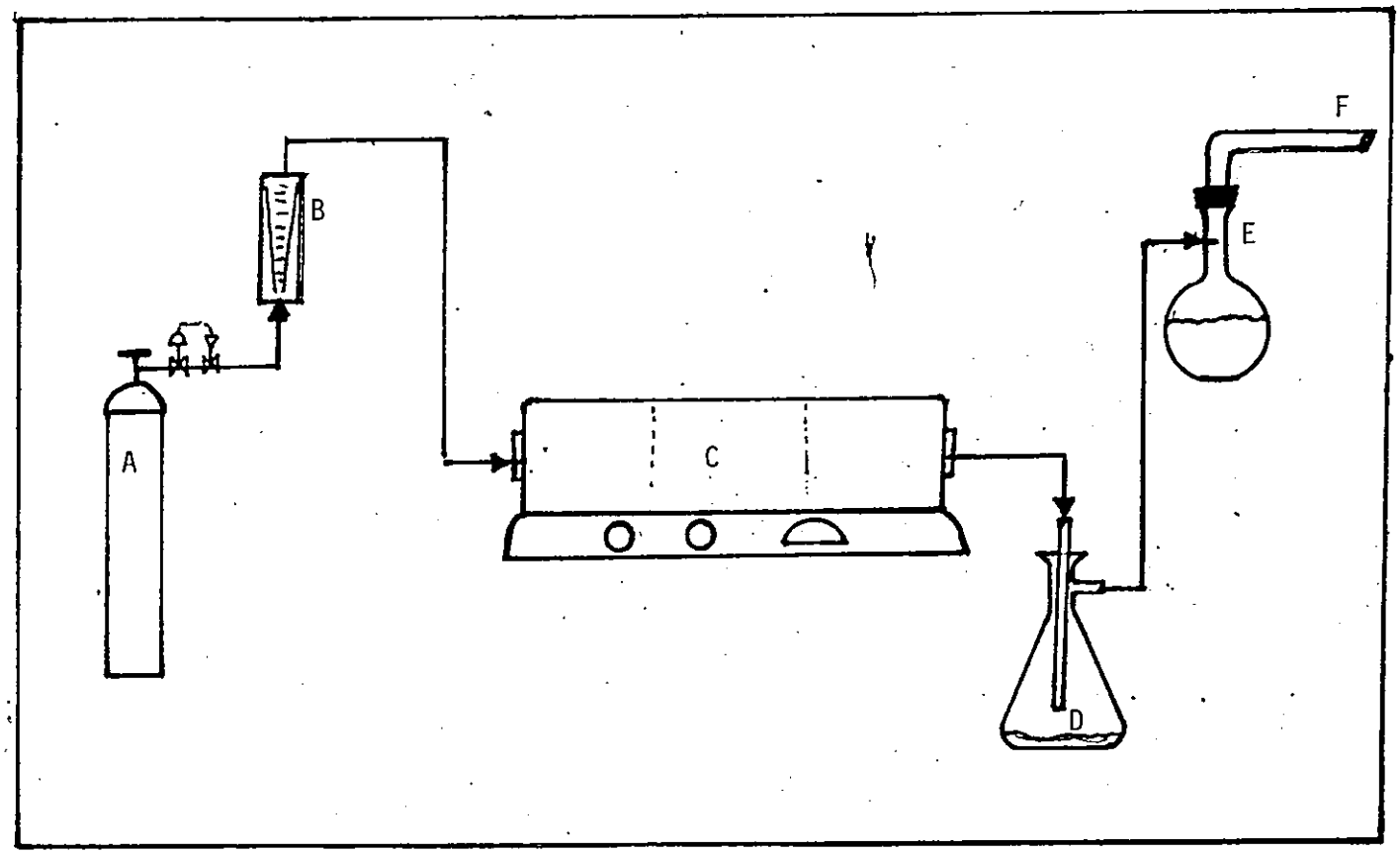

Fgiure F-1 Experimental Setup for Charring

A Nitrogen cylinder
B Brooks Rotameter
C Lindberg Hevi-Duty 3-zone furnace
D Tar collecter
E $Na\ CO_3$ Solution (400 mL H_2O, 150 gm $Na\ CO_3$)
F Fume hood

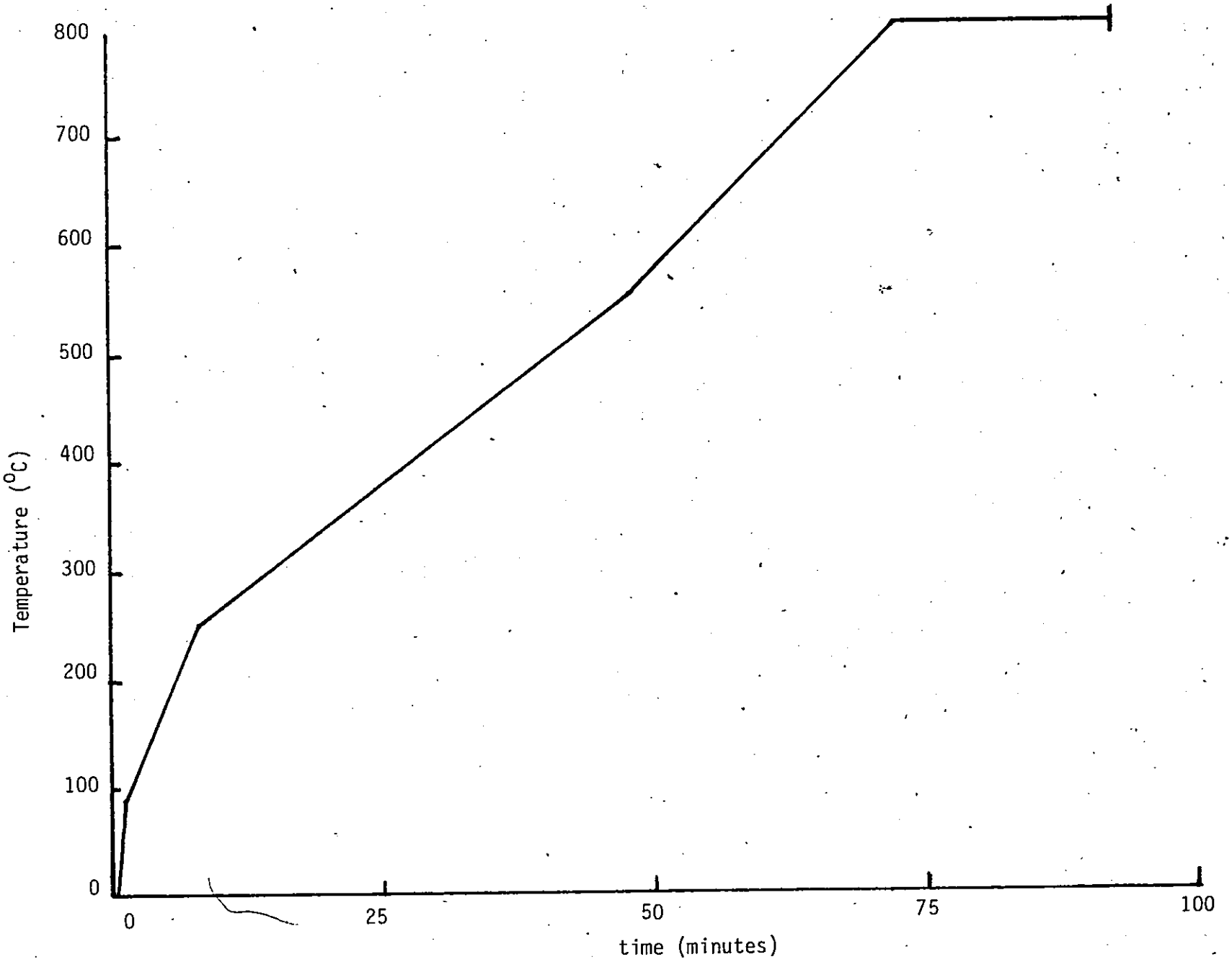

Figure F-2 Typical Temperature Profile During Charring

APPENDIX G

Derivation of F-curve for N-tanks in Series Model

The exit age distribution of the N-tanks in series model is given as:

$$E(t) = \frac{1}{\tau}\left(\frac{t}{\tau}\right)^{N-1} \frac{1}{(N-1)!} \exp(-t/\tau)$$

where t = time (s)

τ = residence time in a single tank (s)

N = number of tanks in series

Since, $E(t)=d(C/C_0)/dt=dF(t)/dt$, the above expression can be integrated to yield the step response.

$$\frac{d(C/C_0)}{dt} = \frac{1}{(N-1)!}\left(\frac{t}{\tau}\right)^{N-1}\left(\frac{1}{\tau}\right)\exp(-t/\tau)$$

$$C/C_0 = \int_0^{\infty} \frac{1}{(N-1)!}\left(\frac{t}{\tau}\right)^{N-1} \frac{1}{\tau} \exp(-t/\tau)\, dt$$

$$C/C_0 = \frac{1}{(N-1)!}\left(\frac{1}{\tau}\right)^{N-1} \int_0^{\infty} t^{N-1} \exp(-t/\tau)\, dt$$

The integral is of the form $x^m e^{ax} dx$, which can be found in tables to be equal to

$$\exp(ax) \sum_{r=0}^{m} (-1)^r \frac{m!\, x^{m-r}}{(m-r)!\, a^{r+1}}$$

where $a = -1/\tau$, $m = N-1$

Thus,

$$C/C_o = \frac{1}{(N-1)!} \left(\frac{1}{\tau}\right)^N \exp(-t/\tau) \sum_{r=0}^{N-1} \frac{(-1)^r (N-1)!\, t^{N-1-r}}{(N-1-r)!\, (1/\tau)^{r+1}}$$

This can be reduced to a simpler expression:

$$C/C_o = \left(\frac{1}{\tau}\right)^N \exp(-t/\tau) \sum_{r=0}^{N-1} \frac{(-1)^r\, t^{N-1-r}}{(N-1-r)!\, (1/\tau)^{r+1}}$$

APPENDIX H

Derivation of Mixed Model Step Response

The mixed model for the reactor consists of a stirred tank in parallel with a plug flow section which are both preceeded by a plug flow section as shown below:

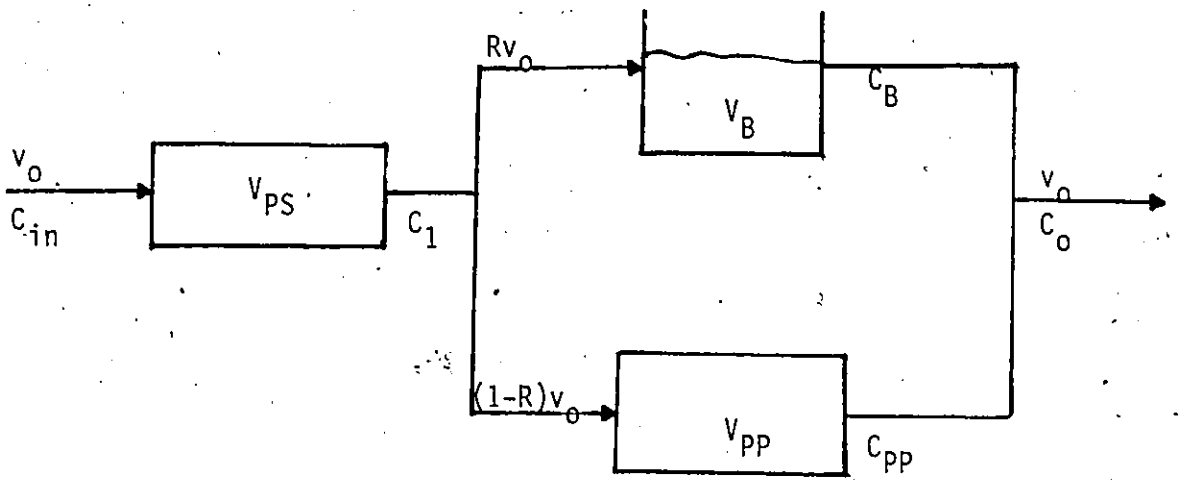

The response of the series plug flow section to a step change in feed composition is given in the time domain by

$$C_1(t) = C_{in} u_t\ (V_{PS}/v_o) = C_{in} u_t\ (T_{PS}) \qquad \text{Equation H-1}$$

and in the Laplace domain by

$$C_1(s) = C_{in}\ \exp(-T_{PS}s)/s \qquad \text{Equation H-2}$$

A material balance over the stirred tank section yields:

$$C_1 - C_B = \frac{V_B}{R\ v_o}\ \frac{dC_B}{dt} = \frac{T_B}{R}\ \frac{dC_B}{dt}\ ;\ C_B(t=0) = 0$$

The solution of this differential equation is given in the time domain by:

$$C_B(t) = C_{in}\,(1-\exp(R(T_{PS}-t)/T_B))\;u_t(T_{PS}) \qquad \text{Equation H-3}$$

The expression for $C_B(S)$ can also be found and is given below as

$$C_B(s) = (C_{in}/s)\;((R/T_B)/(s + R/T_B))\;\exp(-T_{PS}\,s) \qquad \text{Equation H-4}$$

A material balance over the parallel plug flow section yields:

$$C_{pp}(t) = C_1(t)\;u_t(V_{PP}/\;(v_o(1-R)))$$

$$C_{pp}(t) = C_{in}\;\;u_t(T_{PS})\;u_t(T_{PP}/(1-R)) \qquad \text{Equation H-4}$$

In the Laplace domain, this can be described as

$$C_{pp}(s) = (C_{in}/s)\;\exp(-s(T_{PS} + T_{pp}/(1-R))) \qquad \text{Equation H-5}$$

The composition of the exit stream, C_o, can be found by a simple balance and the use of Equations H-3, H-4.

$$Rv_oC_B \;+\; (1-R)v_o\;C_{PP} = v_oC_o$$

$$F(t)=C_o(t)/C_{in}=R(1-\exp(R(T_{PS}-t)/T_B))\;u_t(T_{PS}) \qquad \text{Equation H-6}$$
$$+\;(1-R)\;u_t(T_{PS} + T_{pp}/(1-R))$$

In the Laplace domain, $C_o(S)$ is given by:

$$F(s)=C_o(s)/C_{in}=((R^2/T_B)\;\exp(-T_{PS}s)/(s+ R/T_B) \qquad \text{Equation H-7}$$
$$+\;(1-R)\;\exp\;(-s(T_{PS} + T_{PP}/\;(1-R)))/s$$

APPENDIX I

Derivation of Combined Reactor/Measurement Device Model Step Response

The step response of the combined model for the system can be simply derived by using the Laplace Domain solutions of Appendix H and a material balance over each of the tanks for the measurement device.

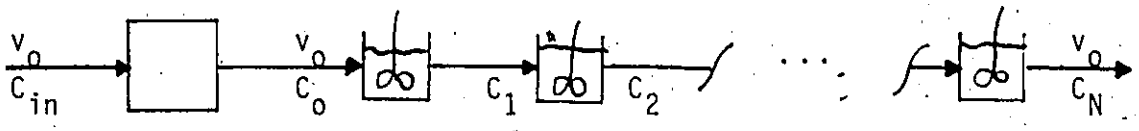

For 1 tank,

$$v_o C_o - v_o C_1 = V\, dC_1/dt$$

If $V/v_o = \tau$, then

$$C_1(s) = \frac{C_o(s)}{(\tau s + 1)}$$

For 2 tanks,

$$v_o C_1 - v_o C_2 = V\, dC_2/dt$$

and

$$C_2(s) = \frac{C_o(s)}{(\tau s + 1)^2}$$

For N equal size tanks in series,

$$C_N(s) = \frac{C_o(s)}{(\tau s + 1)^N} = \frac{1}{\tau^N} \frac{C_o(s)}{(s + 1/\tau)^N} \qquad \text{Equation I-1}$$

Substituting Equation H-7 for $C_o(S)$ yields the required response.

$$C_N(s) = \frac{1}{\tau^N} \frac{1}{(s + 1/\tau)^N} ((R^2/T_B) \exp(-T_{PS}s)/ \quad \text{Equation I-2}$$

$$(s + R/T_B) + (1-R) \exp(-s(T_{PS} + T_{PP}/(1-R))/s)$$

APPENDIX J

Computer Program for Parameter Estimation

A brief description of the Fortran program is provided below:

Reads data ---> MAIN PROGRAM { Calls STAT; Calls ZXMIN; Calls RESID; Calls COVAR } --> Writes output

Reads initial parameter estimates ---> SUBROUTINE ZXMIN { Calls FUNCT; Calls ZXMJN; Calls UERTST } --> Produces converged values of parameters

Reads final parameter values and calculates partial derivatives ---> SUBROUTINE COVAR { Calls FLINV; Calls VTPROF; Calls TANKS; Calls LINV1F; Calls LUDATF } --> Produces Variance-Covariance matrix for parameters

Reads values of parameters at every iteration ---> SUBROUTINE FUNCT { Calls FLINV; Calls TANKS } --> Produces values of C/C_o for both instrument and combined models

Subroutine Name	Description
STAT	- optional, when several values of the dependent variable are available at each time t, this routine calculates the mean and variance for the dependent variable. It also carries out a Bartlett test for equality of variances. (bypassed when IFLAG = 1)
ZXMIN	- IMSL minimization routine used to converge on parameter values (uses a Quasi-Newton method). (ZXMJN, UERTST)
RESID	- routine calculates the weighted or unweighted residual sum of squares. Carries out Derbin-Watson test for serial correlation.
COVAR	- routine that calculates approximate parameter variance-covariance matrix by calculating partial derivative matrix $\underline{X}$ and subsequently $\underline{M}$. Makes use of matrix inversion, matrix multiplication, matrix transposing routines (VTPROF, LINVIF, LUDATF)
FUNCT	- routine that calculates the residual sum of squares, i.e. the function which is being minimized. Uses FLINV to obtain values for the combined model and TANKS to obtain values for the N-tanks in series model.

Subroutine Name	Description
FLINV	- IMSL Laplace inversion routine used to obtain values of $C(t)/C_o$ for the combined model. Algorithm required scaling of both dependent and independent variable.
TANKS	- routine that calculates F(t) for the N-tanks in series model. Maximum number of tanks = 40.

A copy of the program listing is appended.

```
C     PROGRAM CONVERGES ON 5 PARAMETERS; TB,TP,R,TAU2,TD                FIV00010
C                                                                       FIV00020
      IMPLICIT REAL*8 (A-H,O-Z)                                         FIV00030
      EXTERNAL FUNCT                                                    FIV00040
       INTEGER N,NSIG,MAXFN,IOPT                                        FIV00050
       INTEGER NEWTR(25),NEWTS(25),NR,NS,NDR,NDS                        FIV00060
      DIMENSION T(76),YEXP(150),TI(60)                                  FIV00070
       DIMENSION X(5),H(15),G(5),W(15)                                  FIV00080
      DIMENSION TR(25),YR(25),VR(25)                                    FIV00090
      DIMENSION TS(25),YS(25),VS(25)                                    FIV00100
      DIMENSION P(5),FINV(25),FINS(25),FRACT(5)                         FIV00110
      DIMENSION ZZ(76),SAV(25)                                          FIV00120
      DOUBLE PRECISION DIFF(5),AM(5,5),AP(5,5), AMAT(5,5)               FIV00130
      DOUBLE PRECISION COV(5,5),CORR(5,5)                               FIV00140
      COMMON/REACT1/TR,YEXP,FINV,VR,PCOLR,TCT1                          FIV00150
      COMMON/SENSE1/TS,VS,FINS,PCOLS,TCT2                               FIV00160
      COMMON/REACT2/NR,NEWTR,NDR                                        FIV00170
      COMMON/SENSE2/NS,NEWTS,NDS                                        FIV00180
      COMMON/MAIN/C0                                                    FIV00190
      COMMON/MAIN/NT                                                    FIV00200
      C0 = 4.0D0                                                        FIV00210
      T0 = 20.0D0                                                       FIV00220
      NT=40                                                             FIV00230
      IFLAG=1                                                           FIV00240
C                                                                       FIV00250
C                                                                       FIV00260
      NP=5                                                              FIV00270
      NSIG=4                                                            FIV00280
       MAXFN = 500                                                      FIV00290
      IOPT=0                                                            FIV00300
      WRITE(6,202)NT                                                    FIV00310
  202 FORMAT(' ','NUMBER OF TANKS IN SERIES=', I5)                      FIV00320
      READ(5,100) (X(I),I=1,5)                                          FIV00330
  100 FORMAT(5F10.0)                                                    FIV00340
      READ(5,200)NR                                                     FIV00350
  200 FORMAT(I5)                                                        FIV00360
      READ(5,200)NDR                                                    FIV00370
      DO 300   J=1,NR                                                   FIV00380
         READ(5,301)T(J),YEXP(J)                                        FIV00390
          T(J) =T0 * T(J)                                               FIV00400
         YEXP(J) = C0 * YEXP(J)                                         FIV00410
         WRITE(6,304)T(J),YEXP(J)                                       FIV00420
  304   FORMAT(' ',2D13.5)                                              FIV00430
  300 CONTINUE                                                          FIV00440
  301 FORMAT(2F10.0)                                                    FIV00450
      READ(5,302)(NEWTR(L),L=1,NDR)                                     FIV00460
  302 FORMAT(40I1)                                                      FIV00470
      READ(5,105)(FRACT(I),I=1,NP)                                      FIV00480
  105 FORMAT(5E10.0)                                                    FIV00490
C                                                                       FIV00500
      WRITE(6,101)(X(I),I=1,5)                                          FIV00510
  101  FORMAT(' ',5D13.5)                                               FIV00520
      WRITE(6,201)NR                                                    FIV00530
  201 FORMAT(' ',I5)                                                    FIV00540
      WRITE(6,201)NDR                                                   FIV00550
      WRITE(6,303)(NEWTR(L),L=1,NDR)                                    FIV00560
  303 FORMAT(' ',40I1)                                                  FIV00570
C                                                                       FIV00580
      READ(5,200)NS                                                     FIV00590
      READ(5,200)NDS                                                    FIV00600
C                                                                       FIV00610
      WRITE(6,201)NS                                                    FIV00620
      WRITE(6,201)NDS                                                   FIV00630
      DO 400 J=1,NS                                                     FIV00640
      K=NR+J                                                            FIV00650
```

```
      READ(5,301)TI(J),YEXP(K)                                          FIV00660
      TI(J)=T0*TI(J)                                                    FIV00670
C                                                                       FIV00680
      YEXP(K)=C0*YEXP(K)                                                FIV00690
      WRITE(6,304)TI(J),YEXP(K)                                         FIV00700
400   CONTINUE                                                          FIV00710
C                                                                       FIV00720
C                                                                       FIV00730
      READ(5,302)(NEWTS(L),L=1,NDS)                                     FIV00740
C                                                                       FIV00750
      WRITE(6,303)(NEWTS(L),L=1,NDS)                                    FIV00760
C                                                                       FIV00770
C                                                                       FIV00780
C                                                                       FIV00790
      IF(IFLAG.EQ.1)GOTO 769                                            FIV00800
C                                                                       FIV00810
C                                                                       FIV00820
      CALL STAT(T,YEXP(1),NR,NDR,NEWTR,TF,YF,VR,PCOLR,CR)               FIV00830
C                                                                       FIV00840
C                                                                       FIV00850
      DO 450  J=1,NDR                                                   FIV00860
      WRITE(6,500)TR(J),YR(J),VR(J)                                     FIV00870
450   CONTINUE                                                          FIV00880
500   FORMAT(' ',3D13.5)                                                FIV00890
      WRITE(6,550)PCOLR,CR                                              FIV00900
550   FORMAT(' ','POOLED VARIANCE=',D13.5,'  CHI SQ=',D13.5)            FIV00910
C                                                                       FIV00920
C                                                                       FIV00930
      CALL STAT(TI,YEXP(NR+1),NS,NDS,NEWTS,TS,YS,VS,POOLS,CS)           FIV00940
C                                                                       FIV00950
C                                                                       FIV00960
      DO 600 J=1,NDS                                                    FIV00970
       WRITE (6,500) TS(J),YS(J),VS(J)                                  FIV00980
600   CONTINUE                                                          FIV00990
C                                                                       FIV01000
C                                                                       FIV01010
      WRITE(6,550)PCOLS,CS                                              FIV01020
C                                                                       FIV01030
C                                                                       FIV01040
      IF(IFLAG.EQ.0)GOTO 790                                            FIV01050
C                                                                       FIV01060
700   DO 750  K=1,NDS                                                   FIV01070
      READ(5,751)VS(K)                                                  FIV01080
750   CONTINUE                                                          FIV01090
C                                                                       FIV01100
      DO 760  K=1,NDR                                                   FIV01110
      READ(5,751)VR(K)                                                  FIV01120
760   CONTINUE                                                          FIV01130
751   FORMAT(E10.0)                                                     FIV01140
  769   CONTINUE                                                        FIV01150
C                                                                       FIV01160
      DO 770  K=1,NR                                                    FIV01170
      TR(K)=T(K)                                                        FIV01180
770   CONTINUE                                                          FIV01190
C                                                                       FIV01200
      DO 780  K=1,NS                                                    FIV01210
      TS(K)=TI(K)                                                       FIV01220
780   CONTINUE                                                          FIV01230
C                                                                       FIV01240
C                                                                       FIV01250
      DO 1  I=1,NR                                                      FIV01260
    1   VR(I)=0.0                                                       FIV01270
C                                                                       FIV01280
      DO 2  I=1,NS                                                      FIV01290
    2   VS(I)=0.0                                                       FIV01300
C                                                                       FIV01310
C                                                                       FIV01320
C                                                                       FIV01330
```

```
  790    CONTINUE                                                          FIV01340
                                                                           FIV01350
C                                                                          FIV01360
C                                                                          FIV01370
C                                                                          FIV01380
C      CALL ZXMIN(FUNCT,NP,NSIG,MAXFN,IOPT,X,H,G,F,W,IER)                  FIV01390
C                                                                          FIV01400
C                                                                          FIV01410
C                                                                          FIV01420
C                                                                          FIV01430
C      CALCULATING RESIDUALS                                               FIV01440
C                                                                          FIV01450
       CALL RESID(TR,VR,FINV,YEXP(1),NDR,NR,NEWTR)                         FIV01460
C                                                                          FIV01470
       CALL RESID(TS,VS,FINS,YEXP(NR+1),NDS,NS,NEWTS)                      FIV01480
C                                                                          FIV01490
C                                                                          FIV01500
C                                                                          FIV01510
C                                                                          FIV01520
        P(1)=X(1)*X(1)                                                     FIV01530
        P(4)=X(2)*X(2)                                                     FIV01540
        P(5)=DEXP(-X(3)*X(3))                                              FIV01550
        P(2)=(DSIN(X(4)**2 *1.57079D-04))**2                               FIV01560
        P(3)=X(5)                                                          FIV01570
C                                                                          FIV01580
       DO 5050  K=1,NP                                                     FIV01590
         DIFF(K)=FRACT(K) * P(K)                                           FIV01600
         IF(DIFF(K).LT.1.0E-10)DIFF(K)=FRACT(K)                            FIV01610
 5050    CONTINUE                                                          FIV01620
C                                                                          FIV01630
C                                                                          FIV01640
       CALL COVAR(P,DIFF,F,AM,AP,AMAT,CCV,CORR,NP)                         FIV01650
C                                                                          FIV01660
       WRITE(6,900)(P(I),I=1,NP)                                           FIV01670
  900  FORMAT(' PARAMETERS ARE',5D15.7)                                    FIV01680
       WRITE(6,901)(DIFF(I),I=1,NP)                                        FIV01690
       WRITE(6,803)                                                        FIV01700
       WRITE(6,904)((AM(I,J),J=1,NP),I=1,NP)                               FIV01710
       WRITE(6,904)((AP(I,J),J=1,NP),I=1,NP)                               FIV01720
       WRITE(6,804)                                                        FIV01730
       WRITE(6,904)((AMAT(I,J),J=1,NP),I=1,NP)                             FIV01740
       WRITE(6,805)                                                        FIV01750
       WRITE(6,904)((CCV(I,J),J=1,NP),I=1,NP)                              FIV01760
       WRITE(6,806)                                                        FIV01770
       WRITE(6,904)((CORR(I,J),J=1,NP),I=1,NP)                             FIV01780
C                                                                          FIV01790
C                                                                          FIV01800
C                                                                          FIV01810
  901  FORMAT(' ',T10,'DELTAS',5D13.5)                                     FIV01820
  904  FORMAT(' ',5D13.5)                                                  FIV01830
  803  FORMAT(' '/' ','PRODUCT OF X TRANSPOSE X',                          FIV01840
     1'RESPONSE 1 THEN RESPONSE 2'//)                                      FIV01850
  804  FORMAT(' '/' ','M MATRIX,XTX +XTX'//)                               FIV01860
  805  FORMAT(' '/' ','APPROXIMATE PARAMETER VAR-CCV MATRIX'/)             FIV01870
  806  FORMAT(' '/' ','PARAMETER CORRELATION MATRIX'//)                    FIV01880
C                                                                          FIV01890
       STOP                                                                FIV01900
       END                                                                 FIV01910
C                                                                          FIV01920
C                                                                          FIV01930
C                                                                          FIV01940
C                                                                          FIV01950
C                                                                          FIV01960
C      SUBROUTINE SUPPLIED FOR ZXMIN                                       FIV01970
C                                                                          FIV01980
C                                                                          FIV01990
       SUBROUTINE FUNCT(N,X,SS)                                            FIV02000
       IMPLICIT REAL*8 (A-H,O-Z)                                           FIV02010
```

```
      INTEGER N,NSIG,KMAX,IER                                          FIV02020
      INTEGER NEWTR(25),NEWTS(25),NR,NS,NDR,NDS                        FIV02030
      DIMENSION X(5)                                                   FIV02040
      DIMENSION T(76),YEXP(150),TI(60)                                 FIV02050
      DIMENSION TR(25),YR(25),VR(25)                                   FIV02060
      DIMENSION TS(25),YS(25),VS(25)                                   FIV02070
      DIMENSION FINV(25),FINS(25)                                      FIV02080
      COMPLEX*16 F,TB,R,TAU2,TD,TP,DCMPLX                              FIV02090
      COMMON/REACT1/TR,YEXP,FINV,VR,PCOLR,TOT1                         FIV02100
      COMMON/SENSE1/TS,VS,FINS,POOLS,TOT2                              FIV02110
      COMMON/REACT2/NR,NEWTR,NDR                                       FIV02120
      COMMON/SENSE2/NS,NEWTS,NDS                                       FIV02130
      COMMON/PLACE/ TB,TAU2,TD,TP,R                                    FIV02140
       DATA FACT/1.570796D-04/                                         FIV02150
C                                                                      FIV02160
                                                                       FIV02170
      EXTERNAL F                                                       FIV02180
C                                                                      FIV02190
C                                                                      FIV02200
C                                                                      FIV02210
      TB=DCMPLX(X(1)**2,0.0D0)                                         FIV02220
      TP=DCMPLX(X(2)**2,0.0D0)                                         FIV02230
      R=DCMPLX(DEXP(-X(3)**2),0.0D0)                                   FIV02240
C                                                                      FIV02250
      TAU2R=(DSIN(X(4)**2 * FACT))**2                                  FIV02260
      TAU2 =DCMPLX(TAU2R,0.0D0)                                        FIV02270
      TD=DCMPLX(X(5),0.0D0)                                            FIV02280
C                                                                      FIV02290
C                                                                      FIV02300
C                                                                      FIV02310
      NSIG=6                                                           FIV02320
      KMAX=200                                                         FIV02330
      ALPHA = 0.0D0                                                    FIV02340
      WRITE(6,200)(X(I),I=1,5)                                         FIV02350
      WRITE(6,200)TB,TAU2,TD                                           FIV02360
C                                                                      FIV02370
      WRITE(6,200)TP,R                                                 FIV02380
200    FORMAT(' ',6D13.6)                                              FIV02390
C                                                                      FIV02400
      CALL FLINV(F,NDR,TR,ALPHA,NSIG,KMAX,FINV,IER)                    FIV02410
C                                                                      FIV02420
C                                                                      FIV02430
      CALL TANKS(TS,NDS,TAU2R,0.0D0,FINS)                              FIV02440
C                                                                      FIV02450
C                                                                      FIV02460
C                                                                      FIV02470
C                                                                      FIV02480
C                                                                      FIV02490
      DO 75  J=1,NDR                                                   FIV02500
      IF(TR(J).LT.X(5))FINV(J)=0.0D0                                   FIV02510
75    CONTINUE                                                         FIV02520
C                                                                      FIV02530
C                                                                      FIV02540
C     CALCULATING WEIGHTED SUM OF SQUARES                              FIV02550
C                                                                      FIV02560
      JJ=0                                                             FIV02570
      TOT1=0.0D0                                                       FIV02580
C                                                                      FIV02590
      DO 100  K=1,NDR                                                  FIV02600
      KK=NEWTR(K)                                                      FIV02610
      DO 80  J=1,KK                                                    FIV02620
      TOT1= TOT1 + (FINV(K)-YEXP(J+JJ))**2                             FIV02630
80    CONTINUE                                                         FIV02640
      JJ=JJ+KK                                                         FIV02650
100   CONTINUE                                                         FIV02660
C                                                                      FIV02670
C                                                                      FIV02680
      WRITE(6,101)TOT1                                                 FIV02690
```

```
101     FORMAT(' ','TCT =' ,D15.8)                                      FIV02700
C                                                                       FIV02710
C                                                                       FIV02720
        TOT2=0.0D0                                                      FIV02730
        JJ=NDR                                                          FIV02740
        DO 300  K=1,NDS                                                 FIV02750
        KK=NEWTS(K)                                                     FIV02760
        DO 180  J=1,KK                                                  FIV02770
        TOT2=TOT2 + (FINS(K)-YEXP(J+JJ))**2                             FIV02780
180     CONTINUE                                                        FIV02790
        JJ=JJ+KK                                                        FIV02800
300     CONTINUE                                                        FIV02810
C                                                                       FIV02820
C                                                                       FIV02830
        WRITE(6,101) TOT2                                               FIV02840
C                                                                       FIV02850
        SS=TOT1 + TOT2                                                  FIV02860
C                                                                       FIV02870
        WRITE(6,101)SS                                                  FIV02880
C                                                                       FIV02890
        RETURN                                                          FIV02900
        END                                                             FIV02910
C                                                                       FIV02920
C                                                                       FIV02930
C                                                                       FIV02940
C                                                                       FIV02950
C     SUBROUTINE SUPPLIED FOR LAPLACE INVERSE RCUTINE                   FIV02960
C                                                                       FIV02970
C                                                                       FIV02980
        COMPLEX FUNCTION F*16 (S)                                       FIV02990
        REAL*8 C0,DREAL                                                 FIV03000
        COMPLEX*16 S,TB,TP,R,TAU2,CNE,CDEXP,TD                          FIV03010
        COMMON/PLACE/ TB,TAU2,TD,TP,R                                   FIV03020
        COMMON/MAIN/C0                                                  FIV03030
        COMMON/MAIN/NT                                                  FIV03040
        DATA ONE/(1.0D0,0.0D0)/                                         FIV03050
        F=(0.0D0,0.0D0)                                                 FIV03060
        IF(DREAL(ONE-R).LT.1.0D-02)GOTO 10                              FIV03070
        F=(CNE-R)*CDEXP(-S*(TD+TP))/(CNE-R))/S                          FIV03080
10      CONTINUE                                                        FIV03090
        F=F + (R**2/TB) * CDEXP(-TD*S)/S/(S + R/TB)                     FIV03100
        F=F/(S+ONE/TAU2)**NT                                            FIV03110
        F=F/TAU2**NT                                                    FIV03120
        F=C0 *F                                                         FIV03130
        RETURN                                                          FIV03140
        END                                                             FIV03150
C                                                                       FIV03160
        SUBROUTINE COVAR(P,DIFF,SS,AM,AP,AMAT,COV,CORR,NP)              FIV03170
        IMPLICIT REAL*8 (A-H,O-Z)                                       FIV03180
C                                                                       FIV03190
C                                                                       FIV03200
        INTEGER NEWTR(25),NEWTS(25),NR,NS,NDR,NDS                       FIV03210
C                                                                       FIV03220
        DOUBLE PRECISION  P(NP),DIFF(NP),X(5)                           FIV03230
        DOUBLE PRECISION TR(25),TS(25)                                  FIV03240
        DOUBLE PRECISION FINV(25),FINS(25),FC(50),TALL(50)              FIV03250
      DOUBLE PRECISION    YEXP(150),VS(25),VR(25)                       FIV03260
        DOUBLE PRECISION AP(NP,NP)                                      FIV03270
        DOUBLE PRECISION F1(50),F2(50)                                  FIV03280
        DOUBLE PRECISION A(50,5),AM(NP,NP),AMAT(NP,NP)                  FIV03290
        DOUBLE PRECISION AJUNK(5,5)                                     FIV03300
        DOUBLE PRECISION AX(150,5)                                      FIV03310
        DOUBLE PRECISION FUNC(50)                                       FIV03320
        COMPLEX*16 F,TB,R,TAU2,TD,TP,DCMPLX                             FIV03330
        COMPLEX*16 PNEW(5)                                              FIV03340
        DOUBLE PRECISION ATA(15),WKAREA(5),COV(NP,NP),CORR(NP,NP)       FIV03350
        EXTERNAL F                                                      FIV03360
        COMMON/REACT1/TR,YEXP,FINV,VR,FCCLR,TCT1                        FIV03370
```

```
      COMMON/SENSE1/TS,VS,FINS,POOLS,TCT2                               FIV03380
      COMMON/REACT2/NR,NEWTR,NDR                                        FIV03390
      COMMON/SENSE2/NS,NEWTS,NDS                                        FIV03400
      COMMON/PLACE/ TB,TAU2,TD,TP,R                                     FIV03410
      EQUIVALENCE (PNEW(1),TB),(PNEW(2),TAU2),(PNEW(3),TD)              FIV03420
      EQUIVALENCE (PNEW(4),TP),(PNEW(5),R)                              FIV03430
C                                                                       FIV03440
C                                                                       FIV03450
      NSIG=6                                                            FIV03460
      KMAX=200                                                          FIV03470
      ALPHA=0.0D0                                                       FIV03480
      PNEW(1)=  DCMPLX(P(1),0.0D0)                                      FIV03490
      PNEW(4)= DCMPLX(P(4),0.0D0)                                       FIV03500
      PNEW(5)=DCMPLX(P(5),0.0D0)                                        FIV03510
      PNEW(2)=DCMPLX(P(2),0.0D0)                                        FIV03520
      PNEW(3)=DCMPLX(P(3),0.0D0)                                        FIV03530
C                                                                       FIV03540
C                                                                       FIV03550
      NEW=NR                                                            FIV03560
      DO 20  J=1,NEW                                                    FIV03570
      IF(J.LE.NDR)TALL(J) =TR(J)                                        FIV03580
      IF(J.GT.NDR)TALL(J) = TS(J-NDR)                                   FIV03590
20    CONTINUE                                                          FIV03600
C                                                                       FIV03610
C                                                                       FIV03620
C                                                                       FIV03630
      CALL FLINV(F,NEW,TALL,ALPHA,NSIG,KMAX,FO,IER)                     FIV03640
C                                                                       FIV03650
C                                                                       FIV03660
C                                                                       FIV03670
C                                                                       FIV03680
      DO 50   I=1,NP                                                    FIV03690
      PNEW(I)=PNEW(I) + DCMPLX(DIFF(I),0.0D0)                           FIV03700
      IF(I.NE.1)PNEW(I-1)=DCMPLX(P(I-1),0.0D0)                          FIV03710
      CALL FLINV(F,NEW,TALL,ALPHA,NSIG,KMAX,FUNC,IER)                   FIV03720
         DO 40     J=1,NEW                                              FIV03730
            A(J,I)=(FUNC(J)-FO(J))/DIFF(I)                              FIV03740
40       CONTINUE                                                       FIV03750
50    CONTINUE                                                          FIV03760
C                                                                       FIV03770
C                                                                       FIV03780
C                                                                       FIV03790
      DO 55  I=1,NP                                                     FIV03800
      JJ=0                                                              FIV03810
      DO 54    K=1,NEW                                                  FIV03820
      IF(K.LE.NDR)KK=NEWTR(K)                                           FIV03830
      IF(K.GT.NDR)KK=NEWTS(K-NDR)                                       FIV03840
      DO 53  J=1,KK                                                     FIV03850
         AX(J+JJ,I)=A(K,I)                                              FIV03860
53    CONTINUE                                                          FIV03870
      JJ=JJ+KK                                                          FIV03880
54    CONTINUE                                                          FIV03890
55    CONTINUE                                                          FIV03900
C                                                                       FIV03910
      CALL VTPROF(AX,NR,NP,150,ATA)                                     FIV03920
C                                                                       FIV03930
C                                                                       FIV03940
      K=0                                                               FIV03950
      DO 60   I=1,NP                                                    FIV03960
      DO 59    J=1,I                                                    FIV03970
         K=K+1                                                          FIV03980
         AM(I,J)=ATA(K)                                                 FIV03990
         IF(I.NE.J)AM(J,I)=AM(I,J)                                      FIV04000
59    CONTINUE                                                          FIV04010
60    CONTINUE                                                          FIV04020
C                                                                       FIV04030
C                                                                       FIV04040
C                                                                       FIV04050
```

```
      DO 100 I=1,NP                                                     FIV040
      DO 95  J=1,NEW                                                    FIV040
      A(J,I)=0.0D0                                                      FIV040
      IF(I.NE.2)GOTO 91                                                 FIV040
      DELTA=0.0D0                                                       FIV041
      PARM=P(2)                                                         FIV041
      CALL TANKS(TALL,NEW,PARM,DELTA,F1)                                FIV041
      CALL TANKS(TALL,NEW,PARM,DIFF(2),F2)                              FIV041
      A(J,I)=(F2(J)-F1(J))/DIFF(I)                                      FIV041
91    CONTINUE                                                          FIV041
95    CONTINUE                                                          FIV041
100   CONTINUE                                                          FIV041
C                                                                       FIV041
C                                                                       FIV041
      DO 300  I=1,NP                                                    FIV041
      JJ=0                                                              FIV042
      DO 299   K=1,NEW                                                  FIV042
      IF(K.LE.NDR)KK=NEWTR(K)                                           FIV042
      IF(K.GT.NDR)KK=NEWTS(K-NDR)                                       FIV042
      DO 298     J=1,KK                                                 FIV042
        AX(J+JJ,I)=A(K,I)                                               FIV042
298   CONTINUE                                                          FIV042
      JJ=JJ+KK                                                          FIV042
299   CONTINUE                                                          FIV042
300   CONTINUE                                                          FIV042
C                                                                       FIV043
      CALL VTPROF(AX,NR,NP,150,ATA)                                     FIV043
C                                                                       FIV043
      K=0                                                               FIV043
      DO 67   I=1,NP                                                    FIV043
        DO 65   J=1,I                                                   FIV043
        K=K+1                                                           FIV043
        AP(I,J)=ATA(K)                                                  FIV043
        IF(I.NE.J)AP(J,I)=AP(I,J)                                       FIV043
65      CONTINUE                                                        FIV044
67      CONTINUE                                                        FIV044
C                                                                       FIV044
C                                                                       FIV044
C                                                                       FIV044
C                                                                       FIV044
      DO 150 I=1,NP                                                     FIV044
      DO 125 J=1,NP                                                     FIV044
      AMAT(I,J)=AM(I,J)/(TOT1/(NR-NP)) + AP(I,J)/(TOT2/(NS-NP))         FIV044
      AJUNK(I,J)=AMAT(I,J)                                              FIV044
125   CONTINUE                                                          FIV044
150   CONTINUE                                                          FIV045
C                                                                       FIV045
C                                                                       FIV045
      CALL LINV1F(AJUNK,NP,NP,COV,0,WKAREA,IER)                         FIV045
C                                                                       FIV045
C     CALCULATING THE PARAMETER CORRELATION MATRIX                      FIV045
C                                                                       FIV045
      DO 200  I=1,NP                                                    FIV045
        DO 90  J=1,NP                                                   FIV045
        CORR(I,J)=COV(I,J)/DSQRT(COV(I,I)*COV(J,J))                     FIV045
90      CONTINUE                                                        FIV046
200   CONTINUE                                                          FIV046
C                                                                       FIV046
C                                                                       FIV046
      RETURN                                                            FIV046
      END                                                               FIV046
C                                                                       FIV046
      SUBROUTINE STAT(T,YEXP,ND,NN,NEWT,TT,Y,VAR,PCOLS,CHI)             FIV046
C                                                                       FIV046
C                                                                       FIV046
      IMPLICIT REAL*8 (A-H,O-Z)                                         FIV047
      DOUBLE PRECISION T(ND),YEXP(ND),TT(NN),Y(NN),VAR(NN)              FIV047
      INTEGER NEWT(NN)                                                  FIV047
```

```
C                                                                       FIV04740
C                                                                       FIV04750
C     CALCULATION OF DIFFERENT TIME VALUES                              FIV04760
C       CALCULATION OF THE MEAN AND VARIANCE AT EACH TIME               FIV04770
C                                                                       FIV04780
      PREV = -1.0D0                                                     FIV04790
      KJ=0                                                              FIV04800
      DO 450  J=1,ND                                                    FIV04810
         IF(T(J).EQ.PREV)GOTO 450                                       FIV04820
         KJ=KJ+1                                                        FIV04830
         TT(KJ)=T(J)                                                    FIV04840
         PREV=T(J)                                                      FIV04850
 450  CONTINUE                                                          FIV04860
C                                                                       FIV04870
      JJ=0                                                              FIV04880
      DO 460  K=1,NN                                                    FIV04890
        KK=NEWT(K)                                                      FIV04900
         TOT=0.                                                         FIV04910
         DO 455  J=1,KK                                                 FIV04920
            TOT=TOT + YEXP(J+JJ)                                        FIV04930
 455       CONTINUE                                                     FIV04940
         Y(K)=TOT/KK                                                    FIV04950
         JJ=KK+JJ                                                       FIV04960
 460  CONTINUE                                                          FIV04970
C                                                                       FIV04980
      JJ=0                                                              FIV04990
      DO 470 K=1,NN                                                     FIV05000
        KK=NEWT(K)                                                      FIV05010
         TOT=0.                                                         FIV05020
         DO 465  J=1,KK                                                 FIV05030
            TOT=TOT + (YEXP(JJ +J)-Y(K))**2                             FIV05040
 465     CONTINUE                                                       FIV05050
         VAR(K)=TOT/(KK-1)                                              FIV05060
         IF(VAR(K).LE.1.0D-08)VAR(K) = 1.0D-05                          FIV05070
         JJ=JJ+KK                                                       FIV05080
 470  CONTINUE                                                          FIV05090
C                                                                       FIV05100
C                                                                       FIV05110
C                                                                       FIV05120
C     BARTLETT'S TEST FOR EQUALITY OF VARIANCES                         FIV05130
      SUM=0.                                                            FIV05140
      TOT=0.                                                            FIV05150
      DO 1001  J=1,NN                                                   FIV05160
         TOT=TOT + NEWT(J)                                              FIV05170
         SUM=SUM + (NEWT(J)-1)*VAR(J)                                   FIV05180
 1001  CONTINUE                                                         FIV05190
C                                                                       FIV05200
      TOT1=TOT-NN                                                       FIV05210
      POOLS = SUM/TOT1                                                  FIV05220
C                                                                       FIV05230
      C=1. + (TOT-1./TOT)/(3.*(NN-1))                                   FIV05240
C                                                                       FIV05250
      TOT = 0.                                                          FIV05260
      DO 1002  J=1,NN                                                   FIV05270
         TOT = TOT + NEWT(J) * DLOG(VAR(J)/POOLS)                       FIV05280
 1002  CONTINUE                                                         FIV05290
C                                                                       FIV05300
C                                                                       FIV05310
      CHI = -TOT/C                                                      FIV05320
C                                                                       FIV05330
C                                                                       FIV05340
      RETURN                                                            FIV05350
      END                                                               FIV05360
      SUBROUTINE RESID(TT,VAR,F,YEXP,ND,NDATA,NEWT)                     FIV05370
      IMPLICIT REAL*8 (A-H,O-Z)                                         FIV05380
C                                                                       FIV05390
C                                                                       FIV05400
      DIMENSION ZZ(100),TT(ND),VAR(ND),F(ND)                            FIV05410
```

```
      DIMENSION YEXP(NDATA),SAV(100)                                    FIV05420
      INTEGER NEWT(ND)                                                  FIV05430
C                                                                       FIV05440
C                                                                       FIV05450
      WRITE(6,590)                                                      FIV05460
590   FORMAT(' ',20X,'TIME(S)',8X,'VARIANCE',8X,'PRED',                 FIV05470
     1' VALUE',15X,'EXP VALUE',15X,'RESIDUALS'//)                       FIV05480
      JJ=0                                                              FIV05490
      DO 550   K=1,ND                                                   FIV05500
      KK=NEWT(K)                                                        FIV05510
      WRITE(6,600) TT(K),VAR(K),F(K)                                    FIV05520
        DO 525  J=1,KK                                                  FIV05530
       ZZ(J+JJ)=YEXP(J+JJ) -F(K)                                        FIV05540
       WRITE(6,601)YEXP(J+JJ),ZZ(J+JJ)                                  FIV05550
525   CONTINUE                                                          FIV05560
      JJ=JJ+KK                                                          FIV05570
550   CONTINUE                                                          FIV05580
600   FORMAT(' ',T15,D15.6,T30,D15.6,T45,D15.6)                         FIV05590
601   FORMAT(' ',T65,D20.9,T90,D20.9)                                   FIV05600
C                                                                       FIV05610
C                                                                       FIV05620
      DO 900  I=1,2                                                     FIV05630
C DERBIN WATSON TEST FOR SERIAL CORRELATION                             FIV05640
      KK=I-NEWT(1)                                                      FIV05650
      DO 850   K=1,ND                                                   FIV05660
       SAV(K)=ZZ(KK+NEWT(K))                                            FIV05670
      KK=KK +  NEWT(K)                                                  FIV05680
850   CONTINUE                                                          FIV05690
C                                                                       FIV05700
                                                                        FIV05710
       SUM=0.0D0                                                        FIV05720
      TOT=0.0D0                                                         FIV05730
      J=ND-1                                                            FIV05740
      DO 800  K=1,J                                                     FIV05750
      SUM=SUM + (SAV(K+1)-SAV(K))**2                                    FIV05760
      TOT=TOT + SAV(K)**2                                               FIV05770
800   CONTINUE                                                          FIV05780
C                                                                       FIV05790
      TOT = TOT + SAV(ND)**2                                            FIV05800
      D=SUM/TOT                                                         FIV05810
C                                                                       FIV05820
C                                                                       FIV05830
       WRITE(6,998) D                                                   FIV05840
998    FORMAT(' ','DERBIN WATSON TEST, D=',D14.7)                       FIV05850
900    CONTINUE                                                         FIV05860
       RETURN                                                           FIV05870
       END                                                              FIV05880
C                                                                       FIV05890
C                                                                       FIV05900
C                                                                       FIV05910
      SUBROUTINE TANKS(T,N,TAU,DELTA,F)                                 FIV05920
C                                                                       FIV05930
C SUBROUTINE PREDICTS OUTPUT FROM NT TANKS IN SERIES WITH EQUAL         FIV05940
C TIME CONSTANTS                                                        FIV05950
C   NT=NUMBER OF TANKS                                                  FIV05960
C                                                                       FIV05970
      IMPLICIT REAL*8 (A-H,O-Z)                                         FIV05980
      DOUBLE PRECISION T(N),SMALL,TAU,F(N)                              FIV05990
      COMMON/MAIN/CO                                                    FIV06000
      COMMON/MAIN/NT                                                    FIV06010
      DATA ONE/1.0D0/,SMALL/1.0D-04/                                    FIV06020
C                                                                       FIV06030
C  OUTER LOOP CORRESPONDS TO INDIVIDUAL DATA POINTS                     FIV06040
C                                                                       FIV06050
      IFLAG=0                                                           FIV06060
      DO 100  I=1,N                                                     FIV06070
      F(I)=0.0D0                                                        FIV06080
      Q=T(I)/(TAU  + DELTA)                                             FIV06090
```

```
      IF(Q.GE.178)IFLAG=1                                              FIV06100
      IF(IFLAG.EQ.1)GOTO 75                                            FIV06110
      DENOM=1.0D0                                                      FIV06120
C                                                                      FIV06130
      P=DEXP(-Q)                                                       FIV06140
      DO 50 J=1,NT                                                     FIV06150
      L=J-1                                                            FIV06160
      IF(J.NE.1)DENOM=DENOM*L                                          FIV06170
       IF(L.GE.25)GOTO 30                                              FIV06180
      R2=1.0D0                                                         FIV06190
      R1=Q**L                                                          FIV06200
      GOTO 35                                                          FIV06210
30    CONTINUE                                                         FIV06220
      M=L/2                                                            FIV06230
      M1=L-M                                                           FIV06240
      M2=M                                                             FIV06250
      R1=Q**M1                                                         FIV06260
      R2=Q**M2                                                         FIV06270
35    F(I)=F(I) + R1/DENOM*R2                                          FIV06280
50    CONTINUE                                                         FIV06290
C                                                                      FIV06300
C                                                                      FIV06310
      F(I)=F(I)*P                                                      FIV06320
      IF(F(I).LT.SMALL)IFLAG=1                                         FIV06330
75    CONTINUE                                                         FIV06340
      F(I)=CO*(ONE-F(I))                                               FIV06350
100   CONTINUE                                                         FIV06360
C                                                                      FIV06370
      RETURN                                                           FIV06380
      END                                                              FIV06390
C                                                                      FIV06400
C                                                                      FIV06410
```

APPENDIX K

Void Volume Estimates of Char Bed

Estimates of the fractional voids in packed beds are found in Figure 5-53 in Perry's Chemical Engineers handbook (5th Ed.).

		Fractional Voids (ϵ)	
Particle Size	D_p/D_t	Spheres	Granules
0.2 - 0.4 mm	.019	0.333	0.42
0.4 - 1.0 mm	.044	0.358	0.45
1.0 - 1.4 mm	.074	0.36	0.45

The volume of the annular char bed can be calculated as

$$V = \frac{\pi(D_2^2 - D_1^2)h}{4}$$

$D_1 = .125$ in

$D_2 = .625$ in

$h = 3$ in

$V = 14.5\ cm^3$

The volume occupied by the particles is therefore $(1-\epsilon)V$. The range for these volumes is tabulated below:

Particle Size mm	Estimated Volume Occupied by char (cm^3)
0.2 - 0.4	$8.41 < V_p < 9.67$
0.4 - 1.0	$7.98 < V_p < 9.31$
1.0 - 1.4	$7.98 < V_p < 9.28$

APPENDIX L

Approximate Pressure Drop Calculation for Internal Recirculation Reactor

A simplified view of the reactor internals is given below:

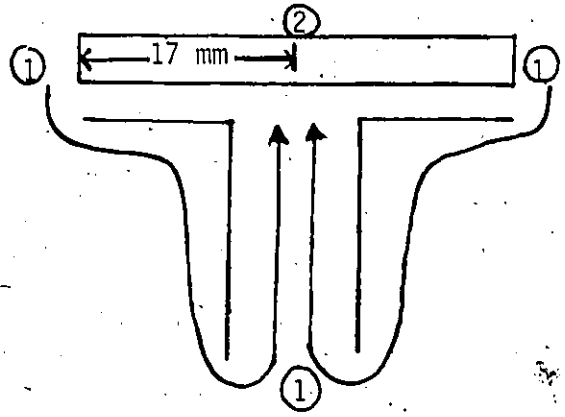

Assuming the gas experiences negligible resistance from the end of the impeller shaft to the bottom of the packed bed, one can get an estimate of the pressure head developed by the impeller and available for gas flow.

A simple Bernoulli equation ignoring any potential energy changes in the system is given below:

$$\frac{1/2\ v^2}{g_c} + \frac{\Delta P}{\rho} = 0$$

$$g_c = 32.17\ \frac{lb\text{-}ft}{lb_f\ s^2} \quad ; \quad v = r\omega = \frac{17\ mm}{25.4\ mm/in}\left[\frac{1\ ft}{12\ in}\right] 2\pi \left[1800\ \frac{rev}{min}\right]\left[\frac{1\ min}{60\ s}\right]$$

$$v = 10.5\ ft/s$$

$$\rho = \frac{P}{RT} = \frac{1\ atm}{82.05\ \frac{cm^3\ atm}{mol\ K}(298)\ K} = 4.1 \times 10^{-5}\ mol/cm^3 = 32.3\ lb/ft^3$$

Substituting these values into the equation gives

$$\frac{(10.5)^2}{2(32.2)} + \frac{\Delta P}{32.2} = 0$$

$$\Delta P = 55.3 \text{ lb}_f/\text{ft}^2 = 0.382 \text{ psi}$$

This is a very small pressure head.

The Ergun equation can be used to calculate the velocity through the drierite/ascarite bed (8 mesh) for this pressure

$$\frac{\Delta P}{L} = 150 \frac{(1-\varepsilon)^2}{g_c \varepsilon^3} \frac{\mu v}{\phi_s d_p^2} + 1.75 \frac{(1-\varepsilon)}{g_c \varepsilon^3} \frac{\rho v^2}{d_p}$$

where $\varepsilon \sim 0.4$

$\phi_s \sim 0.75$

$L = 0.25$ ft

$d_p = 7.75 \times 10^{-3}$ ft

$\Delta P = 55.3 \text{ lb}_f/\text{ft}^2$

The linear fluid velocity in the empty bed is found to be

$$v = 0.321 \text{ ft/s}$$

This velocity is <u>not</u> substantially greater than the inlet fluid velocity which is

$$v_{in} = 1000 \text{ cm}^3/\text{min} \quad \frac{1}{\left(\pi \frac{0.375}{4} 2.54^2 \, 30.48\right)} \quad \frac{1}{60}$$

$$v_{in} = 0.29 \text{ ft/s}$$

This would indicate that there isn't sufficient circulation through the bed.

APPENDIX M

Experimental Data From Mixing Tests

Particle Size —

Gas Flowrate 1000 cm^3/min

Impeller Speed 1800 rpm

Elapsed Time [s]	Measurement Device Response C/C_o	Combined Response C/C_o
0.2	0	0
0.3	0	0
0.4	0.358	0
0.5	0.151	0
0.55	0.275	0
0.6	0.8	0
0.7	0.909	0
0.8	0.936	0.04167
0.9	0.977	0.00417
1.0	0.966	0.02083
1.3	1.0	0.11667
1.7	1.0	0.20833
2.2	1.0	0.41667
2.7	1.0	0.54167
3.2	1.0	0.75
3.7	1.0	0.825
4.2	1.0	0.875
4.8	1.0	0.9167
5.3	1.0	0.95833

Particle Size 0.2 - 0.4 mm
Gas Flowrate 1000 cm^3/min
Impeller Speed 1800 rpm

Elapsed Time [s]	Measurement Device Response C/C_o	Combined Response C/C_o
0.2	0	0
0.3	0	0
0.4	0.358	0
0.5	0.151	0.04
0.55	0.275	0
0.6	0.8	0.06
0.7	0.909	0.032
1.0	0.966	0.2
1.3	1.0	0.38
1.7	1.0	0.56
2.2	1.0	0.616
2.7	1.0	0.76
3.2	1.0	0.86
3.7	1.0	0.90
4.2	1.0	0.928
4.8	1.0	0.952
5.3	1.0	0.96

Particle Size 1.0 - 1.4 mm
Gas Flowrate 1000 cm^3/min
Impeller Speed 1800 rpm

Elapsed Time [s]	Measurement Device Response C/C_o	Combined Response C/C_o
0.2	0	0
0.3	0	0
0.4	0.358	0
0.5	0.151	0
0.55	0.275	0
0.6	0.8	0
0.7	0.909	0
0.8	0.936	0.0980
0.9	0.977	0.0471
1.0	0.966	0.15686
1.3	1.0	0.2353
1.7	1.0	0.4471
2.2	1.0	0.5490
2.7	1.0	0.6941
3.2	1.0	0.8078
3.7	1.0	0.8627
4.2	1.0	0.90196
4.8	1.0	0.9451
5.3	1.0	0.9490

Particle Size 0.2 - 0.4 mm
Gas Flowrate 1000 cm^3/min
Impeller Speed 500 rpm

Elapsed Time [s]	Measurement Device Response C/C_o	Combined Response C/C_o
0.2	0	0
0.3	0	0
0.4	0.358	0
0.5	0.151	0.04
0.55	0.275	0.016
0.6	0.8	0.12
0.7	0.909	0
0.8	0.966	0.12
0.9	0.977	0
1.0	0.966	0.24
1.3	1.0	0.36
1.7	1.0	0.52
2.2	1.0	0.64
2.7	1.0	0.792
3.2	1.0	0.86
3.7	1.0	0.872
4.2	1.0	0.92
4.8	1.0	0.936
5.3	1.0	0.96

Particle Size 1.0 - 1.4 mm
Gas Flowrate 1000 cm^3/min
Impeller Speed 500 rpm

Elapsed Time [s]	Measurement Device Response C/C_o	Combined Response C/C_o
0.2	0	0
0.3	0	0
0.4	0.358	0
0.5	0.151	0
0.55	0.275	0.0392
0.6	0.8	0
0.7	0.909	0
0.8	0.936	0.05882
0.9	0.977	0.07843
1.0	0.966	0.08
1.3	1.0	0.3529
1.7	1.0	0.4706
2.2	1.0	0.5882
2.7	1.0	0.70588
3.2	1.0	0.7843
3.7	1.0	0.8588
4.2	1.0	0.90196
4.8	1.0	0.94118
5.3	1.0	0.9725

Particle Size 0.4 - 1.0 mm
Gas Flowrate 750 cm^3/min
Impeller Speed 900 rpm

Elapsed Time [s]	Measurement Device Response C/C_o	Combined Response C/C_o
0.3	0	0
0.4	0	0
0.5	0	0
0.55	0	0
0.6	0.1481	0.0755
0.65	0.7481	0
0.70	0.9630	0
0.80	0.9555	0.03773
0.90	0.2963	0.09811
1.0	1.0	0.0755
1.3	1.0	0.1509
1.7	1.0	0.2642
2.2	1.0	0.4226
2.7	1.0	0.60
3.2	1.0	0.6566
3.7	1.0	0.7547
4.2	1.0	0.8226
4.8	1.0	0.8679
5.3	1.0	0.8868
6.0	1.0	0.9358

Particle Size 0.4 - 1.0 mm
Gas Flowrate 750 cm^3/min
Impeller Speed 900 rpm

Elapsed Time [s]	Measurement Device Response C/C_o	Combined Response C/C_o
0.3	0	0
0.4	0	0
0.5	0	0
0.55	0	0
0.6	0.1481	0
0.65	0.7481	0
0.70	0.9630	0.0377
0.80	0.9555	0
0.90	0.2963	0
1.0	1.0	0.1132
1.3	1.0	0.2264
1.7	1.0	0.1434
2.2	1.0	0.3396
2.7	1.0	0.5283
3.2	1.0	0.6792
3.7	1.0	0.7170
4.2	1.0	0.7774
4.8	1.0	0.8491
5.3	1.0	0.9057
6.0	1.0	0.9358

Particle Size 1.0 - 1.4 mm
Gas Flowrate 500 cm^3/min
Impeller Speed 500 rpm

Elapsed Time [s]	Measurement Device Response C/C_o	Combined Response C/C_o
0.5	0.01852	0
0.6	0	0
0.65	0.3333	0
0.7	0.3333	0
0.75	0.2407	0
0.80	0.7185	0
0.85	0.8370	0
0.90	0.5926	0
0.95	0.8555	0.0037
1.0	0.9629	0
1.5	1.0	0.0741
2.2	1.0	0.18519
2.7	1.0	0.3148
3.2	1.0	0.4815
3.7	1.0	0.5370
4.2	1.0	0.5926
4.8	1.0	0.6667
5.8	1.0	0.7407
6.5	1.0	0.8148
7.5	1.0	0.8889

Particle Size	0.2 - 0.4 mm
Gas Flowrate	500 cm^3/min
Impeller Speed	500 rpm

Elapsed Time [s]	Measurement Device Response C/C_o	Combined Response C/C_o
0.5	0.01852	0
0.6	0	0
0.65	0.3333	0
0.7	0.3333	0
0.75	0.2407	0
0.80	0.7185	0.03846
0.85	0.8370	0.05
0.90	0.5926	0.01923
0.95	0.8555	0.10
1.0	0.9629	0.01154
1.5	1.0	0.1346
2.2	1.0	0.2692
2.7	1.0	0.3923
3.2	1.0	0.5423
3.7	1.0	0.6077
4.2	1.0	0.71923
4.8	1.0	0.7885
5.8	1.0	0.8346
6.5	1.0	0.90769
7.5	1.0	0.9346

Particle Size 1.0 - 1.4 mm
Gas Flowrate 500 cm^3/min
Impeller Speed 1000 rpm

Elapsed Time [s]	Measurement Device Response C/C_o	Combined Response C/C_o
0.5	0.01852	0
0.6	0	0
0.65	0.3333	0.0037
0.7	0.3333	0
0.75	0.2407	0
0.80	0.7185	0
0.85	0.8370	0
0.90	0.5926	0
0.95	0.8555	0.0037
1.0	0.9629	0.01481
1.5	1.0	0.05926
2.2	1.0	0.16667
2.7	1.0	0.3259
3.2	1.0	0.4074
3.7	1.0	0.48148
4.2	1.0	0.59259
4.8	1.0	0.7037
5.8	1.0	0.7777
6.5	1.0	0.8148
7.5	1.0	0.8778

Particle Size 0.2 - 0.4 mm
Gas Flowrate 500 cm^3/min
Impeller Speed 1000 rpm

Elapsed Time [s]	Measurement Device Response C/C_o	Combined Response C/C_o
0.5	0.01852	0
0.6	0	0
0.65	0.3333	0.00385
0.7	0.3333	0
0.75	0.2407	0.01923
0.80	0.7185	0
0.85	0.8370	0.03846
0.90	0.5926	0
0.95	0.8555	0.02692
1.0	0.9629	0.076923
1.5	1.0	0.17692
2.2	1.0	0.23846
2.7	1.0	0.4538
3.2	1.0	0.44615
3.7	1.0	0.56154
4.2	1.0	0.67308
4.8	1.0	0.75
5.8	1.0	0.8385
6.5	1.0	0.88462
7.5	1.0	0.02308